The Fiber Society
2016 Spring Conference

Textile Innovations—Opportunities and Challenges

May 25–27, 2016

Conference Chairs

Pr. Dominique Adolphe, Pr. Laurence Schacher, Dr. Nabyl Khenoussi

Ecole Nationale Supérieure d'Ingénieurs Sud-Alsace

Venue

University of Haute-Alsace

Ecole Nationale Supérieure d'Ingénieurs Sud-Alsace
Mulhouse, France

ENSISA – Werner 11 – rue Alfred Werner – Mulhouse

Program

Tuesday, May 24

1:00 PM–5:00 PM	Governing Council Meeting: Mechanic Meeting Room, Room 355
5:00 PM–7:00 PM	Early Bird Registration and Reception: ENSISA Werner Bldg. (**B** on map) – Workshop Lane

Chairpersons

Prof. Dominique ADOLPHE
Prof. Laurence SCHACHER
Dr. Nabyl KHENOUSSI

Organizing Committee

Prof. Dominique ADOLPHE
Dr. Emilie DREAN
Prof. Jean-Yves DREAN
Dr. Omar HARZALLAH
Dr. Nabyl KHENOUSSI
Dr. Gaëlle ODING
Prof. Laurence SCHACHER

Scientific Committee

Maria José ABREU – Universidade do Minho - Portugal
Dominique ADOLPHE – University of Haute-Alsace - France
François BOUSSU – ENSAIT - France
Pascal BRUNIAUX – ENSAIT - France
Marie-Ange BUENO – University of Haute-Alsace - France
Christine CAMPAGNE – ENSAIT - France
Emilie DREAN – University of Haute-Alsace - France
Jean-Yves DREAN – University of Haute-Alsace - France
Dominique DUPUIS – University of Haute-Alsace - France
Jean-Paul GOURLOT – CIRAD - France
Adda FERRY – Politecnico di Turino - Italy
Omar HARZALLAH – University of Haute-Alsace - France
Hamidou HAIDARA – IS2M - France
Frederic HEIM – University of Haute-Alsace - France
Tanveer HUSSAIN – National Textile University - Pakistan
Michael JAFFE – New Jersey Institute of Technology - USA
Stefan JOCKENHÖVEL – RWTH Aachen University - Germany
Nabyl KHENOUSSI – University of Haute-Alsace - France
Mourad KRIFA – University of Texas at Austin - USA
Bipin KUMAR – University of California at Davis - USA
Victor KUZMICHEV – Ivanovo State Polytechnic University - Russian Federation
Yordan KYOSEV – Hochschule Niederrhein University of Applied Sciences - Germany
Abdelaziz LALLAM – University of Haute-Alsace - France
Gildas L'HOSTIS – University of Haute-Alsace - France
Margarita NEZNAKOMOVA – Sofia Technical University - Bulgaria
Vincent PLACET – University of Franche-Comté - France
Ron POSTLE – New South Wales University - Australia
Ivelin RAHNEV – College of Sliven - Bulgaria
Laurence SCHACHER – University of Haute-Alsace - France
Artan SINOIMERI – University of Haute-Alsace - France
Damien SOULAT – ENSAIT - France

Wednesday, May 25

7:30   Registration (ENSISA Werner Building – Main Hall – **B** on the map) and Breakfast (Workshop Lane)

8:30   Welcoming Remarks, Business, and Announcements – Amphitheatre Hadamard-FST (**A** on the map)

Christine Gangloff-Ziegler, President of the University
Laurent Bigue, Director of ENSISA
Marie-Ange Bueno, Director of Laboratory (LPMT)
Konstantin Kornev, President, The Fiber Society
Laurence Schacher, Conference Chair

8:45–
9:25   **Speaker:** Michael Ellison, Clemson University, *The Fiber Society: In the Beginning, May 1941*

9:25   Move to Session Rooms (ENSISA Werner Building – **B** on the map)

Morning Session

	Amphi Richard Adrien Schutz (RAS)	Amphi 116
	Session: Fiber Formation, Structure, and Properties ***Chair, Bhuvenesh Goswami***	**Session: Yarn Processes, Structures, and Properties** ***Chair, Yordan Kyosev***
9:45	*Homogeneity of Finest Fiber Nonwovens* Ingo Windschiegl, Institute of Textile Technology and Process Engineering	*Automatic Online Controlling Linear Density and Blend Ratio of Rotor Spun Yarn Spinning Process* Rui-Hua Yang, Jiangnan University
10:10	*Structure and Properties of Cellulose Diacetate Fibers by Melt Spinning with Imidazole Ionic Liquid as Plasticizing Agent* Na Liu, Donghua University	*High-temperature Polymer Yarns for Through Thickness Reinforcement of Carbon Fibre Laminates* Cormac McGarrigle, Ulster University
10:35	*Effect of Stress and Temperature on the Molecular Orientation of Melt-spun Poly(3-hydroxybutyrate) Fibers* Rudolf Hufenus, Empa	*open*

11:00–11:20	***Break***	

	Session: Fiber Formation, Structure, and Properties ***Chair, Janice R. Gerde***	**Session; Dyeing, Finishing, and Wettability** ***Chair, Ian Hardin***
11:20	*Wettability of Carbon Fibers at the Microscale* David Seveno, KU Leuven	*Influence of UV Protecting Finish and Color on Spectral and Thermophysiological Properties of Sports Textiles* Bianca-Michaela Woelfling, Hohenstein Institute for Textile Innovation
11:45	*Hydrodynamics of Fiber Drawing from Polymer Solutions* David Lukáš, Technical University of Liberec	*On the Relevance to Test the Robustness of the Textile Hydrophobic Properties* Florence Biguenet, University of Haute-Alsace
12:10	*open*	*Wetting of Complex-shaped Fibers* Konstantin Kornev, Clemson University
12:35	*Structural Development of Poly(ethylene terephthalate) Undrawn Filament Upon Cold Drawing Assisted with Infusion of Ethanol* Takeshi Kikutani, Tokyo Institute of Technology	*Formation of Alcohol Repellent Medical Nonwoven Fabrics via Electrospraying* Mehmet Dasdemir, University of Gaziantep

1:00–2:45	***Lunch—at the Campus Restaurant (C on the map)***	

Afternoon Session

	Session: Apparel, Fashion, and Marketing *Chair, Maria José Abreu*	Textile Testing and Control *Chair, René Rossi*
2:45	*Textile Design with Integrated Smart Textile Applications* Zuzana Hrubošová, Technical University of Liberec	*New Method for Evaluation of the Trauma and the Penetration Depth Through Multilayer Textiles* Priscilla Reiners, Hochschule Niederrhein University of Applied Sciences
3:10	*ANN and Fuzzy Techniques for Modeling the Residual Bagging Height of Denim Fabrics as Function of Frictional Properties* Boubaker Jaouachi, University of Monsatir	*Biochemical Remedy of Contaminated Forests and Fields of Fukushima Area of Japan Using Kassei-chip Method* Masatomo Minagawa, Dream-Create-Laboratories
3:35	*Photonic Textile Design Practice: A Case Study* Zi-qian Bai, Donghua University	*Wear of Carbon Nanotubes Grafted on Carbon Fiber* Claire Guignier, University of Haute-Alsace
4:00	*open*	*Investigation of Flammability Behaviour of Woven/Glass Fabric Reinforced with Vinyl Ester Composites Used in Wind Turbines* Tugba Ozturk, Gaziantep University

4:25–4:45	**Break**

4:45–7:00	*Laure Ledoux, Artist – Coctail de Vernisage* In the frame of a Residency supported by Kunsthalle (Contemporary Art Gallery and Art Exhibition) and the University of Haute-Alsace, Laure Ledoux spent 2 months in ENSISA–Textile Department. The program was designed to stimulate collaborative problem-solving using an interdisciplinary approach. Together, the artist and scientists explored issues of visual representation and communication, and worked toward a better understanding of the complexities of artistic and scientific behaviors. Those interactions led to the influence of the artist point of view and initiated a series of photos that will be presented in the frame of this exposition. During her residency, Ledoux mainly worked on a technical pleated textile called Vertilap®, developed by a local textile manufacturer (N. Schlumberger) that she transformed, tortured, and assembled in order to develop shapes and clothes that have been the object of her thoughts and photographic works.

Thursday, May 26

8:00   Registration (ENSISA Werner Building – Main Hall – **B** on the map) and Breakfast (Workshop Lane)

8:30–9:10   **Speaker:** Francisco Chinesta, Ecole Centrale de Nantes, *From Short to Long: Fiber Behaviors in Reinforced Polymers and Composite Processing* (in Amphitheatre Richard Adrien Schutz-RAS)

9:10   Move to Session Rooms

Morning Session

	Amphi Richard Adrien Schutz (RAS)	Amphi 116
	Session: Nanofibers by Electrospinning or Other Methods *Chair, Xungai Wang*	Session: Fabric Processes, Structures, and Properties *Chair, Michael Ellison*
9:25	*open*	*Slash and Penetration-resistant Hybrid Fabrics of Superior Performance* Donald Sturgeon, Multifibers LLC
9:50	*Titanium-Magnesium Oxide Hybrid Nanofibers* Yakup Aykut, Uludağ University	*Development of Wicking Interfaces in Single Jersey Knitted Fabric for Better Moisture Management Properties* Jawairia Umar, University of Agriculture

10:15	Polyimide Nanofibers/Carbon Woven Fabrics Hybrid Hot Gas Filter Qiuran Jiang, Donghua University	Comfort Effects of Weft-knitted Structures on Rowing Shirts Using IR Thermography Maria José Abreu, University of Minho
10:40–10:55	*Break*	
	Session: Nanofibers by Electrospinning or Other Methods *Chair, Caroline Schauer*	**Session: Fabric Processes, Structures, and Properties** *Chair, Marie-Ange Bueno*
10:55	*Unconfined, Melt-edge Electrospinning for Scale-up* Russell Gorga, North Carolina State University	*Weft-backed Woven Structures for Enhanced Color Effect and Structure Integration of Colorful and Jacquard Fabrics* Tao Hua, Hong Kong Polytechnic University
11:20	*Exploring the Potential of Nanofibers in Gas and Water Filtration, Including a Gateway to Mass Production* Xiaohong Qin, Donghua University	*The Influence of Repeated Washing on Abrasion Resistance of Nonwoven Cleaning Materials/Cloths/Wipes Produced with Different Process Conditions* Emel Çinçik, University of Erciyes
11:45	*Increasing Surface Available Biotin and Improving Water Stability of PLA/PLA-b-PEG Nanofibers* Larissa Shepherd, Cornell University	*Investigation of Dimension Stability of Knitted Fabrics Made of Single- and Double-plied Yarns* Ebru Çoruh, Gaziantep University
12:10	*Piezoelectric Properties of Natural Polymer Electrospun Fibers* Caroline Schauer, Drexel University	*The Effect of Yarn on the Air Permeability of Plain Knitted Fabrics Produced by Different Count, Raw Material, and Twist Ratios* Züleyha Değirmenci, University of Gaziantep
12:35	*Thin Film, Nanofibrous Composite Membranes Prepared by Electrospray Technique and Hot-pressing Treatment for Water Purification* Lindgi Shen, Donghua University	*Geometrical Modeling of Flat and Tubular Triaxial Braided Structures* Yordan Kyosev, Hochschule Niederrhein University of Applied Sciences
1:00–2:30	*Lunch—at the Campus Restaurant*	

Afternoon Session

	Session: Polymers and Smart Applications *Chair, Takeshi Kikutani*	**Session: Functional Fibers and Structures** *Chair, Kostya Kornev*
2:30	*Nanocellulose-based Textile Coatings for Smart Textiles* Sergiy Minko, University of Georgia	*Enhancing the Efficiency of Diesel Fuel Filters by the Usage of Bicomponent Fibers with Water-guiding Channels* Inga Noll, RWTH Aachen University
2:55	*Cellulose Dissolution: Promising Approach for the Preparation of Composite Materials* Noureddine Abidi, Texas Tech University	*Luminescent and Glucose-sensitive Hybrid Biofiber Based on Bacterial Nanocellulose* Jingjing Yao, Donghua University
3:20	*Development of Composite Filament by Conventional Melt Extruder* Ali Afzal, University of Haute-Alsace	*How to Flame Retard Polyamide-6 Fibers* Mathilde Casetta, University of Lille
3:45	*Flexible Solar Textiles with Style for Future Smart Clothing System* Youngjin Chae, Singapore University of Technology and Design	*Mechanical and Functional Characterization of Basalt Woven Structures* Zuzana Hrubošová, Technical University of Liberec
4:10–4:35	*Break*	
4:35–6:00	**Poster Session and Competition: Room 202 and Dedicated Corridors**	

6:00–7:00	Transportation to Gala Dinner at the Automotive Museum via Tram (LPMT PhD Students will Serve as Guides)	
7:00–11:00	Gala Dinner Speaker: Marc Renner, *1746–2016: Opportunities and Challenges for Textile Innovation in Mulhouse*	

Friday, May 27

8:00   Breakfast (ENSISA Werner Building – Workshop Lane – **B** on the map)

8:30–
9:10   **Speaker:** Damien Durville, Ecole Centrale Paris-France, *Finite Element Simulation of Fibrous Materials* (in Amphitheatre Richard Adrien Schutz-RAS)

9:10   Move to Session Rooms

	Amphi Richard Adrien Schutz (RAS)	Amphi 116
	Session: Fabric Processes, Structures, and Properties *Chair, Rudolf Hufenus*	**Session: Fibers for Medical Applications** *Chair, Sergiy Minko*
9:25	*Artificial Finger for Textile Fabrics* Marie-Ange Bueno, University of Haute-Alsace	*Antibacterial Activity and Washing Durability of Bamboo Fabrics Treated with Different Metal Salts* Mustafa Tutak, Erciyes University
9:50	*Sound Absorption Properties of Spunmelt Multilayer Nonwovens* Dilan Canan Çelikel, Gaziantep University	*Development of Antibacterial Braided PET Suture* Faten Debbadi, Monastir University
10:15	*Electromagnetic Characterization of Textile Materials for the Design of Wearable Antennas* Caroline Loss, University of Beira Interior	*Wearable Sensors and Therapy Devices Based on Photonic Textiles* René Rossi, Empa

10:40–10:55	*Break*	

	Session: Natural Fibers; Composite Processes, Properties, and Modeling *Chair, David Seveno*	**Session: Fibers for Medical Applications** *Chair, Frederic Heim*
10:55	*Characteristics and Prospective Applications of Powders Derived from Natural Fibers* Rangam Rajkhowa, Deakin University	*Sustained Release of VEGF from Silk Fibroin Nanoparticle-modified, Bacterial Cellulose-based Scaffold for Tissue Engineering* Baoxiu Wang, Donghua University
11:20	*The Effect of Titanium Dioxide on the Processing Time of Composites Made of Commingled Glass and PA 6 Fibres* Robert Brüll, RWTH Aachen University	*Functionalization and Biocompatibility Evaluation of Drawn Fibers for Neural Tissue Implants* Kateřina Strnadová, Technical University of Liberec
11:45	*Mechanical and Structural Characteristics of a High-performance, Fully-thermoplastic, Fiber-reinforced Composite* Andres Leal, Empa	*High-modulus, Melt Spun Polycaprolactone Fibres for Biomedical Grafts* Tom O'Haire, University of Leeds
12:10	*open*	*Mechanical Behavior of Rat Tendons Under Cyclic Tensile Loadings* Gilles Arnold, University of Haute-Alsace
12:35	*open*	*Textile Prosthetic Heart Valve Designs to Reduce Reynolds Shear Stress* Antoine Vaesken, University of Haute-Alsace

1:00	*Close of Conference*	

2:30	*Visit of the Textile College of Engineering and Laboratory Facilities*	

Poster Session

Thursday, May 26, 4:20 p.m.–6:00 p.m., Room 202 and Dedicated Corridors

Presenter	Title
Alenka Ojstršek	*Surface Morphologies of Nylon Knitted Textiles Coated with Different Zeolites*
Darinka Fakin	*Applicability of Porous Three-dimensional Aluminosilicates for Cellulose Surface Modification*
Ahsan Nazir	*Effect of Electrospinning Parameters on Air and Water Vapour Permeability of PP Nonwoven Substrate Coated with PA-6 Nanoweb*
Shiyan Chen	*In Vitro Biodegradability of Bacterial Cellulose by Cellulase and Compatibility In Vivo*
Ngan Yi Kitty Lam	*The Application of Chitosan/Cotton Blend Yarn for Addressing Functional Clothing Needs of Patients Suffering from Epidermolysis Bullosa*
Boubaker Jaouachi	*Sewing Thread Consumption of Overegged Three-thread Stitch Type 504*
Guangbiao Xu	*Structure and Properties of Polytetrafluoroethylene (PTFE) Fiber*
Inga Noll	*Correlation of Polyethylene-based Precursor Properties on the Sulfonation for Stabilization*
Robert Brüll	*Meltspun Polyamide 6-Graphite Fibres: Manufacturing and Analysis with Additional Comparison of Pre- and Inline Compounding*
Tae Jin Kang	*Effect of Concentration of Hydrophobicity of Polydimethylsiloxane Fiber Mat by Electrospinning*
Michel Tourlonias	*Carbon Yarn/Yarn and Fiber/Fiber Friction*
Benjamin Glauβ	*Multicomponent Filaments Process for the Use as Sensors*
Ruihua Yang	*Numerical Analysis and Comparison of Airflow in Rotors with U and V Groves During Rotor Spinning Process*
Tao Hua	*Effect of the Proportion of Meta-aramid Fibers on Flammability of Meta-aramid/Wool-blended Yarn and Fabric*
Maria José Abreu	*Lexicon for Sensory Evaluation of Tactile Textiles in Brazil*
Floriane Leclinche	*Fabric Friction Sound Characterization in Dry and Wet State*
Yakup Aykut	*Titanium Isopropoxide/Magnesium Acetate/PVP Composite Nanofibers via Electrospinning*
Michael Ellison	*Understanding Factors Influencing Cellular Response to Spider Silk*
Cheng Cheng	*GO/SiO$_2$ Ultrafiltration Composite Membrane Based on PAN Nanofibrous Substrate for Oil-Water Emulsions Treatment*
Xufeng Yu	*Thin Film Nanofibrous Composite Hemodialysis Membranes with High Permeability and Great Selectivity*
Min Wang	*Co-deposition of Dopamine and Poly(ethyleneimine) Complex Nanofibrous Membranes for Dye Adsorption*
Wujun Ma	*Hierarchically Porous Carbon Black/Graphene Hybrid Fibers for High-performance Flexible Supercapacitors*

Plenary Speakers

The Fiber Society: In the Beginning, May 1941

Dr. Michael Ellison
Clemson University

ellisom@clemson.edu

An overview of the inception and early years of The Fiber Society, culled from the Society's collection of original documents. The documents include minutes from Governing Council and Annual Business Meetings, some synopses of research presentations, correspondence, and photographs. Additionally, some research into the historical record outside of Fiber Society archives is included. The changes in the Society, often as a consequence of shifting personnel and their influence, as well as the effects of outside influences (WWII, for example), are discussed.

From Short to Long: Fiber Behaviors in Reinforced Polymers and Composite Processing

Dr. Francisco Chinesta

Ecole Centrale de Nantes

francisco.chinesta@ec-nantes.fr

Over the last decades, an increasing number of functional and structural parts, made so far with metals, have been progressively reengineered by replacing metallic materials with polymers, reinforced polymers, and composites. The motivation for this substitution might be weight reduction, a simpler, cheaper, or faster forming process, or the ability to exploit additional functionalities.

The fillers usually employed cover a broad range involving many scales: (1) the nanometer scale (e.g., carbon nanotubes, graphene, fullerene, nanodiamonds); (2) the micrometer to the millimeter scale (particles and short fibers); (3) the centimeter scale of fibers used in SMC and BMC composite processes; and (5) the macroscopic scale, where fibrous reinforcements are made of continuous fibers arranged in bundles.

When load-bearing capacities are especially desired, continuous fiber-reinforced polymers are selected. In this case, the impregnation of the reinforcement with a low-viscosity polymer involves the flow of a Newtonian or non-Newtonian fluid in the complex multiscale microstructure related to the fiber and tow arrangement. Reinforced polymers are selected instead of high-performance polymers of equivalent properties, since the latter are generally more expensive.

When looking for functional properties, the use of nanocharges opens a wide spectrum of possibilities, but is also raises new challenges, such as dispersion of charges into the polymer matrix and the occurrence of aggregation and disaggregation mechanisms. Suspensions of practical interest involve many scales and many concentration regimes, the latter ranging from diluted to highly concentrated.

In all cases, efficient simulation strategies that are able to perform real-time calculations, which are specially needed when optimizing materials and processes when performing inverse analysis or during the simulation-based control of processes, are urgently needed.

In this talk, we revisit some major challenging processes and describe advanced modeling and simulation strategies, the last being able to proceed in real time, allowing for real-time decision making.

Finite Element Simulation of Fibrous Materials

Dr. Damien Durville
Ecole Centrale Paris–France

damien.durville@centralesupelec.fr

A global approach is proposed and presented for the simulation by the finite element method of the mechanical behavior of fabrics and fabric-reinforced composites. The research work is based on the representation of all fibers constituting woven fabric structures by means of 3D beam models, taking into account contact-friction interactions between fibers.

Few parameters are available to describe and predict the complex, global, mechanical behavior of textile composite materials at a macroscopic scale, as well as very localized phenomena, such as breakings at the microscopic scale of fibers.

Fiber Formation, Structure, and Properties

Homogeneity of Finest Fiber Nonwovens

Ingo Windschiegl, Martin Dauner, Andreas Ullrich, Götz T. Gresser
Institute of Textile Technology and Process Engineering, Germany
ingo.windschiegl@itv-denkendorf.de

OBJECTIVE

Due to their statistic fiber orientation nonwovens are basically inhomogeneous. This inhomogeneity is balanced with increasing web weights. One way to reduce the irregularities to this scale are finest fibers technologies (fibers < 1 µm) as meltblow (MB) or centrifugal spinning (CS). But if we optimize the homogeneity by use of finest fibers, we have to readjust the evaluation; the finer the fibers the smaller the inhomogeneous areas.

INTRODUCTION

In filtration fine fibers act by their size/mass proportion, small pores in separation, low inertia in sound insulation, low stiffness for comfort. There is another, rarely discussed, seemingly obvious effect connected to the fiber size of nonwovens: the finer the fibers are, the more homogeneous the lay down of the fibers will be (keeping the web weight constant and considering a constant area, let's say a disc of 100 cm², as it is used for standard area weight tests). Only from view one may know that spunbond webs having fiber sizes > 10 µm look less homogeneous than meltblow webs of 1 µm fiber diameter. Moreover finest fiber webs of 0.1 µm fiber diameter seems to be even more homogeneous (at same web weight). That is connected to the stochastic nature of nonwovens and is given by the number of fibers involved respectively. Nevertheless there are some irregularities, even in finest fiber webs.

Yet typical filter media of finest fibers are extremely light < 1 g/m² to keep the pressure drop low. Hence their homogeneity cannot be measured using a standard weighing scale. Air permeability measurements combined with porosimetry and SEM are used alternatively as filter tests require an enormous effort. In textile world area weight is referred to m² (i.e., g/m²) on samples of some min. 100 cm² (DIN EN ISO 29073-1); thickness is measured on an area of 25 cm² (DIN EN ISO 9073-2), air permeability on an area of 20 cm² (DIN EN ISO 9237). Common testing methods do not reflect small areas and, even more important, irregularities of nonwovens are usually in even a smaller scale. Alternatively we used samples of 10 mm diameter.

On the one hand Meltblow is well known as pretty homogenous, but even though the process is stochastic and thus there are some irregularities. On the other hand centrifuge spinning, a productive technology for finest fibers webs, bears a special risk of inhomogeneity due to the pattern of the lay down. As substrate and reference we set paper and meltblow filter media, which are considered to be best in homogeneity.

MATERIALS AND METHODS

As substrate (for centrifugal spinning) and reference a high precise filter paper (by Stora Enso, FI; 214 g/m² +/- 13%) was chosen. Additionally some commercial meltblow webs for filtration were evaluated to see differences, weak spots in evaluation and set standard.

At ITV Denkendorf the technologies meltblow and centrifugal spinning were examined with regard to homogeneity.

The prototype centrifugal spinning technology was developed by the ITV and Reiter OFT Winnenden, Germany, designed by 3 centrifuges on 1 m working width (Fig. 3-4). The technology has been lent from the painting industry; the set up was adapted to nonwoven processes. Trials were performed with 1 to 3 centrifuges at up to 40.000 turns/min. Means to optimize the web weight were forming air, distance of centrifuges and electrostatic field, resp.. Finest fibers of cellulose acetate were applied on the filter paper with very low area weight (0.1 – 0.3 g/m²) and with > 3 g/m². A second polymer solution system, polyamide 6/ formic acid, was applied on a warp knit (by Roekona, FI; 45 g/m² +/- 2%) with area weights > 1 g/m².

The meltblow line at ITV has a working width of 500 mm with 561 capillaries and 0.3 mm in hole diameter. For direct comparability among technologies, the webs were spun with polyamide 6 as well, with area weights of 10-50 g/m², self-supporting. Means of optimizing was airflow/ suction, polymer throughput, distance of die to collector (DCD).

The finest fiber webs (and/or the substrate) were punched to samples of 10 mm diameter (0.785 cm²) with a distance in between 2 samples of 10 mm. These samples were weight on a high resolution lab scale (Mettler Toledo) to 0.01 mg +/- 0.001 mg.

The parameters are summed up:
- Substrate and reference:
  Filter paper by Stora Enso, FI: 214 g/m² +/- 13%.
  Warp knit by Roekona, FI; 45 g/m² +/- 2%
  Commercial meltblow web, > 20 g/m²
- Target of var.-coeff.: < 15%
- Finest fiber web weight target for CS: 3 - 10 g/m²
- Finest fiber web weight target for MB: 10 - 50 g/m²
- Polymers:
  CS - Cellulose acetate (CA)
  CS/MB - Polyamide 6 (PA 6)
- Solvent:
  Acetic acid: acetone (2:1)
  Formic acid
- Measure: Web weight
- Measuring sample size: Ø 10 mm (0,785 cm²).
- High resolution lab weigh (Mettler Toledo), 0,01+/- 0,001 mg

RESULTS

To set a reference for deviation of weight the filter paper was examined with standard size measurement acc. DIN EN

ISO 29073-01 and the higher, new measuring-resolution subsequently. The variation coefficient was measured to +/- 1.5% for standard sample-size (100 cm²) and to +/- 13 % for small samples (0,785 cm²). Thus we set our deviation measure for "high" evaluation to < 15%.

For centrifugal spinning the trials were started with only one centrifuge with polymer-solvent-system cellulose acetate/ acetic acid: acetone (2:1). A standard setting was used. As a parameter the Die-Collector-Distance was varied. The result was a double peak web as expected and described in Fig. 1. Consider a circular (stationary) lay down of the fibers generated by the centrifuge. The result is a ring with broad rim. There will be significantly less fibers in the center. In combination to the movement of the conveyor belt the web weight in the center is distinctly lower compared to both sides (Fig. 2, above). The weight proportions depend a lot on the parameters. Higher DCD gave less variation, yet still very high, so the var.-coeff. was not calculated.
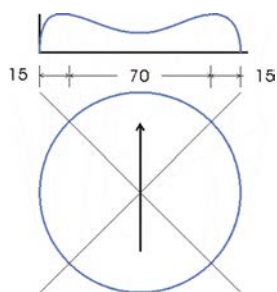
Figure 1: Sketch of fiber deposition in the centrifuge process. Above: weight-related front view with a double peak; below: top view on stat. fiber lay down almost to a ring.

The final combination of forming air, throughput/ centrifuge, web speed and DCD led to homogenous fiber deposition with a variation coefficient of 14%.

Transferring the results from one centrifuge to the three centrifuges line gave a fair var.-coeff. (94-03: 26%). This result could further be improved by interactive adjustment of the forming air and the positioning of the centrifuges (94-04: 1%) as shown in Fig. 2. A var.-coeff. of 14% in this context means a weight variance of 1 g/m² among max. and min. absolute weight.
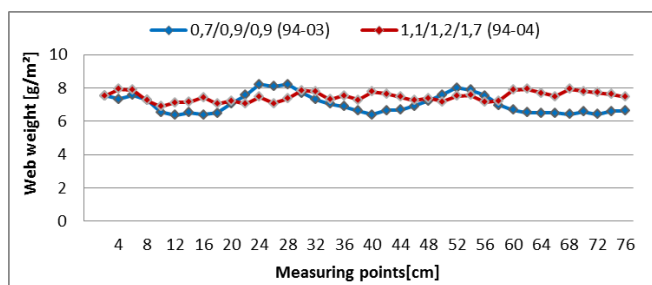

Figure 2: Web weight distribution = f(forming air) (3 centrifuges)(Measuring points: diam. 10 mm; 38 points) Var.-coeff.: 94-03: 26%; 94-04: 14%.

The transfer of all these results was done with polymer-solvent-system, polyamide 6 in formic acid. A further challenge of this system was the corrosivity of the solvent,

which need an improvement in conveying system. Additionally polyamide 6 was spun in meltblow process to have a direct comparability. Both of those spun web showed homogeneity with a var.-coeff. < 15% (Fig. 3).
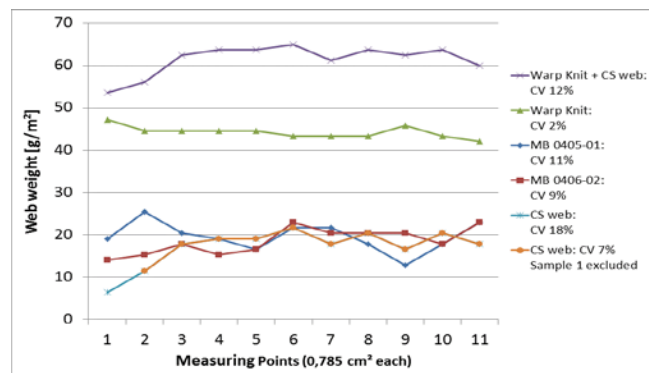

Figure 3: Web weight distribution = f(3 centrifuges & meltblow) (Measuring points: diam. 10 mm; 11 points)→ Var.-coeff.: < 15%.

With regard to manufacturing finest fibers in meltblow process, the parameters temperature (in polymer to reduce viscosity and of the air) and airflow were exhausted the most. As a consequence the lay down of fibers became more complex due to air turbulences and poses the risk of irregularities.

DISCUSSION
In the textile world, as already said, area weight is referred to square meters (i.e., g/m²) on sample sizes of 100 cm²; thickness is measured on an area of 25 cm², air permeability on an area of 20 cm².

Some filters, like e.g., blood or fuel filters, are smaller than these measuring areas. And even for large filters it isn´t sufficient to ignore weak spots. Moreover the optimization leads to further increase of filter productivity or helps to reduce them in size.

A control scheme using smaller areas than the filter size is stringently required to ensure or improve high quality.

CONCLUSION
- Small area filters need adjusted homogeneity control.
- Uncontrolled web formation at centrifuge spinning results in twin peak distribution.
- Web weight distribution in CS depends mainly on:
  → centrifuge positions (CD, z-axis)
  → forming air
- Web weight distribution in MB depends mainly on:
  → airflow
  → temperature (polymer and air)
- Web weight homogeneity with a var.-coeff. < 15% is achieved in centrifuge spinning and meltblow process and strikes the quality of a high quality filter paper.

Structure and Properties of Cellulose Diacetate Fibers by Melt Spinning with Imidazole Ionic Liquid as Plasticizing Agent

Na Liu, Weixia Yan, Huaping Wang

State Key Laboratory for Modification of Chemical Fibers and Polymer Materials, College of Materials Science and Engineering, Donghua University, Shanghai, China

liuna@dhu.edu.cn

As regenerated cellulose fibers, cellulose diacetate (CDA) fibers have played an irreplaceable role in the family of natural and synthetic fibers for decades and have been widely applied in textiles, for medical care and filter materials.[1] They exhibit softness and suppleness with a silk-like handle, a pleasant feel on the skin, excellent draping qualities, natural crease resistance, low moisture absorption and distinct filtering effect, which combine the merits of synthetic fibers and cellulose fibers，therefore have been the subjects of extensive current researches.[1-5]

CDA fibers are commercially manufactured by dry spinning. Large quantities of acetone are needed during the spinning process, which incurs both environmental and health concerns as acetone is highly volatile and flammable，and also lowers the production throughput. Furthermore, the produced CDA fibers from using acetone have relatively low mechanical strength, typically in the range of 1.06-1.23cN/dtex.[1] This has limited the application scope in textiles. A new environmental friendly process to fabricate CDA fibers with enhanced mechanical properties is highly demanded.

Our group has done a lot of work in this area to fabricate a melt spinning method of CDA plasticized by ILs. In our previous research work, imidazole ionic liquids were used as plasticizers of CDA and it was proved that ILs as plasticizers can be effective in improving the melt processability of CDA. [6,7] In this study, a type of ionic liquids, 1-Butyl-3-methylimidazolium terafluoroborate ([BMIM]BF$_4$) was used as plasticizing agent of CDA and then CDA fibers were produced by melt spinning. The rheological behavior of plasticized CDA was tested. The structure and properties of CDA fibers were then investigated.

CDA powder was provided by Natong Cellulose Fibers Co., Ltd. (degree of polymerization was 692, DS=2.4). It was dried in vacuum oven at 80 ℃ for 12 h before use. [BMIM]BF$_4$ was purchased from Shanghai Chengjie Chemical CO., LTD, China. CDA and [BMIM]BF$_4$ were mixed at room temperature with mass ratio of 75:25, subsequently blend in the twin-screw extruder (Eurolab16, Thermo-Hakke, Germany) at 180 ℃-190 ℃ to obtain pellets for further investigation. Then the pellets were injection molded using a SZ-5-C injection molding machine (Dehong Rubber and Plastic Machinery Co., China). The injection temperature and mold temperature were 245°C and 55°C respectively, the injection pressure was 0.5 Mpa and the dwell time was 6 s. Finally plasticized CDA samples with diameter of 25 mm and thickness of 2 mm were obtained for the rheological test.

The rheological test was performed on a rotational rheometer, ARES-G1 (TA Instrument Corporation, USA). It is clear that the plasticized CDA exhibits the typical shear-thinning behavior, with the temperature increasing, the apparent viscosity tended to decrease (Fig. 1). It is also apparent that when the temperature was over 230 ℃, η at different temperature was close under the same shear rate.
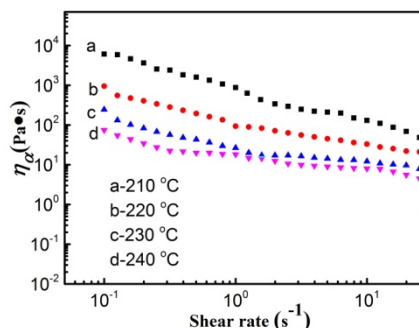

Fig. 1. Relationships of apparent viscosity vernus shear rate of CDA plasticized by 25 wt % [BMIM]BF$_4$ at different temperature.

Structural viscosity index ($\Delta\eta$) is a very important and common experimental parameter to evaluate the spinnability of spinning dope. $\Delta\eta$ can be described by the following equation[8]: $\Delta\eta = -[d(\lg\eta_a)/d\gamma^{1/2}] \times 100$, where η_a refers to apparent viscosity and γ shear rate. For non-Newtonian fluids, the values of $\Delta\eta$ are positive and smaller $\Delta\eta$ reflects better spinnalibity of fluids.

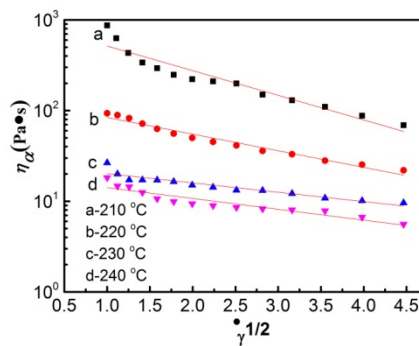Fig. 2. Relationships of lgη_a vernus $\gamma^{1/2}$ of CDA plasticized by 25 wt % [BMIM]BF$_4$ at different temperature.

The relationships of logη_a vernus $\gamma^{1/2}$ of CDA plasticized by 25 wt % [BMIM]BF$_4$ at different temperature are given in Fig. 2. Fitting curves of the experimental data in linear formula are also shown. It can be seen that the plots of experimental data exhibit good linear relationship. The values of $\Delta\eta$ were calculated as 27.17, 18.35, 10.29 and 11.95 at 210 ℃, 220 ℃, 230 ℃ and 240 ℃, respectively. It is obvious that $\Delta\eta$ has a minimum value at 230 ℃. The

decreasing $\Delta\eta$ can be attributed to the decrease of entanglement and easier movements of CDA chains with increasing temperature before 230 ℃. However $\Delta\eta$ at 240 ℃ is less than that at 230 ℃, which attribute to thermal decomposition of CDA at 240 ℃. Therefore，the melt spinning temperature was set as 230 ℃ for CDA plasticized by 25 wt % [BMIM]BF$_4$ in this study.

The spinning pellets were dried in vacuum oven at 80 ℃ for 40 h prior to melt spinning. Plasticized CDA fibers were melt spun by a MATE-V spinning device (Ube, Japan) at 230 ℃. The spinneret with 18 orifice of 0.4 mm was used. The as-spun fibers were taken up by means of winders at 100 m/min- 300 m/min, washed by deionized water and then dried in vacuum oven at 100 ℃ for 12 h.

Glass transition temperature (T$_g$) of CDA raw material, as-spun CDA fiber and washed CDA fiber were determined by DMA (Fig. 3). Tan Delta (Tanδ) is a damping term defined as the ratio of energy dissipated as heat to the maximum energy stored in the material. It is an index of material viscoelasticity. The temperature of the peak is related to T$_g$. As is shown in Fig. 3, T$_g$ of unwashed fiber is much less than that of CDA raw material and washed fiber, which is caused by [BMIM]BF$_4$. [BMIM]BF$_4$ in unwashed fiber weakened hydrogen bonds in CDA, resulting in decreasing in T$_g$. After washed, [BMIM]BF$_4$ was removed from the CDA fibers, hydrogen bonds in CDA Partially restored, thus washed fiber exhibits higher T$_g$ than unwashed fiber.
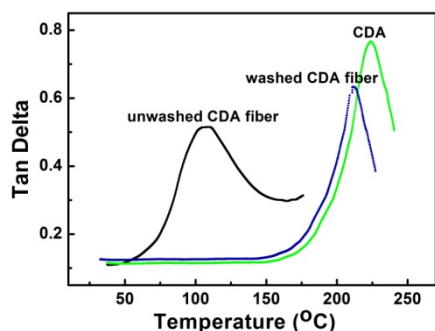

Fig. 3. The loss tangent and temperature curves of unwashed CDA fiber, washed CDA fiber and CDA.

It was very clear that there were no distinct flaws or crevices in the surface of the CDA fibers (Fig. 4a). The cross-section image showed that there were many hollows in the CDA fibers (Fig. 4b), which were caused to a great extent by the escape of BMIMBF$_4$.
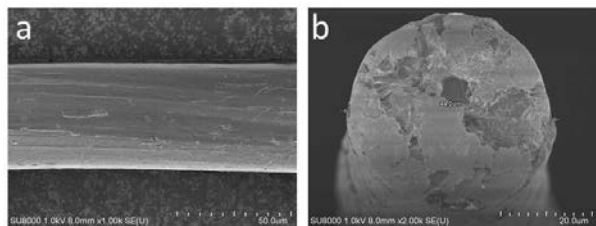

Fig. 4. SEM images of surface (a) and cross section (b) of washed CDA fiber (taken-up speed was 100 m/min).

The mechanical properties of washed CDA fibers at different taken-up speed were list at table I. Commercial CDA fibers purchased from Hangzhou Xinxie Fiber Co., Ltd, China was also tested for comparison. From the data, the fineness of melt spun CDA fibers decreases from 34.3 dtex to 18.1 dtex with the increase of taken-up speed from 100 m/min to 300 m/min. The tensile strength improves from 0.92 cN/dtex to 1.78 cN/dtex, whereas the elongation at break decreases from 15.4 to 12.8. Compared with that of the commercial CDA fibers (1.44 cN/dtex), the melt spun CDA fibers with taken-up speed above 200 m/min have comparable or higher tensile strength despite of the greater fineness. The tensile strength of melt spun CDA fibers is also greater than that reported in literature (1.06-1.23 cN/dtex).[1]

Table I. Mechanical properties of CDA fiber from different spinning process

Sample	Taken-up speed (m/min)	Fineness （dtex）	Tensile strength (cN/dtex)	Elongation at break (%)
Commercial	/	3.83	1.44	24.90
Melt-spun fiber	100	34.3	0.92	15.40
	200	25.4	1.31	14.70
	300	18.1	1.78	12.80

To conclude, The CDA fibers have been successfully processed by melt spinning with [BMIM]BF$_4$ as plasticizer. The optimal tensile strength of CDA fibers can reach 1.78 cN/dtex with the fineness of 34.3 dtex, compared favorably with the fineness (3.83 dtex) and tensile strength (1.44 cN/dtex) of the commercial CDA fibers. We believe there is still a broad room to improve the mechanical properties of the CDA fibers by optimizing the spinning conditions. The added environmentally benignness of the IL should make this approach attractive for future textile applications.

REFERENCES
1. R C. Law. *Macromol. Symp.*, 2004, 208: 255-66.
2. I. Munaweera, A. Aliev, K.J. Balkus, Jr. *ACS Appl. Mater. Interfaces.*, 2014, 6: 244-51.
3. R. Nasser, Jr., M.E.S. Taqueda. *Ind. Eng. Chem. Res.*, 2008, 47: 8376-83.
4. D.A. Rubenstein, S.M. Venkitachalam, D. Zamfir, F. Wang, H. Lu, M. D. Frame, W. Yin. *J. Biomater. Sci. Polym. Ed.*, 2010, 21: 1713-36.
5. T. Matamá, R. Araújo, G. M. Gübitz, M. Casal, A. Cavaco-Paulo. *Biotechnol. Progr.*, 2010, 26: 636-43.
6. Z. Li, N. Liu, Y. Yao, S. Chen, H. Wang, H. Wang. *RSC. Adv.*, 2015, 5: 901-07.
7. N. Liu, J. Zhang, H. Wang, *Adv. Mater. Res.*, 2014, 936: 1002-06.
8. J. Cai, P. Fei, Z. Xiong, Y. Shi, K. Yan, H. Xing, *Carbohydr. Polym.*, 2013, 92: 11-18.

Effect of Stress and Temperature on the Molecular Orientation of Melt-spun Poly(3-hydroxybutyrate) Fibers

Rudolf Hufenus, Felix A. Reifler

Empa, Swiss Federal Laboratories for Materials Science and Technology, Switzerland

rudolf.hufenus@empa.ch

OBJECTIVE

In a previous work we presented the successful spinning of poly(3-hydroxybutyrate) (P3HB) fibers applying an upscalable melt-drawing method [1, 2]. This work aims to an understanding of the effect of stress and temperature on the molecular orientation of melt-spun P3HB fibers. To this end, the physical and structural properties of the produced filaments are characterized applying wide angle X-ray diffraction (WAXD) in combination with tensile and heating stages.

INTRODUCTION

The use of inherently biodegradable polymers is an opportunity to reduce the amount of plastic waste that cannot be assimilated by microorganisms. P3HB is a sustainable and biocompatible, semi-crystalline thermoplastic polyester produced by bacteria for intracellular carbon and energy storage [3]. The bacteria build the polymer chains perfectly linear and isotactic, which guarantees superior properties [4]. Due to its biological background, P3HB is truly biodegradable in aerobic (e.g. in soil or compost) and anaerobic (e.g. in drainage pits or sea mud) conditions without forming toxic by-products [5]. In addition, P3HB is water insoluble, hydrophobic, and comparatively resistant to hydrolytic degradation [6]. Due to its exceptional properties, as well as reasonable production costs via the relatively simple biosynthesis process, P3HB is a promising substitute for conventional petrochemical plastics [7]. Its thermoplastic nature qualifies it for a continuous production of filaments via melt-spinning, which is arguably the most efficient process to produce fibers, and thus for the use in numerous textile and medical applications [8].

However, its rapid thermal degradation at temperatures just above the melting temperature, and the brittleness of native P3HB, pose technical and scientific challenges [9]. Other difficulties for industrial transfer include the raw polymer impurity, varying viscosity, broad molecular weight distribution, and complex crystallization behavior [10]. As these are inherent weaknesses of P3HB processed from natural resources, we proposed the use of additives to improve its melt-spinnability [1]. On one hand we proved that nucleating agents control and stabilize crystallization, on the other hand we showed how plasticizers damp viscosity fluctuations and enable a decrease of processing temperatures, resulting in reduced thermal degradation (loss of molecular weight). In addition to the incorporation of additives, we installed an intermediate godet in the draw-off unit to address the poor melt strength and the complex crystallization behavior of P3HB. By introducing the intermediate godet, we accomplished an oriented crystallization before complete solidification. Thus the extrudate could withstand the drawing forces induced by melt-spinning, and filaments dominated by longitudinally oriented lamellae rather than spherulitic structures were obtained. Secondary crystallization could be suppressed, which otherwise would lead to brittleness and poor mechanical performance.

In the equatorial 2Theta scan of the WAXD patterns, we observed a series of local maxima. We postulated a highly ordered amorphous phase, which is kinetically trapped between the aligned lamellae of the crystalline α-phase [1]. This is in contrast to the previous literature, where diffraction signals in this region are commonly described as one reflection, assigned to the so-called "β-form" of P3HB. In our model, the local maxima in the 2Theta scan correspond to preferred distances between polymer chains that are oriented nearly parallel to, but irregularly arranged along the fiber direction.

For the present study, P3HB fibers are subjected to various tensions and temperatures while tracing their structural response by *in-situ* WAXD.

EXPERIMENTAL APPROACH

Fiber melt-spinning of P3HB (Biomer P209, Biomer, Krailling, Germany) was carried out on Empa's custom-made pilot melt-spinning plant [10]. The analytical tools applied included wide angle X-ray diffraction (WAXD), recorded on a Bruker Nanostar U diffractometer (Bruker AXS, Karlsruhe, Germany) with $Cu_{K\alpha 1}$ radiation.

RESULTS AND DISCUSSION

From the WAXD pattern of fully drawn P3HB fibers under tension (Fig. 1) it can be seen that the intensities of the highly oriented crystalline reflections (020) and (110) decrease with increasing tension.
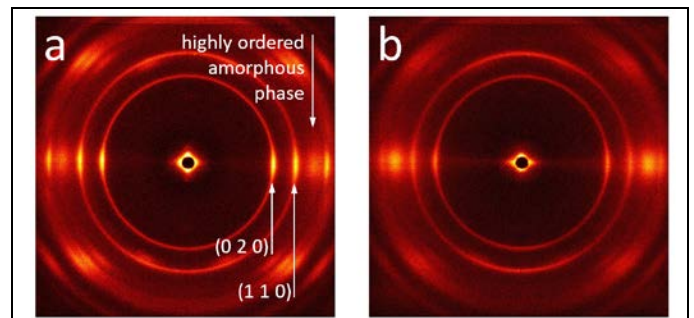

Figure 1: WAXD pattern of a P3HB fiber under tension. (a) 0 N (0 MPa, strain 0 %); (b) 1.05 N (165 MPa, strain 59 %).

Since the total intensity of the (020) reflection (including the reflections of the poorly oriented crystallites on the whole

ring) remains constant, this intensity drop can be explained by a reduction in highly oriented crystalline lamellae, i.e. by a smaller relative amount of highly oriented crystals. Simultaneously, the intensity of the reflections assigned to the highly ordered amorphous phase is considerably increasing.
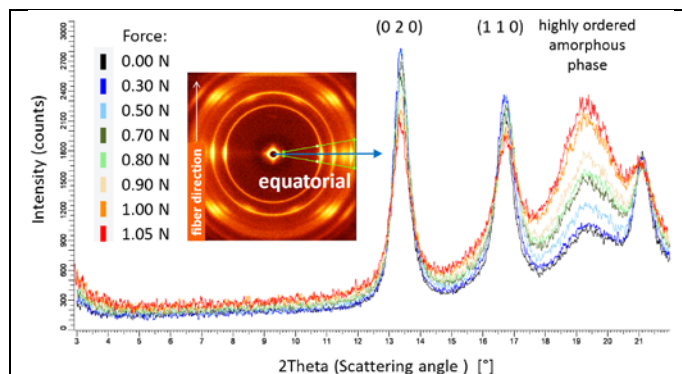

Figure 2: Structural response of the P3HB fiber in Fig. 1 to increasing tensional forces: 2Theta scan of the equatorial sector indicated by the green wedge cursor in the WAXD pattern.

2Theta scans of the equatorial sectors in WAXD patterns recorded under increasing tensional forces (Fig. 2) show this behavior in a more detailed way: enhanced orientation of the amorphous phase is realized to the disadvantage of the orientation of the crystalline phase. While the orientation of the amorphous polymer chains between the shish-kebab structures within the fiber is increasing, these chains can enforce a tilting of some of the crystalline lamellae, which in turn results in local bending of the shish. From the literature it is known that the shish have a certain flexibility [11].

The evaluation of WAXD patterns recorded under a cyclic change of load reveals a high degree of reversibility for these phenomena. Thus, the proposed bending of the shish-kebab structure is partly reversible, depending on the external load. The detected reversibility also supports our model of the highly ordered amorphous phase described in the introduction.

Annealing under tension remarkably increases the orientation of the crystalline phase: annealing at a temperature of 110 °C with a static load of 25 grams (equal to 25 % of the ultimate tensile strength of the fiber) increases the amount of highly oriented lamellae from 21 % to 50 %. At the same time, the ultimate tensile strength increases from 163 MPa to 189 MPa.

CONCLUSION
WAXD data of our P3HB fibers suggest that besides the oriented and unoriented crystalline lamellae dominating the fiber structure, a highly oriented amorphous phase is present in the fibers. Under load, the orientation of the amorphous phase is enhanced, to the disadvantage of the orientation in the crystalline phase. Cyclic drawing experiments with simultaneous WAXD support this model.

REFERENCES
1. Hufenus, R., et al. "Molecular orientation in melt-spun poly(3-hydroxybutyrate) fibers: effect of additives, drawing and stress-annealing." *European Polymer Journal*, 2015, 71: 12-26.
2. Hufenus, R., F.A. Reifler, M.P. Fernández-Ronco. "Molecular orientation in melt-spun P3HB fibers." *The Fiber Society Spring Conference Proceedings*, 2015, Shanghai, China.
3. Sudesh, K., H. Abe, Y. Doi. "Synthesis, structure and properties of polyhydroxyalkanoates: biological polyesters." *Progress in Polymer Science*, 2000, 25(10): 1503-55.
4. Pan, P., Y. Inoue. "Polymorphism and isomorphism in biodegradable polyesters" *Progress in Polymer Science*, 2009, 34(7): 605-40.
5. Bonartseva, G.A., et al. "Aerobic and anaerobic microbial degradation of poly-β-hydroxybutyrate produced by Azotobacter chroococcum." *Applied Biochemistry and Biotechnology-Part A Enzyme Engineering and Biotechnology*, 2003, 109(1-3): 285-301.
6. Zinn, M., R. Hany. "Tailored material properties of polyhydroxyalkanoates through biosynthesis and chemical modification." *Advanced Engineering Materials*, 2005, 7(5): 408-11.
7. Laycock, B., et al. "The chemomechanical properties of microbial polyhydroxyalkanoates." *Progress in Polymer Science*, 2013, 38(3-4): 536-83.
8. Ziabicki, A. *Fundamentals of Fibre Formation*. London: John Wiley & Sons, Ltd., 1976.
9. Barham, P.J., A. Keller. "Relationship between microstructure and mode of fracture in polyhydroxybutyrate." *Journal of Polymer Science. Part A-2, Polymer Physics*, 1986, 24(1): 69-77.
10. Hufenus, R., et al. "Biodegradable Bicomponent Fibers from Renewable Sources: Melt-Spinning of Poly(lactic acid) and Poly[(3-hydroxybutyrate)-co-(3-hydroxyvalerate)]." *Macromolecular Materials and Engineering*, 2012, 297(1): 75-84.
11. Keller, A., H.W.H. Kolnaar. "Flow-Induced Orientation and Structure Formation." *Materials Science and Technology*, 2006, Wiley-VCH Verlag GmbH & Co. KGaA.

Wettability of Carbon Fibers at the Microscale

Si Qiu[1,2], C.A. Fuentes[1], Dongxing Zhang[2], Aart Willem Van Vuure[1], <u>David Seveno</u>[1]

[1]Department of Materials Engineering, KU Leuven, Leuven, Belgium; [2]School of Material Science and Engineering, Harbin Institute of Technology, Harbin, China

david.seveno@mtm.kuleuven.be

INTRODUCTION

Carbon Fiber-reinforced polymer (CFRP) composites have received considerable attention due to outstanding characteristics and wide applications in many fields such as aircraft and marine industries [1]. The strength of the adhesion between the reinforcing carbon fibers and the matrix plays a decisive role in determining the final mechanical properties of the composite material [2]. The wettability of carbon fibers exercises great influence on the interfacial adhesion and can be obtained by measuring the contact angles between liquids and fibers. The Wilhelmy balance method is a frequently used method which consists of measuring the capillary force $F_{Capillary}$ exerted by a liquid on a solid substrate when it is partially immersed at a constant velocity [3]. If the diameter of the fiber d and the liquid/vapor surface tension γ_{LV} are known then the dynamic contact angle θ can be calculated according to the Wilhelmy equation, $F_{Capillary} = \pi d \gamma_{LV} cos\theta$. However, testing the wettability of single carbon fibers with micron scale diameters is highly challenging as slight variations of the fiber diameter and the measured capillary forces can greatly influence the contact angles. However, it is a common practice to assume that the tested carbon fibers share nearly the same diameter [4], despite Scanning Electron Microscopy (SEM) showed that they have a given variability. Moreover, much attention has been paid to the dynamic advancing contact angle at extremely low velocity, assuming it has a value close to or even equal to the value of the static advancing contact angle [5] while advancing contact angle measurements at contact line velocities above 10 mm/min have never been studied. This lack of clarity leads to controversial static contact angle values ranging from 62º to 79º for desized T300 carbon fibers and de-ionized water. In the present study, reliable and accurate water contact angles around single carbon fibers are reported. We propose a methodology which permits to measure dynamic contact angles taking into consideration both the intrinsic variability of the carbon fiber diameter and the signal to noise ratio level of the microbalance used in the frame of this study. The effectiveness of the method was demonstrated by fitting the experimental contact angle values by the Molecular-kinetic theory (MKT) [6] which permits to assess the static advancing contact angle as well as the dynamic wetting parameters of the carbon fiber.

MATERIALS AND METHODS

FT300-3000-40A polyacrylonitrile-based carbon fibers manufactured by Toray Carbon Fibers Europe S.A. were used in this study. To obtain clean surfaces, the fibers were washed in ethyl alcohol and dried at 80ºC for 1h. This gentle cleaning procedure removes dust and grease without altering the sizing that is typically present on commercial carbon fiber. N-Hexane (Acros) and deionized water (Millipore Direct Q-3 UV) with respectively a liquid/vapor surface tension of 18.4 and 72.8 mN/m were used as probe liquids. Advancing and receding contact angles were measured with a high-precision Force Tensiometer – Krüss K100SF [7]. During the experiments, a single carbon fiber was attached to the sample holder and set perpendicular to the surface of the liquid. The fiber is then dipped in and later withdrawn from the liquid bath with testing velocities ranging from 0.5mm/min to 500mm/min.

N-hexane is supposed to perfectly wet the fibers, i.e. $\theta = 0º$, leading to a simplified version of the Wilhelmy equation which permits to obtain the fiber diameter. To assess the reliability of the methodology, 20 fibers were randomly extracted from a tow and measured twice. Once accurate and reliable fiber diameters were obtained, contact angle measurements with deionized water were implemented. Every fiber was dipped in and withdrawn from the liquid vessel repeatedly for 3 times at a constant velocity to measure respectively a series of dynamic advancing and receding contact angles. 10 fibers with known perimeters were tested per velocity for a total of 120 measurements. For every measurement, fibers were cleaned and fresh water was used to avoid contamination. After the contact angle measurements, every tested fiber was observed in a FEI XL30 FEG scanning electron microscope to double check the values of the diameters obtained with the tensiometer. The fibers were dried to remove the water on the surface and then attached by double-sided adhesive tape on the SEM stage. The immersed sections were imaged at a magnification of 5000x under a voltage of 12kV. Three pictures were taken over the length of the immersed sections of the carbon fibers and diameters were measured at 3 different locations for each picture. The MKT was finally used to model the contact line motion during wetting. It considers a dissipation process occurring close to the contact line where liquid atoms jump on the solid surface from one adsorption site to another. In its general form, the MKT predicts the following relationship between the equilibrium and dynamic wetting properties:

$$V = 2\kappa^0 \lambda sinh\left[\frac{\gamma_{LV}\lambda^2}{2k_BT}(cos\theta^0 - cos\theta)\right] \qquad (1)$$

with V the contact line velocity, θ^0 the static contact angle, λ the atomic jump length, κ^0 the atomic jump frequency, k_B the Boltzmann's constant, and T the temperature. The purpose is here to check if the experimental dynamic wetting data can be modelled by such standard approach [8]. If successful, this fitting procedure would support the experimental methodology and give access to θ^0. However, it will neither validate the measurements nor the theory as λ and κ^0 are molecular parameters which cannot be measured experimentally. Typical values of around one nanometer for λ and one megahertz for κ^0 are expected [8].

RESULTS AND DISCUSSION

The wetted diameters of 20 carbon fibers obtained from both the tensiometer and SEM are shown in Figure 1. There is a very good agreement between the average results obtained from the SEM method (6.83 ± 0.44 μm) and the tensiometer method (7.13 ± 0.44 μm) which validates the proposed methodology. Most diameters obtained from the SEM show however slightly lower values than those obtained with the tensiometer. A possible explanation for this variation is that the fibers may not be strictly vertical when touching the water/air interface, leading to a higher apparent wetted perimeter. Hereafter, the diameters obtained from the SEM technique are selected to calculate the contact angles with water.
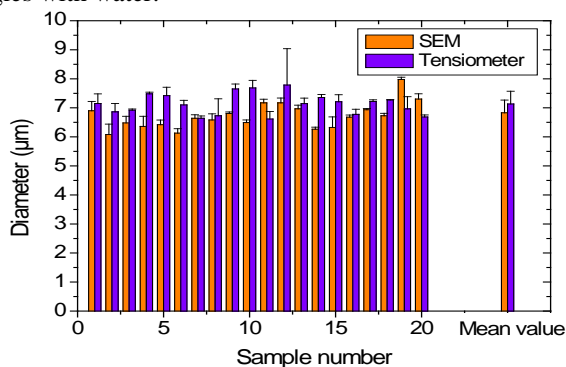
Figure 1: Comparison of carbon fiber diameters obtained from the wetting experiments and by SEM.

To have a better overview of the wettability of a single fiber, the distribution of contact angles of every tested fiber is calculated thanks to the measurement of the precise wetted perimeter. Dynamic advancing contact angles show finite values, the receding ones have basically values fluctuating between 20º and 0º regardless of the contact line velocity. If this methodology provides highly accurate force and fiber diameter measurements, it is anyhow insufficiently accurate to derive reliable small contact angles especially sensitive to tiny force fluctuations. For wetting velocities ranging between 0.5mm/min and 500mm/min, dynamic advancing contact angles (between 10000 at the lower velocities and 300 at the higher velocities) were then calculated from the force measurements. The distributions of these contact angles are narrow enough to allow for the calculation of an average and standard deviation values as shown in Figure 2. The contact angles vary from 65.7±10.0º to 92.0±4.8º with increasing wetting velocity. The modelling of the contact angle dynamics was carried out with the G-Dyna software [9] so that the quality of the fit and the distributions of the free parameters can be obtained and their consistency evaluated. Figure 2 also shows that the experimental data can be modelled by the MKT quite well with fitted values of 0.15 ± 0.1 Mhz, 1.0 ± 0.1 nm, and 65.8 ± 2.9° for respectively κ^0, λ, and θ^0. This static contact angle is a key parameter to determine the surface energy components of the fiber and will be further used in forthcoming studies. The model also indicates that the dynamic contact angles measured at low velocities, from 0.5mm/min to 20mm/min, are not dissimilar to the equilibrium value. That is to say, dynamic contact angles measured within this range of velocity can give a reliable approximation of θ^0.
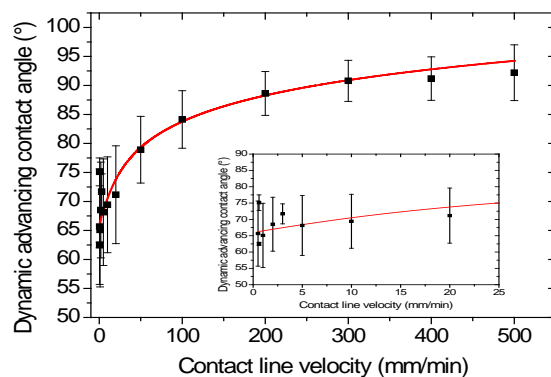

Figure 2: Dynamic advancing contact angle versus contact line velocity fitted by the MKT (red full line).

CONCLUSIONS

A new method was developed to measure the dynamic contact angles of a single carbon fiber at low and high velocities (0.5mm/min-500mm/min), taking into consideration both the intrinsic variability of the carbon fiber diameter and the signal to noise ratio level of the tensiometer. SEM analysis confirmed the accuracy of the wetted length measurement by the tensiometer method. The capillary forces ensure the correct measurement of the calculated contact angles. MKT modelling has been used to closely fit the experimental data, demonstrating the effectiveness of the new method and also providing the value of the static contact angle for carbon fiber in deionized water (65.8±2.9º). Contact angle values measured at different velocities suggest that dynamic contact angles measured below 20mm/min can be used to calculate the surface energy components of the carbon fibers investigated in this research. In summary, dynamic contact angle tests in water were conducted in a more reliable and accurate way than in previous studies and this will improve the prospect of employing tensiometry to better understand the wetting behavior of carbon fibers.

ACKNOWLEDGMENT

REFERENCES

[1] Suzuki, M. *Carbon*, 1994, 32: 577-86.
[2] Karger-Kocsis, J., Mahmood, H., Pegoretti, A. *Progress in Materials Science*, 2015, 73: 1-43.
[3] Ma, L., Meng, L., Fan, D., He, J., Yu, J., Qi, M., Chen, Z., Huang, Y. *Applied Surface Science*, 2014, 296: 61-68.
[4] Li, M., Gu, Y., Liu, Y., Li, Y., Zhang, Z. *Carbon,* 2013, 52: 109-21.
[5] Wu, Z., Meng, L., Liu, L., Jiang, Z., Xing, L., Jiang, D., Huang, Y. *Journal of Adhesion Science and Technology*, 2014, 28: 444-53.
[6] Blake, T., Haynes, J. *Journal of Colloid and Interface Science*, 1969, 30: 421-23.
[7] Fuentes, C., Tran, L.Q.N., Dupont-Gillain, C., Van Vuure, A., Verpoest, I. *Colloids and Surfaces A: Physicochemical and Engineering Aspects*, 2011, 380: 89-99.
[8] Blake, T.D. "Dynamic Contact Angles and Wetting Kinetics" in *Wettability*, J.C. Berg, Ed., New York: Marcel Dekker, 1993, 49: 251-309.
[9] Seveno, D., Vaillant, A., Rioboo, R., Adao, H., Conti, J., De Coninck, J. *Langmuir*, 2009, 25: 13034-44.

Hydrodynamics of Fiber Drawing from Polymer Solutions

M. Sivan[1], P. Mikes[1], J Chaloupek[1], E. Kostakova[1], M. Tunak[1], K. Strnadova[1], Michal Rezanka[2], D. Lukas[1,2]

[1]Department of Nonwovens and Nanofibrous Materials, Technical University of Liberec

[2]Institute for Nanomaterials, Advanced Technologies and Innovation, Technical University of Liberec,

Liberec, Czech Republic

david.lukas@tul.cz

ABSTRACT

A hypothesis based on hydrodynamic analysis is proposed to predict conditions for creation of relative stable liquid threads from polymeric solutions by drawing. Analytical estimations are performed, predicting the fastest growing rate and the assigned wavelength of the Plateau-Rayleigh instability developing on the viscose thread. We show comparing analytical results with experimental data that the coexistence and creation of the thread from a sessile solution droplet has a character of an immediate liquid-solid transition, where the solid has a form of a gel. Model predictions show a good agreement to our drawing experiments on PVA solution as well as to the data available in the literature.

INTRODUCTION

Drawing a single fiber is a fascinating technique to produce polymeric (nano) fibers in diameter range from tens of nanometers [1] to hundreds of micrometers. The process itself is rather simple and versatile. A drawing lab-device is generally based on a micromanipulator that moves with a needle, micropipette or AFM tip, i.e., with a drawing element in general. When the polymeric solution has a suitable concentration, the drawing element is withdrawn from the polymer solution droplet and is moved away rapidly. The drawing element pulls a fiber that attained in a length from one millimeter up to tens of centimeters. The pulled fiber is deposited by touching the surface with the extremity of the drawing element. This method allows the deposition of fibers in predetermined patterns, i.g., highly oriented patterns.

The very promising field of the utilization of such highly oriented fibers made by drawing is tissue engineering. Drawing can be used for scaffold fabrication which will serve for replacement of tissues with oriented structure, e.g. smooth muscles or nerves. As it was published previously, the in vitro tests show that highly oriented fibers are preferred by neuronal cells compared to the randomly organized fibers and the cells proliferate better [2]. In these experiments the commonly used method of oriented scaffold fabrication is electrospinning [2, 3]. Even though electrospinning is much more productive than drawing, drawing provides single fibers which can be handled separately and placed in any direction thus we are able to prepare defined scaffold structure. Therefore, drawing is a very promising method. For each specific application, a narrow range of fiber diameters is required to optimize their performance. That is why, fiber diameter control based on a detailed knowledge of the drawing process is essential.

HYDRODYNAMICS OF FIBER DRAWING

One of the analytical models of drawing an individual thread is the Chandrasekhar stability analysis of viscous jets and cylinders [4]. Using the poloidal-toroidal decomposition he found an analytical relationship between the growing rate σ and the wave number k in an implicit form.

The dependence of the dimensionless growth parameter $\sigma R^2 / \nu$ on the dimensionless wave number $x = kR$ is plotted in Figure 1. The most bottom curve corresponds to the smallest value of the parameter $J = \gamma\, R / (\rho \nu^2)$.
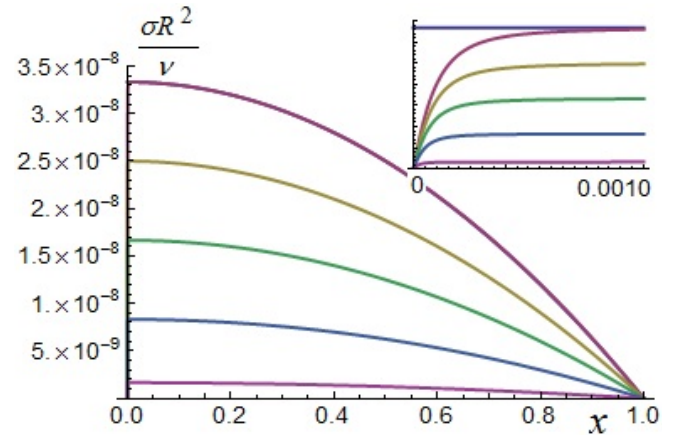

Fig. 1: The dependence of the dimensionless growth parameter on the dimensionless wavenumber. The curves are plotted sequentially for the following values of the parameter J = 1·10^-5, 5·10^-5, 10·10^-5, 15·10^-5 and 20·10^-5. The smallest value of J corresponds to the most bottom curve. The inserted figure shows details of the curves in the vicinity of the x axes origin.

Numerical coordinates, ie. $\left(x, \sigma R^2 / \nu\right)$, of extremal values of these relationships on the interval $x \in (0,1)$ are obtained using Wolfram Mathematica and the computed numerical values are introduced in Tab.1.

Table 1: Values of the parameter J and assigned extremal values of the dimensionless growth parameter and the wave number x. The kinematic viscosity ν is calculated from J values. The characteristic hydrodynamic time $\tau = 1/\sigma$ is determined from the dimensionless growth parameter. The liquid jet radius R = 75 [μm] is taken from experiments.

J	$\sigma R^2 / \nu$	$x = kR$	ν [$m^2 s^{-1}$]	λ [m]	$\tau = 1/\sigma$ [s]
10^{-5}	$1.6 \cdot 10^{-6}$	0.0272	0.0181	0.017	0.18627
10^{-6}	$1.6 \cdot 10^{-7}$	0.0153	0.0573	0.030	0.58845
10^{-7}	$1.6 \cdot 10^{-8}$	0.0086	0.1814	0.054	1.86025
10^{-8}	$1.6 \cdot 10^{-9}$	0.0048	0.5738	0.097	5.88204
10^{-9}	$1.6 \cdot 10^{-10}$	0.0027	1.8145	0.172	18.6001
10^{-10}	$1.6 \cdot 10^{-10}$	0.0015	5.7380	0.306	58.8179
$1.3 \cdot 10^{-2}$	$2.0 \cdot 10^{-3}$	0.1600	0.0005	0.002	0.0054

The numerical evaluation of the wavelength and corresponding relaxation time is carried out for the original 15%wt PVA aqueous solution, from which the liquid jet is drawn. Poly(vinyl alcohol) PVA, brand Sloviol was purchased from Novacke chemicke zavody, Novaky, Slovakia, with predominant molecular weight 60 000 g/mol. Fresh 16% w/w solutions were prepared by dissolving the Poly-vinyl-alcohol in distilled water. This solution has the following physico-chemical parameters: the specific gravity $\rho = 1.0091 \cdot 10^3$ kg/m^3, kinematic viscosity $\nu = 5.0109 \cdot 10^{-4}$ m^2/s and a surface tension $\gamma = 44.3 \cdot 10^{-3}$ N/m.

It is well-known, that a pooling a fiber requires a material with an appropriate viscoelastic behavior to undergo strong deformations, while being cohesive enough to support the stresses developed during the drawing. On the other hand, the above mentioned data provide with the instability parameters indicated in the last row of Tab. 1 that admit the liquid thread existence for five microseconds only as opposed to the experimental experience. This contradiction leads to the conclusion that the treat has to have four orders higher viscosity than the polymeric solution from which it is created. Therefore, the drawn threat form the liquid polymeric droplet is some form of a solid phase.
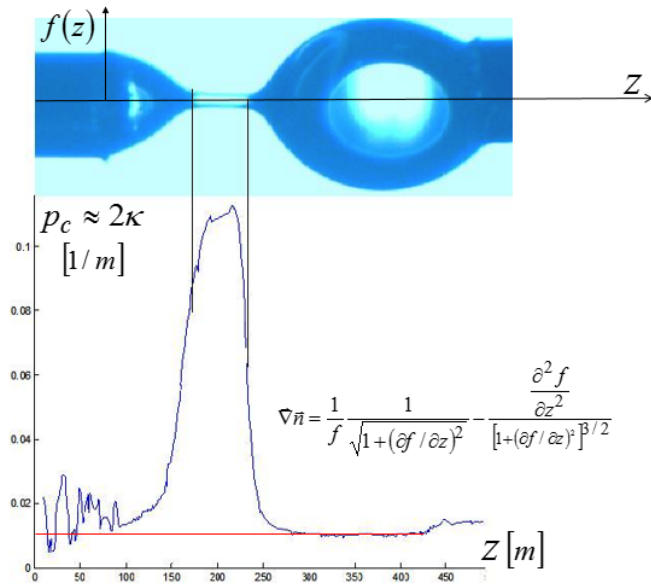

Fig. 2: An aqueous solution of PVA is deformed using a drawing element (left) into a relatively stable thread bridging two droplets.

The threat is longer than the Plateau limit, $\lambda > 2\pi r$. This exhibits an apparent violation of stability rules for liquid bodies for which the Laplace pressure is constant anywhere. A nonuniform distribution of the capillary pressure p_c inside the threat is obtained using the calculation of twice the mean curvature from the equation (1).

An experimental method aided by image analysis is used to study the Laplace pressure distribution inside a threat-droplet co-existence body. The distribution of the Laplace pressure p_c provides with a direct evidence of the liquid-solid transition between the liquid droplet and the tough gel, from which the thread has to be at least partly formed. For the Laplace pressure holds, $p_c = 2\gamma \vec{\nabla} \vec{n}$. Here the divergence

of the normal $\vec{\nabla} \vec{n}$ has the meaning of twice the mean curvature, $\vec{\nabla} \vec{n} = 2H$. For the axisymmetric surface takes force the following relation

$$\vec{\nabla} \vec{n} = \frac{1}{r\sqrt{1 + r'^2}} - \frac{r''}{\left(1 + r'^2\right)^{3/2}}, \qquad (1)$$

where the prime denotes the space derivative d/dz and $r(z)$ is a local radius of the liquid body.

An experimental setup is composed of two metallic capillaries connected to syringes that supply them with the solution. Each of the capillaries is of 1 mm of the outer radius. Capillaries are laterally adjusted in the grooves of the cylindrical pedestal that ensures their axial alignment. One of the capillaries is fixed in the space while the other is connected to the device providing it with a linear movement. This assembly is placed under a microscope that enables video-recording of the drawing process from the upper view.

The Figure 2 depicts the basic steps of PVA solution drawing. At first, droplets are created at the rims of both capillaries by pooling the polymer solution from them using syringes. Than the moveable capillary is shifted until both droplets come into contact. Next, the movable capillary is displaced horizontally with a constant velocity and stopped at a predetermined distance.

CONCLUSION
The discrepancy between hydrodynamic stability, physico-chemical parameters of the original polymeric solution from which the fiber is drawn and experimental measurement of capillary pressure distribution is a subject of our next research. Thermodynamic of the pulled material is probably the most critical item, since the drawing process is probably accompanied by a solidification caused by pronounced evaporation of the solvent that transforms a liquid spinning material into a solid one.

KEYWORDS
Drawing a fiber, hydrodynamic stability, Poly(vinyl alcohol), capillary pressure.

REFERENCES
[1] Ondarçuhu, T., Joachim, C. *Europhys. Lett.*, 1998, 42(2): 215-20.
[2] Corey, J.M., Lin, D.Y., Mycek, K.B., Chen, Q., Samuel, S., Feldman, E.L., Martin, D.C. "Aligned electrospun nanofibers specify the direction of dorsal root ganglia neurite growth." *J. Biomed. Mater. Res. A*, 2007, 83(3): 636-45,
[3] Lee, Y.-S., Livingston Arinzeh, T. "Electrospun Nanofibrous Materials for Neural Tissue Engineering." *Polymers*, 2011, 3: 413-26.
[4] S. Chandrasekhar. *Hydrodynamics and Hydromagnetic Stability*. New York: Dover Publications, 1982. 540.

Structure Development of Poly(ethylene terephthalate) Undrawn Filament Upon Cold Drawing Assisted with Infusion of Ethanol

Rina Khanum[1], Wataru Takarada[1], Arun Aneja[2], <u>Takeshi Kikutani</u>[1]
[1]Department of Organic and Polymeric Materials, Tokyo Institute of Technology
[2]Department of Engineering, East Carolina University (Formerly, Senior Research Associate, DuPont Company)
kikutani.t.aa@m.titech.ac.jp

INTRODUCTION

In this paper, "Infusion" is defined as the transport of solvent and solute into filament driven by the drawing process. This paper focuses on the infusion behavior and structural development of low oriented amorphous poly(ethylene terephthalate) (PET) filaments upon cold drawing in ethanol at room temperature. Along with the absorption of ethanol into filament, dyes dissolved in ethanol also could be transported into filament during the drawing process. Occurrence of crystallization at room temperature for the filaments drawn in ethanol was also confirmed. It should be noted that any structural change cannot be induced by merely immersing undrawn PET filament or PET filament drawn in air or water into ethanol. Accordingly, when drawing is performed in ethanol/dye solution, the color from dyes was observed only in the drawn segments when draw ratio was lower than the natural draw ratio. In any case, single step process of drawing and dyeing at room temperature accompanied by the fiber structure development with molecular orientation and crystallization can be achieved utilizing the "infusion" process.

EXPERIMENTAL

Low oriented (PET) filament with a fineness of 125 dtex was prepared through the melt spinning process of PET (IV= 0.68) at extrusion temperature of 290 $^{\circ}$C and take-up velocity of 0.4 km/min. Drawing of as-spun PET filament was performed in ethanol/water solution using a horizontal mini tensile tester. In some experiments, ethanol/water solution with 0.5 wt% of dye was used. For comparison, drawing was also performed in air and water. The drawn filaments of various draw ratios were observed under an optical microscope. The differential scanning calorimetry (DSC, Q100, Texas Instruments) measurements was performed at a constant heating rate of 10 K/min. Weight loss percentage of filaments with the increase of temperature was measured by thermogravimetric analysis (TGA, Thermo Plus TG-8120, Rigaku). Wide-angle X-ray diffraction (WAXD) patterns and small-angle X-ray scattering (SAXS) patterns were obtained using an X-ray diffractometer equipped with a CCD detector (Rigaku).

RESULTS AND DISCUSSION

Drawing of as-spun PET filament in pure ethanol

During the drawing process of as-spun PET filament, necking deformation was observed. SEM photographs of the necking regions for the drawing in air and pure ethanol are compared in Fig. 1. When the PET filament was drawn in

ethanol, multiple necking with extremely narrow transition regions from undrawn to drawn parts was observed.
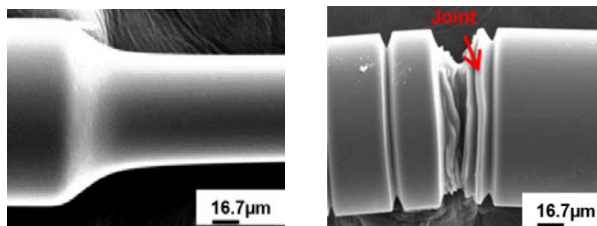

Fig. 1: Shape of drawing region for drawings in air and in ethanol.

Stress-strain behaviors measured during the drawing process of PET in air, water and ethanol are compared in Fig.2. Less prominent yielding behavior, lower yielding and neck-drawing stresses, and higher natural draw ratio are the features of the drawing in ethanol in comparison with the drawings in air and water.
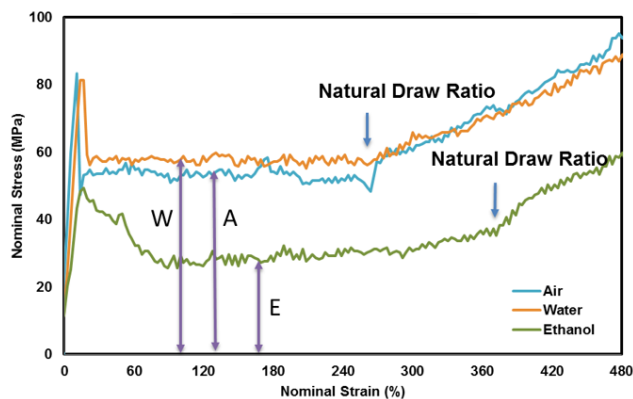

Fig. 2: Stress-strain behaviors measured during drawing of PET filament in air, water and ethanol.

WAXD and SAXS patterns of filaments drawn in air and ethanol are compared in Fig.3. Filaments drawn in ethanol exhibited distinct crystalline reflections of highly oriented triclinic crystals of PET, whereas only the concentration of amorphous halo on the equator was observed for the filament drawn in air. In additions, PET filaments drawn in ethanol exhibited distinct equatorial streak in the SAXS pattern. It should be noted that no crystallization was detected when the undrawn filament and the filament drawn in air or water were immersed in ethanol. In other words, crystallization proceeded only when undrawn filament was drawn in the ethanol.
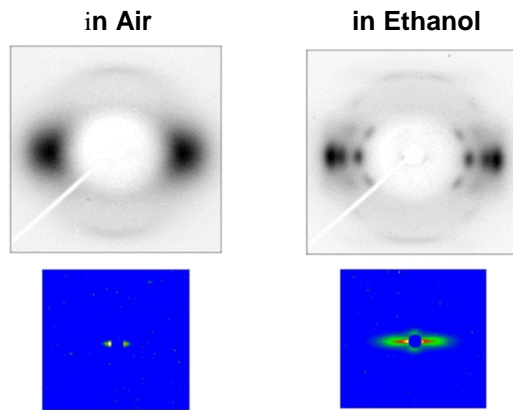
in Air **in Ethanol**

Fig. 3: WAXD and SAXS patterns of PET filament drawn in air and ethanol.

Effect of ethanol concentration on drawing behavior

Through the comparison of TGA and DSC analyses, it was confirmed that the endothermic peak area observed between 50 and 150 °C in the DSC thermogram is attributable to the amount of ethanol infused into PET filament upon cold drawing. Heat of cold crystallization was also detected in the DSC analysis. Variations of endothermic heat representing the vaporization of ethanol and exothermic heat representing the cold crystallization of PET are plotted against draw ratio for the filaments drawn in ethanol/water solutions of various ethanol concentrations as shown in Fig. 4. Amount of infused ethanol increased with the increases of draw ratio and ethanol concentration. Before reaching the natural draw ratio, amount of infused ethanol increased and heat of cold crystallization decreased linearly with the increase of draw ratio. These behaviors correspond to the increase of drawn region and reduction of undrawn region during the necking drawing. Sudden additional increase of the amount of infused ethanol was observed when draw ratio exceeded natural draw ratio. This result corresponds to the additional infusion of ethanol upon starting of the further stretching of the drawn region.
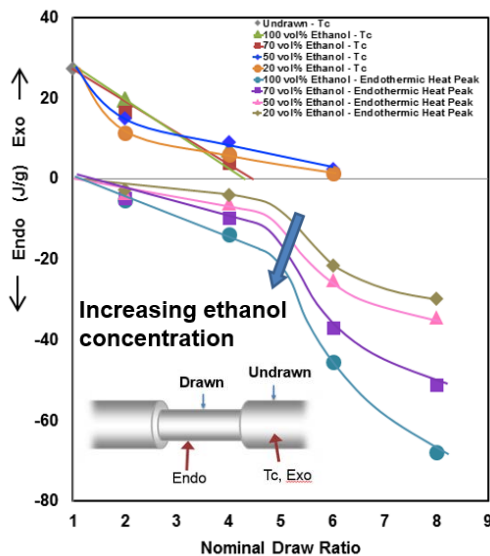

Fig. 4: Variations of exothermic heat of cold crystallization and endothermic heat of the vaporization of ethanol with the increase of draw ratio for drawing of as-spun PET in ethanol/water solutions of various ethanol concentrations.

Photographs of fibers drawn in ethanol/water solution of various ethanol concentrations containing 0.5 wt% of disperse dye are shown in Fig.5. Only the drawn part of filaments were colored with dye. Color concentration reduced with the reduction of ethanol concentration.
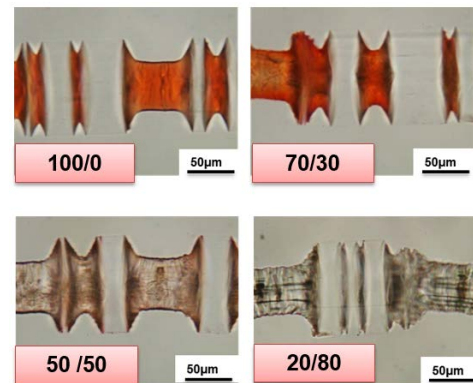

Fig. 5: Photomicrographs of PET filaments drawn to draw ratio 3 in ethanol/water solutions of various ethanol concentrations containing 0.5 wt% of disperse dye.

Effect of drawing speed on drawing behavior

During drawing of PET filament in ethanol, multiple neck appears. Number of necking decreases with the increase of draw ratio through the consumption of undrawn part and merge of two drawn regions. Number of necking observed at the draw ratio 2 during drawing of PET filament in pure ethanol are plotted against drawing speed as shown in Fig. 6. Number of necking increased steeply with the increase of drawing speed at low drawing speed region. Propagation speed of necking was estimated from the drawing speed, necking draw ratio and number of necking. The result is also shown in Fig.6, Neck propagation speed increased almost linearly with the increase of draw ratio. It was also found that the amount of infusion of ethanol decreased with the increase of drawing speed. This result suggests that the speed of infusion of ethanol into filament is comparable with the propagation speed of necking. Even though amount of ethanol was decreased with the increase of drawing speed, crystallization and dyeing of PET filament were still possible at high drawing speeds.
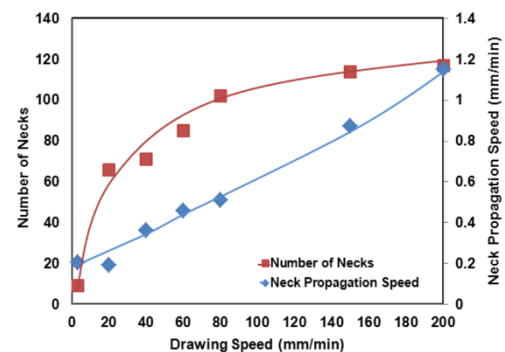

Fig. 6: Number of necking and necking propagation speed at draw ratio 2 for drawing of PET in pure ethanol at various drawing speeds.

REFERENCES

R. Khanum. et al. *Polymer*, 2015, 59: 26-34.
R. Khanum, et al. *Polymer*, 2015, 70: 19-29.
R. Khanum, et al. *Sen'i Gakkaishi*, 2015, 71: 273-283.

Yarn Processes, Structures, and Properties

Automatic Online Controlling Linear Density and Blend Ratio of Rotor Spun Yarn Spinning Process

Rui-Hua Yang, Ming-Rui Guo, Yuan Xue, Wei-Dong Gao
Key Laboratory of Science & Technology for Eco-Textiles, Education Ministry, Jiangnan University,
Wuxi, Jiangsu Province, China
yangrh@jiangnan.edu.cn

INTRODUCTION

Rotor spinning is well known for its high production rate and good evenness of the yarn, which is the only real alternative to ring spinning for producing coarser yarn counts[1]. The basic principle of rotor spun yarn spinning process involves the separation of the sliver fed into individual fibers, which are gathered on the collection groove of the rotating rotor, inserting twist into the fibers. The yarn produced is then taken up onto a cross wound package, eliminating the need for a separate winding process, as in ring spinning.

Since 1965, the first rotor spinning machine showed in International Textile Machinery Exhibition of Brno, there are many new technical advances:
  *Cheap raw materials is available including noils, linters, slips, waste cotton,
  *There is less waste,
  *High speed of twist insertion and delivery speed up to 300 m/min,
  *High speed of rotor speed up to 200000 rpm,
  *High speed of opening roller up to 10000 rpm,
  *Wide fineness of yarn 3.5-60S,
  *High drawing of sliver up to 400.
  In the paper, we mainly discuss some important works for the development of rotor spinning machine.

THREE FEEDING ROLLERRS

Three separate fiber feed system was modified on rotor spinning machine, by which three sliver can be feed separately and simultaneously as shown by Figure 1. It is implemented by a creative mechanical structure design of feed roller which is combined of three separate feed rollers side by side and controlled by servo motors with PLC. Using this new method, three different slivers can be fed and controlled by each feed roller individually (the feeding speeds can be the same or different and can be changed on line) [2]. This yarn is named as Digital yarn because yarn structure parameters including linear density and blend ratio can be controlled and realized by asynchronous drafted slivers. Besides blended yarns, colorful yarns can be produced by changing the proportion of fed colorful fiber strands on line. For example, fiber strands can be three basic colors: Red, Yellow, and Blue. Sample yarns are showed by Figure 2. The results demonstrate the advantages and development potentials of Digital yarns in spinning flexibility and products variety.
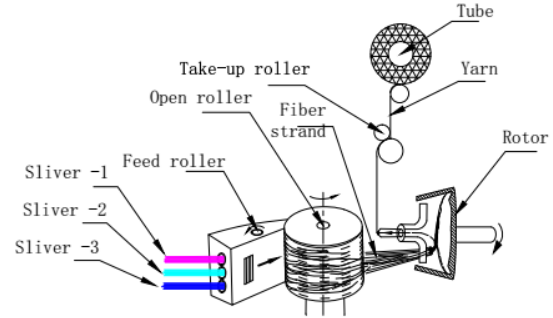

Figure 1: Schematic diagram of rotor-spun yarns spinning process with three feeding rollers.
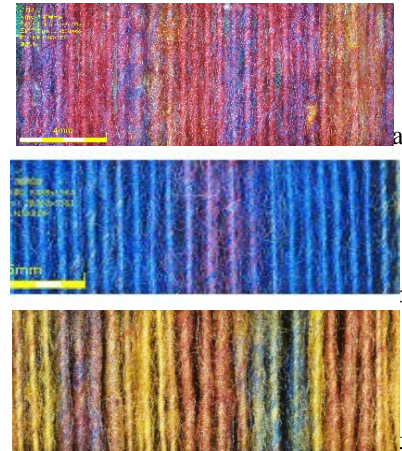

Figure 2: Colorful yarns produced by rotor-spun yarns spinning process with three feeding roller by three roving colored by three primary colors, respectively (a-R/Y/B=7/1/2, b- R/Y/B=1/1/8, c-R/Y/B=2/7/1).

TROIS OPENING ROLLERS

Increasing number of opening rollers from one to three may improve fiber orientation, blending in the final yarn and improve production by gradual speed of the opening roller. In the new spinning box, one opening roller is upgraded to three, which are speeded up separately[3], as demonstrated in Figure 3. Slivers were opened, weeding, combed into single fibers after they went through three opening roller. As the speed of three opening rollers keep increasing incrementally, for example, the first one 5000 rpm, the second one 7500 rpm, the third one 11250, the new system can work more efficient than one opening roller. The differences are illustrated in Table 1 by comparing Autocoro 360 with the new modified rotor machine with three opening rollers, producing 28tex cotton yarn. The output of the new machine can be improved by 6.27/4.18=1.5 times.
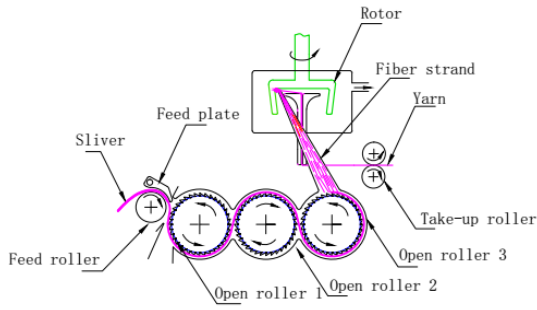
Figure 3: Schematic diagram of rotor-spun yarns spinning process with three opening roller.

Table 1: Illustration of spin boxes with one opening roller and with three.

Type	Autocoro360	Rotor spinning with three opening rollers	
Speed of opening roller (rpm)	7500	First roller	5000
		Second roller	7500
		Third roller	11250
Fiber numbers on surface of opening roller	15	First roller	33.8
		Second roller	22.5
		Third roller	15
Speed of sliver(m/min)	0.929	1.393	
Taking-up speed of yarn(m/min)	149.3	223.9	
Rotor speed(rpm)	107197	160760	
Output of yarn（g/min）	4.18	6.27	

Besides one feed plate, there are also two and three feed plates with three opening rollers as shown in Figure 4and 5separately[4], which can produce blend yarn and fancy yarn easily with higher output and better yarn quality. The slivers can be the same or different types or colors of fibers. Their feeding speed can be the same or different, which are controlled by electrical machine separately. The production can be Mix variety.
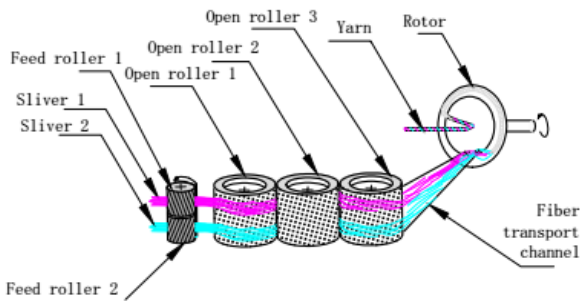

Figure 4: Schematic diagram of rotor-spun yarns spinning process with three opening rollers and two feeding rollers.
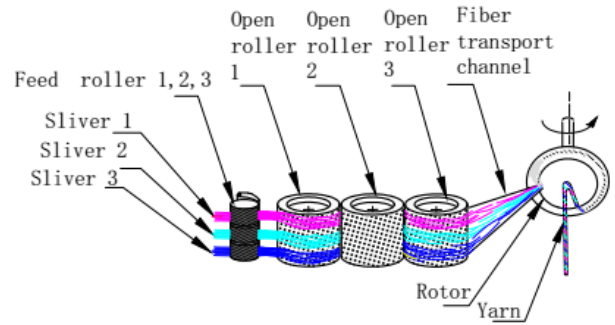

Figure 5: Schematic diagram of rotor-spun yarns spinning process with three opening rollers and three feeding rollers.

CONCLUSION
New progresses of rotor spinning machine are introduced. For traditional rotor spinning, there is one feed roller. While then there are two kinds of two feed rollers, one kind for two sliver separately, another kind for sliver and filament separately. Also there are three feed rollers. And the newest rotor spinning machines are designed with three opening roller and one feed roller or two or three, which can achieve a higher output and produce blended yarn, fancy yarn and colored yarn more efficiently because yarn structure parameters including linear density and blend ratio can be controlled and realized by asynchronous drafted slivers.

KEYWORDS
Rotor spinning, Devices, Feed roller, Asynchronous drafting; Structure parameters of yarn.

REFERENCES
[1] Xue, Y., Gao, W.D., Yang, R.H., Guo, M.R. "Automatic online controlling linear density and blend ratio of rotor spun yarn by three orderly arranged opening rollers and three independent drafting systems." *China*, CN201510518853.9, November 18, 2015, and PCT/CN2015/000737.

[2] Yang, R.H., Wang, S.Y. "Effects of spinning conditions on convergent point in rotor-spun composite-yarn spinning process." *Journal of The Textile Institute*, 2009, 100(7): 654.

[3] Xue, Y., Gao, W.D., Yang, R.H., Guo, M.R. "Automatic online controlling linear density and blend ratio of rotor spun yarn by three orderly arranged opening rollers." *China*, 201510520954.X, November 18, 2015, and PCT/CN2015/000734.

[4] Xue, Y., Gao W.D., Yang, R.H., Guo, M.R. "Automatic online controlling linear density and blend ratio of rotor spun yarn by three orderly arranged opening rollers and two independent drafting systems." *China*, CN201510516137.7, November 18, 2015, and PCT/CN2015/000738.

High-temperature Polymer Yarns for Through Thickness Reinforcement of Carbon Fibre Laminates

Cormac McGarrigle, Thomas Dooher, Dorian Dixon, Edward Archer, Alistair McIlhagger
Engineering Research Institute, School of Engineering, Ulster University, Jordanstown
mcgarrigle-c2@email.ulster.ac.uk

OBJECTIVE

To produce and characterize high temperature polymer yarns which will then be used to stitch carbon fibre laminates together to provide through thickness reinforcement and improve delamination resistance. To the best of the authors knowledge that these composites have not been previously investigated for this purpose.

INTRODUCTION

Fibre-reinforced composite laminates support a significant improvement in overall material weight when compared with metals and other materials traditionally used in engineering. This makes them highly desirable in both the aerospace and the automotive industries in which a low material weight is essential to reduce fuel consumption.[1]

Carbon fibre composites typically consist of thin carbon fibre layered to give the desired thickness and properties. when subjected to interlaminar stress these multi-layered, or laminate, composites are highly susceptible to delamination. This is a loss of local stiffness in a composite material which is subjected to either static loading or cyclic loading.[2]

Through thickness reinforcement is a method of reducing delamination in a laminate composite by increasing its interlaminar properties. This is performed by means of a third directional reinforcement of through thickness fibres in the z-direction. Stitching holds great promise in this area.[3]

Currently commercially available polymers, such as polyparaphenylene terephthalamide, are used as through thikcness fibre reinforcement despite not meeting all of the desired criteria for a reinforcement material, for example retaining their properties during the knotting process of stitching.

Producing reinforcement yarns with tailored properties could be used for more effective and target reinforcement of carbon fibre laminate.

MATERIALS

Polysulfone, polyethersulfone, polyphenylsulfone and polyetherehterketone were sourced in powder form. Tenax® HTA 40 67 tex spread yarn carbon fibre was used a reinforcement material.

METHOD

In a precautionary step to avoid moisture and reduce any variability between the production of the various yarns all of the polymers used were heated in an oven for 4 hours at 180^{0}C. The dehumidified polymers were then stored in airtight containers until required for the extrusion process.

Yarns were then manufactured using a 16mm twin-screw extruder with an L:D ratio of 25:1 (ThermoScientific, Haake Rheomex OS PTW16). The cutting blade from the pelletizer on the extruder was removed, leaving behind only a wheel capable of drawing the polymer out of the extruder. This allowed the yarn to be drawn at a constant rate.

Each polymer powder listed in table one were removed from their container and individually poured into the hopper to be extruded. The temperature and speed of the screws along with the draw off speed of the pelletizer as follows:

Polymer Name	Screw Temperature	Screw Speed	Pelletizer Draw-off Speed
Polysulfone	360°C	7	7
Polysulfone & Carbon Fibre	380°C	7	4
Polyethersulfone	360°C	7	7
Polyethersulfone & Carbon Fibre	360°C	7	4
Polyphenylsulfone	385°C	7	7
Polyphenylsulfone & Carbon Fibre	385°C	7	4
Polyetheretherketone	385°C	7	7
Polyetheretherketone & Carbon Fibre	385°C	7	4

Table I: Extruder Set Up

The polymers were individually fed into the extruder and fed out through a single hole die. They were then hot drawn by being fed from the extruder into the pelletizer wheel, where it was then hand wound onto a bobbin.

For the polymers containing carbon fibre reinforcement the same process was employed, except on this occasion a roll of carbon fibre was placed on a spindle above the extruder and fed into the hopper, along with the dried polymer. The extruder screws have two compounding regions which break the carbon fibre up and allow it to mix with the polymer.

RESULTS

Figure 1 shows an SEM image of PEEK containing carbon fibre. Variation in the diameter of the fibre is evident from the measurements taken on the SEM. This could be attributed to a number of things: the carbon fibre clumping in sections in the polymer, leading to necking. The possibility exists of the carbon fibre affecting the melt temperature of the polymer resulting in the polymer carbon fibre mix not getting fully melted and exiting the extruder before it has had the opportunity to complete the entire extrusion process. Had the mix not been fully extruded irregular hot drawing of the polymer mix would occur, thus affecting the fibre diameter.[4]
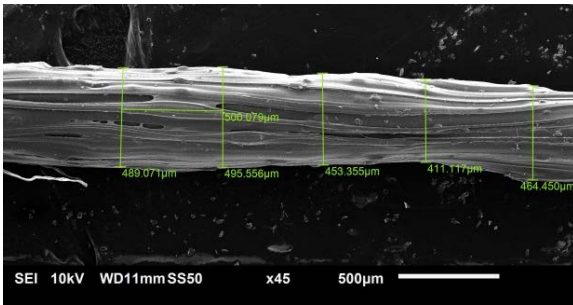
Figure 1: SEM of Extruded PEEK & CF

However, the polymer yarns, without carbon fibre presented a much more consistent diameter, as can be seen in Figure 2.
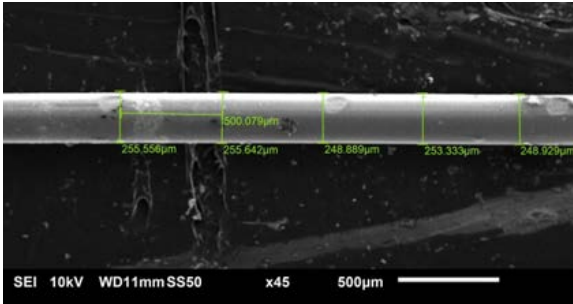

Figure 2: SEM of Extruded PEEK

Micrograph images of all of the polymers display a striate surface. This could be attributed to machining marks within the die, generated during its manufacture, affecting the surface of the polymer. Wight et al. observed similar striated surfaces on their extruded polymers.[2]

PPSU fibres produced the most consistent diameter fibres, with a standard deviation between diameter results at 8.2, thus a Cpk anaylsis was performed upon the PPSU fibre diameters, as seen in Figure 3.
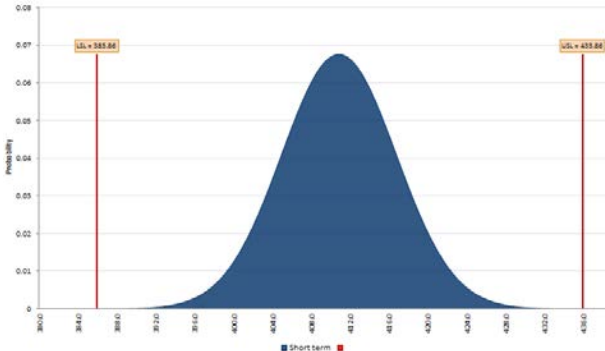

Figure 3: Cpk Analysis

The Cpk analysis, with the upper and lower limits being 25micrometers either side of the average diameter, of PPSU gave a figure of 1.4, surpassing the usually desired 1.3. A Cpk analysis was also performed on the PPSU yarns which contained carbon fibre, giving a poor 0.11 Cpk value, deeming the process unsuitable for the production of a fibre with a consistent diameter. Cpk analysis was performed on all of the polymer yarns.

Further microscope analysis revealed the arrangement and distribution of carbon fibre within the polymers was random, as can be seen in Figure 4. This yielded a polymer yarn with an uneven distribution of carbon fibres within the yarn. Both this and the possibility that the carbon fibre affected the melt temperature of the polymer composite mix potentially resulted in the polymer carbon fibre mix not getting fully melted and exiting the extruder before the material has had the opportunity to complete the entire extrusion process.
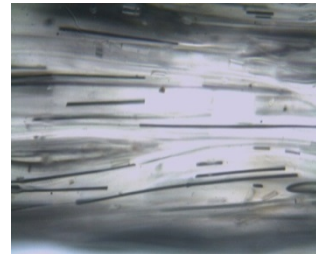

Figure 4: Micrograph of PPSU and CF

This would account for the variation in diameter of the fibres containing carbon fibre, but cannot be concluded without further testing.

In some cases these randomly aligned fibres even protruded through the polymer.

CONCLUSION

The polymer only yarns yielded fairly consistent diameters, with a standard deviation of the PPSU diameters being as low as 8.2 over 25 measurement samples.

Variation in the diameter of the fibres containing carbon fibre is evident from the diameter measurements taken on the SEM. This and the lower draw off speed can be attributed to the cause of the uneven distribution of carbon fibres within the polymer.

REFERENCES
[1] Aktas, A., Potluri, P., Porat, I. "Multi-needle stitched composites for improved damage tolerance." *17th Int Commitee Compos.*, 2009.
[2] Jain, L.K., Dransfield, K., Mai, Y-W. "Effect of Reinforcing Tabs on the Mode I Delamination Toughness of Stitched CFRPs." *J Compos Mater.*, 1998, 32(10): 2016-41.
[4] Dell'Anno, G., Cartié, D.D., Partridge, I.K., Rezai, A. "Exploring mechanical property balance in tufted carbon fabric/epoxy composites. *Compos Part A Appl Sci Manuf*, 2007, 38(11): 2366-73.
[4] Wright, D.D., Lautenschlager, E.P., Gilbert, J.L. "The effect of processing conditions on the properties of poly(methyl methacrylate) fibers." *J Biomed Mater Res*, 2002, 63(2): 152-60.

Dyeing, Finishing, and Wettability

Influence of UV Protecting Finish and Color on Spectral and Thermophysiological Properties of Sports Textiles

Bianca-Michaela Woelfling, Martin Harnisch, Edith Classen
Hohenstein Institute for Textile Innovation gGmbH, Boennigheim, Germany
b.woelfling@hohenstein.de

INTRODUCTION

In summer clothing worn during endurance sports, like biking or running, needs to offer sun protective properties and good sweat management. In this manner sun protection is related to shortwave ultraviolet radiation (UV) and long wave infrared radiation (IR). UV rays damage human skin, harm function of sweat glands and therefore decrease sportsmen's performance[1]. One long term effect of UV light is skin cancer[2], wherefore this risk is higher for endurance sportsmen[2, 3]. Furthermore human body is producing heat by metabolism, e.g. 140 W when walking slowly to more than 1000 W during sprints[4]. In summer sun is causing an additional heat source due to IR radiation.
A study by Nielsen et al. showed a heat uptake of the body by sunlight of 120 W, what was 20% of overall heat production[5]. Of cause this heat needs to be released to avoid overheating of the body, maintain wear comfort of clothing and performance of sportsmen[4]. At high temperatures during summer "dry" heat loss by convection and conduction is relatively low, while sweat evaporation is more important.

UV protection depends on the fiber composition of the textile. Textiles made of natural fibres (e.g. cotton, wool) provide lower UV protection than synthetic fibres (e.g. polyester)[6]. Additional protection can be achieved by finishes like TiO_2 or ZnO[7, 8] and by dark colour[9, 10]. Furthermore it is well known that fibres, textile construction and finishes influence sweat management as well as wear comfort of clothing, e.g. Harnisch et al.[11].

Nielsen compared different T-shirts (white vs. black, polyester vs. cotton) in subject trials simulating a sunny summer day[12]. He found lower heart rate and sweat loss in trials with polyester in comparison to cotton and benefits of black shirts when compared to white ones. Kato et al. found no differences between black and white clothing subject trials in the field in regards to body core and skin temperature, but higher sweat rates when wearing white clothes, too[13]. Therefore Nielsen[12] and Kato et al.[13] summarized that white clothing allows higher transmission rates and leads to higher sweat rates. On the other hand EMPA compared a beige and a black shirt by torso measurements and found lower sweat rates for the none-black shirt[14].

No papers were found on spectral/sun protective properties and thermophysiological properties in dependency of fibre chemistry, knit construction and finish.

APPROACH

Four fabrics were chosen to represent sports shirts and as basis for finishing in the laboratory. Every two of them built a pair of similar fibre chemistry (PES/EL and CLY/PP/EL), but varied knit (single and piqué). PES fibers of samples 1 and 2 included an optical brightener and had been white. CLY/PP/EL fibers of samples 3 and 4 were not finished in any way and naturally grey. Fabrics were finished and dyed in the laboratory (red and black, BEMECRON for PES, BEZAKTIV for CLY/PP, all dying agents from BEZEMA AG). Two commercially available UV protection finishes were used, an inorganic one based on TiO_2 (finish 1 – f1, CHT BREITLICH GmbH) and an organic one based on heterocyclic compounds and benzophenone derivates (finish 2 – f2). In combination with those finished fabrics were tested in non-dyed state, red and black.

UV protective properties were characterized according to UV standard 801[15] in dry and wet state. Sun protection in regards to heat transfer through the fabrics was characterized according to EN 410 (g-value)[16].

Sweat management was characterized by means of a sweating guarded hot plate. Based on human thermoregulation and resulting wear situations different sweat rates from vaporous to heavy liquid sweating were simulated and according values were measured. Water vapour resistance Ret was measured according to DIN EN ISO 11092[18]. Higher sweat rates were characterized by buffering capacity of vaporous sweat F_d[11] and the liquid sweat transport F1[11, 19].

RESULTS AND DISCUSSION

Spectral properties

The UPF-values according to UV standard 801 of the base samples 1 to 4 as well as the finished ones show that the PES ones have a higher UV protection, caused by the additional brightener within the fiber. The UPF of PES samples 1 and 2 increases by UV protective finish. On the other hand the UV protection of CLY/PP/EL sample 3 and 4 could not be improved by the use of an UV protection finishing.

The base samples 3 and 4 out of CLY/PP show a lower, better g-value than the PES ones. By applying an UV protection finishing the g-value is significantly decreased. Therefore less IR radiation transmits the sample and the space between wearer and sample is warmed up less.
Further investigation deal with the influence of the colour on the UPF- and g-value. The results show that the UPF- as well as the g-value of the black samples show better results than the red and non-colored ones.

Thermophysiological properties

Water vapor resistance (R_{et}) of the PES fabric is better than CLY/PP fabric and the single jersey is better compared to piqué. Looking at UV protective finish leads to slightly higher values in comparison to non-finished state. Overall

vapor resistance R_{et} of all fabrics (new state, dyed or finished) show a good water.

In regards to buffering capacity of vaporous sweat all fabrics show similar values. Transport of liquid sweat F1 is higher for PES fabrics compared to CLY/PP fabrics. F1 values of piqué samples are lower in comparison to single jerseys. For PES fabrics the inorganic finish has a negative effect, while comparison of non-finished to UV protective organic finish shows approximately same values. In CLY/PP organic finish has a benefit for both knits in regards to F1, while inorganic one just shows a benefit in piqué.

Table 1: Thermophysiological properties of new state and finished textiles.

	finished by	Ret [m2 Pa/W]	Fd [-]	F1 [g/m² h hPa]
1	-	2,30	0,76	20,9
1	f1	2,59	0,65	19,8
1	f2	2,61	0,65	20,9
2	-	2,83	0,65	20,3
2	f1	3,24	0,64	18,5
2	f2	3,12	0,67	19,8
3	-	3,36	0,64	17,7
3	f1	3,90	0,61	17,5
3	f2	3,63	0,64	19,1
4	-	3,78	0,60	16,0
4	f1	4,25	0,59	17,6
4	f2	4,00	0,62	18,2

CONCLUSION
PES samples show less UV protection, a higher g-value and an inferior thermophysiological comfort in comparison to CLY/PP. By coloring the samples UV protection and g-value was improved. The better g-value was reducible to higher light absorption, which could lead to warming of the skin when tightly fitting clothes were worn. Further no influence of dying on the thermophysiological properties has been observed.

In comparison to dying the finishing has less effect on the UV protection and g-value. A clear statement on the influence of the UV finishing on thermophysiological comfort is not possible.

KEYWORDS
UV protective properties, g-value, thermophysiological properties, sports textiles

ACKNOWLEDGMENT

REFERENCES
[1] Lambert, M.I., Manna, T.J., Dugas, P. *Thermoregulation and Human Performance-Physiological and Biological Aspects.* Basel: Karger, 2008: 104-20.
[2] Möhrle, M. "Outdoor sports and skin cancer." *Clin Dermatol,* 2008, 26, 1: 12-15.
[3] Möhrle, M. "Ultraviolet exposure in the Ironman triathlon." *Med Sci Sport Exer*, 2001, 33, 8: 1385-86.
[4] de Marées, H. *Sportphysiologie.* Bochum: Verlag Sport und Buch Strauss, 2003.
[5] Nielsen, B., Kassow, K., Aschengreen, F. "Heat balance during exercise in the sun." *Eur J Appl Physiol O*, 1988, 58, 1: 189-96.
[6] Djam, M., Rosinskaja, C., Kizil, Z., Weinberg, A. "Assessment Method for UV Protection of Woven Fabrics-A Study." *Melliant Int*, 2001, 7, 6: 144-46.
[7] Haug, J.-P. "Schützen alle Textilien gut vor UV-Strahlen. " *aha!news*, 2008, 2: 14-15.
[8] Mallik, S.K., Arora, T. "UV Radiations: Problems and Remedies." *Man Made Textiles India*, 2003: 164-16.
[9] Achwal, W.B. "UV Protection by Textiles." *Colourage*, 2000, 4: 50-51.
[10] Hunt, R. "Opportunities in UV Protection." *Knitting International,* 2003, 2: 51-53.
[11] Harnisch, M., Klepser, A., et al. "Grundsatzuntersuchung zur Leistungssteigerung durch Sporttextilien mit komprimierenden Eigenschaften. " Final Report IGF 16868 N. 2014.
[12] Nielsen, B. "Solar heat load: heat balance during exercise in clothed subjects." *Eur J Appl Physiol O*, 1990, 60, 6: 452-56.
[13] Kato, M., Ha, M., Tokura, H. "The effect of black and white garments on thermoregulation under warm conditions with sun radiation." *Environ Ergon*, 1996: 279-82.
[14] Schoeller. "Coldblack®: Sun Reflector–UV Protector." Available at www.coldblack.ch/ uploads/media/coldblack_Product_Info_Sheet_German_01.pdf. Accessed 2012-02-22.
[15] "UV Standard 801." Available at http://www.uvstandard801.de/. Accessed 2011-02-13.
[16] DIN EN 410. *Bestimmung der lichttechnischen und strahlungsphysikalischen Kenngrößen von Verglasungen.* 2011.
[17] Gagge, A.P. A new physiological variable associated with sensible and insensible perspiration." Am J Philology, 1937, 120: 277-86.
[18] DIN EN ISO 11092. *Textiles-Physiological effects-Measurement of thermal and water-vapour resistance under steady-state conditions.* 2014.
[19] DIN CEN/TR 16422:2013-03. *Classification of thermoregulatory properties.* 2013.

On the Relevance to Test the Robustness of Textile Hydrophobic Properties

Florence Biguenet, Safi Melki, Dominique Dupuis
Laboratoire de Physique et Mécanique Textiles, CNRS-UHA, ENSISA, Mulhouse, France
florence.biguenet@uha.fr

OBJECTIVE

Controlling wetting behavior has recently attracted a great attention due to the wide applications in technologies (medical, printing, cleaning processes…). This study examines the influence of textile structures on the hydrophobicity but also on the robustness of this property. A laboratory test method to evaluate this robustness is proposed.

INTRODUCTION

Wetting properties depend on a combination of surface chemistry and surface roughness. Many studies have been performed on the effects of model textured surfaces on the hydrophobicity [1][2][3]. Fewer have explored the wetting behavior of surfaces with non-perfect pattern structures as textile surfaces [4]. Such surfaces combine different roughness scale levels related to the yarns, the fibers and sometimes to nanofibers or nanoparticles grafted on the primary structure [5]. Additionally, the different elements constituting a fabric are highly deformable.

The main characteristic of the wetting properties of non planar surfaces is the apparent contact angle. Another important characteristic is the contact angle hysteresis which is the difference between the advancing and the receding contact angle. This hysteresis is related to the pinning of the drop when the solid surface is tilted. It is proportional to the force required to start a drop moving on a surface. The present discussion focuses on the necessity to introduce another characteristic parameter to express the robustness of the hydrophobic property of rough surfaces and especially here textile surfaces.

Some hydrophobic fibrous structures were prepared to prospect for the influence of textile structures on the natural and forced wetting properties.

APPROACH

All samples were submitted to the same sizing treatment in order to obtain hydrophobic surfaces. Two main classes of fabrics are considered: classical fabrics and flocked ones.

For the classical fabrics, different arrangement of the yarns and different geometries of the yarns are considered. The warp is made of cotton yarns. The weft is made of cotton, cotton/PET blend or PET yarns. PET yarns are continuous multifilament yarns while cotton and cotton/PET yarns are made of staple fibers which induces some pilosity. In order to modify the roughness at the yarn scale, two different weaves have been chosen: satin weave (SW) and plain weave (PW).

Flocked textiles are composed of a cotton substrate (canvas fabric) on which the viscose hairs of various diameters and lengths are stuck.

To measure the robustness of the hydrophobic property, a laboratory tester has been designed and produced. It allows measuring the contact angle of a water droplet before and after compression on the surface.
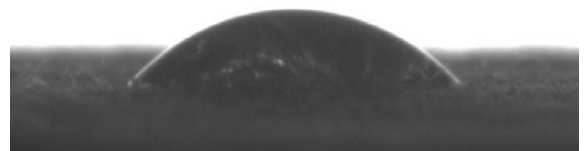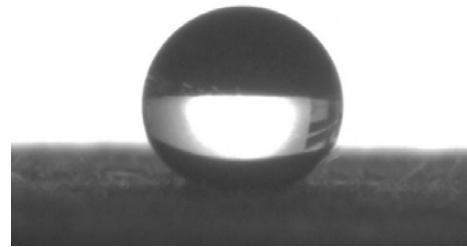

Fig. 1: Example of a drop before and after compression

RESULTS AND DISCUSSION

The classical fabrics are characterized by several scales of roughness corresponding respectively to the crosslinks of the yarns (weaving), the yarn structure and the fibers geometry. Our woven samples, exhibiting approximately the same natural contact angle (125° to 130°), show significant different forced wetting behavior. The fibers geometry and the weaving structure seems to complementary influence the contact angle hysteresis and the robustness of the hydrophobic property. The sateen weave clearly displays the influence of the type of weft yarn on the hysteresis and the robustness of the hydrophobic property. Indeed, the contact area of the liquid drop with these yarns is more important than in the case of plain weave.

The pile fabrics are characterized by a greater contact angle (142° to 147°) and ability for the drop to roll on it.

Nevertheless, when an external pressure is applied to the drop, the pile samples lose their hydrophobicity with contact angles being able to decrease up to 50°. The drop is, at rest, in a Cassie state and undergoes a wetting transition to the Wenzel state after compression. But the problem is more complicated than for model surfaces since the hairs are deformable and bend during the compression which significantly modifies the initial structure. As observed for the woven samples, the pile samples, of approximatively the same static wetting properties, appear to resist differently to compression.

CONCLUSION

The measure of the static wetting properties (natural contact angle, hysteresis, roll-off angle) is not sufficient to characterize the wetting dynamic behavior of a textile surface. Such measurements have to be completed by a study on the influence of an external stress. Here, a laboratory test method is proposed to evaluate the robustness of hydrophobicity. This property can be characterized by the smaller pressure required to induce the lost of hydrophobicity.

REFERENCES
1. Reyssat, M., Yeomans, J.M., Quéré, D. "Impalement of fakir drops." *Europhys Lett*, 2008, 81: 26006.
2. Yoshimitsu, Z., Nakajima, A., Watanabe, T., et al. "Effects of Surface Structure on the Hydrophobicity and Sliding Behavior of Water Droplets." *Langmuir*, 2002, 18: 5818-22.
3. Marmur, A. "Wetting on hydrophobic rough surfaces: to be heterogeneous or not to be?" *Langmuir*, 2003, 19: 8343-48.
4.. Michielsen, S., Lee, H.J. "Design of a superhydrophobic surface using woven structures." *Langmuir,* 2007, 23: 6004-10.
5. Zimmermann, J., Reifler, F.A., Fortunato, G., et al. "A Simple, One-Step Approach to Durable and Robust Superhydrophobic Textiles." *Adv Funct Mater*, 2008, 18: 3662-69.
.

Wetting of Complex-shaped Fibers

Chengqi Zhang[1], Mars Alimov[2], Konstantin G. Kornev[1]

[1]Department of Materials Science and Engineering, Clemson University, Clemson, SC, USA
[2]Kazan Federal University, Kazan, Russia

kkornev@clemson.edu

ABSTRACT

Experimental and theoretical study of wetting of the complex-shaped fibers will be reported. Different modes of wetting are analyzed. First, we will discuss the: capillary rise of menisci on the blade-like fiber. It is shown that at the sharp edges of the blade, the contact line makes a jump. In the wetting case, the contact line sitting at each side of the blade is lifted above the points where the meniscus first meets the blade edges. In the non-wetting case, the contact line is lowered below these points. The contours of the constant height emanating from the blade edges generate unusual singularities with infinite curvatures at some points at the blade edges. The meniscus forms a unique surface made of two mirror-symmetric sheets fused together. Each sheet is supported by the contact line sitting at each side of the blade.

We then consider a C-type fiber and study behavior of menisci formed on the vertically and horizontally placed fibers. In the capillary rise experiment, the indented part of the C-fiber either enhance wetting (for hydrophilic walls) or hinders it (for hydrophobic wall). Meniscus on the edges of the C-fiber is universal, yet its transition to the indentation and protuberance is drastically different.

On horizontally placed fibers, the drop show different scenarios of wetting. A clam-shell configuration of a droplet can be formed only in the cases when a small drop is placed on the bulged side of the C-fiber. As soon as the drop contact line reaches the edge and crawls on the indented side of the fiber, it never stops until gets inside the C-channel.

An overview of the drop behavior on a bundle of the C-shaped fibers will be given. Some practical implications of these results will be provided with examples from biology.

Formation of Alcohol Repellent Medical Nonwoven Fabrics via Electrospraying

Mehmet Dasdemir, Hatice İbili
Textile Engineering Department, University of Gaziantep, Gaziantep, Turkey
dasdemir@gantep.edu.tr

STATEMENT OF PURPOSE
The purpose of this study is to achieve highly alcohol repellent medical nonwoven fabrics via electrohydrodynamic atomization (electrospraying) technique as a novel finishing application.

INTRODUCTION
Alcohol is typically used in medical industry for its bioactive characteristic. This certain characteristic helps to reduce the undesired microbial contamination [1]. Although alcohol's bioactivity can reduce the contamination, it may not remove the risk of cross-contamination via alcohol containing fluids. Therefore alcohol repellency is required for medical textile products. Water and alcohol present different behaviour on surface for repellency because of their surface tension properties (water- 72.8 $mN.m^{-1}$, isopropyl alcohol- 22 $mN.m^{-1}$) [1]. Although alcohol repellency is an essential characteristic for medical textiles' surfaces, it is difficult to obtain this characteristic due to alcohol's very low surface tension which facilitates spreading out the alcohol on the textile surfaces.

Electrohydrodynamic atomization or electrospraying is a novel and promising method for adding functionality to textile surfaces [2]. It can provide obtaining nano sized coating which can bring several advantages such as high surface area, thinner coating layer and low coating weight for many textile surface treatment applications [3]. In addition to these advantages, fabric breathing characteristic and fluid barrier characteristic can be provided [4]. However, the potential of electrospraying application as a finishing treatment on textile surfaces especially for the achievement of alcohol repellency hasn't been explicitly discovered yet.

APPROACH
Our main objectives in this study are to investigate alcohol repellencies of nonwoven fabrics which were coated with a commercial textile repellent agent using a novel approach named electrospraying and to compare them with padded fabrics as a traditional solution. For this purpose, alcohol contact angle measurements for raw, electrosprayed and padded nonwovens were analyzed. Also, fabric comfort properties such as water vapor permeability and air permeability were evaluated based on the statistical analysis (ANOVA) of the results. In order to investigate the morphology of the applied coating on surface fibers SEM images were taken.

RESULTS AND DISCUSSION
For the evaluation and comparison of alcohol repellencies, contact angle measurements of raw, electrosprayed and padded nonwoven fabrics were taken against varying isopropyl alcohol/water (v/v%) mixtures. Figure 1 shows the measured alcohol contact angles (ACAs) for raw and coated nonwoven fabrics. Degrees of alcohol repellencies for electrosprayed fabrics were higher than these for padded fabrics at all alcohol/water mixtures. Also electrosprayed fabric maintained hydrophobic characteristic (ACA>90°) against alcohol/water mixture even at 70 % alcohol concentration with ACA of 96.5° (±5.7°).
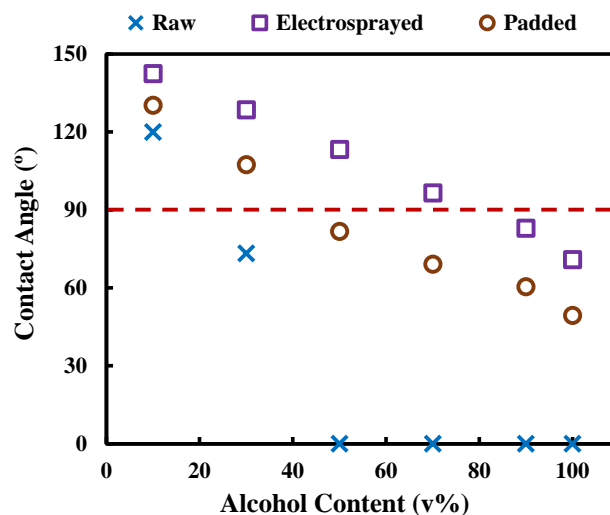

Figure 1: Alcohol repellencies of raw, padded and electrosprayed nonwoven fabrics [2]

In order to investigate the morphology of the coated surfaces, SEM images were taken for raw nonwovens and electrosprayed nonwovens (Figure 2). It was observed that electrosprayed fluorochemicals resided on only surface fibres of nonwovens. Also, they were mostly observed on the uppermost side of the surface fibres. It was concluded that these properties of the coating obtained by electrospraying led to the achievement of high degree of alcohol repellency in this study.
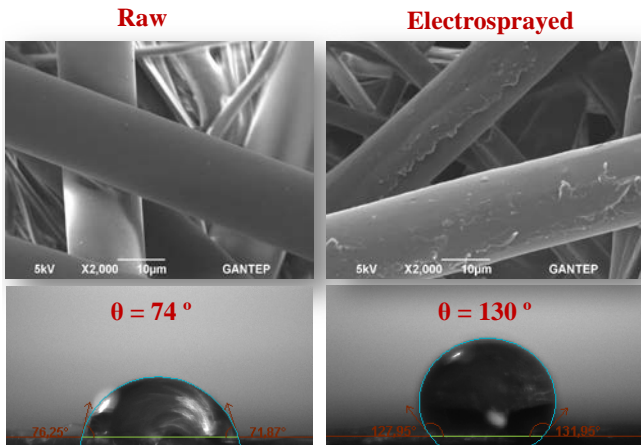
Figure 2: SEM and alcohol contact angle images of raw and electrosprayed nonwoven fabrics [2]

Transmission of water vapor through fabric and air permeability are important comfort characteristics for medical textiles which are directly contact with human skin [5]. In this regard, WVTRs and air permeability of nonwoven fabrics before and after applications were examined (Table 1). After the application of fluorochemical with padding and electrospraying WVTR and air permeability of the fabrics did not significantly change compared to raw fabric. These results indicated that comfort properties of nonwoven fabrics were not affected by applied padding and electrospraying treatments.

Table 1: Water vapor and air permeability of raw, electrosprayed and padded nonwoven fabrics [2]

	WVTR (g.m^{-2}.24 hr^{-1})	Air Permeability (cm^3.s^{-1}.cm^{-2})
Raw	888 (±6)	252 (±6)
Electrosprayed	884 (±11)	256 (±12)
Padded	875 (±4)	239 (±4)

CONCLUSIONS

In this study, electrosprayed nonwovens were shown to be alcohol repellent against alcohol/water mixture of 70/30 (v/v%) whereas that was 30/70 (v/v%) for padded nonwovens. In addition to these, it was revealed that comfort properties of fabrics did not change after the coating which is an advantage for the wearer. This is because electrospraying application not only provides thinner coating on the uppermost side of surface fibers but may also prevent the aggregation of functional finishing agents. Also, it was speculated that there must be some additional contribution of small roughness effect achieved on the fiber surfaces.

REFERENCES

[1] Baldwin, AF. "Process for applying a water and alcohol repellent microbiocidal finish to a fabric and product so produced." U.S. Patent No. 4,411,928. 25 Oct. 1983.

[2] Dasdemir, M., Ibili, H. "Formation and characterization of superhydrophobic and alcohol repellent nonwovens via electrohydrodynamic atomization (electrospraying)." *J Ind Text*, 2016. Accepted Paper.

[3] Graham, K., Schreuder-Gibson, H., Gogins, M. "Incorporation of electrospun nanofibers into functional structures." *Proceedings of International Nonwoven Technical Conference*, 2003.

[4] Dastjerdi, R., Montazer, M., Shahsavan, S. "A new method to stabilize nanoparticles on textile surfaces." *Colloids Surf A Physicochem Eng Asp,* 2009, 345(1): 202-10.

[5] Lee, S., Jeong-Sook, C., Gilsoo, C. "Antimicrobial and blood repellent finishes for cotton and nonwoven fabrics based on chitosan and fluoropolymers." *Tex Res J*, 1999, 69(2): 104-12.

Apparel, Fashion, and Marketing

Textile Design with Integrated Smart Textile Applications

Zuzana Hrubošová

Technical University of Liberec, Faculty of Textile Engineering, Liberec, Czech Republic

zuzana.hrubosova@tul.cz

ABSTRACT

At the market, there are available many various kinds of textiles which are finished by some kinds of prints and applications, but usually there is no other added value except aesthetic one. This research deals with functional kinds of textile prints and their practical application. In this paper, application of 3D textile print in form of Braille symbols is discussed enabling easier communication between blind people and world through the care symbols applied on apparel and textile, see figure 1. These care symbols in Braille are much larger in size compared to classical labels and therefore integration of this functional application to classical aesthetic textile print on right side of clothes is one of favorable possibilities. Experimental part of this paper deals with description of preparation of these special 3D applications on different textile structures and examines effect of textile substrate and type of printing paste on its performance. Stability of 3D print during washing and drying cycles and influence of spot level on readability of Braille symbols is also studied. All findings are based on direct cooperation with visual disable people.

KEYWORDS

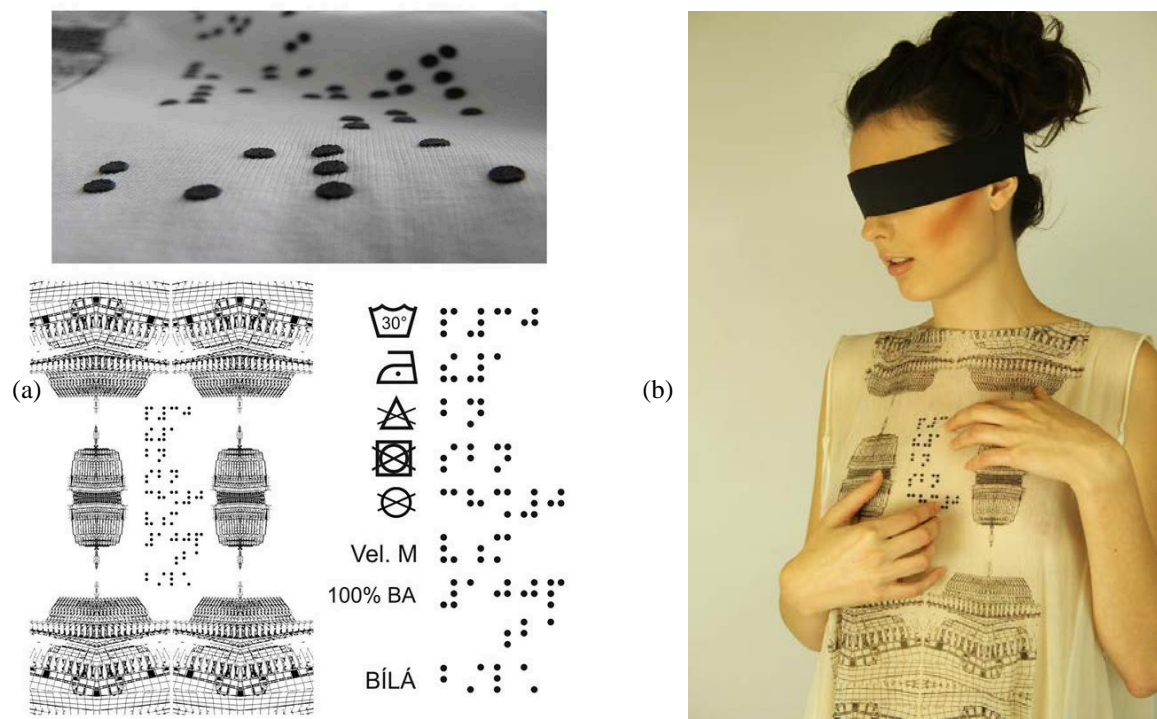Braille writing, care symbols, 3D textile print, textile design

Fig. 1. 3D printed Braille application (a) care symbols, (b) application integrated to printed pattern in apparel.

ANN and Fuzzy Techniques for Modeling the Residual Bagging Height of Denim Fabrics as Function of Frictional Properties

Boubaker Jaouachi[1,2], Mouna Gazzah[1], Faouzi Sakli[1]
[1]Textile Engineering Laboratory, University of Monastir-Tunisia
[2]National Engineering School of Monastir, University of Monastir-Tunisia
boubaker_jaouachi@yahoo.fr

STATEMENT OF PURPOSE

This work deals with the evaluation and prediction of the residual bagging height of denim fabric specimens. It also provides the impact of each frictional input parameter in our experimental field of interest to simulate the bagging phenomenon after several denim clothing uses.

INTRODUCTION

Modeling of the bagging behaviors by deciphering the relationship between both the yarn and fabric properties can be considered as a fruitful field in textile research. In fact, it seems important from the industrial and user's viewpoint, because it affects the appearance quality of the garments. Statistical regression modeling techniques are used by many researchers to predict the bagging behaviors of knitted and woven fabrics[1,2,3,4].

Some intelligent techniques such as fuzzy logic and neural network approaches are used in large textile applications, due to their flexibility and accuracy of modeling complex textile phenomena. In addition, to evaluate fabric-bagging behaviors, Young et al.[5] used the neural network to modeling fabric bagging when evaluating the subjective perception data of the bagging appearance which can be predicted from the images of the bagged fabrics. In this work, the neural network and fuzzy logic-based models are compared and discussed to predict the residual bagging height as function of the studied frictional parameters.

RESULTS AND DISCUSSION

In total, 29 twill 3/1 denim fabric samples were industrially produced, investigated and studied in the present work. The methods and materials details are described in several works[6,7].

Predicting the residual bagging height using the Artificial Neural Network

Neural network algorithm is used for the bagging modeling due to the high accuracy of this system in learning nonlinear process data. The denim fabric samples are divided into a training set (20 samples) and a test one (9 samples). The validation set is used to achieve training done with the training set. Since neural network is an alternate statistical method, the root mean square error (RMSE), the relative mean absolute error (RMAE) and correlation coefficient (R) are used as performance criteria to carry out the best suitable models. Here, the number of hidden neurons is considered optimal when the training and test root mean square errors are both in the same order and as small as possible.

As shown in Figure 1 there are good agreements between predicted and observed data values. Thus, our findings seem improved widely
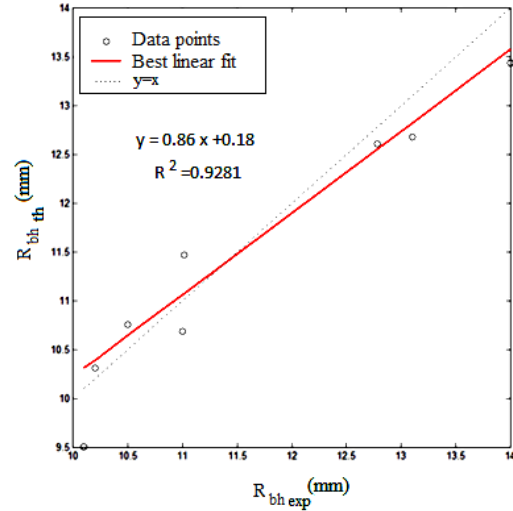

Figure 1. Artificial Neural Network predicting of the residual bagging height.

Table I shows the *RMSE*, *MRAE*, and the correlation coefficient R of training and test samples given by the neural network. The neural network model gives high and acceptable coefficient value for both training ant test samples. In fact, the correlation coefficients are ranged from 0.885 to 0.977 which are close to 1. The MRAE values are ranged between 0.61% and 1.06% which are considered low. Consequently, it may be concluded that the neural network methodology is helpful towards a better understanding of the relationship between the frictional parameters and the bagging behavior of denim fabric samples.

Table I. Performance evaluation of the Neural Network model.

. Performance variables	R_{bh} (mm)
$RMSE_{Training}$	786.09
$RMSE_{Test}$	617.23
$MRAE_{Training}$	0.61%
$MRAE_{Test}$	1.06%
$R_{Training}$	0.885
R_{Test}	0.977

Predicting the residual bagging behaviors using the fuzzy logic theory

All input and output values are converted to three fuzzy subsets: low, medium and high. In fuzzy inference, the Mamdani method was used for calculating the output inferred by a set of fuzzy rules.

Four different membership functions "Triangular" (Trimf), "Trapezoidal" (Trapmf), "Gaussian" (Gaussmf) and "Generalized-bell" (G-bell shape) are chosen and applied. Figure 2 shows the results obtained using the fuzzy logic theory.
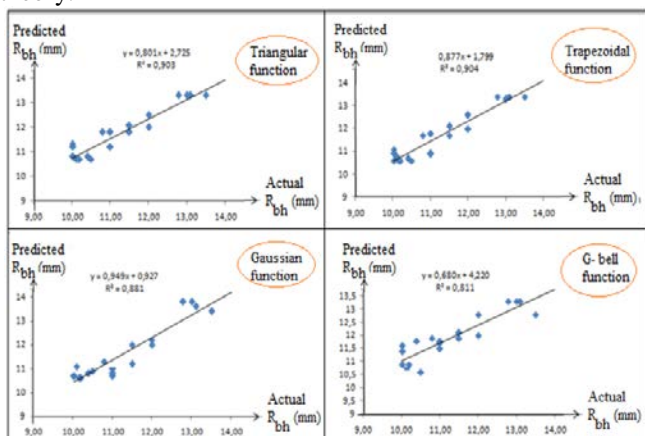

Figure 2. Linear regression evolutions between predicted and actual R_{bh} values using fuzzy logic models.

The regression models present good regression coefficient values, which improve the effectiveness of the developed fuzzy models. Thus, we can deduce that the R_{bh} seems predictable sufficiently in our experimental design of interest. Besides, compared to the experimental results, our theoretical findings give more accurate prediction of the residual bagging height, R_{bh}. Moreover, the root mean square error (RMSE), the relative mean absolute error (RMAE) and the correlation coefficient (R) are used as performance criteria to get higher suitable models (see Table II) which can be applied further.

Table II. Performance evaluation of the different fuzzy logic models relative to R_{bh}.

	Fuzzy membership functions			
	Trimf	Trapmf	Gaussmf	G-bell shape
RMSE	0.61	0.55	0.54	0.81
MRAE	0.47%	0.11%	0.41%	0.64%
R	0.95	0.95	0.94	0.90

Comparison between fuzzy and neural prediction performance

Basing on the results obtained, it is revealed that the fuzzy models are slightly powerful than the neural models. The performance criteria are better for fuzzy models compared to those for neural models. Applying the best fuzzy function in each residual bagging property, there is a more significance of fuzzyfied values than those saved using neural network technique. These findings can help industrial and researchers to predict widely the bagging ability of

tested denim samples in our experimental design of interest. Moreover, basing on the obtained results, it seems possible to prevent, evaluate and optimize the denim fabric bagging properties as function of frictional inputs.

CONCLUSION

In this work, we have predicted the residual bagging height of denim fabric samples using two theoretical methods: fuzzy logic theory and neural networks. Our findings showed that the prediction performance is high for the fuzzy models. Indeed, the results show, also, that the change of fuzzy membership function affects enormously the prediction accuracy of the residual bagging characteristics. Compared to experimental results, it may be concluded that overall theoretical models using fuzzy technique are marked by relatively good and significant correlation coefficients. However, the fuzzy technique remained the best-applied method to evaluate studied bagging height. Indeed, we have concluded either, that the error values (RMSE and MRAE) between theoretical and experimental results traduce the effectiveness of both the fuzzy and the neural models to predict and evaluate bagging behavior.

KEYWORDS

Residual bagging height, denim fabric, frictional properties, fuzzy modelling, ANN technique.

REFERENCES

1. Gazzah, M., Jaouachi, B. "Evolution of residual bagging height along knitted fabric lengths." *Research Journal of Textile and Apparel*, 2014: 70-75.
2. Gazzah, M., Jaouachi, B., Sakli, F. "Recovery Velocity Evaluation of Bagged Denim Fabrics as Function of Frictional Parameters." *International Journal of Clothing Science and Technology*, 2015, 27(2): 302-14.
3. Hossein, H., Sanaz, H.Z., Sanaz, B. "Bagging behavior of different fabric structures knitted from blended yarns using image processing." *Journal of Engineered Fibers and Fabrics*, 2012, 7: 8-15.
4. Zhang, X., Dhingra, R.C., Miao, M. "Garment Bagginess." *Textile Asia*, 1997, 28: 50-52.
5. Yeung, K.W., Li, Y., Zhang, X. "Evaluating and Predicting Fabric Bagging with Image Processing." *Textile Research Journal*, 2002, 72: 693-700.
6. Gazzah, M., Jaouachi, B., Sakli, F. "Optimization of bagged denim fabric behaviors using the genetic algorithms and the ant colony optimization methods." *International Journal of Clothing Science and Technology*, 2015, 27(6): 772-92.
7. Gazzah, M., Jaouachi, B. Sakli, F. "Study of the influential inputs on the bagged denim fabric behaviors using the Principal Component Analysis method." *International Journal of Clothing Science and Technology*, 2015, 27(6): 922-39.

Photonic Textile Design Practice: A Case Study

Zi-qian Bai[1], Jeanne Tan[2]
[1]Shanghai International College of Fashion and Innovation, Donghua University, China
[2]Institute of Textiles and Clothing, The Hong Kong Polytechnic University, Hong Kong
vera.bai @dhu.edu.cn

INTRODUCTION

POFs (Polymer Optical Fibers) have been widely utilized in innovative photonic textile and fashion design, due to its compatibility to textile processing. When coupled with light source, POF fabric can emit light if the cladding of POF is partially damaged by chemical corrosion, mechanical abrasion, laser engraving, etc (Daum et al.; Endruweit, Long and Johnson). In contrast to the never-changing color of conventional textiles, the POFs in the photonic textile can be connected to different Light Emitting Diodes (LEDs) sources to transform the textile color to adapt to the user's preference. With the integration of sensors, the photonic textiles can detect and respond to the stimuli from the users, and therefore promote interaction between textiles/user, and user/user (Bai and Tan; Bai et al.; Bai, Tan and Tao). The developing process of interactive photonic textile involves technology implementation, engineering techniques and design, which makes developing a user-friendly product a big challenge. Conventional technology-driven development of smart photonic textiles lacks the considerations from a designer's standpoint. The objective of this research is to address some issues during the design and development process by taking a developed photonic textiles prototype as a case study. How to bridge the gaps between different disciplines are discussed.

CASE STUDY

One piece of illuminating creation based on POF fabric has been developed. During the development process, it is found that technology-centered development approach does not necessarily yield a prototype with satisfactory user experience. The main issues are discussed below.

Fashion vs Function

Design and development of interactive photonic textiles require knowledge from multiple areas (design, textiles, wearable electronics, sensor, etc). During this multi-disciplinary design process, the designer should understand the knowledge of technical parts. How to communicate with technical experts and engineers is a big challenge to designers, since the language the designer uses is very different from the language the engineer uses. Discussions should be carried out during the whole design process between different parties (Figure 1).

Figure 1: Discussion between designer and engineer during the design process.

Smart textiles are always developed by technical researchers, who concern more about the technology and function. There is a lack of consideration about the appearance, aesthetics and comfort of the prototype, which significantly influence the usability of the end product. Therefore, the development of interactive photonic textiles must combine technology and design, fashion and function. The designer and engineer must work closely to continuously refine the prototype until the preset requirements from both functional and aesthetic points of view are met.

Unobtrusive Design

One of the main challenges in development of POF textiles is how to integrate POFs and LEDs into fabrics without interfering much with the user, while still maintain the desired illuminating effect. Especially in smart clothing application, as the POF fabric is worn next to skin, the integrated electronic components must be safe, less-bulky, comfortable, easy care and fashionable as well.

Conventional method to couple LEDs to POFs is to attach LEDs to the ends of a group of POFs by transparent glue. The glue needs to be solidified using ultraviolet radiation to ensure the fixation. Due to the size of LED, only a small amount of POFs can be coupled to one LED. This makes the coupling procedure a time-consuming and labor-intensive process. Experiments in this study indicate that the utilization of cable glands significantly reduces the time required for POFs coupling compared to the Ultraviolet bonding technique. This technique involves the use of a customized coupler based on a cable gland. A Tri-color

LED is fixed inside the coupler, and is connected to PCB via wires. A bundle of POFs is inserted into the coupler, and then is fastened by the cable gland without the fussy gluing and curing process. This technique is labor efficient and produces bright illumination. The developed prototype uses less LEDs and wires, is less bulky, and therefore imposes less impact to the wearer.

User Experience

Previous study on smart textiles and clothing focused mainly on the technology development. Experiments are always designed to test the functional performance of the prototypes. However, very few studies have been conducted to research the user experience of the prototype, and how to use the feedback from users to refine the design.

In this research, when a prototype is finished, surveys are conducted to obtain the feedback from users. Each performance is given a numerical grade from 1 (very unsatisfactory) to 7 (very satisfactory). The overall grade is obtained by taking average of the grades from all subjects. Results from surveys provide valuable directions for further refinement of the prototypes (Figure 2).
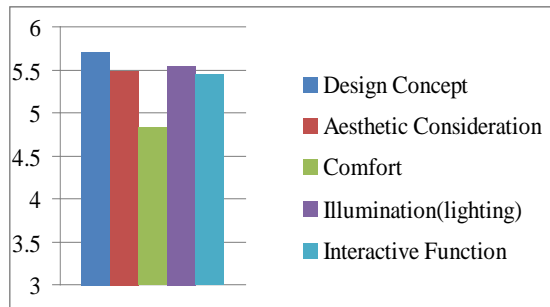
Figure 2: Numerical grades.

Imperfection is Perfect

In the creation developed in this research, the POF fabric is engraved by laser to achieve an illuminating effect. During laser engraving, due to the wrong setting, some POFs are over-burned. Therefore more light emit from the over-burned area than other areas, and this makes the over-burned area lighter than other areas (Figure 3). From a technological point of view, the over-burned area is a consequence of wrong setting and failed treatment. However, from a designer's viewpoint, this creates a unique appearance and illuminating effect, which is acceptable. The development process is rather design-driven than technology-driven.
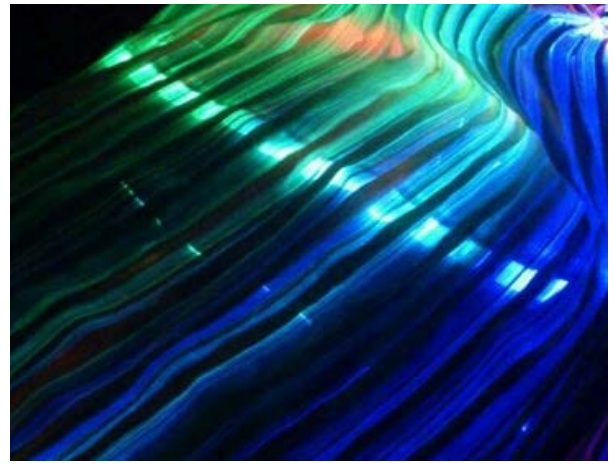
Figure 3: Illuminating fabric.

CONCLUSION

The challenges in the development of smart photonic textiles are discussed. It is concluded that:

1) In order to create user-friendly smart photonic textiles prototype, the design process needs to combine fashion and function, design and technology.
2) Research on smart photonic textiles needs to consider the needs and feedback of end users. Unobtrusive design can satisfy the user physically and psychologically in terms of minimizing the impact on the users. Surveys also offer a useful tool to collect the feedback from the users to further improve the prototypes.
3) Development of smart photonic textiles is not only driven by technology, but also driven by design.

KEYWORDS

Fashion Design, Photonic Textiles, POFs

REFERENCES

Bai, Z. Q., J. Tan, X.M. Tao. "Surface Printing and Photonic Fibers for Interactive Interior Textiles." *The Fiber Society 2011 Spring Conference Proceedings*.

Bai, Z.Q., J. Tan. "Innovative Design of Polymeric Optical Fiber Fabric for Interior Textiles." *Research Journal of Textile and Apparel*, 2013, 17.2: 10-15.

Bai, Z.Q., et al. "Enhancing the Functionality of Traditional Interior Textiles with Integration of Optical Fibers." *Research Journal of Textile and Apparel*, 2012, 16.4: 31-38.

Daum, W., et al. *Pof Polymer Optical Fibers for Data Communication*. Berlin: Springer, 2002.

Endruweit, A., A.C. Long, M.S. Johnson. "Textile Composites with Integrated Optical Fibres: Quantification of the Influence of Single and Multiple Fibre Bends on the Light Transmission Using a Monte Carlo Ray-Tracing Method." *Smart Materials & Structures*, 2008, 17.1.

Textile Testing
and Control

New Method for Evaluation of the Trauma and the Penetration Depth Through Multilayer Textiles

Priscilla Reiners, Yordan Kyosev, Meike Siemes, Jenny Becker, Annika Mihm, Alena Cordes
Hochschule Niederrhein University of Applied Sciences, Mönchengladbach, Germany
priscilla.reiners@hs-niederrhein.de

PROBLEM

Stab resistance tests are normally carried out according to the German Test Standard [1] with a standard knife which falls from a specific height, depending on the required energy level. The knife is driven by a defined weight onto the test sample, which is lying on a box with ballistic plasticine. The penetration depth in the plasticine is measured after removing the plasticine on one side of the penetration channel. The deformation depth is determined by measuring the deepest point of the stab impact, where the trauma impact is not taken into account [2–4]. Figure 1 shows two identical engraving results, but with varying degrees trauma, which is not considered. This means that the hole, which is caused by the stab test, has to be dug out carefully and the exposed hole has to be measured using a ruler. In practice, this measurement method is, however, quite difficult to implement and lead to frequent discarding of the stab. When digging, it may happen that the stab hole is touched and so falsifying the measuring result or becomes unusable. While three samples should be measured according to the standard and to ensure reproducible and meaningful results, it becomes quite difficult and expensive to get enough test material in case of the discard of many measurement results. These problems led to the development of a more productive method of measurement, which is described following.
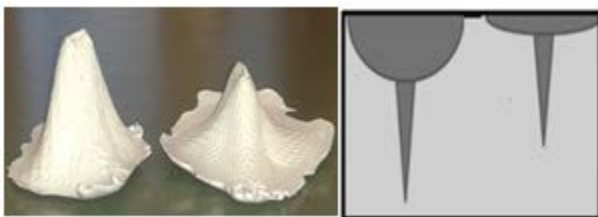

Figure 1: Identical stab depth results with varying trauma

NEW METHOD

The new evaluation method is described, where the deformation depth and the trauma can be poured out in plasticine and the deformation of the lowest fabric layer can be fixed. Thereby the puncture can be measured accurately and fixed plastically. The plasticized samples can also be measured in order to analyze and simulate movement, deformation and energy absorption.

During the test preparation a cup is filled with plasticine, with no air bubbles and placed below the knife tip. Then, the investigated multiple layer sample is positioned on it, and the test is performed by dropping the knife from a specified height as usual. To fix the lowest fabric layer, the upper layers of tissue have to be removed carefully and it must be ensured that the lowermost fabric layer just remains in its position. Subsequently, the cup can be carefully removed

from the testing area, so that next test can be performed there.

First, the fabric is fixed in its deformed state with quick-drying adhesive. After the hardening, the puncture in the plasticine is poured out and after hardening of the resin, the trauma can be filled with silicone. Using cups allows the testing of multiple samples in succession and simultaneous processing. Thus, the individual steps must not be carried out directly after each test. Also there is no need for time-consuming digging out of the puncture, which also has a low success rate, as results will be damaged easily like described before. Using this method, measurable samples are available in a short time. Due to fixation of their three-dimensional form, the poured out puncture and the trauma of a sample can be easily compared with those of another sample. This is useful in addition to the pure measurement of the penetration depth because the differences between samples can be recognized and assessed visual. In the following, the individual processes are explained in detail.

DEFORMATION OF THE LOWEST LAYER

The fabric is fixed with adhesive in its deformed state, where the wetting is performed by a pipette with collodion. To obtain a particularly good and stable result, several layers collodion are applied. Once the adhesive has dried, the prepared fabric layer can be removed from the plasticine and investigated. Picture 2 shows a hardened fabric layer of aramid, which has been tested against puncture resistance, which allows qualitative and quantitate analysis of the deformations.

Figure 2: Deformed lowest layer fixed with collodion

DEFORMATION DEPTH OF THE PUNCTURE

The performed methodology makes easier the measurement of the deformation depth and enables rapid processing of multiple samples simultaneously, since the individual measurements are carried out in removable cups. First, an epoxy resin composition (mixing ration to hardener 8:1) is prepared, with which the groove is poured. The resin is filled in dropwise into the puncture. Thereby it has to be ensured, that the resin can be completely flow into the puncture and bubbles have the opportunity to escape. In addition to be able to pour out the trauma, it is important to fill the resin accurately up to the puncture beginning. The used epoxy resin has a curing time of approximately twelve hours. After this time, the sample is ready for further processing and can be removed out of the plasticine. Figure 3 shows the pour out puncture after the drying time. On the form it is possible to measure the penetration depth of the blade on its straight side.

Figure 3: Pour out puncture

It can be seen clearly, how exactly the puncture was poured out. The cut surface of the blade is exactly recognizable and also the beginning of the trauma can be seen. It can be constructed as the stitch can be attached to the trauma, to visualize the action of the knife and the impact energy.

In addition to the penetration depth, it is possible to fix the resulting trauma. Here, a silicone compound is filled directly into the deformation in plasticine. Figure 4 shows the fixed trauma.

Figure 4: Silicone compound traumas

Out of the values weight and density, the energy absorption behavior of different materials can be compared trough the volume of the trauma, determined by weighting of the silicone piece:

$$V[cm^3] = \frac{m[g]}{\varrho\left[\frac{g}{cm^3}\right]}$$

with m for the mass of the poured trauma and ϱ for the density of the silicone compound material with 1.24 g/cm³. The trauma volume gives additional information about the distribution of the energy in the investigated system compared to the single value of the trauma heights.

EXPERIMENTAL

Tests were carried out to compare samples without and with a pretension of 1.5N in total to analyze the influence of the fabrics pretension on the stab test results. In Figure 5 and Figure 6 the stab depths of samples with different sizes are compared together with the trauma depth and the trauma volume. The results show, that the pretension has no influence onto the stab depth but on the trauma size. The trauma volume and height is bigger for samples where the fabric is tested in free state, without pretension.
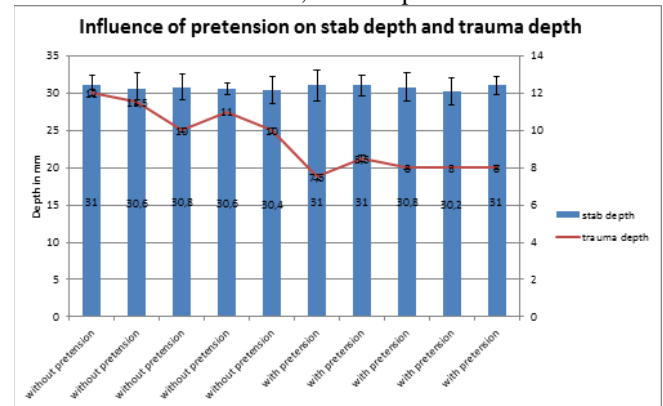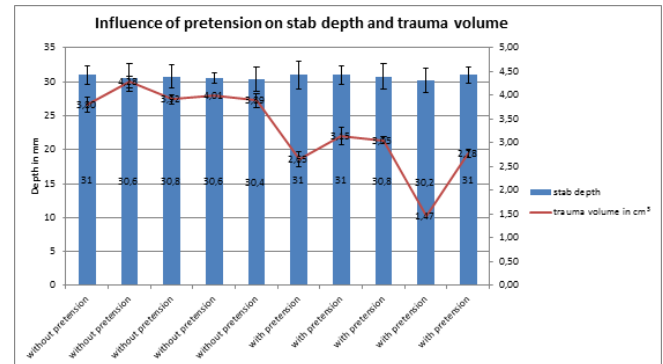

Figure 5: Results for stab and trauma depth

Figure 6: Results for stab depth and trauma volume

CONCLUSIONS

A new method for analysis of the stab depth, trauma height and trauma volume was developed. The investigation shows, that the fabric pretension has significant influence on the trauma depth and the trauma volume.

REFERENCES

1. *VPAM KDIW 2004 Stab and Impact Resistance- Requirements, Classifications and Test Procedures*. 2011.
2. Egres, Jr,, R.G., et al. "Stab resistance of shear thickening fluid (STF)-Kevlar composites for body armor applications." *World Scientific*, 2004.
3. Horsfall, I., et al. *Impact Perforation Testing of Stab- resistant Armour Materials*, 1995.
4. Suhaimi, S.A., et al. "Puncture resistance of Twaron fabric layers with different stitching patterns." *International Journal of Textile Science*, 2012, 5: 44-48.

Biochemical Remedy of Contaminated Forests and Fields of Fukushima Area of Japan by Using Kassei-chip Method

Msatomo Minagawa[1], Hideaki Akashi[2], Tatsuya Kajikuri[3]

[1]NPO, Dream-Create-Laboratories, Yonezawa, Yamagata, Japan
[2]Higashi-Nippon International University, Iwaki, Fukushima, Japan
[3] Research Institute for Recycle-Society, Murakami, Niigata, Japan
gakusai-minagawa@memoad.jp

ABSTRACT

The Kassei-chip method was tentatively applied in Fukushima area (Kawamae in Fig.1) to check the intensity change of Cs (radioactive specie) derived from Atomic Reactor Accident in Fukushima. When Kassei-chip (compost-fertilizer) was mixed with contaminated **soil** and kept exposed in a flexible bag, temperature increased gradually ($\sim40^o$C) and the radiation intensity of Cs decrease. In a few days, the initial intensity decreased below its half value ($\sim1/2$). Not only contaminated soil but also contaminated cow's droppings and wood chips showed similar reduction, the extent of which was different from the kind of materials. The most remarkable result was obtained in cow's drops ($\sim1/5$). The reason why the intensity decreases, when special enzymes in the Kassei-chip propagate in the presence of cellulose, has not been clarified. We estimate that hydration around encapsulated (Cs) particle at a molecular level plays a significant role for the intensity reduction. Here the possible mechanism is discussed.

INTRODUCTION

More than 5 years have already passed since the Giant Earthquake and Tsunami attacked Fukushima Area, South Tohoku of Japan (March 11, 2011). We can hear a voice of the completion of re-construction of Fukushima area, but we have seen many un-repaired housings in the Ghost towns. Figure 1 shows contamination map, which indicates how to spread the radioactive specie (Cs) from the Broken Atomic Reactors (Fukushima I-III). We can understand easily how difficult to remedy (purify) the contaminated region, wood forests, cultivating fields, rivers, bonds and green mountains in this area. Contaminated surface area is extremely large, and
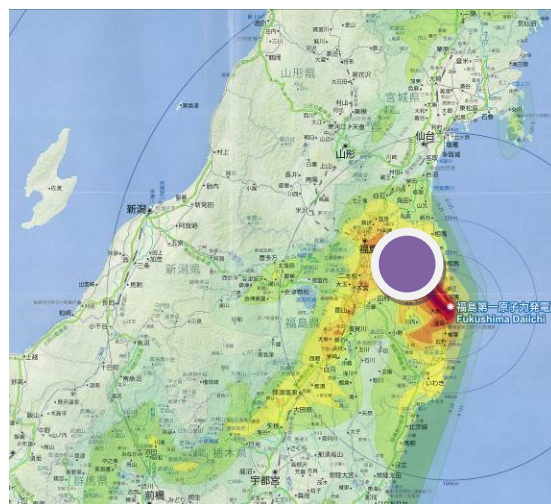

Figure 1. Contamination map (7th ed.) prepared by Prof. Y. Hayakawa (Gunma University).

therefore, some kind of epoch-making powerful procedures are strongly required. The Kassei-chip (compost-fertilizer, VCS) is quite adequate for this purpose. The procedure is very simple and its powerful effect has already been confirmed in other field of agriculture, such as to strengthen the life of aged pine trees or insect-damaged green trees in the forests. Here we report the application of this method and the solution of radioactive (Cs) problems in Kawamae (indicated by circle in Fig.1) by this procedure.

RERSULTS AND DISCUSSION

Figure 2 shows the intensity variation of the soil. The intensity decreased rapidly, and the extent of which was about one/half (1/2). That is, the original value of 4,000 Bq/Kg decreased to 2,000 Bq/Kg. In the case of cow's droppings, its effectiveness was more remarkable (Fig. 3). The initial value 5,000 Bq/Kg decreased to 1,000 Bq/Kg, to be about one/five (1/5). In the case of wood chips, the results were similar to those of soil ($\sim1/2$). In this way, three kinds of substances showed similar decrease of
radiation intensity of cesium (Cs).

There exist more than 100 kinds of micro-organs (enzymes) in the Kassei-liquid (original compost liquid), and 10 % of which have anti-radiation property. It is worth-while noting that simple propagation of some kinds of enzymes appears
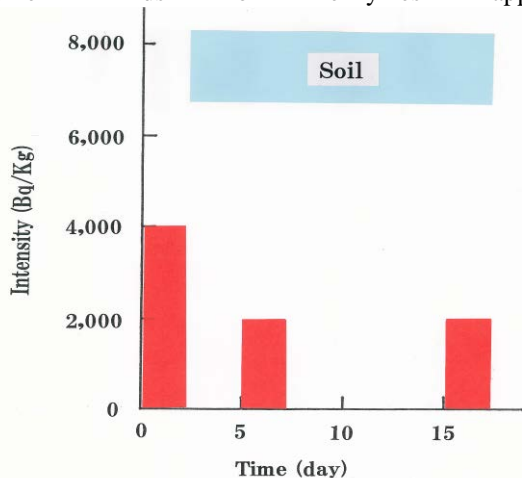

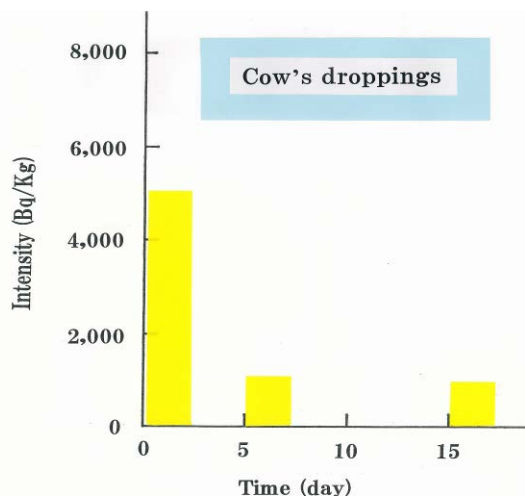Figure 2. Intensity variation of soil of Kawamae.

Figure 3. Intensity variation of cow's droppings.

not to affect the irradiation intensity. However, if some of these enzymes will micro-capsule of cesium particles at a molecular level to form a very thin membrane, then such an effect may be observed. Namely, simple micro-capsule covering may cause the change of hydration state around the outer atmosphere of Cs particle (Fig. 4). The capsule-covering may play a role of an environmental anchor attracting water molecules. The intensity variation would be possible in terms of the shielding effect by water molecules around Cs through enzymes.
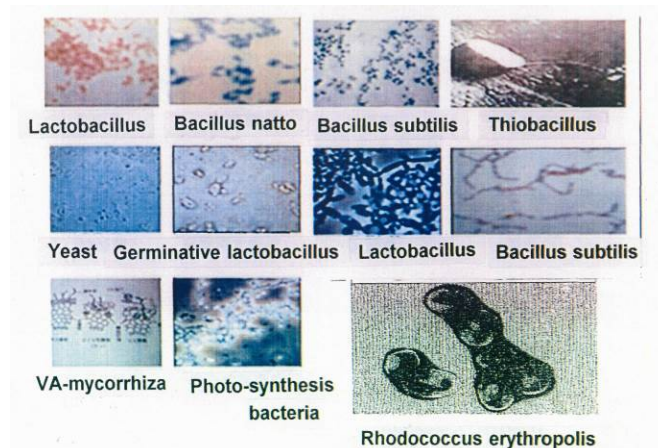

Figure 4. Possible micro-capsulating enzymes in Kassei liquid.

CONCLUSION

1. Kassei-chip method was applied on the field of Kawamae by the courtesy of Mr. C. Sakai, a leader of this area. Contaminated material (600L) was mixed with Kassei-chip (400L), and exposed in a flexible bag under strictly controlled conditions.

2. Radiation intensity of Cs was monitored by two methods, one is direct monitoring by us at Kawamae using (ALOKA), and the other was done by moving it to National Testing Organization in Nagaoka (Niigata) in the next day. In both measurements, the intensity decreased rapidly. The results by the latter were shown in Figs. 2-3.

3. The above results were explained in terms of the bio-chemical reactions, the variation of hydration state around cesium. Microscopic capsule covering by special enzymes may play a role of the formation of outer atmosphere attracting water molecules.

REFERENCES
M Minagawa, T. Kajikuri, H. Akashi. Preprints of 24th Annual Meeting of MLS, July 5-6, 2013, Kyoto Inst. Tech., Kyoto: 57-60.

Wear of Carbon Nanotubes Grafted on Carbon Fiber

Claire Guignier, Marie-Ange Bueno, Brigitte Camillieri, Thang Le Huu, Bernard Durand, Florence Biguenet
Laboratoire de Physique et Mécanique Textiles, Ecole Nationale Supérieure d'Ingénieurs Sud-Alsace,
Université de Haute-Alsace, Mulhouse, France
claire.guignier@uha.fr

INTRODUCTION

Carbon nanotubes (CNTs) grafted on carbon fibers (CFs) are widely used to reinforce composites and particularly to improve the fiber/matrix interface. However, the good comprehension of the CFs/CNTs interface is necessary. During the industrial process of composite fabrication, the fabric is guided with some cylindrical metallic piece between the weaving and the shaping. This cause some stresses on the CNTs grafted CFs which can create some damage on the CNTs, particularly friction. The aim of this study is to determine the behavior of the CNTs grafted CFs under a stress like friction, and particularly to highlight a wear mechanism.

APPROACH

The carbon filaments used are ex-PAN CFs, with high tenacity and a standard modulus from Toho Tenax, with a diameter of 7 µm. They are assembled in a 6 K multifilament and then they are woven in a plain weave fabric with fine weft in glass E. The raw material is treated by acid sulfuric to eliminate the epoxy-based sizing. Multi-walled carbon nanotubes are produced directly on the surface by the flame method, developed by Donnet et al. [1-2], using a metallic catalyst. This method as the benefit of rapidity, but the structure of CNTs (number of walls, diameter…) is not well controlled. Several ferrous catalysts have been tested in preliminary studies. For this study, the two ferrous catalysts (noted Cat.1 and Cat.2) selected are those that give the best quality and density of MWCNTs. The conditions of fabrication are the same for the two catalysts in terms of temperature and growth period. The only difference is in the particle size distribution, which is thinner for Cat.2 than Cat.1.

Friction tests are realized on a linear reciprocating tribometer, with a cylindrical slider (stainless steel, with a diameter of 20 mm), in order to approach a rolling on a metallic piece. The normal load is applied by means of dead weights, under a normal load of 1 N, at a sliding speed of 20 mm/s and a sliding distance of 20 mm.
SEM observations were conducted in order to see the evolution of the surface.

RESULTS AND DISCUSSION
Characterization of the produced CNTs

Figure 1 shows virgin carbon fibers (a), and the CNTs grafted CFs (b-c). We can clearly see that the carbon nanotubes cover the entire carbon surface, by creating a film (b). At small-scale (c) carbon nanotubes are totally and randomly entangled on the surface.
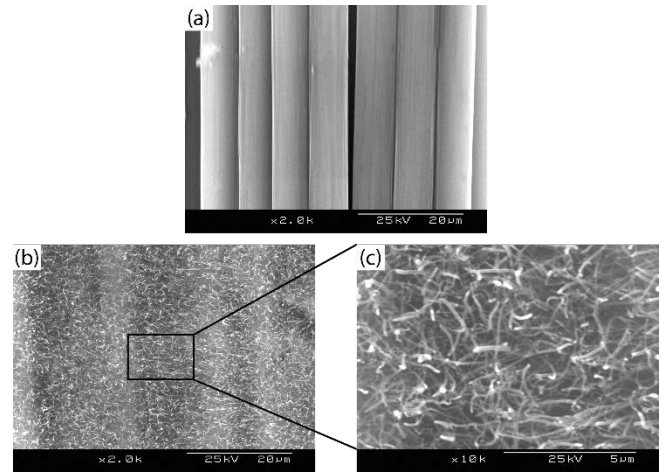

Figure 1: SEM pictures of (a) virgin carbon fibers, (b-c) CNTs grafted carbon fibers at different magnification.

The CNTs structures have been determined and it appears that the CNTs present a diameter of around 50 nm with Cat.1 and around 30 nm with Cat.2. The link between the size particles of the catalyst and the diameter of the CNTs is confirmed.

Study of the wear in the first friction cycles

The aim of this study is to determine the behavior of CNTs under friction strain, corresponding to the solicitations applied during the guidance of the fabric. Friction tests are realized cycle by cycle and SEM observations are made exactly in the same place in the fabric between each friction test.
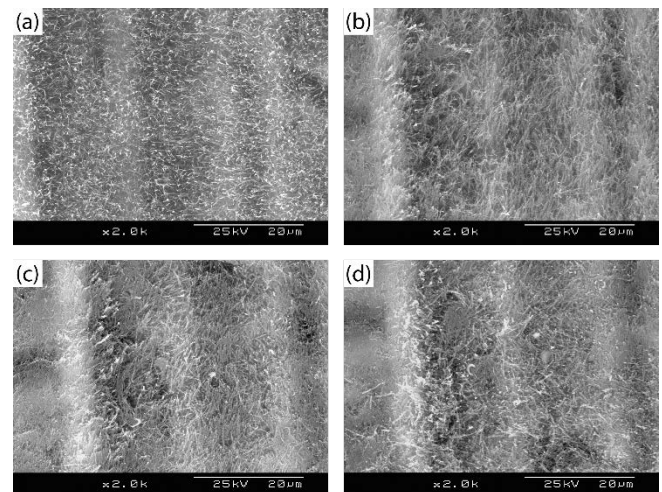

Figure 2: SEM pictures showing the evolution of the surface state of the CNTs during the first cycles of friction: (a) before friction, (b) 1st cycle of friction, (c) 5th cycle of friction and (d) 10th cycle of friction.

Figure 2 shows the SEM pictures obtained, for the surface with Cat. 2, the results are the same for both catalysts. Before friction (a), CNTs are entangled on the surface, after one friction cycle (b), CNTs are aligned in the axis of fibers (in the friction direction). When the friction goes on, CNTs are more and more aligned and crushed on the surface until the creation of a transfer film. After 5 friction cycles (c), the transfer film is present on the all surface and no modifications are noticed on it as the friction goes on until 10 cycles (d).

We can conclude that CNTs are resistant to 10 cycles of friction, however they are changing the surface state, they are no more entangled but aligned and crushed on the surface.

A chemical analysis of the transfer film showed that it mostly composed of carbon and some ferrous particles, which come from the catalyst particles. On the slider, some residues, composed only of carbon are present after the tests.

Study of the time stability of the transfer film
This study have been realized to determine the stability of the transfer film under repeated friction cycles, in order to see the influence of the catalyst on the time stability of the CNTs. In a first study, the different step of the wear mechanism were determined related to the number of the cycles [3]. However, the grafting conditions were optimized, in order to increase the resistance of the grafting.
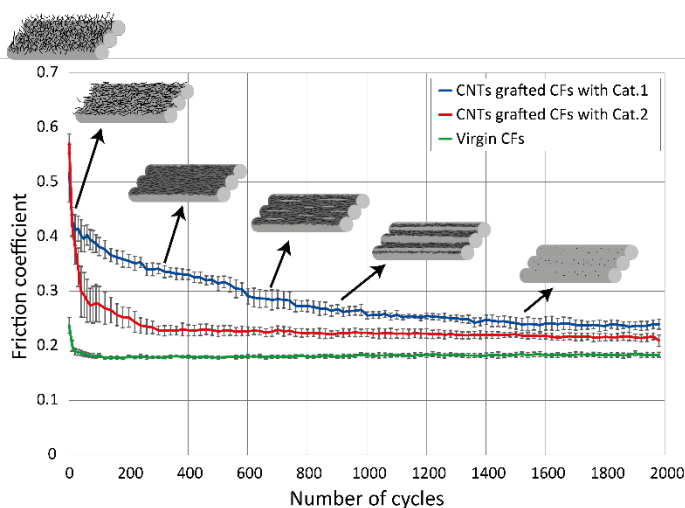

Figure 3: Evolution of friction coefficient function of the number of cycles for 3 states of surface under 1N.

For the virgin CFs, the decrease in the first cycles is due to the reorganization of the textile structure, and then the friction coefficient (COF) is stable around 0.18. The presence of CNTs grafted on the CFs increase the COF. For the CNTs grafted surfaces, COF decrease more rapidly with the number of cycles for Cat.2 than Cat.1 and then become stable. SEM observations during the friction showed the formation of the transfer film and the breaking appears at around 100 cycles of friction for Cat.2 while for Cat.1, the transfer film do not present crack before 500 cycles. That is why, the decrease of the COF is slow while the transfer film resists to the friction stress, but the decrease becomes rapid

when the transfer film breaks, and then the COF is more and more close to the COF of the virgin carbon surface.

The different steps of the wear mechanism that occurs during the friction of the CNTs grafted CFs were added on the friction curve for the Cat.1. First there is an alignment of the CNTs (1st friction cycles), then the formation of the transfer film. At around 600 cycles, the first cracks appears in the film, and then the film particles are gradually evacuated in less stressed areas. All this steps takes place also with the Cat.2, but in the 300 first cycles of friction. So the resistance of the CNTs grafted CFs in greater with the use of the Cat.1 than Cat.2. This result has also been highlighted under different normal load [4].

Study of the wettability of the CNTs with epoxy resin
Given that carbon fabric grafted with CNTs will necessarily suffer some friction damage before the manufacturing of composite, the CNTs will not be entangled at the surface but aligned and crushed on the surface. In this case, it is necessary to evaluate the wettability behavior of the used fabric with composite resin.

The resin used is epoxy and the results shows no impregnation difference between the surface no used and the used surface. So we can presume that the wear of the CNTs will not change the potential mechanical properties of composites.

CONCLUSION
This study enables us to highlight the behavior of the CNTs grafted CFs under friction stresses. When friction starts, CNTs are directly aligned and crushed on the surface. However it do not change the wettability behavior of the surface, which is a main thing for the manufacturing of composite. The catalyst, essential to the growth of CNTs, influences the time durability of the transfer film, and it appears that the use of the Cat.1 give the greatest friction resistance.

KEYWORDS
Carbon nanotubes (CNTs), carbon fibers (CFs), friction, wear

REFERENCES
[1] Donnet, J.-B., Pontier, Johnson M., Norman, D.T., Le Huu, T., Oulanti, H. "Method and systems for synthesis on nanoscale materials." US Patent 7833505 B2. 2010.
[2] Donnet, J.-B., Pontier, Johnson M., Norman, D.T., Le Huu, T., Oulanti, H. "Methods for production of carbon nanomaterials in the presence of a carbon black catalyst." US Patent 2011/0059006 A1. 2011.
[3] Guignier, C., Bueno, M.-A., Camillieri, B., Tourlonias, M., Durand, B. "Tribological behavior and wear of carbon nanotubes grafted on carbon fibres." *Composites Part A: Appl Sci Manuf*, 2015, 71: 168-75.
[4] Guignier, C., et al. "Tribological behavior and adhesion of carbon nanotubes grafted on carbon fibres". *Tribology International*, 2015.

Investigation of Flammability Behaviour of Woven/Glass Fabric Reinforced With Vinyl Ester Composites Used in Wind Turbines

Nazan Avgio Avcioğlu Kalebek, Tugba Ozturk
Gaziantep University, Fine Art Faculty, Textile and Fashion Design Department, Gaziantep, Turkey
tugbaozturk@gantep.edu.tr

Flame retardant (FR) fabrics are most profitable niche markets in the global textile complex. Most of the textile materials are flammable, therefore using flame retardant fibres, such as carbon, aramid and e-glass, to textile fabrics becomes necessary to assure humans safety under many circumstances. In this study, woven/glass fabric reinforced with vinyl ester resin are produced with different weight, structure and treated with vinyl ester resin in different volume ratio (% 1,3,5) for determining the flammability behaviour. These results show that fabric weight, structure and vinyl ester resin volume ratio have negative effect on improving flammability behaviour and char length of fabrics.

KEYWORDS: e-glass fabric, vinyl ester, composites, flammability.

INTRODUCTION
Textiles are traditionally an important part of the human life involving all types of building, such as homes, offices, hotels, and hospitals, as well as industrial systems, such as factories, dams, laboratories or electric power stations. In that respect, textiles serve three basic purposes; decoration, comfort and safety. More specifically, technical textiles are used for their functional properties rather than their aesthetic or decorative characteristics [1,5].

Flame retardant (FR) fabrics are most profitable niche markets in the global textile complex. Most of the textile materials are flammable, therefore using flame retardant fibers, such as carbon, aramid and e-glass, to textile fabrics becomes necessary to assure humans safety under many circumstances. Most recently established federal regulations on the flammability of the fabrics indicate that FR textiles will steadily increase in the near future. The increasing use of FR materials in industry has put lot of thrust on the scientific community to develop new polymer materials, FR chemicals, and fiber combinations to a wide range of end use applications [6,9].

EXPERIMENTAL APPROACH
Materials
In this study, woven/glass fabric (Table 1) reinforced with vinyl ester resin are produced with different weight, structure and treated with vinyl ester resin (Figure 1) in different volume ratio (% 1,3,5) for determining the flammability behavior.
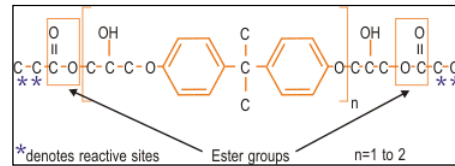

Figure 1: Chemical structure of vinyl ester resin

Table 1. Technical properties of composites

	Fabric Structure	Weight (g/m^2)	Thickness (mm)	Weight (g/m2)	Thickness (mm)
1		100+300	8.17	100+450	8.92
2	Plain	200+300	8.89	200+450	9.00
3		300+300	9.02	300+450	9.08
4		500+300	9.10	500+450	9.17
1		100+300	9.08	100+450	9.25
2	Twill	200+300	9.41	200+450	9.43
3		300+300	9.68	300+450	9.69
4		500+300	9.76	500+450	9.79

Methods
The vertical test method is used to measure flammability resistance of samples according to ASTM D6413-08 standard under controlled laboratory conditions (Table 2). The conditions of the fabrics and environment were on a average temperature ranged between 20 ℃ and 22 ℃, and relative humidity (RH) ranged between 65 and 67 %. This test method determines the response of textiles to a standard ignition source, deriving measurement values for after flame time and afterglow time.

Table 2. Vertical Flammability Test Adjustment

Gas Mixture	99 % pure methane
Gas Pressure (kPa)	17.2±1.7
Flame Height (mm)	3
Timer- Test Flame Duration (s)	12

In addition, the e-glass fabrics are examined by an optical microscope (Leica DM 1000 equipped with digital image analysis software). Figure 2 shows the top views of the fabrics.
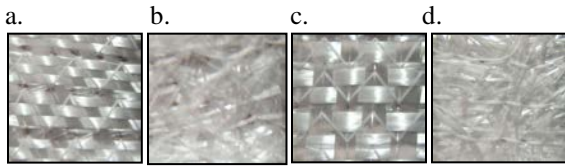
Figure 2: Sample of composites (a. 300+300 front, b. 300+300 back, c. 500+450 front, d. 500+450 back)

RESULTS AND DISCUSSION

Flammability tests were carried out machine direction (MD) and cross direction (CD), respectively. In Table 4 and 5, selected flammability resistance of the composites tested in this study is displaced. These tables reveal that, e-glass felt reinforced vinyl ester resin composites in the direction of MD are slightly higher than in the direction of CD. According to the results of the tests for all thicknesses, FR chemicals played positive effects on flammability resistance and char length of composite fabrics.

Table 3. Flammability Resistance Test Results (MD)

Weight (g/m²) / FR (%)	After flame (s)			Afterglow (s)			Char length (mm)		
	1	3	5	1	3	5	1	3	5
100+300	5.5	4.0	3.1	a	a	a	3.2	2.7	1.5
200+300	4.0	3.3	2.0	a	a	a	2.4	1.5	1.0
300+300	3.1	2.4	1.6	a	a	a	1.0	1.1	0.7

* a=no burning is occurred; b=partial combustion occurred; c=fabric is completely burned.

Table 4. Flammability Resistance Test Results (CD)

Weight (g/m²) / FR (%)	After flame (s)			Afterglow (s)			Char length (mm)		
	1	3	5	1	3	5	1	3	5
100+450	6.8	2.2	1.8	1.0	0.8	a	2.5	1.3	1.1
200+450	3.4	1.8	1.0	1.8	0.7	a	2.0	1.0	0.8
300+450	2.6	1.1	1.0	2.4	0.5	a	1.2	1.0	0.6

CONCLUSION

The results obtained from this study can be summarized as follows: These results show that while fabric weight, structure and vinyl ester resin volume ratio have negative effect on improving flammability behavior and char length of fabrics, FR has positive effect.

FUTURE WORK

Further studies have to be carried out to ascertain the mechanical and physical properties of the composites made of glass fibers reinforced with epoxy and/or polyester resin esters.

REFERENCES

[1] D. Özdemir, H.D. Mecit, N. Seventekin, T. Öktem. "Glass Fibers." *Tekstil ve Konfeksiyon*, 2006, 1: 281-86.

[2] S.M. Mostashari, S.Z. Mostashari. "Verification Concerning the Relative Superiority of a Cellulosic Fabric with Regard to Polyester in Terms of Flammability." *Polymer-Plastics Technology and Engineering*, 2008, 47: 313-17.

[3] J.G. Allen, H.M. Stapleton, J. Vallarino, E. McNelly, M.D. McClean, S.J. Harrad, C.B. Rauert, J.D. Spengler. Exposure to Flame Retardant Chemicals on Commercial Airplanes." *Environmental Health,* 2013, 12: 2-12.

[4] C.D. Papaspyrides, S. Pavlidou, S.N. Vouyiouka. "Development of Advanced Textile Materials: Natural Fibre Composites, Anti-Microbial, and Flame-Retardant Fabrics." *Materials: Design and Applications*, 2009, 223: 91-102.

[5] B. Patel, H.S. Patel. "Synthesis, Characterization, and Glass Reinforcement of Flame Retardant Acrylated Poly (Ester-Amide) and Flame Retardant Poly (Ester-Imide) Resins Based on Brominated Epoxy Resin." *International Journal of Polymeric Materials and Polymeric Biomaterials*, 2013, 62: 455-61.

[6] R.I. Shekar, T.M. Kotresh, P.M. Damodhara Rao, M.N. Kumar, S. Rahman. "Flammability Behavior of Fiber-Fiber Hybrid Fabrics and Composites." *Journal of Applied Polymer Science*, 2011, 122: 2295-2301.

[7] Z. Shi, R. Fu, S. Agathopoulos, X. Gu, W. Zhao. "Thermal conductivity and fire resistance of epoxy molding compounds filled with Si_3N_4 and $Al(OH)_3$." *Materials and Design*, 2012, 34: 820-824.

[8] X. Chen, S. Zhang, G. Xu, X. Zhu, W. Liu. "Mechanical, Flammability and Crystallization Behavior of Polypropylene composites Reinforced by Aramid Fibers." *Journal of Applied Polymer Science*, 2012, 125: 1166-75.

[9] L. Yusriah, M. Mariatti, A.A. Bakar. "Mechanical Properties of Particulate-Filler/Woven-Glass-Fabric-Filled Vinyl Ester Composites." *Journal of Vinyl & Additive Technology,* 2010, 16: 98-104.

Nanofibers by Electrospinning or Other Methods

Titanium-Magnesium Oxide Hybrid Nanofibers

Yakup Aykut

Uludağ University, Engineering Faculty, Textile Engineering Department, Gorukle, Bursa, Turkey

aykut@uludag.edu.tr

INTRODUCTION

Nanofibrous form of ceramic materials have been produced and used for photocatalytic applications because specific surface are increase tremendously as a result of production the material in nanoscale [1-2]. Magnesium loading in TiO_2 nanofibers is another research interest since microstructural phases are changed and hence photocatalytic properties of TiO_2 are enhanced [3-4]. In this study, effects of Mg^{2+} doping on the morphology and microstructural evaluation of electrospun titanium magnesium oxide hybrid nanofibers were examined by controlling Ti/Mg molar ratios. Four different calcinations temperatures 400, 500, 650 and 800 ^oC were performed to evaluate the effect of phases. Morphology of the calcined nanofibers was analyzed with Scanning electron microscopy. Crystal phase formations and transformations of the nanofibers were investigated with X-ray diffractometer and Raman spectra.

EXPERIMENTAL

Electrospun Ti (IV) isopropoxide/Magnesium Acetate/PVP composite nanofibers at different with MgAc contents respect to Ti (IV) isopropoxide of 0, 15, 30, 50 wt% were calcined at 400, 500, 650 and 800 ^oC in air environment and their SEM and XRD characterization were conducted
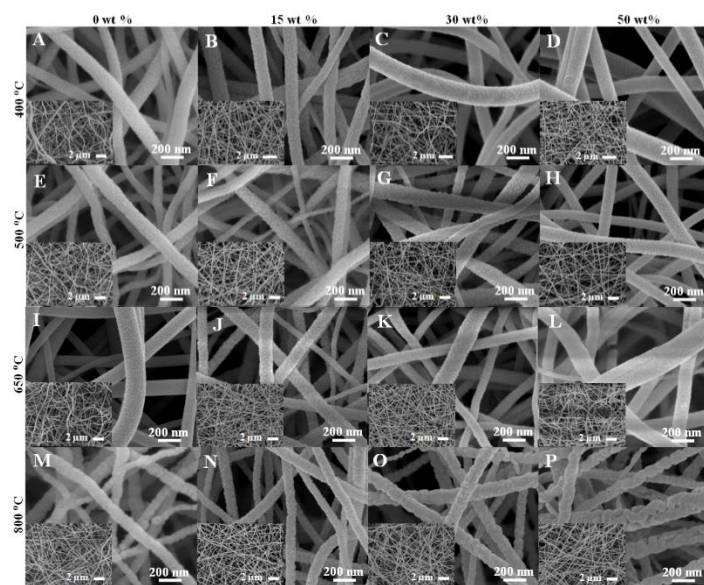

Figure 1. Scanning Electron Micrographs of calcined Ti (IV) isopropoxide/Magnesium Acetate/PVP composite nanofibers at different calcination temperature and with MgAc contents respect to Ti (IV) isopropoxide: A) 400°C, 0 wt%; B) 400°C, 15 wt%,; C)400°C, 30 wt%; and, D) 400°C, 50 wt%, E) 500°C, 0 wt%; F) 500°C, 15 wt%,; G)500°C, 30 wt%; and, H) 500°C, 50 wt%, I) 650°C, 0 wt%; J) 650°C, 15 wt%,; K) 650°C, 30 wt%; and, L) 650°C, 50 wt%, M) 800°C, 0 wt%; N) 800°C, 15 wt%,; O)800°C, 30 wt%; and, P) 800°C, 50 wt%.

RESULTS AND DISCUSSION

Morphological and surface analysis of calcined titanium magnesium oxide hybrid nanofibers performed with SEM and the images are given in Figure 1A- 1D (for 400°C), Figure 1E- 1H (for 500°C), Figure 1I- 1L (for 650°C), and Figure 1M- 1P (for 800°C).

As seen from the SEM images, surface of the calcined nanofibers rough as a result of removal of organic species and conversion of precursors into ceramic nanofibers. Outcropping on the nanofibers surfaces are indicative of small individual crystals that have been growth individually or transformed from another crystals in the nanofibers. Porous structure on the nanofibers is seen at the samples calcined at 800 ^oC samples especially at 50 wt% ratio sample. To better investigate these crystals, X-ray diffraction and Raman spectra analyses were conducted for all calcined samples.
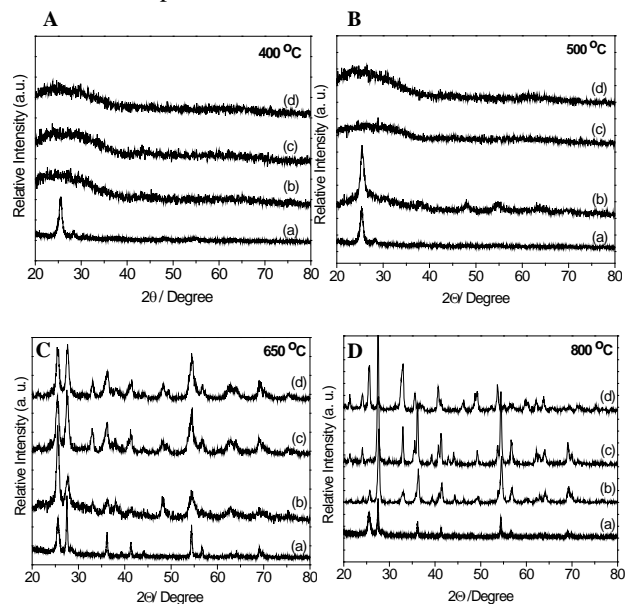

Figure 2. X-Ray Diffraction patterns of TiO_2/MgO mixed nanofibers calcined at A)400°C, B)500°C, C)650°C, and D)800°C, with MgAc contents respect to Ti (IV) isopropoxide in the precursor Ti (IV) isopropoxide/Magnesium Acetate/PVP NF: a) 0 wt%; b) 15 wt%,; c) 30 wt%; and, d) 50 wt%.

Microstructural investigations of calcined nanofibers were performed with wide angle X-ray diffraction technique and the results are demonstrated in Figure 2A (for 400°C), Figure 2B (for 500°C), Figure 2C (for 650°C), and Figure 2D (for 800°C).

The results revealed that at 400°C calcination temperature no crystallized magnesium phase are present and only anatase crystals TiO_2 forms. Even addition of magnesium prevents anatase TiO_2 phase formation at 400 and 500°C. At

500°C Mg free and 15 wt% Mg added sample shows anatase phase but increasing Mg content again causes the prevention of anatase crystal formation. As seen from the diffraction peaks anatase TiO_2 crystal peaks are seen at 2θ ~25.5° and 27.4° which correspond to the (101) and (002) crystal planes and rutile peaks at 2θ ~ 27.7°, 36.1°, 41.2°, 43.9°, 54.4° corresponding to (110), (101), (111), (210), and (211) crystal planes of TiO_2 [5]. With increasing calcination temperature to 650 and 800 °C rutile phases of TiO_2 are form and some anatase crystals transform to rutile phase [5].

To further investigate the microstructural properties of titanium magnesium oxide hybrid nanofibers, Raman spectra were performed and the results are demonstrated in Figure 3.
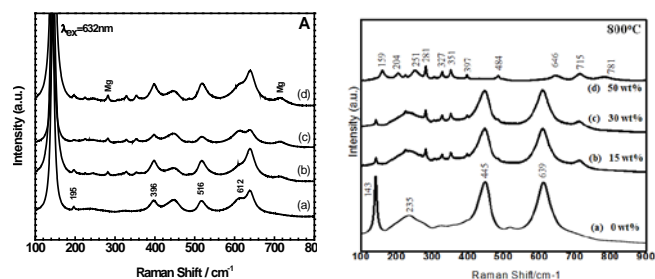

Figure 3. Raman Spectra of TiO_2/MgO mixed nanofibers calcined at A)650°C, and, B)800°C, with different MgAc contents respect to Ti (IV) isopropoxide in the precursor Ti (IV) isopropoxide/Magnesium Acetate/PVP NF: a) 0 wt%; b) 15 wt%,; c) 30 wt%; and, d) 50 wt%.

Raman spectra conducted for 650 and 800 °C calcined samples. The samples calcined at 650°C, weak rutile crystal peaks of TiO_2 are observed at the characteristic Raman bands at 143, 235, 445, and 612 cm[-1][5]. At a calcinations temperature of 800°C, the intensities of the peaks representing the anatase phase in the fibers decreases (395 and 639 cm^{-1}), and the intensities of rutile peaks at 445 and

612 cm^{-1} become stronger as a result of formation and phase transformation from anatase to rutile in the structure of titanium magnesium oxide hybrid nanofibrous system. Increasing Mg content, the intensities of rutile peaks decrease at 800 sample °C event disappeared in 50wt% calcined sample.

CONCLUSION

Scanning electron microscopy, X-Ray diffraction and Raman Spectral characterization of titanium magnesium oxide hybrid with different MgAc contents respect to Ti (IV) isopropoxide in the precursor Ti (IV) isopropoxide/Magnesium Acetate/PVP nanofibers (0, 15, 30 and50 wt%) at four different calcination temperature 400, 500, 650, 800 °C have been conducted. The results reveal that magnesium addition prevents crystal formation at lower calcination temperatures. Only anatase crystals of TiO_2 are forms at low temperatures and rutile crystals are present with increasing calcination temperatures. Such materials can be potentially used for photocatalytic applications.

REFERENCES

1. Li, D., Xia, Y. *Nano Letters*, 2003, 3: 555-60.
2. Shao, C., Guan, H., Liu, Y., Mu, R. *Journal of Materials Science*, 2006, 41(12): 3821-24.
3. Lopez, T., Hernandez, J., Gomez, R. *Langmuir*, 1999, 15: 5689-93.
4. Bandara, J., Hadapangoda, C.C., Jayasekera, W.G. *Applied Catalysis B: Environmental*, 50 (2): 83-88.
5. Aykut, Y., Saquing, C., Pourdeyhimi, B., Parsons, G.N., Khan, S.A. *ACS Applied Materials and Interfaces*, 2012, 4 (8): 3837-45.

Polyimide Nanofibers/Carbon Woven Fabrics Hybrid Hot Gas Filter

Qiuran Jiang[1,2,3], Qiannan Wang[2], Yuying Bai[2], Yiping Qiu[1,2,3]
[1]Key Laboratory of Textile Technology, Ministry of Education, Shanghai, China
[2]Department of Technical Textiles, College of Textiles, Donghua University, Shanghai, China
[3]Key laboratory of Science & Technology of Eco-Textiles, Ministry of Education, Shanghai, China
jj@dhu.edu.cn

OBJECTIVE

In this study, a multi-scale fibrous filter combined with polyimide (PI) nanofibers as the filtration layer and the carbon woven fabrics as the supporting layer was developed for potential hot gas filtration with a high filtration efficiency to remove particles around PM 2.5.

INTRODUCTION

The demand for hot gas filtration is driving by serious air pollution resulted from a wide variety of blooming industries, such as thermal power regeneration, metal refining/recycling, and biomass/coal gasification [1]. The design of filters is a compromise between filtration efficiency, pressure drop and the cost of manufacturing and operation. Comparing to the conventional cyclones and electrostatic precipitators, bag type dust collection is gaining increasing attention due to its high filtration efficiency and convenience in operation and maintenance [2]. Filter media are the key element for the bag type dust collection. The filter media for hot gas filtration should be able to withstand corrosive and high temperature atmosphere [3]. Moreover, to block particles smaller than PM 2.5, the filter media should possess small pore sizes with large surface areas [4]. Nanofiber mats with small fiber diameters and pores are more promising to serve as filter media due to their potential efficient blocking to small particles and an acceptable low pressure drop generated from the gas slip effect [4]. However, mats with a nanofibrous structure do not have sufficient mechanical properties for filtration, thus require for supporting materials. Polyimide show outstanding mechanical properties, thermal stability and inertness to solvent and radiation resistance [5]. In this study, multi-scale polyimide/carbon fibers hybrid filters were developed for hot gas filtration, which PI electrospun nanofibers served as the filtration layer and the carbon fabrics as the supporting layers.

APPROACH

The precursor of PI, poly(amic acid) (PAA) was synthesized from of pyromellitic dianhydride (PMDA) and 4,4'-oxydianiline (ODA) at a molar ratio of 1:1 in N, N-dimethylacetamide (DMAc), and obtained the stock PAA solution with a concentration of 20%. The spinning solutions were prepared by diluting of the stock PAA solution with DMAc to 12%, 14%, 16%, 17%, 18%. Electrospinning was carried out with a solution feeding speed at 0.2 ml/h and a gap distance of 20 cm at 11-14 kV. PAA fibers were collected onto the carbon woven fabrics fixed on the drum roller. The areal densities of PAA nanofiber membranes could be easily controlled by adjusting the deposition time. PAA/carbon hybrid filters were kept at 100, 200, 300 and 350 °C for 30 min at each temperature with a temperature elevation rate at 3 °C /min. The morphologies of the filters were observed under a scanning electron microscope (SEM) and the chemical components of the nanofibers were confirmed by their flourier transform infrared spectra (FTIR). The filtration performance of filters was evaluated by a TSI Model 8130 Automated Filter Tester with a continuous airflow fixed at 20 ± 2 L min^{-1}.

RESULTS AND DISCUSSION

Imidization of PAA has been confirmed by FTIR shown in Fig. 1. The PAA spectrum displayed absorption bands in the range of 3000–4000 cm^{-1}, which were attributed to stretching vibrations of O-H (in carboxyl group) and N-H (in amide group) in PAA. These bands were no longer identifiable in the PI spectrum.
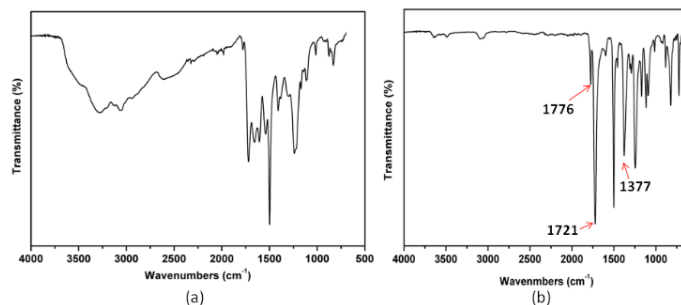

Figure 1. FTIR spectrum of PAA nanofiber mat (a) and PI nanofiber mat (b).

Even nanofibers with fiber diameters around 200 nm could be produced from the PAA solution at a concentration of 17%. After filtration, the dust cake of particulates around 0.3 µm could be generally formed on the top of polyimide filtration layer (Fig. 2(B)), while limited dusts were entrapped in the bulk of supporting layers (Fig. 2(A)). It was indicated that filtration layers composed with ultrafine fibers played the key role in removal of fine dusts other than supporting layers fabricated from regular fibers. The filtration efficiency, increasing with the formation of the cake layer, could be maintained above 95.0 % after 9 min and reached a maximum value of 99.4 %. This research proved that the multi-scale polyimide/carbon fibers hybrid filters possessed the potential to serve as filtration media in bag filters for hot gas filtration.
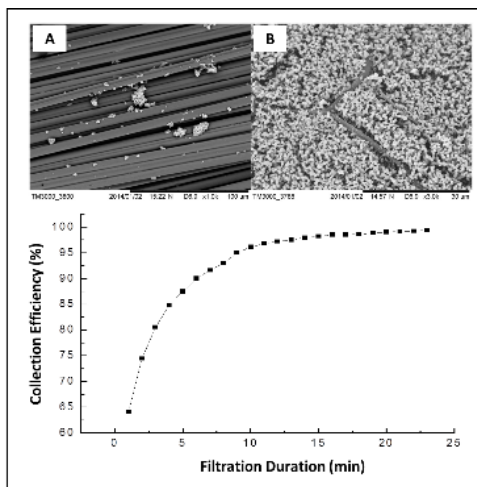
Figure 2. Morphologies of supporting layer (A) and dust cake accumulated on filtration layer (B) after filtration and filtration efficiency of the three layer hybrid filter.

CONCLUSION

Uniform PAA nanofibers around 200 nm in diameter could be produced from the solution at 17% concentration, and be imidized into PI nanofibers. The hybrid filter with PI nanofibers and carbon woven fabrics showed a high filtration efficiency at 99.4 %. The majority of particles were blocked by the PI nanofiber mat, which served as the main filtration layer.

FUTURE WORK

It is of our interest to investigate the filtration efficiency and pressure drop when PI nanofibers are obtained on different supporting materials and performs in a hot gas environment.

KEYWORDS

hot gas filtration, nanofiber, carbon fiber, polyimide

REFERENCES

[1] Finley, J. "Hot gas filtration: diesel—how prepared is the filtration industry?" *Filtration & Separation*, 2006, 43: 16-20.

[2] Tanabe, E.H., Barros, P.M., Rodrigues, K.B., Aguiar, M.L. "Experimental investigation of deposition and removal of particles during gas filtration with various fabric filters." *Separation and Purification Technology*, 2011, 80: 187-95.

[3] Lupión, M., Gutiérrez Ortiz, F.J., Navarrete, B., Cortés, V.J. "Assessment performance of high-temperature filtering elements." *Fuel*, 2010, 89: 848-54.

[4] Podgórski, A., Bałazy, A., Gradoń, L. "Application of nanofibers to improve the filtration efficiency of the most penetrating aerosol particles in fibrous filters." *Chemical Engineering Science*, 2006, 61: 6804-15.

[5] Lingaiah, S., Shivakumar, K. "Electrospun high temperature polyimide nanopaper." *European Polymer Journal*, 2013, 49: 2101-08.

Unconfined, Melt-edge Electrospinning for Scale-up

Qingqing Wang[1], Addison Randolph[2], Nagarajan Muthuraman Thoppey[3],
Jason R. Bochinski[4], Laura I. Clarke[4], Russell E. Gorga[3]

[1]School of Textiles & Clothing, Jiangnan University; [2]Biomedical Engineering, NC State University; [3]Fiber and Polymer Science Program, NC State University; [4]Department of Physics, NC State University
regorga@ncsu.edu

OBJECTIVE

The purpose of this work is to demonstrate melt electrospinning from an unconfined (needleless) system using conventional thermoplastics such as polyethylene and polypropylene.

INTRODUCTION

Thermoplastics can be processed by needle-based electrospinning in the melt phase, however this approach is notoriously unpopular due to persistent fundamentally detrimental system issues such as needle clogging and relatively large fiber size (due in part to difficulties in pumping viscous fluids at very low feed rates) [1] . However, despite such challenges, recently research efforts in melt electrospinning have been rapidly increasing, driven by the potential of creating fibers having enhanced mechanical properties, the ability to utilize of a wider range of materials, and most importantly, increasing awareness of the environmental impact of manufacturing, which motivates interest in limiting or eliminating solvent use in industrial scale fabrication processes. In this work, an unconfined spinning geometry, instead of a needle, is utilized where a strong electric field at the plate edge causes many parallel fiber-forming jets to spontaneously form on a sheet of molten polymer, and subsequently, electrospin a commercial polyethylene material creating meso-scale fibers.

APPROACH

The melt-electrospinning apparatus (Figure 1) consists of an aluminum source plate (14 × 5 × 0.5 cm with additional upturned (0.8 cm tall) ends on three sides) placed directly on a commercial hot plate (Fisher Scientific model 11-500-78H). The 1 cm region of the source plate closest to the collector tapers in thickness to an edge value of 0.03 cm, which is ultimately where the spinning occurs. The source plate is placed off-center in order that the tapered edge protrudes over the hot plate edge by 1 cm. A type J thermocouple (Omega) is pressed between two ceramic (1.5 × 1.4 × 0.5 cm) plates (bound together by four screws) and affixed to the source plate to monitor temperature. The opposite side of the source plate is connected to ground potential with a thick wire. The 20 × 30 cm isolated aluminum collector (covered with aluminum foil) situated 10 cm from the source plate is held at negative electric potential by a high voltage source (Glassman High Voltage Model FC60R2). The region between source and collector is only incidentally warmed via convection of ambient air from the source plate; it is not intentionally heated or temperature controlled.
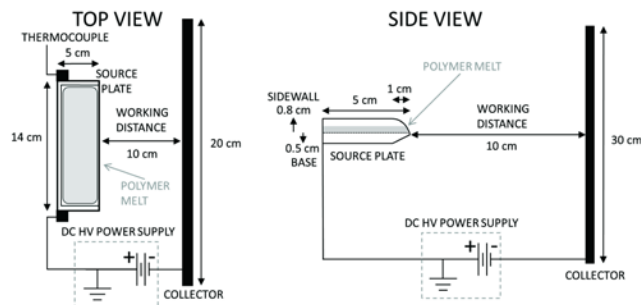

Figure 1. Schematic diagram of the experimental apparatus as viewed from above (top) and side. (Note: For clarity of viewing, hot plate not shown.)

RESULTS AND DISCUSSION

Unconfined melt electrospinning is demonstrated with three different polymer systems. Jet-to-jet spacing of ~5 mm is obtained in all cases (see Figure 2), which is generally much smaller than the possible site spacing when electrospinning from multiple confined source, e.g., an array of needles. Fundamental analysis shows the important physical parameters that control inter-jet spacing and flow rate. As in confined melt electrospinning, one of the most dominant effects influencing the process is the melt viscosity. Comparing results from PE at 170-190°C (40-60 °C above Tm) and PCL at 100 °C (40 °C above Tm), which have similar surface tension values (~37 mN/m and 26 mN/m, respectively), we observe that for the lower viscosity material system (PCL) produces the expected jet number and provides high throughput per jet with a lower resultant fiber diameter. For the higher viscosity polymer system (PE), the time to form or re-form perturbations and jets is longer, not all perturbations transition into fiber-forming jets, and the formed fibers have a larger diameter. However, electrospinning, with moderate quality fibers and significant throughput, is still readily achievable. The effect of shear thinning on flow rate is clearly demonstrated for PE, indicating that the strongest result of increased voltage is a decrease in effective viscosity: utilizing such an approach may be useful in spinning high quality fibers from innately high-viscosity melt systems. From a technological perspective, the fabrication of fibers of the same quality as in the needle approach but at a much higher throughput (up to 80 mg/min) with no possibility of nozzle clogging opens the door to significant-scale production of microstructures (and perhaps even nanostructures) from a wide variety of thermoplastic systems, even high viscosity melts which may not be suitable for needle electrospinning. From a fundamental perspective, these experiments increase our understanding of highly viscous fluids under the influence of a strong electric field.
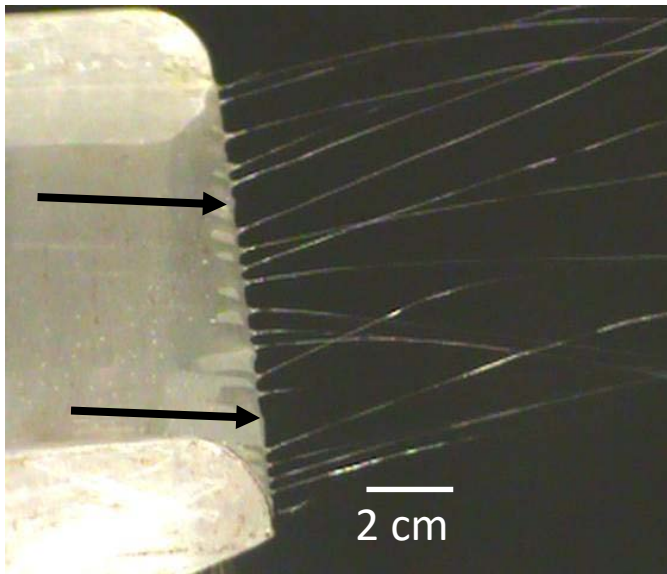
Figure 2. Image of electrospinning from a polymer melt coated source plate (PE at 170 °C, -45 kV) in steady state (i.e., after ~30 minutes). The black arrows indicate non-jetting perturbations.

CONCLUSION

Commercial grade polyethylene and polypropylene are melt electrospun from a thin film of unconfined molten polymer on a heated, electrically-grounded plate. Under the influence of an applied electric field, the melt spontaneously forms fingering perturbations at the plate edge which then evolve into emitting fiber-forming jets. Jet-to-jet spacing (~5 mm), which is dependent on the applied voltage amplitude, is in agreement with estimates from a simple theoretical treatment. The broad applicability of the approach is verified by spinning a third, dissimilar polymer - polycaprolactone. In both cases, the fabricated fibers are similar in quality to those obtained under needle melt electrospinning; however for this method, there are no nozzles to clog and an enhanced production rate up to 80 mg/minute is achieved from approximately 20-25 simultaneous parallel jets. The process of jet formation, effective flow rates, cone-jet diameters, as well as limits on jet density and differences with polymer type are compared with theoretical models. This particular approach allows facile, high throughput micro- and nano-fiber formation from a wide variety of thermoplastics and other high viscosity fluids without the use of solvents or the persistent issues of clogging and pumping that hamper traditional methods, resulting in mechanically strong meso-scale fibers highly desirable for industrial applications.

Main points:
- Melt electrospinning of thermoplastics (polyethylene, polypropylene and polycaprolactone) from an unconfined plate edge;
- Multiple jets spun simultaneously with 5 mm jet spacing with fiber diameters ~ 1 mm;
- Approach allows high throughput meso-fiber production without the use of a solvent or persistent issues of clogging a small orifice.

REFERENCE
Hutmacher, D.W., Dalton, P.D. *Melt Electrospinning Chem.-Asian J*, 2011, 6: 44-56.

Exploring the Potential of Nanofibers in Gas and Water Filtration, Including a Gateway to Mass Production

Xiao-Hong Qin

Shanghai Key Laboratory of Advanced Micro & Nano Textile Materials,
College of Textiles, Donghua University, Shanghai, China
xhqin@dhu.edu.cn

NANOFIBERS IN WATER & GAS FILTRATION

The paper explores the application of nanotechnology in water and gas decontamination. These ultra-thin materials offer a huge surface area on a comparatively tiny volume and thus potential of economically dealing with a range of pollutants right from the usual indoor air particles such as microorganisms, dust, and allergens to dangerously toxic agents. Air devoid of particulates is of critical importance in a number of areas including chemical, foods and beverages, pharmaceuticals, and electronic assembling industries among others. In addition, clean air and water are part and parcel of the well-being of earth's inhabitants. Our research group is actively pursuing the fabrication of nanofibers via different methods and looking at nanotechnology in general as a remedy to serious problems associated with air and water contamination; a result of aggressive industrialization, research and careless disposal that is becoming a problem to urban dwellers, water dwellers and users[1]. Application of nanofiber membranes for this purpose boasts of quite a number of advantages over traditional water purification methods such as scalability, low power consumption, and the non-usage of chemicals. During the usage of conventional water filters, membrane fouling by microorganisms and heavy metals is one of the major problems faced.

surface functionalization through blending, grafting, coating, and interfacial polymerization a line that is being pursued to tackle intense biofouling as experienced in the conventional water filters. Besides this, nonwoven webs of fibers formed via electrospinning possess nano-scale pore sizes, high and controllable porosity, high specific surface areas, and extreme flexibility with regard to the materials used.

MASS PRODUCTION OF NANOFIBERS

One of the key stumbling blocks to the commercial application of this technology has been failure to have a sustainable and economically viable mass production procedure. However, at Donghua University we have developed a cutting edge free surface electrospinning technology[2] aimed at efficient, low energy based high through put intended to transform the conventional needle based approach into a multiple jet simultaneous output. This needless setup has a stepped pyramid-shaped spinneret as the electrospinning operator. This works on a principle that the free surface edges influence the generation of an electric field gradient that in turn enables the ejection of multiples jets on the surface. Also, the setup allows for the excess solution to flow back into the solution.
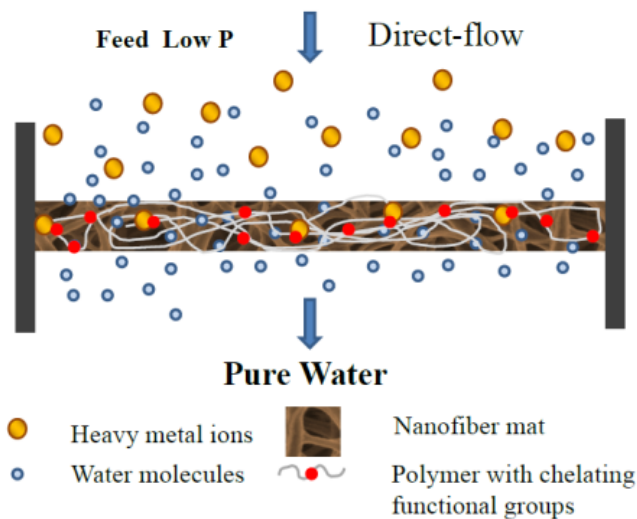

Figure 1: Nanofiber-based adsorptive composite membrane.

Nanoscale materials can display dramatically different physical and chemical properties from their bulk counterparts with radically improved specific surface areas, significant increases in surface reactivity, and tunable energy gaps and electronic structures providing a recipe for
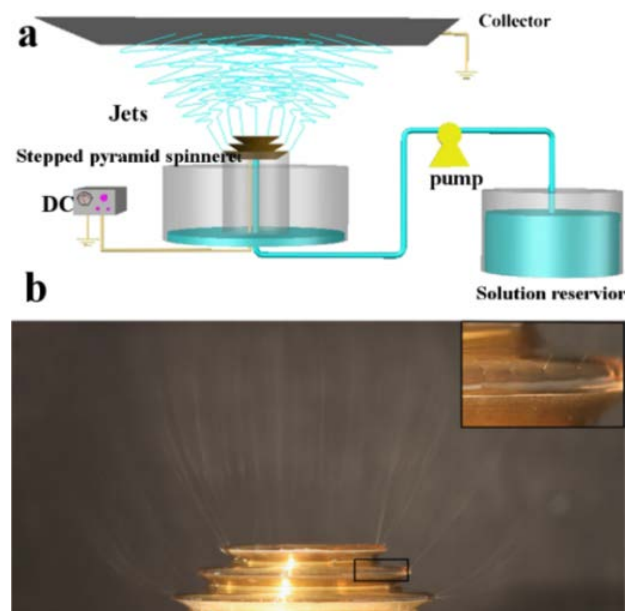

Figure 2: (a) An electrospinning apparatus setup using a stepped pyramid spinneret. (b) Picture of the actual process ongoing with the inset showing the magnified jets. (Courtesy of Prof. XiaoHong Qin Donghua University)[2].

REFERENCES

1. Ramakrishna, S., et al. "Science and engineering of electrospun nanofibers for advances in clean energy, water filtration, and regenerative medicine." *Journal of Materials Science*, 2010. 45(23): 6283-312.

2. Jiang, G., Zhang, S., Qin, X. "High throughput of quality nanofibers via one stepped pyramid-shaped spinneret." *Materials Letters*, 2013, 106: 56-58.

Increasing Surface Available Biotin and Improving Water Stability of PLA/PLA-b-PEG Nanofibers

Larissa M. Shepherd[1], Edurne Gonzalez[1], Laura Saunders[2], Esther Chen[3], Margaret W. Frey[1]
[1]Department of Fiber Science & Apparel Design, Cornell University, Ithaca, NY; [2]Department of Chemical and Biological Engineering, University at Buffalo, Buffalo, NY; [3]Department of Biomedical Engineering, Cornell University, Ithaca, NY
lb468@cornell.edu

STATEMENT OF PURPOSE

In this work we use the Avidin/Biotin complex and the thermodynamics of polymer/polymer phase separation to develop selective binding enabled nanofibers. This work lays the foundation to incorporate antibodies into poly(lactic acid), (PLA)/PLA-b-poly(ethylene glycol), (PEG) electrospun fibers as a means of selective contamination detection.

INTRODUCTION

Nanofibers tailored to be hydrophilic, non-water soluble, and functionalized at the fiber's surface can be used for biosensor applications. Nanofibers are an attractive candidate for biosensors as they have a high surface area to volume ratio and porous structure. (Li et al., Senecal et al., Luo et al.)

Li et al. incorporated biotin into PLA nanofibers, and was able to detect a non-linear relationship between the amount of biotin added to the solution and the amount of biotin at the fiber's surface. (Li et al.) In this study we investigate the effect of adding block copolymers of PLA-b-PEG along with biotin in the electrospinning dopes as a means increase the hydrophilicity of the fiber and increase the biotin available at the fiber's surface. We also present the first study of the stability of these fibers in water over time.

Previously, PLA and copolymers with varying block lengths of PLA-b-PEG were electrospun at varying weight percent (wt %) PEG in the final fiber. The final properties (i.e. water uptake, fiber diameter, and amount of PEG reaching the fiber's surface) of fibers was a function of block length and wt % of PEG. Compared to PLA fibers, a 1,300 % increase in water wicking was achieved for commercially bought copolymer PLA1000-b-PEG5000 at 12 wt % of PEG in the final fiber. This copolymer resulted in the greatest amount of PEG at the fiber's surface. (Buttaro et al.)

RESULTS AND DISCUSSION

We synthesized copolymers of PLA730-b-PEG5000 and electrospun them using a modified apparatus (Buttaro et al.) at 12 wt % PEG in the final fiber; previously found to be the optimum copolymer and wt % PEG for maximum water uptake. By comparing PLA and PLA/PLA-b-PEG nanofibers at 0, 5, 10, and 18 wt % biotin in the final fiber composition, we showed that the copolymer is critical to increasing surface functionalization.

Using a Pierce™ Biotin Quantitation Kit from ThermoScientific, we reconstituted HABA/Avidin solution to be analyzed using UV-Vis spectrophotometry. By measuring the change in absorbance at 500 nm between the control solution and the solution post fiber introduction we are able to calculate the amount of biotin per gram of fiber

from Equation 1 where A^0_{500} is the absorbance of the solution prior to the addition of nanofiber, A_{500} is the absorbance of the solution post nanofiber exposure, Mw_{biotin} is the molecular weight of the biotin (244.3 g/mol), V is the volume of the solution (L), b is the cuvette path length (1 cm) and ε is the extinction coefficient of the HABA/Avidin complex at 500 nm (3.4×10^{10} L/(mol cm)).

$$surface\ available\ biotin\ (mg\ biotin/g\ fiber) = (A^0_{500} - A_{500}) \left(\frac{Mw_{biotin}V}{\varepsilon bW}\right) \qquad \text{Equation 1}$$

At 5, 10, and 18 wt % biotin, fibers containing copolymer have more biotin available at the fiber's surface (Figure 1). (González et al.) At 18 wt % biotin there is a 506 % increase of biotin available at the surface for fibers containing PLA-b-PEG compared to PLA fibers. While PLA/PLA-b-PEG results in a more hydrophilic fiber than PLA fibers, the increase in biotin at the fiber's surface is not attributed to the hydrophilic nature. By adding a surfactant (Tween 20) to PLA nanofibers, there was no significant increase in biotin at the fibers surface (Li et al.), therefore the PLA-b-PEG merely aids in the phase separation of biotin to the fiber's surface.
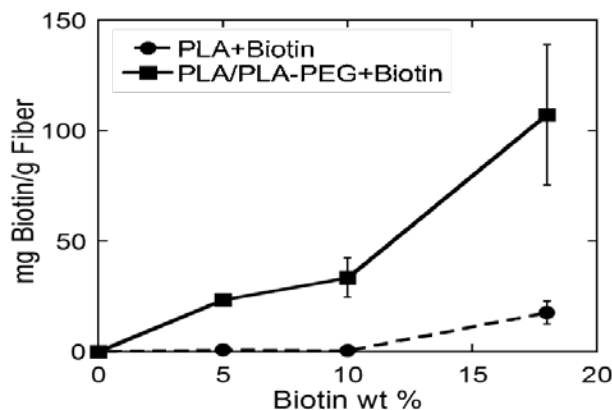

Figure 1. Available biotin at the fiber's surface for fibers containing 0, 5, 10, and 18 wt % biotin. (González et al.)

Samples were then immersed in DI water for either one day or seven days to determine the water stability of fibers. Samples were weighed prior to exposure to water, and re-weighed post exposure after they were dried in a vacuum oven for 24 hours (Figure 2) (González et al.). The weight lost after the first day is attributed to biotin, as PLA/PLA-b-PEG fibers containing no biotin had little to no weight loss after one day. The weight loss after one week, however, is due to both biotin and PLA-b-PEG leaching into the aqueous phase.

Fabrics containing 18wt% biotin were again analyzed using UV-Vis after water stability tests. PLA fibers after one day had an increase of biotin at the fiber's surface due to migration of the biotin, while PLA/PLA-b-PEG samples had decreased to approximately no biotin at the surface. After seven days there was approximately no biotin at the fiber's surface for PLA or PLA/PLA-b-PEG fibers.
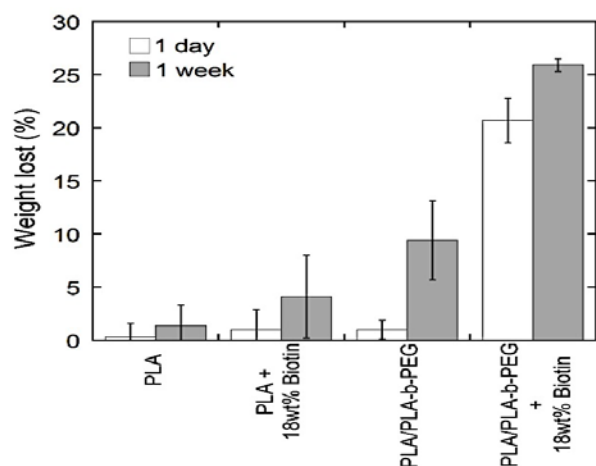

Figure 2. Water stability was determined by the amount of weight lost by the control electrospun fibers and fibers containing 18wt% of biotin when immersed in DI water for one day and one week. (González et al.)

CONCLUSION
By incorporating PLA-b-PEG copolymers with biotin into PLA nanofibers we are able to increase the amount of biotin at the surface of the fibers by over 500 % compared to PLA fibers with biotin. The biotin itself is not stable in aqueous environments. PLA-b-PEG is more stable than biotin, however, it too eventually migrates to the aqueous phase.

FUTURE WORK
As biotin is a small molecule, it readily migrates into aqueous solutions to which it is exposed. When used in microfluidic channels with HABA/Avidin, we observed the color change from orange to yellow, indicating there is biotin at the surface (Figure 3). The color change is not instantaneous, however, leaving the collection vial orange for a short time prior to turning yellow.
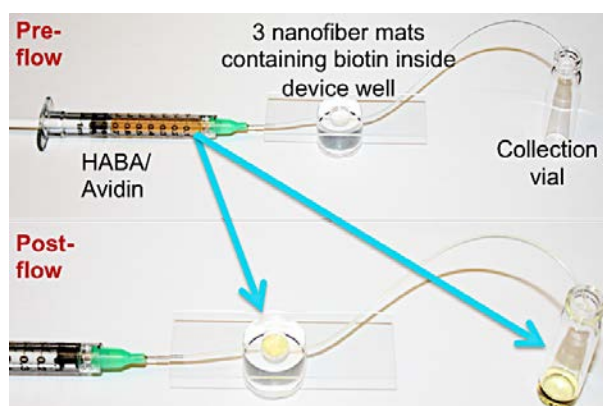

Figure 3. (Top) HABA/Avidin mixture pre-flow through 12 wt % PEG from PLA730PEG5000 with10 wt % Biotin in the final fiber. (Bottom) Post flow of HABA/Avidn through fiber mats, and change in color observed at the collection vial.

Future work includes minimizing the migration of biotin so that, when samples are used for detection, leaching is not a source of error in measurements. In order to find the appropriate length where copolymers do not migrate to solution, we are tailoring the block lengths of the copolymers added to electrospinning dopes. After tailoring the length, biotin will be attached to the copolymer. Studies to determine the amount of available biotin at the fibers surface when attached to the copolymer will be performed.

REFERENCES
Buttaro, Larissa M., et al. "Phase Separation to Create Hydrophilic yet Non-Water Soluble Pla/Pla-B-Peg Fibers Via Electrospinning." *Journal of Applied Polymer Science,* 2014, 131.19.

González, Edurne, et al. "Surface Functional Poly (Lactic Acid) Electrospun Nanofibers for Biosensor Applications." *Materials,* 2016, 9.1: 47.

Li, D.P., et al. "Electrospun Polylactic Acid Nanofiber Membranes as Substrates for Biosensor Assemblies." *Journal of Membrane Science,* 2006, 279.1-2: 354-63.

Li, Dapeng, et al. "Availability of Biotin Incorporated in Electrospun Pla Fibers for Streptavidin Binding." *Polymer,* 2007, 48.21: 6340-47.

Luo, Yilun, et al. "Surface Functionalization of Electrospun Nanofibers for Detecting E. Coli O157:H7 and Bvdv Cells in a Direct-Charge Transfer Biosensor." *Biosensors & Bioelectronics*, 2010, 26.4: 1612-17.

Senecal, Andre, et al. "Development of Functional Nanofibrous Membrane Assemblies Towards Biological Sensing." *Reactive & Functional Polymers*, 2008, 68.10: 1429-34.

Piezoelectric Properties of Natural Polymer Electrospun Fibers

Tatyana D. Huseynova, Prashant Chandrasekaran, Xin Xu, Wan Shih, Wei Shih, Lin Han, Caroline L. Schauer
Drexel University, Philadelphia, Pennsylvania
cschauer@coe.drexel.edu

STATEMENT OF PURPOSE

Naturally occurring piezoelectricity has focused mainly on ceramic materials. However, many biological systems have been found to use piezoelectricity such as bone, teeth and butterfly wings. Here we report the piezoelectricity of electrospun natural polymer, chitin. The nanofibers were measured both on a custom designed nanogenerator as well as using piezoelectric force microscopy.

INTRODUCTION

Materials that respond on a nanoscale level to both an electrical and/or mechanical stimulus are promising candidates for sensor applications [1]. Piezoelectrics are a unique class of materials that are able to respond to both electrical and mechanical stimulation by producing a voltage when mechanically deformed or conversely, mechanically deform in response to an applied voltage. Typically these materials are ceramics and are utilized in electronic, energy, sensor technology, and electromechanical applications. Polymers however can introduce an entirely new range of properties and functionalities to piezoelectric sensors due to their flexibility, versatility, and facile processing techniques. The two known piezoelectric polymers, polyvinylidene fluoride (PVDF) and its copolymer polyvinylidene fluoride trifluoroethylene (PVDF-TrFE) have been previously processed using the technique of electrospinning, which creates a network of non-woven fibers that possess very high surface area to volume ratios at the nanoscale [2-5].

Chitin occurs in nature as ordered nanofibers and is a major structural component in shrimp shells, exoskeleton of crabs and insect cuticles. Its popularity in the research field is attributed to the physiochemical properties as well as biocompatibility and biodegradability in nature. The piezoelectric nature of chitin is currently not well understood. For example, the butterfly wing, whose major component is chitin, does not have ceramics but has been identified as piezoelectric.

APPROACH

Pure chitin aligned and random nanofibers are electrospun from hexafluoroisopropanol (HFIP). A 1.55 wt/v% solution of chitin in HFIP is spun at a voltage of 17kV, distance of 10 cm and pump rate of 1mL/h.

RESULTS AND DISCUSSION

As seen in Figure 1, the nanofibers are electrospun aligned or random depending on the collector used.
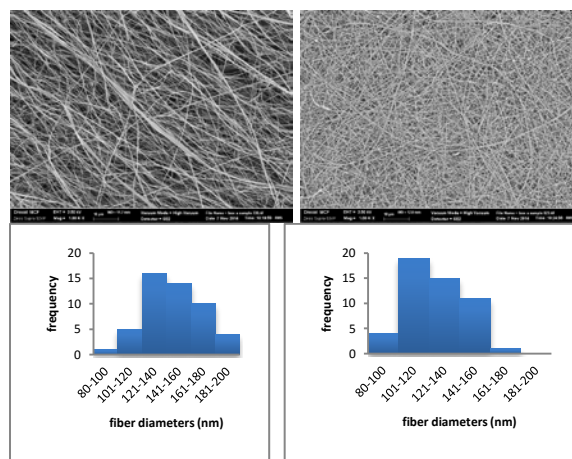

Figure 1: SEM images of aligned and random chitin fibers electrospun from HFIP. Histogram of average diameters for aligned nanofibers (130 nm average) and random (115 nm average).

The mechanical properties of aligned *vs.* random nanofibers as shown in Figure 2 are statistically different in the chitin samples. Tensile tests were performed in triplicate on an Instron.
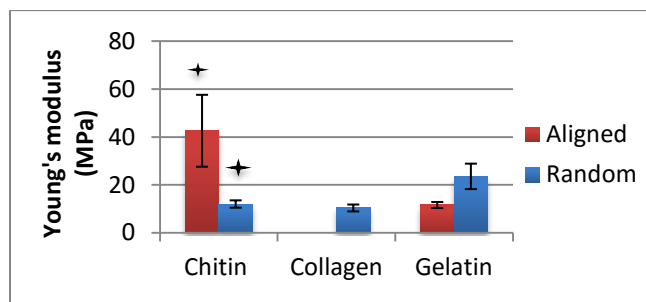

Figure 2: Tensile testing of biopolymer nanofibers in both the aligned and random formation. The stars indicate statistical difference with $p < 0.05$. Values presented are avg. mean, standard error, n = 3 samples.

Using the designed nanogenerator, the nanofibers are placed between two electrodes and a cantilever is used to control the force displacement. Figure 3 identifies the piezoelectric response of the aligned and random natural polymer nanofibers. The green line indicates the bare nanogenerator's response.
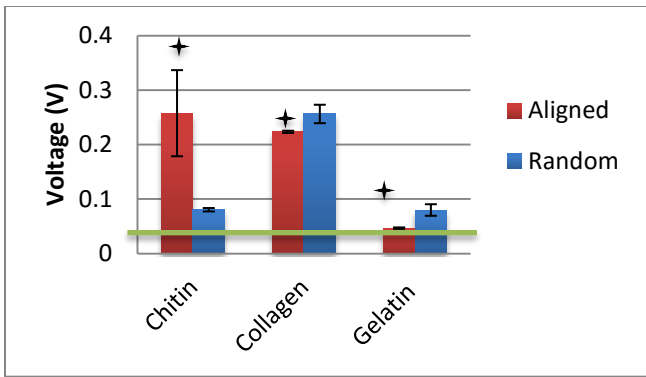
Figure 3: Piezoelectric testing on the nanogenerator of biopolymer nanofibers in both the aligned and random formation. The stars indicate statistical difference with p < 0.05. Values presented are avg. mean, standard error, n = 3 samples. The green line is the limit of detection of the nanogenerator.

Piezoelectric Force Microscopy Conducted piezoelectric force microscopy (PFM) testing supported the evidence gathered from the nanogenerator experiment. Single, aligned chitin fibers electrospun from HFIP were found to be piezoelectric when tested using the PFM function of a Bruker AFM (Bruker, Camarillo, CA) (Figure 4). The surface area, noise and energy transfer provided a stronger piezoelectric response from a single fiber than from the aligned group (Figure 5). Aligned fibers had a greater piezoresponse then the randomly deposited ones possibly due to the increase in polymer organization within the fibers.
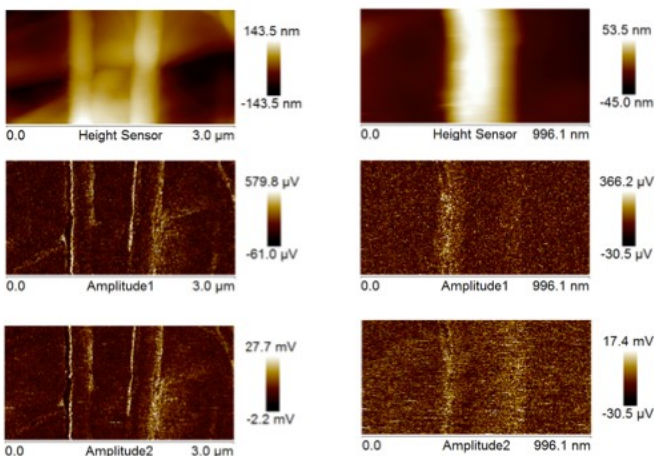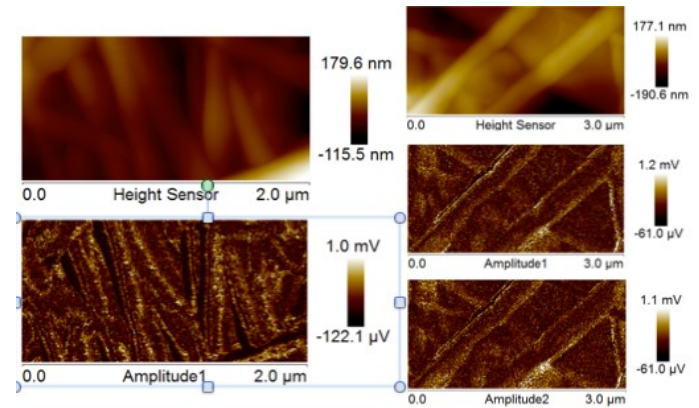

Figure 4: PFM on chitin aligned single fiber.

Figure 5: PFM on chitin aligned fibers.

FUTURE WORK
Fully understanding the internal organization of the chitin within the electrospun fibers will allow for controlled replication of the piezoelectricity. We are currently measuring the crystallinity of the chitin fibers to identify the packing arrangement within the fibers.

ACKNOWLEDGMENTS

REFERENCES
1. Miao, H., Srinivasan, K., Aksyuk, V. "A microelectromechanically controlled cavity optomechanical sensing system." *New Journal of Physics*, 2012, 14(7): 075015.
2. Cozza, E.S., Monticelli, O., Marsano, E., Cebe, P. "On the electrospinning of PVDF: influence of the experimental conditions on the nanofiber properties." *Polymer International,* 2013, 62(1): 41-48.
3. Dhakras, D., Borkar, V., Ogale, S., Jog, J. "Enhanced piezoresponse of electrospun PVDF mats with a touch of nickel chloride hexahydrate salt." *Nanoscale*, 2012, 4(3): 752-56.
4. Sharma, T., Langevine, J., Naik, S., Aroom, K., Gill, B., Zhang, J.X.J. "Aligned electrospun PVDF-TrFE nanofibers for flexible pressure sensors on catheter." In: *Solid-State Sensors, Actuators and Microsystems (TRANSDUCERS & EUROSENSORS XXVII), 2013 Transducers & Eurosensors XXVII: The 17th International Conference on 16-20 June 2013*: 422-25.
5. Persano, L., Dagdeviren, C., Su, Y., Zhang, Y., Girardo, S., Pisignano, D., Huang, Y., Rogers, J.A. "High performance piezoelectric devices based on aligned arrays of nanofibers of poly(vinylidenefluoride-co-trifluoroethylene)." *Nat Commun*, 2013, 4: 1633.

Thin Film, Nanofibous Composite Membranes Prepared by Electrospray Technique and Hot-pressing Treatment for Water Purification

Lingdi Shen[1], Xuefen Wang[1], Benjamin S. Hsiao[2]

[1]State Key Lab for Modification of Chemical Fibers and Polymer Materials, Donghua University, Shanghai, China
[2]Department of Chemistry, Stony Brook University, Stony Brook, New York, USA
wenqingshen_go@163.com; wangxf@dhu.edu.cn

INTRODUCTION

The shortage of clean, fresh water has lead to many serious problems which have attracted increasing worldwide attention. The composite filtration membranes with hierarchical structures have drawn much attention in water treatment due to their priorities of high rejection, good permeability and pressure resistance[1]. In recent years, electrospun nanofibrous mats have often been used as the substrate for the preparation of the thin film nanofibrous composite (TFNC) membrane due to their excellent advantages including high surface area, high porosity, area-to-volume and length-to-diameter ratios, interconnected porous structure and so on[2]. Surface coating is a very common and simple way for the barrier layer preparation[2,3]. However, easy penetration of the coating solution into the highly porous nanofibrous substrate is hardly avoided which results in a much thicker barrier layer. To solve these problems, our group proposed a novel route to fabricate ultra-thin barrier layer on nanofibrous substrate by electrospraying hydrophilic polymer nanobeads combined with hot pressing treatment as illustrated in Figure 1. The resultant composite membranes show excellent nanofiltration or ultrafiltration performance in different wastewater treatment systems.

Figure 1: Illustration of the fabrication process for TFNC membrane based on PAN nanofibrous substrate and hydrophilic barrier layer.

PVA/PAN TFNC Membrane Prepared by Electrospray Technique and Hot-pressing Treatment

Inspired by conventional powder coating technology[4], a simple and controllable fabrication process was proposed to prepare the composite membranes containing poly(vinyl alcohol) (PVA) barrier layer and polyacrylonitrile (PAN) nanofibrous substrate[5].

PVA nanobeads were electrosprayed onto the electrospun PAN substrate. PVA top layer was moistened by absorbing moisture in a moistener with humidity of ~90% and then sandwich heated by two hot plates to melt and to be pressed into an integrated layer. The moistened electrosprayed PVA nanobeads could be easily melted or softened to be pressed imperceptibly into an integrated barrier film on the supporting layer at a certain temperature. Finally, the as-prepared PVA/PAN composites were crosslinked by glutaraldehyde (GA) in water/acetone solution.
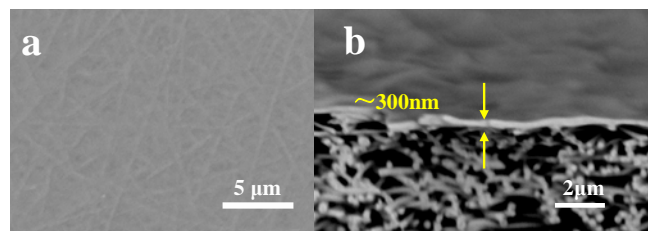

Figure 2: Surface (a) and cross-sectional (b) SEM images of the resulting PVA TFNC membranes.

Depositing time of 18 min for PVA electrospray, moistcuring time of 90 s, heating temperature of 60 °C and curing time of 4 min were optimized for the PVA/PAN TFNC membrane preparation. The surface and cross-sectional SEM image of the optimized PVA/PAN membrane was shown in Figure 1. The PVA film layer was very thin (~300 nm) and no obvious evidence of the penetration of PVA top layer could be observed.
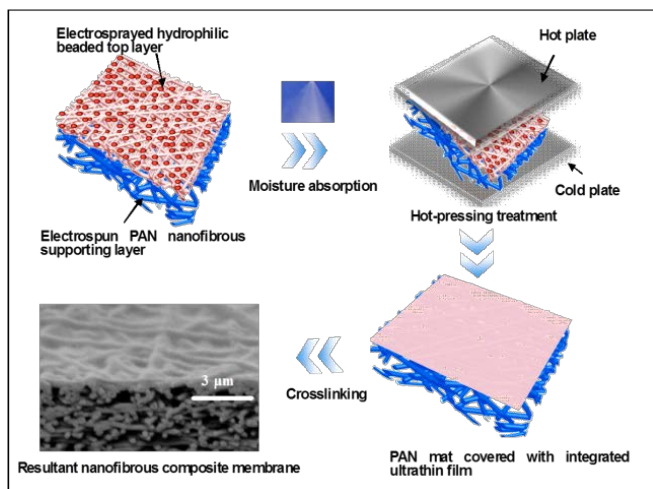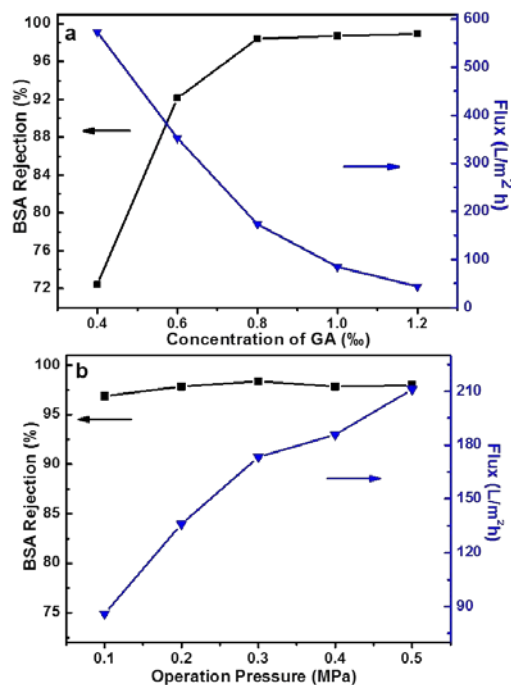
Figure 2 the Effect of GA concentration (a) and operation pressure (b) on the filtration performance of PVA TFNC membranes using BSA aqueous solution.

Different amount of GA was used to finely adjust the compactness of PVA barrier layer as shown in Figure 2a, and GA concentration of 0.8 wt‰ was chosen for BSA separation. The as-prepared composite membrane showed good anti-pressurizing property as depicted in Figure 2b.

CS-PEO-PEGDMA/PAN TFNC Nanofiltration Membrane with High Performance for Anionic Dyes Separation

It is believed that the hot pressing strategy for fabricating TFNC membranes described above can be extended easily to fabricate membranes from many other polymeric membrane materials. UV-cured chitosan (CS)-polyethylene oxide (PEO)-polytriethylene glycol dimethacrylate (PEGDMA)/PAN TFNC membranes for anionic dyes nanofiltration were demonstrated here.
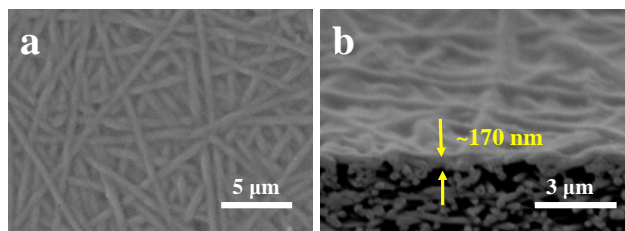

Figure 3: Surface (a) and cross-sectional (b) SEM images of the resulting CS-PEO-PEGDMA TFNC membrane.

Hydrophilic CS-PEO-triethylene glycol dimethacrylate (TEGDMA) nanobead was firstly electrosprayed on PAN nanofibrous substrate. Then the hydrophilic top layer was acidic moistcured and hot pressed to form an integrated barrier film on the supporting layer. Finally, the top layer was UV-cured to form CS-PEO-PEGDMA semi-interpenetrating polymer networks to physically crosslink CS.

Depositing time of 30 min for electrospray, acidic moistcuring time of 60 s, heating temperature of 50 ℃ and curing time of 4 min were selected to achieve an optimized integrated barrier layer on PAN nanofibrous substrate. The CS-PEO-PEGDMA film layer was ultrathin (~170 nm) and no obvious evidence of the penetration of CS-PEO-PEGDMA top layer could be observed as shown in Figure 3.

The resultant membranes exhibited unexpected high nanofiltration performance for anionic dyes separation with permeate flux (~117.5 L/m^{2}h) and rejection (~99.9%) to Direct Red 80 solutions at 0.2 MPa, whose permeate flux to anionic dye at very low operation pressure was three or more times of those flux value ever-reported as seen in Figure 4.

KEYWORDS

Thin-film Nanofibrous Composite Membrane, Wastewater Treatment, Hot Pressing Treatment
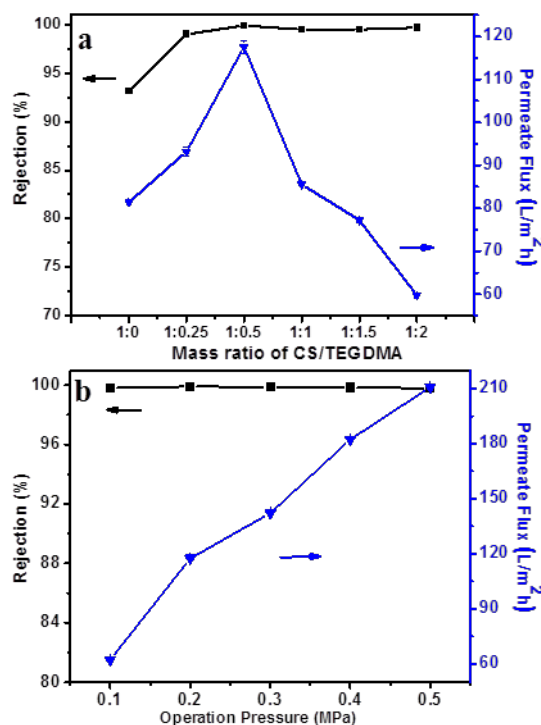
Figure 4: Effect of CS/TEGDMA mass ratio (a) and operation pressure on the permeate flux and rejection rate of the CS-PEO-PEGDMA TFNC membranes using 100 mg/L Direct Red 80 solution as a feed solution (b).

REFERENCES

[1] Zhao, Z.G., Zheng, J.F., Wang, M.J., Zhang, H.Y., Han, C.C. *J. Membr. Sci.*, 2012, 394: 209-17.
[2] Ma, H.Y., Burger, C., Hsiao, B.S., Chu, B. *J. Membr. Sci.*, 2014, 454: 272-82.
[3] Wang, X., Fang, D.F., Hsiao, B.S., Chu, B. *J. Membr. Sci.*, 2014, 469: 188-97.
[4] Luo, Y.F., Zhu, J., Ma, Y.L., Zhang, H. *Int. J. Pharm.*, 2008, 358: 16-22.
[5] Shen, L.D., Yu, X.F., Cheng, C., Song, C.L., Wang, X.F., Zhu, M.F., Hsiao, B.S. *J. Membr. Sci.*, 2016, 499: 470-79.
.

Fabric Processes, Structures, and Properties

Slash and Penetration-resistant Hybrid Fabrics of Superior Performance

Donald L.G. Sturgeon
Multifibers LLC
multifibers@outlook.com

PURPOSE

The purpose of this work was to determine the extent to which novel hybrid fabric designs that utilized low cost commodity fibers could equal or exceed the cut and penetration protection offered by premium performance fabrics made with high strength and modulus aromatic polyamide fibers or ultrahigh molecular weight polyethylene.

INTRODUCTION

The integrity of fabrics made with a variety of natural and manmade fibers used in luggage, upholstery, protective clothing, tenting, awnings, transportation tarps and architectural membrane coverings are vulnerable to natural and manmade cutting damage, often the result of accidents, robbery or vandalism. Products with improved cut resistance have been developed to meet the requirements of industrial safety, law enforcement and the military, based on high performance fibers like Kevlar*, Spectra* and Dyneema*, that have not achieved widespread sales in commoditized retail segments due to their high cost to the consumer.

APPROACH

Our approach was to: (a) clarify the mechanics of cutting of fibrous assemblies; (b) determine what in the metallurgy of the inorganic component was critical to its effectiveness; (c) evaluate the relative contribution to cut and penetration resistance of the kind, form, amount and distribution of both the organic and inorganic components of the composite; (d) exploit the flexibility of derivative weave designs to produce hybrids with a wide variety of useful end-use functionalities; and (e) measure the cut and penetration resistance of test items vs. controls in a pragmatic test that defined a Cut Through Force (CTF) to discriminate among the contending materials.

In order to converge more rapidly on the materials and design of the eventual co-woven hybrids that had the desired higher cut resistance, hybrid simulations were constructed that were reasonably predictive of their performance without the need to weave a multitude of tentative samples.

RESULTS AND DISCUSSION

The resultant hybrid cut-resistant fabric design developed incorporated a metallic wire component in both the warp and fill directions in a derivative weave structure (1). The fabrics were a triple weaves having a top face and a bottom face consisting predominantly of a commodity non-metallic yarn and a co-woven metallic commodity component extending substantially between these two faces. The result was a metal wire grid integrally configured into a unitary single co-woven layer of hybrid fabric of outstanding cut resistances. The CTFs of the hybrids ranged from 18 lbs. for the lighter constructions to well in excess of 20 lbs. for the heavier fabrics. These compared to CTFs of 2 to 4 lbs. for widely used non-hybridized compositions and equaled those of premium aramid fabrics that ranged from 10 lbs. to in excess of 20 lbs. A range of hybrid basis weights were produced by varying the relative amount of the steel wire metallic component to the nylon non-metallic ingredient. The relatively high basis weights (20 oz./sq.yd.) produced were representative of transportation tarps and architectural awnings, the intermediate basis weights (15 oz./sq.yd.) were as those found in upholstery and soft sided luggage, and the lower (12 oz/sq.yd.) were more typical of personal protective clothing and equipment.

CONCLUSION

A new class of economical woven hybrid fabrics was developed that combined organic and metallic commodity fibers into woven structures of outstanding resistance to very sharp natural and manmade hazards.

Because the price of commodity fibers and wires is significantly less than that of premium organic high performance fiber specialties, and only relatively minor modifications are required to weave these hybrid fabrics on
.

existing equipment, their production economics are extremely favorable. Indeed, both input materials and weaving costs at commercial production rates should be in the present range of commodity organic industrial fabrics and commodity steel wire cloth, and thus provide the opportunity for the market introduction of products with a heretofore unavailable combination of higher performance and more affordable price.

*Registered trademarks.

1. LONGITUDINAL SECTION OF THE TRIPLE WEAVE HYBRID FABRIC

Warp Direction

TOP FACE

TOP ORGANIC WARP

TOP ORGANIC FILL

C

D

METALLIC WARP

METALLIC FILL

A

B

BOTTOM FACE

BOTTOM ORGANIC WARP

BOTTOM ORGANIC FILL
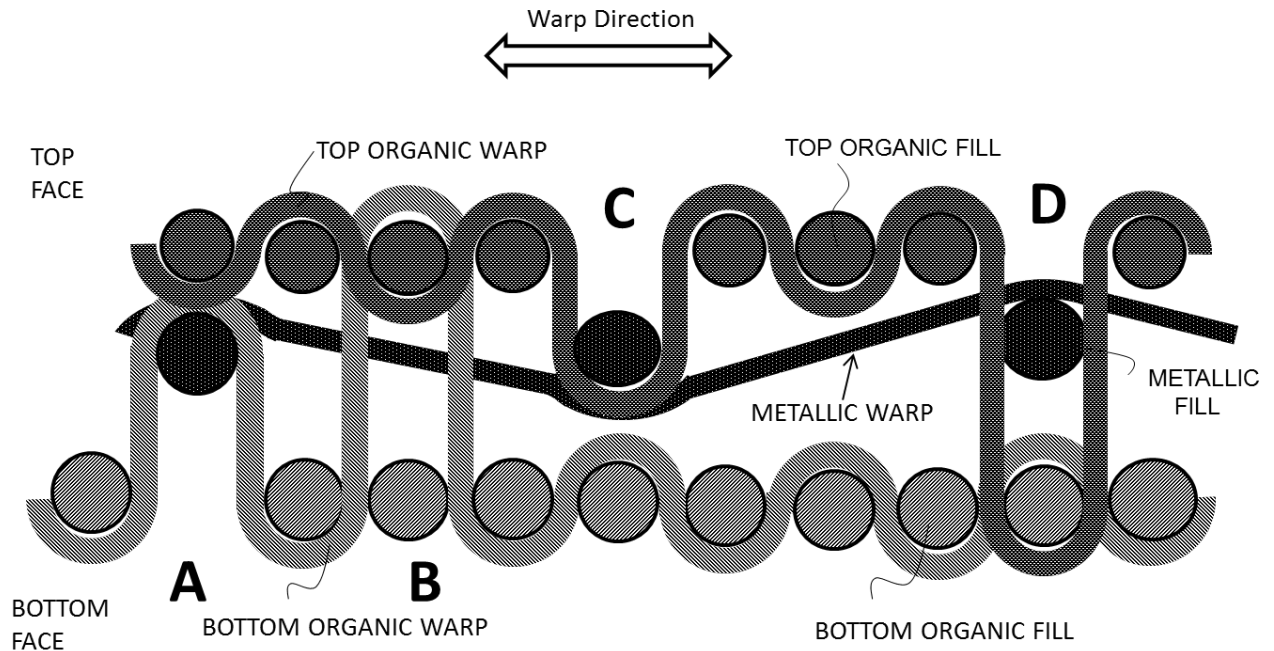
TOP FACE WIRE COUPLER LOOP AT 'A'
TOP INTERFACE LOOP AT 'B'
BOTTOM WIRE COUPLER LOOP AT 'C'
BOTTOM INTERFACE LOOP AT 'D'

Development of Wicking Interfaces in Single Jersey Knitted Fabric for Better Moisture Management Properties

Jawairia Umar[1], Tanveer Hussain[2], Assad Farooq[1], Ahsan Nazir[2]
[1]Department of Fibre and Textile Technology, University of Agriculture, Faisalabad, Pakistan
[2]Department of Textile Processing, National Textile University, Faisalabad, Pakistan
jiaumar@gmail.com

STATEMENT OF PURPOSE

This study aims to improve the moisture management properties of a knitted single jersey fabric utilizing comfort properties of cotton along with cheaply available polyester yarn in alternate positions in order to produce wicking interstices for better moisture transport.

KEYWORDS

Moisture management, Moisture management tester, wicking interfaces, single jersey, sweat shirt

INTRODUCTION

Better sweat management has been a center of researcher's interest since long with the rapid growth of sports textiles in the global market. Therefore comfort of the garment is becoming more important criterion for garment selection in the modern consumer market. The consumers, now a days, not only consider the aesthetics of a garment but also most keenly prefer a comfort factor. This is due to more consciousness in the consumer of modern era regarding feel good philosophy of a better life. The most significant comfort factors of a garment related to ease of movement, garment fit and sweat protection.

Efficient clothing is expected to transfer sweat to the atmosphere in order to maintain the physiological thermal balance of the human body. Since this transfer of body moisture to the atmosphere under transient humidity conditions is very important factor in order to maintain the body's comfort zone especially in dynamic conditions which is more likely our practical situation. [1]

It is very necessary for the human skin to remain dry in order to avoid the blockage of skin pores due to extreme humidity by perspiration and to minimize this one should capable of effectively release this moisture in the atmosphere when the body has stopped sweating. [2] Wicking also plays a vital roles in transferring the moisture out leaving dry skin, higher the wicking capacity of a fabric higher will be its moisture spreading property which leads to quicker evaporation of moisture in the atmosphere. This is due to higher spreading of liquid fills the space between the fabric interstices which builds a capillary pressure. [1]

Fabric construction plays an important role in the moisture management properties of textile clothing. [3, 4] Sweat shirts are normally made by synthetic yarns providing better moisture spreading but lacking comfort properties of cotton.

Therefore an alternative hydrophilic and hydrophobic channeled fabric was manufactured to maximize the moisture spreading rate as compared to 100% cotton sweat shirt with higher moisture regain and 100% polyester with low tactile comfort properties of fabric.

APPROACH

For this purpose five different types of polyester yarns: spun polyester, macro filament polyester, micro filament polyester, channeled polyester and cationic polyester were taken as hydrophobic yarns as shown in Table I. All these hydrophobic yarns were knitted in combination with 100% comb cotton yarn in alternate positions to produced plain weft knitted structures. Moisture management properties were measured on Moisture Management Tester M290 SDL Atlas, UK and air permeability was examined on Air Permeability Tester M021S SDL Atlas, UK. [5, 6, 7] The results were analyzed using ANOVA by a statistical software Minitab 17.

Table I: Type of yarns used in study.

No.	Type of Yarn	Nature	Linear Density, tex
Yarn 1	Cotton	Hydrophilic	30Ne, 19.68
Yarn 2	Spun PES	Hydrophobic	30Ne, 19.68
Yarn 3	Macro Filament PES 75D/36	Hydrophobic	75D/36, 8.33
Yarn 4	Micro Filament 75/144	Hydrophobic	75D/144, 8.33
Yarn 5	Channeled PES	Hydrophobic	80D/36, 8.89
Yarn 6	Cationic PES	Hydrophilic	150D, 16.67

RESULT AND DISCUSSIONS

It was observed that among the different cotton/polyester channeled samples of knitted fabrics, the combination of yarn 1 and yarn 2 (Table I) channeled fabrics has showed superior comport properties with respect to air permeability, moisture spreading speed and overall moisture management as compare to other combinations. Which is also the cheapest option among all.

CONCLUSION

Combination of one hydrophilic and one hydrophobic yarn dramatically changes the comfort properties of the fabric when compared with 100% hydrophilic or 100% hydrophobic fabric, moreover blending of cotton and polyester in fabric showed superior comfort properties in terms air permeability, moisture spreading speed and maximum wetted radius over 100% cotton fabric with comparable OMMC. In polyester cotton blended fabric blending of cotton with filament polyester showed superior overall properties when compared with the cotton blended fabric with spun polyester. Different Aesthetic benefits can also be achieved by such cotton polyester blending as we can play with dyeing to have same of different tonal striper effect which can be shown below in Figure 1.
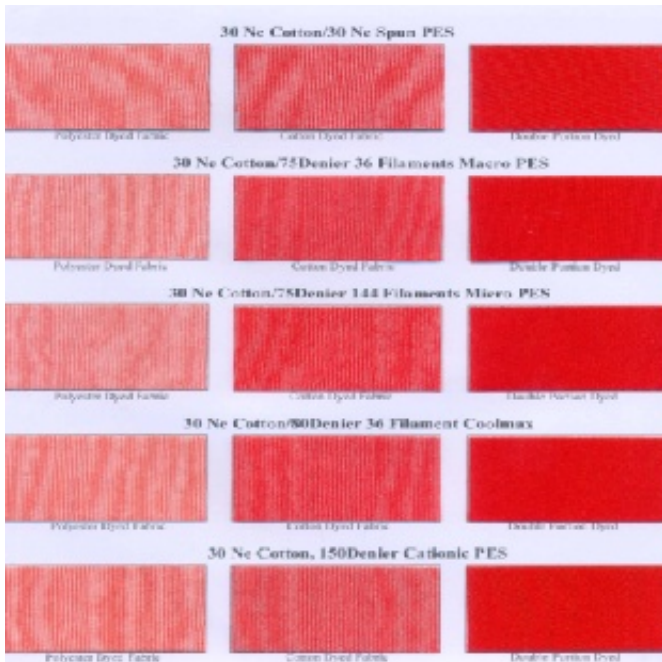

Figure 1: Different dyeing effects with cotton polyester blended fabric.

FUTURE WORK

This study was an initial work to see the effect of creating channeled fabric using different yarns with different moisture behavior. Besides cotton and polyester the method can be advanced by studying the behavior of others yarns to develop super comfort fabric with excellent moisture transport properties.

REFERENCES

[1] B. Das, A. Das, V.K. Kothari, R. Fanguiero, M. De Araújo. "Part I : Processes involved in moisture transmission and the factors at play." *AUTEX Research Journal*, 2007, Vol. 7, No. 2: 100-10.

[2] G. Supuren, N. Oglakcioglu, N. Ozdil, A. Marmarali, "Moisture management and thermal absorptivity properties of double-face knitted fabrics." *Textile Research Journal*, 2011, Vol. 81, No. 13: 1320-30.

[3] C. Prahsarn, R.L. Barker, B.S. Gupta. "Moisture Vapor Transport Behavior of Polyester Knit Fabrics." *Textile Research Journal,* 2005, Vol. 75, No. 4: 346-51.

[4] H.N. Yoon, A. Buckley. "Improved Comfort Polyester Part I: Transport Properties and Thermal Comfort of Polyester/Cotton Blend Fabrics." *Textile Research Journal*, 1984, Vol. 54, No. 5: 289-98.

[5] Moisture Management Tester Operation Manual.

[6] AATCC Test Method 195-2011. "Liquid Moisture Management Properties of Textile Fabrics*." AATCC Technical Manual,* 2012: 366-70.

[7] J. Hu, Y. Li, K.-W. Yeung, A.S.W. Wong, W. Xu, "Moisture Management Tester: A Method to Characterize Fabric Liquid Moisture Management Properties." *Textile Research Journal*, 2005, Vol. 75, No. 1: 57-62.

Comfort Effects of Weft-knitted Structures on Rowing Shirts Using IR Thermography

M.J. Abreu[1], A.P. Catarino[1], N. Haeussermann[2]

[1]University of Minho, Department of Textile Engineering, 2C2T, Campus de Azurém, Guimarães, Portugal
[2]Applied Universityof Niederhein, Moenchengladbach, Germany
josi@det.uminho.pt

ABSTRACT

A fundamental factor in high performance sportswear is the thermo-physiological wear comfort. The sportswear is responsible to support the thermal comfort of the wearer and consequently the thermoregulation, which means helping in body's heat regulation by maintaining the skin temperature of 33°C and body's core temperature of 37°C. Each sport has its own requisites and rowing is no exception.

In the following investigation there were examined three different groups of water-repellent finished functional rowing shirts, featuring different knitting structures. The shirts were tested in a climatic chamber with a thermal manikin under constant conditions and afterwards analyzed using infrared thermography. The objective was to find out which sample shirts and knitting structures provide the best performance under different environmental conditions.

INTRODUCTION

Rowing is a periodic movement always repeating several phases. These phases are catch, drive, finish and recovery. One cycle of this periodic movement is called stroke. The stroke count gives the amount of strokes per minute. In order to provide a comfortable microclimate, sportswear design for rowing must always follow the principle that clothing should prevent the wearer to feel too hot or/and cold. A rowing shirt should then provide the following factors: Elasticity; Breathability; Fitting; Water-repellent; Moisture Transport; Windproof; Easy Care; Seamless; Pilling Resistance. Due to the high movement during the activity of rowing, the sport shirt need to have high elasticity. Even simple movements of the body like bending an elbow leads to a skin stretching of 50% (Shishoo, 2005). Breathability is also an important factor. Due to the maintenance of the core temperature of 37°C and the human perspiration, the textile material needs to be able to transport moisture to the outside. Less energy is wasted by cooling the body and the heart rate is lower if fabrics with good moisture transport are used. Consequently more energy is reserved for the rowing activity. Due to the fact that rowing is practiced in an outdoor area of water, like rivers or lakes, the rowing shirt needs to be water-repellent and wind shield. Wind can cool down the athlete causing a higher heat loss in thermoregulation using a high amount of energy. The high rate of movement, especially of the arm area, requires that the shirt should have a high pilling resistance due to the high abrasion rate during rowing. (Shishoo, 2005).

MATERIALS AND METHODS

With the purpose of developing a t-shirt for rowing, several t-shirts were produced with different structures and fiber compositions, as table 1 shows. The same machine and production conditions were used.

Table I. Composition and structure of each one of the t-shirts used in this study.

Code	Code in graphs	Composition	Structure
A	(1)	100% Cotton (CO)	Single jersey
B	(2)		Composition of structures in different areas used in t-shirt B1, B2 and B3
B1	(3)		False Rib 1
B2	(4)	60% Polyamide (black);	False Rib 2
B3	(5)	35% Polyester (grey);	Single jersey jacquard 1
D	(6)	5% Elastane (transparent);	Composition of structures in different areas used in t-shirt D1, D2 and D3
D1	(7)		Single jersey jacquard 2
D2	(8)		Single jersey jacquard 3
D3	(9)		False Rib 3

As reference, type A is a white shirt made with 100% cotton, with sewed side seams, round neck and long sleeves. Type B, C and D were produced with no side seams, tight fit due to the presence of elastane, raglan design and long sleeves. Due to the capabilities of full jacquard, Type B shirt contains the three different structures, B-1, B-2 and B-3. Other three shirts were made using exclusively one of the three B structures. The same was done for type D shirt. The first one contains the three structures D-1, D-2, D-3, in different regions, and three additional shirts were made using each one single structure. All t-shirts were treated with the same water-repellent finishing. The study was conducted using a climatic chamber at the Center of Textile Science and Technology of University of Minho. In order to reproduce the conditions in the climatic chamber similar to a rowing environment the selected country was Portugal, in particular the North of the country, specifically Oporto region, where the majority of rowing clubs exist, about 65% (http:fluvialremo.no.sapo.pt, 2014).

Figure 1. Images of t-shirts type B (left) and type D (right) under study and detail of the structures used.

It was considered two extreme climatic conditions, as shown in table 2. However, it was not possible to simulate the lower temperature with the climatic chamber, so an annual average temperature and humidity was used instead (http:weather.com, 2014).

Table 2. Climatic conditions selected for testing the t-shirts on the manikin inside the climate chamber. (A) and (B) refer to the conditions actually tested, since January's conditions were not possible to reproduce.

Month	Average Max. Temperature	Average Rel. Humidity
January	13.5°C	79%
July (A)	24.5°C	75%
Annual (B)	19.0º C	77%

A thermal manikin TM 3.2 / R 110 of PT-Teknik made in Denmark was also used in order to develop heat in a homogeneous distribution. This is a female model, selected because it is known that exist more variability regarding thermal behavior in the clothing of women compared to men. The Manikin was inside the climate chamber, placed around 0.1m above the floor with hanging arms and legs. The Manikin's temperature during the complete study was maintained at around 33 ±0.2 °C. Each 5 minutes of the running tests a picture was taken with the infrared camera. As a common scale for both test series ranging from 23°C-35°C in order to compare the series properly.

RESULTS
Figure 2 illustrates two pictures taken during test series A and test series B. Pre-determined points were measured for comparison purposes.
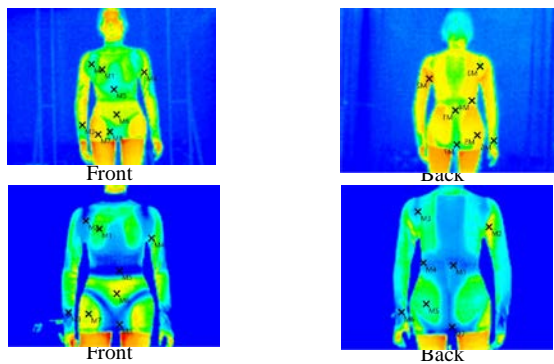

Figure 2. IR pictures for t-shirt code B, for test series A (top) and test series B (bottom).
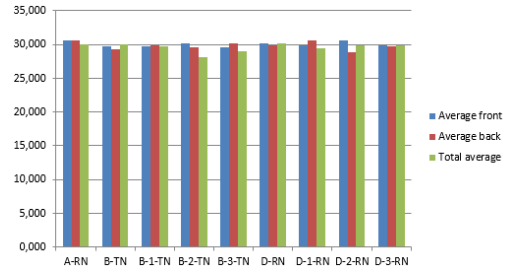

Figure 3. Average temperature of the t-shirts in test series A.

The difference between front and back is relatively equalized. In the front the highest number has sample D-RN and in the back B-TN. In general D-RN followed by B-TN and A-RN represent the hottest surface. Consequently it can be said that the mother shirts have the highest average of the temperature points. The coldest average stands for sample B2-TN.
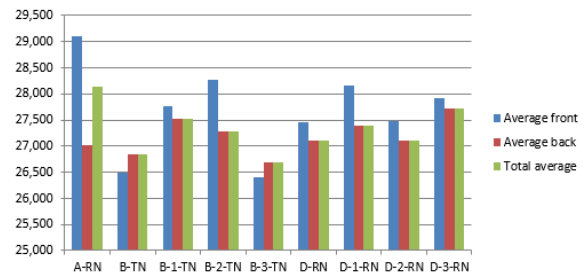

Figure 4. Average temperature of the t-shirts in test series B.

In series B one can observe high variations between front and back. By far the highest temperature reveals in the front part sample A-RN. T-shirt D3-RN has the highest temperature in the back part. The highest total average temperatures is A-RN. The coldest shirt is B3-TN in total as for the front and back part as well.

CONCLUSION
From the results obtained one can state that for weather conditions similar to summer, all t-shirts behave more or less the same, however, for a colder environment there are differences and the material as well as the structure used can be a factor of importance, retaining heat. The combination of different structures in the same t-shirt does not seem to be as important as initially hypothesized. However, one should consider the results for cold weather with care in further studies since it was not possible to simulate winter conditions.

REFERENCES
1. Shishoo, R. *Textiles in Sport*. Cambridge: Woodhead Publishing Ltd., 2005.
2. http:fluvialremo.no.sapo.pt. 2014.
3. http:weather.com. 2014.

Weft-backed Woven Structures for Enhanced Color Effect and Structure Integration of Colorful and Jacquard Fabrics

Tao Hua, Wing Yan Chiu

Institute of Textiles and Clothing, The Hong Kong Polytechnic University, Hong Kong

tcthua@polyu.edu.hk

OBIECTIVE

This study aims at developing modified weft-backed woven structures for enhancing color effect of colorful and jacquard fabrics based on single colored warp and multicolored weft yarns. Two types of weft-backed structures were designed for the yarn color mixing and the resultant fabric color performance was evaluated and compared for these two fabric structures.

INTRODUCTION

Jacquard woven textiles often refer to colorful and figured woven fabrics. With multicolored warp and/or filling yarns, jacquard fabrics are made using jacquard looms. As a result, colorful, intricate patterns or figures are created all over the fabrics. With the intricate structures and unique features on pattern, color and texture, jacquard woven fabrics are nowadays widely used for fashion, home furnishings and decorations. In the design of colorful and jacquard woven fabrics, weave design and yarn color design are two important factors affecting the color and figure effects of the resultant woven fabrics. A number of studies have been carried out to develop design methods as well as investigate the color and weave effects for jacquard fabrics. Osaki proposed a method for the development of high quality color reproduction on silk Jacquard textiles from digital color images [1-2]. Gabrijelcic et al. explored the possibility of color values corrections of woven fabrics by changing of constructional parameters [3]. Mathur et al. developed a geometric model combined with a color model to predict the color contribution of each precolored yarn in terms of color attributes of each area of a Jacquard pattern [4]. Chae et al. proposed the geometrical and colorimetrical modelings for single-layered colorful woven structures with improved accuracy in color prediction [5-6].

Multicolored warp and filling yarns are commonly used in the jacquard woven fabric production to obtain good color and figure effect of jacquard fabric. However, with the modern weaving looms, weft yarns in different colors are used easily in woven fabric production while the preparation of warp yarn is more demanding and complicated than that of the filling yarn. Therefore, if only single colored warp yarns are used, the design of weft yarn color as well as woven structure becomes the key issue for the jacquard fabric compared to that using both multicolored warp and filling yarns. In this study, we tried to develop modified weft-backed woven structures for enhancing color effect of colorful and jacquard fabrics based on single colored warp and multicolored weft yarns.

APPROACH

In this study, two types of weft-backed structures were designed for the yarn color mixing. One is a conventional weft-backed structure that consists of face layer and back layer, as shown in Fig. 1. Based on this structure, a modified weft-backed structure was proposed by adding a color regulating layer between face and back layers, as shown in Fig. 1.

Conventional structure   Modified structure

(a) Weave 1

Conventional structure   Modified structure
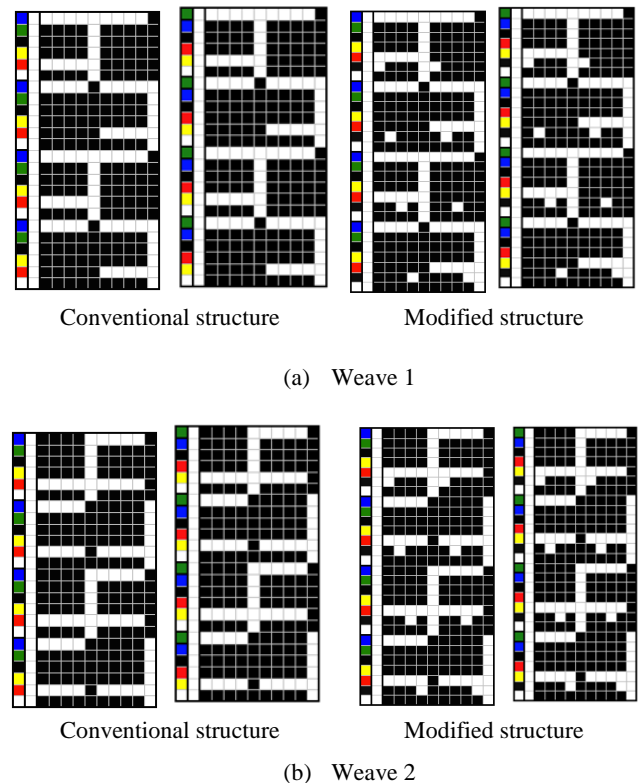
(b) Weave 2

Fig. 1. Weaves for conventional and modified structures.

Based on the coloring principle of woven fabric, weft yarns of 175 D polyester filament in six different colors of red, green, blue, yellow, black and white together with white warp yarn of 100 D polyester filament were used to create the desired colors and figures for the colorful and jacquard fabrics in this study.

Total fifty-six two-colors mixed woven fabric samples were produced by using the above-mentioned colored yarns and two weft-backed structures via a LX 3202 Staubl jacquard machine. The two color mixings are red-blue mixing and green-yellow mixing with different proportions of two colored yarns for face color, respectively. The fabric density is 47 ends/cm and 68 picks/cm and 58 picks/cm for conventional and modified weft-backed structures, respectively.

The color performance of the resultant colorful fabric samples was evaluated by using a X-rite 7000A spectrophotometer. The colorimetric data in terms of CIE

$L*$, $a*$, $b*$, $C*$ and h^o values were calculated to investigate the effect of fabric structure on fabric color performance.

RESULTS AND DISCUSSION
Tables I and II show the fabric samples and their attributes by using conventional and modified weft-backed structures and red-blue mixing and green-yellow mixing modes. The results demonstrate that there is a significant color difference between two types of weft-backed fabrics. For red-blue color mixing mode, the modified weft-backed fabric has higher blueness but lower redness than that of the conventional fabric, and for green-yellow color mixing mode, the modified weft-backed fabric has lower greenness and yellowness than that of the conventional fabric. Combining the structure analysis and color evaluation, the modified weft-backed fabric presents deeper color performance, more even color appearance as well as more stable fabric structures compared to the conventional weft-backed fabric because the regulating layer of the modified structure that consists of black weft floats reduces the lightness of the face color, lessens the effect of color of back yarns and enhances the structure integration for the fabric.
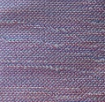
Table I: Color attributes of fabrics by red-blue mixing.
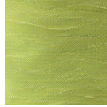
Color attributes	Conventional structure	Modified structure
L*	52.222	48.501
a*	7.012	3.464
b*	-8.875	-11.497
C*	11.310	12.008
h^o	308.313	315.169
$\Delta E_{CMC (2:1)}$	5.921	
(a) Using weave 1		

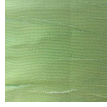|	Conventional structure	Modified structure
L*	52.788	50.699
a*	17.586	16.987
b*	1.076	0.181
C*	17.619	16.988
h^o	3.500	7.101
$\Delta E_{CMC (2:1)}$	1.33	
(b) Using weave 2		

Table II: Color attributes of fabrics by green-yellow mixing.

Color attributes	Conventional structure	Modified structure
L*	65.398	58.720
a*	-18.092	-17.728
b*	19.366	11.991
C*	26.502	21.402
h^o	133.052	145.926
$\Delta E_{CMC (2:1)}$	5.821	
(a) Using weave 1		

	Conventional structure	Modified structure
L*	69.834	68.307
a*	-12.172	-10.797
b*	32.138	28.879
C*	34.366	30.831
h^o	110.744	110.499
$\Delta E_{CMC (2:1)}$	1.837	
(b) Using weave 2		

CONCLUSION
In this study, based on the yarn color mixing principle and the features of weft-backed structure for face color mixing of the fabric, a modified weft-backed structure was developed by adding a color regulating layer between face and back layers and compared to the conventional structure. The experimental study demonstrates that such kind of innovative structure based on single colored warp and multicolored wefts is capable of expressing deeper color performance and creating more even color appearance and more stable fabric structure integration for the colorful and figured fabrics.

REFERENCES
[1] Osaki, K.. "Reproduction of various colors on jacquard textiles by only eight kinds of color wefts." *Proceedings of SPIE*, 2002, 4421(4): 740-44.
[2] Osaki, K. "High quality color reproduction on jacquard silk textile from digital color images." *AUTEX Research Journal,* 2003, 3(4): 173-79.
[3] Gabrijelcic, H., Dimitrovski, K. "Influence of yarn count and warp and weft thread density on color values of woven surface*." Fibers and Textiles in Eastern Europe,* 2004, 12 (1): 32-39.
[4] Mathur, K., Seyam, A.M., Hinks, D., Donaldson, R.A. "Towards automation of color/weave selection in jacquard designs: model verification through visual assessment." *Color. Technol.,* 2007, 124: 48-55.
[5] Chae, Y., Xin, J.H., Hua, T. "Color prediction models for digital jacquard woven fabrics." *Color Research and Application,* 2016, 41(1): 64-71.
[6] Chae, Y., Xin, J.H., Hua, T. "Color prediction of woven structure for digital jacquard fabrics: model evaluation." *The Fiber Society Spring 2014 Conference Proceedings*, Liberec, Czech Republic, May 21-23, 2014.

The Influence of Repeated Washing on Abrasion Resistance of Nonwoven Cleaning Materials/Cloths/Wipes Produced with Different Process Conditions

Emel Çinçik, S. Cansu Yildiz, Özge Yildirim
University of Erciyes, Textile Engineering Department, Turkey
emelcincik@erciyes.edu.tr

OBJECTIVE

The aim of this study is to investigate the effects of repeated washing cycles on abrasion resistance of nonwoven cleaning cloths/wipes manufactured with different process conditions and areal weights. For this purpose, nonwoven materials with different areal weights and production conditions were exposed to repeated washing cycles and physical properties (areal weight, thickness, bulk density), dimensional changes and abrasion resistance of all the samples were determined. The properties of unwashed and washed samples were compared with each other and the influence of washing cycles and production conditions on structure, dimensional change and abrasion resistance of the samples were evaluated.

INTRODUCTION

Nonwoven materials have been among the most demanded textile materials in many application areas in recent years due to the easy and lower number of processes in manufacturing line, higher production rates and lower costs compared to the similar woven or knitted products and diverse characteristics and properties. Nonwoven cleaning materials/wipes are one of the most widely used nonwoven products which constitute 16% of the whole nonwoven market share with dry and wet wipes [1, 2].

These materials are generally constituted from viscose, polyester, polypropylene, cotton fibers and their mixtures by needle punching method followed by thermal bonding process applied either by calendering or through air bonding. The properties of these products closely related with the fiber type and fiber characteristics constituting the nonwoven, the structural arrangement of fibers in the web and the bonding constructions which are influenced by the production method and production parameters [3, 4]. During their usage, these cleaning materials are exposed to short washing processes conducted with warmer water by hand again and again. Besides, as it determines the using life of the product, the abrasion resistance is the most critical performance property for nonwoven cleaning materials/wipes.

Therefore; this study handles the effect of repeated washing processes on abrasion resistance of nonwoven cleaning materials produced with different process conditions. For this aim; 5 different nonwoven cleaning cloth produced with different conditions and areal weights were subjected to washing with different numbers of washing cycles ; 0, 1, 5 and 10 cycles. The physical properties such as areal weight (g/m^2), thickness (mm), bulk density (g/cm^3) and most important performance property named abrasion resistance of unwashed and washed samples were measured. Also, the dimensional changes in samples were determined after each washing cycles. The structural properties and abrasion resistance of unwashed and washed samples were compared and the influence of production conditions and washing cycles on these properties were explained in detail.

EXPERIMENTAL APPROACH

Materials

Five different nonwoven cleaning cloths constituted by different viscose and polyester mixtures and produced with needle punching process followed by different thermal bonding procedures were used as material in this study. All the samples were cross-lapped before needling processes. The coded names and properties of the samples can be seen in Table I. C identifies the calendering whereas T means through air bonding as thermal bonding process.

Also the numbers such as 90 shows the target areal weight of the samples during production step.

Table I. Nonwoven samples used in the study

	Fiber Content	Punch. Den. (p/cm²)	Thermal Process	Areal Weight (g/m²)	Thickn. (mm)	Bulk Den. (g/cm³)
S-C90	%65 V (1.5d X 51mm) %25 P (1.5d X 51mm) %10 BP (4d X 51mm)	200	Calendered at 200°C	95.83 (4.34)	1.173 (10.48)	0.0817
S-C120	%80 V (1.5d X 51mm) %10 P (1.5d X 51mm) %10 BP (4d X 51mm)	200	Calendered at 200°C	129.04 (6.89)	1.377 (4.41)	0.0937
S-C140	%80 V (1.5d X 51mm) %10 P (1.5d X 51mm) %10 BP (4d X 51mm)	200	Calendered at 200°C	148.73 (5.06)	1.529 (3.75)	0.0973
S-T90	%88 V (1.5d X 51mm) %12 BP (4d X 51mm)	330	Through air bonded at 185°C and cold calendered	93.20 (7.02)	1.258 (7.81)	0.0745
S-T120	%88 V (1.5d X 51mm) %12 BP (4d X 51mm)	330	Through air bonded at 185°C and cold calendered	122.00 (5.17)	1.481 (4.87)	0.0823

V: Viscose, P: Polyester; BP: sheath/core Bi-component polyester melting point of 110°C
The values in parenthesis shows the CV(%) values

Methods

The samples were cut into 4 pieces and first piece was kept for unwashed samples. The other 3 samples were marked with benkmarks to determine dimensional change according to AATCC TM -135-2000 test standard[5]. The samples were subjected to washing together following home laundering process by home laundering machine with different numbers of washing cycles; 0, 1, 5 and 10 cycles specified in AATCC TM-135-200 test method. During laundering; 66±5g Standard Reference Detergent was used and the washing temperature and duration was selected as 40±3°C, 50 minutes, respectively. Although cleaning cloths are generally exposed to hand washing with colder water, harder conditions were selected in this study to reveal the abrasion resistance of the samples in harder conditions. The dimensional change values of the samples were measured in both machine and cross direction after flat drying.

The areal weight, thickness of the samples were measured following NWSP 130.1 and NWSP 120.1 [6, 7] test standards, sequentially. The bulk density (d_n; g/cm^3) of the samples were calculated by using areal density (W; g/cm^2), thickness (t; mm) as follows.

$$d_n = \frac{W}{1000 * t} \tag{1}$$

The abrasion resistances of the samples were conducted on James H. Heal Martindale abrasion tester following NWSP 20.5 [8] test standard and using woolen fabric as an abradant. The abrading cycles that create a hole in the fabric was reported to determine abrasion resistance of the nonwoven samples.

RESULTS AND DISCUSSION

The dimensional change, areal weight, thickness test results and calculated bulk density results were demonstrated in Table II, III, IV and V, respectively. As seen from the Table II, the dimensions of all the samples decreased after all washing cycles and the decrease in dimensions increased with increasing washing cycles. The decrease of dimension in cross direction was higher than that of machine direction due to the higher number of fibers oriented in CD. Generally, higher dimension decrease was obtained for through air bonded nonwoven samples. This was attributed to the closer bonding structure in thickness way provided by calendering

process where pressure was applied to the fibers. Because of the higher heat transfer applied by contact of calenders, stronger bonds could be constituted between the fibers which result in smaller dimensional change after washing cycles.

Table II. Dimensional change results of the samples

W. Cycles	S-C90		S-C120		S-C140		S-T90		S-T120	
	MD	CD	MD	CD	MD	CD	MD	CD	MD	CD
1	-1.78 (2.2)	-1.89 (1.7)	-2.56 (3.0)	-3.22 (0.8)	-3.22 (0.5)	-2.67 (2.3)	-3.44 (3.3)	-3.11 (3.8)	-7.33 (2.5)	-4.22 (3.2)
5	-2.33 (3.4)	-6.22 (2.8)	-3.22 (1.6)	-4.78 (2.1)	-3.56 (1.5)	-4.56 (1.6)	-8.55 (2.8)	-5.88 (3.1)	-13.88 (2.7)	-7.11 (2.2)
10	-3.78 (1.8)	-7.22 (0.9)	-4.67 (1.7)	-6.00 (1.4)	-4.67 (1.2)	-5.11 (1.1)	-12.00 (2.4)	-8.55 (1.9)	-14.56 (3.9)	-8.11 (3.3)

Table III. Areal weight change results of the samples

Samples	Washing Cycles						
	0	1		5		10	
	Value	Value	Variation (%)	Value	Var.* (%)	Value	Var.* (%)
S-C90	95.83	93.13	-2.82	106.14	+10.76	105.58	+10.17
S-C120	129.04	136.38	+5.69	144.72	+12.15	145.14	+12.48
S-C140	148.73	162.83	+9.48	168.93	+13.58	169.12	+13.71
S-T90	93.20	100.71	+8.06	115.42	+23.84	110.21	+18.25
S-T120	122.00	142.35	+16.68	160.91	+31.89	159.59	+30.81

*: variation compared to unwashed sample

Table IV. Thickness change results of the samples

Samples	Washing Cycles						
	0	1		5		10	
	Value	Value	Variation (%)	Value	Var.* (%)	Value	Var.* (%)
S-C90	1.193	1.156	-3.10	1.282	+7.46	1.319	+10.56
S-C120	1.377	1.380	+0.22	1.472	+6.89	1.489	+8.13
S-C140	1.529	1.542	+0.85	1.537	+0.52	1.848	+20.86
S-T90	1.251	1.294	+3.44	1.335	+6.72	1.457	+16.47
S-T120	1.483	1.571	+5.93	1.694	+14.23	1.763	+18.88

Table V. Bulk density change results of the samples

Samples	Washing Cycles						
	0	1		5		10	
	Value	Value	Var.* (%)	Value	Var.* (%)	Value	Var.* (%)
S-C90	0.0803	0.0806	+0.29	0.0828	+3.07	0.0801	-0.35
S-C120	0.0937	0.0988	+5.46	0.0983	+4.91	0.0975	+4.02
S-C140	0.0973	0.1056	+8.56	0.1099	+12.99	0.0915	-5.92
S-T90	0.0745	0.0778	+4.47	0.0865	+16.05	0.0756	+1.53
S-T120	0.0823	0.0906	+10.15	0.0949	+15.47	0.0905	+10.04

The areal weights and thicknesses of the samples increased with washing cycles due to the shrinkage comprised after washing processes. Therefore, the bulk densities of the samples generally increased. The increase in areal weight and thickness was generally higher for through air bonded samples compared to calendered identical areal weighted samples.

The abrasion resistance of the samples before and after washing cycles were illustrated in Table VI. According to the table, the abrasion resistance of the unwashed calendered samples were higher than that of unwashed through air bonded nonwovens, if the abrasion resistances of the same areal weighted samples investigated. The punching density of the through air bonded nonwovens are higher compared to the calendered samples. Increased punching density provided better interlocking of the fibers and fabrics resisted to abrading action. On the other hand, by increasing the punching density the number of fibers migrated from un-bonded region of the web towards to interior of fabric increased. Since the mass per unit area was same for two groups of the samples, higher punching density also caused the number of fibers in un-bonded region to decrease and un-bonded regions got weaker for abrasion action [8]. The abrasion resistance of all the samples decreased with increasing washing cycles except 1 washing cycle of $140g/m^2$ calendered sample, 1 and 5 washing cycle of $120g/m^2$ through air bonded samples. The repeated washing process result in shrinkage in the samples and the holes constituted by needles and un-bonded regions increases in a constant area. Thus, the abrasion force affects more weaker area

and abrasion resistance decreases. Also, the washing process may damage the fibers.

Although unwashed calendered samples possess higher abrasion resistance, the abrasion resistance of washed through air bonded samples were higher that of washed calendered samples for identical areal weights. As the increase in thickness of the through air bonded fabrics were slightly higher than thicknesses of through air bonded ones after washing cycles, the abrasion of the through air bonded samples were higher after washing cycles. During abrasion test, abrasion force first affects the fibers and bonds on the surface and then fibers and bonds in other layers in thickness direction. Since the abrasion cycle which causes a hole in the sample is determined during the test, the higher thickness resulted in higher abrasion resistance.

Table VI. Abrasion resistance change results of the samples

Samples	Washing Cycles					
	0	1		5		10	
	Value	Value	Var. (%)	Value	Var. (%)	Value	Var. (%)
S-C90	11613	4439	-61.76	4375	-62.33	3375	-70.94
S-C120	16125	13188	-18.21	12475	-22.64	6925	-57.05
S-C140	15025	15525	+3.33	14191	-5.55	11125	-25.96
S-T90	7427.5	6733.3	-9.35	4578.3	-38.36	3554	-52.15
S-T120	11600	12525	+7.97	12725	+9.69	9762.5	-15.84

CONCLUSION

As a result of experimental study, it was determined that areal weight, thickness and bulk density of the nonwoven samples generally increased after washing cycles due to the dimensional shrinkage occurred after washing procedures. The abrasion resistance of all samples generally decreased after washing cycles except some samples. The abrasion resistance of through air bonded samples were slightly higher compared to that of calendered samples after washing processes due to the higher thickness and higher needling density.

FUTURE WORK

For further studies the other performance properties of the nonwoven cleaning cloths may be evaluated. The effect of repeated washing on nonwoven samples produced with other methods may be investigated.

KEYWORDS
nonwoven, cleaning cloth/wipe, repeated washing, abrasion resistance

REFERENCES
1. *EDANA 2012 Nonwoven Production Statistics*, www.edana.org. 2015.
2. Batra, S.K., Pourdeyhimi, B. *Introduction to Nonwovens Technology*, Destech Publications, USA. 2012.
3. Desai A.N., Balasubramanian, N. "Critical factors affecting the properties of thermal-bonded nonwovens with special reference to cellulosic fibres." *Indian Journal of Fibre & Textile Research*, 1994, Vol 19: 209-15.
4. "AATCC TM-135-2000: Standard test method for determining dimensional changes in automatic home laundering of fabrics." *AATCC Research Journal*.
5. "NWSP 130.1: Standard test method for determining mass per unit area of nonwovens." *INDA & EDANA Worldwide Strategic Partners*, 2012.
6. "NWSP 120.1: Standard test method for determining thickness of nonwovens." *INDA & EDANA Worldwide Strategic Partners*, 2012.
7. "NWSP 20.5: Standard test method for determining abrasion resistance of nonwoven fabrics using a nonwoven modified martindale abrasion." *INDA & EDANA Worldwide Strategic Partners*, 2012.
8. Koç. E., Çinçik, E. "An analysis on abrasion resistance of polyester-/viscose-blended needle-punched nonwovens." *The Journal of The Textile Institute*, 2013, Vol. 104, Issue 8: 852-60.

Investigation of Dimensional Stability of Knitted Fabrics Made of Single- and Double-plied Yarns

Ebru Çoruh
Gaziantep University, Fine Art Faculty, Department of Fashion and Textile Design
Gaziantep, Turkey
ecoruh@gantep.edu.tr

OBJECTIVE

In this study, we observed weft knitted fabrics which are produced with different production techniques by applying ten laundering and drying processes one after the other. Then dimensional stability are measured. In these tests we used %100 cotton, cotton/polyester and cotton/acrylic blended raw material and also we used fabrics which are produced from single plied and double plied yarns, in different yarn counts, rotor spinning system. These tests are done on fabrics which have plain, lacoste, 1x1 rib structures. After the tests, the datas are grouped and showed in graphics according knit structure. It's observed that double plied and synthetic blended fabrics have less shrinkage values than others.

INTRODUCTION

Knitted fabrics are constructed by the interlocking of a series of loops made from one or more yarns, with each row of loops caught into the preceding row. Three basic stitches are used to make weft knitted fabrics: plain, lacoste and rib. During use or refurbishing, fibers, yarns or fabrics of various structures change their dimensions. This kind of distortion, especially in knit fabrics is of equal concern to the fabric manufacturer, retailer, garment maker, and consumer. It has also been one of the most extensively discussed subjects in both industry and research. Dimensional change of fabrics, especially due to repeated laundering, is a critical attribute and, hence, its accurate quantification is a major concern for all sectors of the textile industry.

During the knitting process, the yarns forming the fabrics are constantly under stress. As a result, the fabric on machine is more distorted than its natural relaxed state. When the fabric is removed from the machine, it has time to relax and overcome these stresses, a form of relaxation that is easily recognizable by the changes in dimensions. Mackay, Anand, and Bishop are investigated acrylic, cotton, and wool rib knitwear fabrics have been subjected to several laundering cycles using a variety of washing and drying conditions[1]. Quaynor, Nakajima, and Takahashi are studied deformation by laundering is investigated for single jersey and rib flat knit silk and cotton fabrics with yarns of varying linear densities and fabric tightness[2]. Another study of Quaynor, Nakajima, and Takahashi, is on the effects of laundering and laundering temperatures on surface properties and dimensional stability are investigated for plain flat knit silks, cotton, and polyester fabrics with varying cover factors[3]. Higgins et al. are observed factors during tumble drying that influence dimensional stability and distortion of cotton knitted fabrics[4]. Marmaralı is researched the dimensional and physical properties of cotton/spandex single jersey fabrics are investigated and the results compared with fabrics knitted from cotton alone[5]. Our further aims in this work are to examine the ways in which the conditions chosen for domestic laundering can affect the mechanical and sensory properties of knitted fabrics over a large number of wash cycles, and to identify and damaging aspects of the laundering process for individual fiber types.

EXPERIMENTAL APPROACH

Materials

Experiments were carried out with cotton, cotton/acrylic, cotton/polyester blend yarns with a 20 tex linear density and smilar twist level. Such yarns are regularly used in knitting processes for various textile products. Structure of yarn; according to yarn production method rotor yarns, which are single plied yarn and double plied yarn are used. Knit structure; plain, lacoste, rib fabrics are used. The fibres used in the study are given in Table I.

Table I. Characteristics of cotton, acrylic and polyester.

Fibers	Fibre length (mm)	Fibre fineness (dtex)	Fiber strength (g/d)
Cotton	28,2	1,9	3,7
Acrylic	32	2,5	2
Polyester	32	2,22	5,5

Systematically the effect of the principal washing and drying variables on the dimensional stability and distortion of knitted fabrics are investigated. The fabrics are subjected to ten laundering cycles followed by tumble drying. Changes in the dimensions are fully measured after each process.

Methods

All experiments were carried out in a standard atmosphere 65%RH and 20 ± 2^{0}C temperature for testing according to Standard ISO139 (2002). The main characteristics of the yarn used are given in Table II.

The dimensional stability of grey and dyed samples were tested, using a Wascator washing tester according to the standard of EN ISO 6330 and EN ISO 5077.

RESULTS AND DISCUSSION

Dimensional change of fabrics, especially due to repeated laundering, is a critical attribute and, hence, its accurate quantification is a major concern for all sectors of the textile industry.

Table II. Test samples and specifications.

Fabric structure	Raw material	Fiber Fineness (mic.)	Fiber Length (mm)	Yarn Count (Ne)	Twist (tpm)
Plain	%100 Co	5	29,5	30/1	850
	%100 Co	4,3	29,5	30/2	800
	%50Co+%50Pac	4,5	29,5	30/1	800
	%50Co+%50Pes	4,5	29,5	30/1	800
Rib	%100 Co	4,4	29	30/1	800
	%100 Co	4,4	29,5	30/2	850
	%50Co+%50Pac	4,3	29,5	30/1	800
	%50Co+%50Pes	4,3	29	30/1	850
Lacoste	%100 Co	3,8	29	30/1	850
	%100 Co	4,3	29,5	30/2	800
	%50Co+%50Pac	4,3	29,5	30/1	800
	%50Co+%50Pes	4,3	29	30/1	800

Table III. Dimensional change.

Fabric Structure	Fabric Composition	Yarn Count (Ne)	Dimensional change	
			Width(%) 10.cycle	Length(%) 10.cycle
Plain	%100 Co	30	13,8	14,1
	%100 Co	30/2	11,7	11,8
	%50Co+%50Pac	30	8,3	7
	%50Co+%50Pes	30	8	6,8
Rib	%100 Co	30	23,8	18
	%100 Co	30/2	17	14,8
	%50Co+%50Pac	30	9,2	10,2
	%50Co+%50Pes	30	8,8	8
Lacoste	%100 Co	30	14	17
	%100 Co	30/2	12,0	14,0
	%50Co+%50Pac	30	9,0	11,0
	%50Co+%50Pes	30	8,8	10,7

CONCLUSIONS

The tests were performed on produced with different production techniques by applying ten laundering and drying process one after the other. Detailed analysis of many factors (count of yarn, ply of yarn, knit type, raw material) were made. The results show that structural differences of yarn ply take a large part to define the dimensional stability of these fabric types. Causes of major fabric changes were discussed in terms of the wash process variables (agitation level, detergent product, and drying method) and the different physical properties of the fiber types. Various fabric characteristics such as fiber properties have important effects on the shrinkage behavior of weft knits.

REFERENCES

[1] Mackay, C., Anand, C.S., Bishop, P.D. "Effects of Laundering on the Sensory and Mechanical Properties of 1x1 Rib Knitwear Fabrics, Part I: Experimental Procedures and Fabrics Dimensional Properties." *Textile Res. J.*, 1996, 66(3): 151-57.

[2] Quaynor, L., Nakajima, M., Takahashi, M. "Dimensional Changes in Knitted Silk and Cotton Fabrics with Laundering." *Textile Res. J.*, 1999, 69(4): 285-91.

[3] Quaynor L., Nakajima, M., Takahashi, M. "Effects of laundering on the surface properties of dimensional stability of plain knitted fabrics." *Textile Research Journal*, 1999, 70(1): 28-35.

[4] Higgins, L., Anand, S.C., Hall, M.E., Holmes, D.A. "Factors during tumble drying that influence dimensional stability and distortion of cotton knitted fabrics." *International Journal of Clothing Science and Technology*, 2003, 15(2): 126-39.

[5] Marmaralı Bayazıt, A. "Dimensional and physical properties of cotton/spandex single jersey fabrics." *Textile Research Journal*, 2003, 72(2): 164-69.

The Effect of Yarn on the Air Permeability of Plain Knitted Fabrics Produced by Different Count, Raw Material, and Twist Ratios

Züleyha Değirmenci

[1]University of Gaziantep, Department of Textile Engineering, Gaziantep, Turkey
degirmenci@gantep.edu.tr

ABSTRACT
Air permeability is an important property which is related with comfort of the fabrics. This characteristic depends on the structural properties of the fabrics such as thickness, weight, stitch density, porosity, pattern and any finishing applications. Beside these, the characteristic of the yarn is quite important. For this aim in this study, the effect of raw material, count and twist ratio of the yarn on the air permeability of the knitted fabrics are investigated.
Keywords: air permeability, twist ratio, yarn count

INTRODUCTION
Knitted fabrics can be used for different purposes. Circular knitted plain fabrics are generally used as underwear and summer clothes. For these types of garments air permeability is very important property. Therefore the air permeability is known as one of the comfort related properties. In the literature there are many studies about air permeability of knitted fabrics [1-6]. As the air permeability of the fabrics is related with the characteristics of the yarn; the count, raw material and the twist ratio of the yarn are also important. Among these variables twist is quite important one. The twist in a yarn binds the fibres together and helps to keep them in the respective positions. It thus gives coherence to yarn. Twist effects on yarn and fabric physical properties. As the twist level in a yarn is increased it becomes more compact because the fibres are held more tightly together, so giving a harder feel to the yarn. Because of decrease in the yarn diameter, its covering power is reduced. A fabric made from a high-twist yarn will therefore feel harder and will also be thinner. A fabric produced from a low-twist yarn will have a soft handle but at the same time weaker yarn thus resulting in pilling and low abrasion resistance of fabric. High twist holds the fibres tight thus restricting water to enter. Such a high twist yarn is used where a high degree of water repellency is required, e.g. in gabardine fabric. Low twist yarn is used where absorbency is required. With an increase in twist level wearing properties (abrasion and pilling) are improved. High level of twist helps to resist abrasion as the fibres can't easily pulled out of the yarn. The same effect also helps to prevent pilling (which result from the entanglement of protruding fibres). The level of twist in yarn alters its appearance both by changing the thickness and light reflecting properties. Different patterns can be produced in a fabric by using similar yarns but with different twist levels; a shadow stripe can be produced by weaving alternate bands of S and Z twist yarns. In the available literature there is no study about the effect of twist on the air permeability of knitted fabrics [7-9]. Then in this study it is aimed to investigate the effect of yarn twist, count and raw material on the air permeability of plain knitted fabrics.

APPROACH
In this study eighteen knitted fabrics are produced by single feeder knitting machine with same loop length (2,7). The raw material of the yarn varies as polyester, viscose and polyester-viscose (50-50 %). The count of yarn varies as Ne 25/1 and Ne 40/1 and the yarns are spun by different twist ratios with 3α, 3.5α and 4α. Obtained samples are conditioned and then structural characteristics and the air permeability of the samples are tested according to the international standards [10-14]. The results of the measurements are compared by graphics and tables.

RESULTS AND DISCUSSION
In the study, wales per cm, courses per cm, unit weight and the thickness of the samples are measured and the average of the measurements are presented in Table 1.

Table 1. Structural properties of sample knitted fabrics.

	cpc	wpc	Thickness (mm)	Unit Weight (g/m^2)
Pes25-3α	7.75	10.5	0.63	1.089
Pes253.5α	8.5	10	0.64	1.109
Pes25-4α	9	10.5	0.72	1.198
Vis25-3α	6.5	10.25	0.50	0.882
Vis25-3.5α	8.5	10.75	0.55	1.088
Vis25-4α	8.5	10.80	0.63	1.112
PesVis25-3α	9	11.75	0.53	0.972
PesVis25-3.5α	7.5	10.5	0.55	1.108
PesVis25-4α	7.75	10.25	0.68	1.117
Pes40-3α	10.75	11.25	0.48	0.713
Pes40-3.5α	9.5	10.5	0.57	0.739
Pes40-4α	10.5	11.5	0.59	0.796
Vis40-3α	7.5	11.75	0.43	0.737
Vis40-3.5α	9.25	10.75	0.44	0.737
Vis40-4α	8.5	10.5	0.51	0.678
PesVis40-3α	9	10.5	0.43	0.676
PesVis40-3.5α	8.75	11	0.56	0.749
PesVis40-4α	10.75	11.75	0.57	0.727

According to the test results given in Table 1, when the twist ratio of the samples increase, the stitch density (wpc*cpc), the thickness and the unit weight increase. The thickness and the unit weight of fabrics produced by Ne 40/1 yarns are lower than those of fabrics produced by Ne 25/1 yarns. The raw material does not affect the structural properties of the samples identically.

The air permeability of sample knitted fabrics are measured by SDL Atlas Air Permeability Tester and listed in Table 2 and the comparison of the test results are emphasized in Figure 1.

Table 2. Air permeability of sample knitted fabrics.

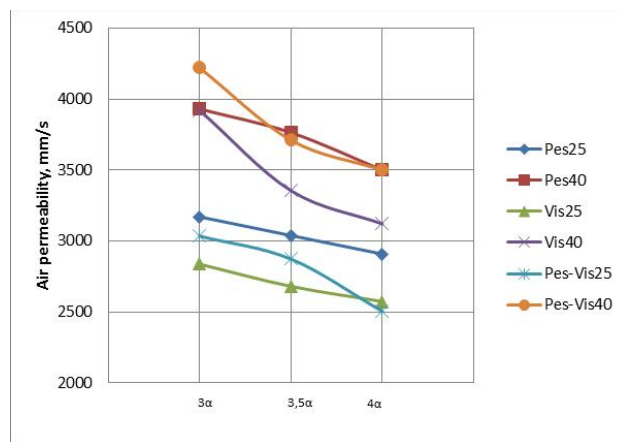| Air permeability, mm/s			
	3α	3,5α	4α
Pes25	3170	3038	2908
Pes40	3930	3764	3500
Vis25	2836	2680	2573
Vis40	3920	3354	3120
Pes-Vis25	3034	2872	2504
Pes-Vis40	4220	3710	3500

Figure 1. Air permeability of sample knitted fabrics versus yarn twist ratios.

Figure 1 and Table 2 show that while the twist ratio increases from 3 α to 4 α; air permeability decreases. The air permeability of the fabrics are affected by yarn fineness while are not affected by raw material directly

CONCLUSION

According to the results of the study when the twist ratio per inch increases the thickness and the unit weight of the fabric increase so the air permeability of the samples decrease.
When the fineness of the yarn increases the air permeability of the sample knitted fabrics decreases.
There is no significant effect of raw material on the air permeability of the sample knitted fabrics.

FUTURE WORK

In the following studies different patterns can be knitted to see the effect of pattern and twist ratios on the air permeability of the fabrics.

ACKNOWLEDGMENT

.REFERENCES
1. Prakash, C., Ramakrishnan, G., Koushik C.V. "The effect of loop length and yarn linear density on the thermal properties of bamboo knitted fabrics." *AUTEX Research Journal*, 2011, 11: 102-105.
2. Bivainytė A., Mikučionienė D. "Investigation on the air and water vapour permeability of double-layered weft knitted fabrics." *Fibres & Textiles in Eastern Europe*, 2011, 19: 69-73.
3. Čiukas, R., Abramavičiūtė, J. "Investigation of the air permeability of socks knitted from yarns with peculiar properties." *Fibres & Textiles in Eastern Europe,* 2010, 18: 84-88.
4. Majumdar, A., Mukhopadhyay, S., Yadav, R. "Thermal properties of knitted fabrics made from cotton and regenerated bamboo cellulosic fibres." *International Journal of Thermal Sciences*, 2010, 49: 2042-48.
5. Kane, C.D., Patil, U.J., Sudhakar, P. "Studies on the influence of knit structure and stitch length on ring and compact yarn single jersey fabric properties." *Textile Research Journal*, 2007, 77: 572-82.
6. Oğlakcioğlu, N., Marmarali A. "Effects of regenerated cellulose fibers on thermal comfort properties of compression stockings." *Textile and Engineer*, 2010, 17, 77.
7. Au, K.F. *Advances in Knitting Technology*. Cambridge: Woodhead Pub. CRC Press, 2011.
8. Booth, J. E. (1968). *Principles of Textile Testing: An Introduction to Physical Methods of Testing Textile Fibres, Yarns and Fabrics*. 3rd ed. London: Heywood Books, 1968.
9. Banerjee, P.K., Alaiban, T.S. "Geometry and Dimen- sional Properties of Plain Loops Made of Rotor Spun Cotton Yarns, Part III: Spirality of the Wale Line." *Textile Res. J.*, 1988, 58(5): 287-290.
10. *Standard Practice for Conditioning and Testing Textiles*. ASTMD1776-08e1. 2009.
11. *Textiles Determination of Permeability of fabrics to Air*. TS 391 EN ISO 9237. 1999
12. *Standard Test Methods for Mass per Unit Area (Weight) of Fabric*. ASTM D3776/D3776M-09a. 2013.
13. *Standard Test Method for Thickness of Textile Material*. ASTM D1777-96(2011)e1. 2011.
14. *Textile-Knitted Fabrics-Determination the Number of Stitches in a Unit Area*. ISO 14971:2006, Geneva, Switzerland, 2006.

Geometrical Modeling of Flat and Tubular Triaxial Braided Structures

Yordan Kyosev
Hochschule Niederrhein – University of Applied Sciences,
Research Institute of Textile and Clothing, Mönchengladbach, Germany
yordan.kyosev@hs-niederrhein.de

INTRODUCTION

Braided structures are widely used for composites, medical, technical and other applications. The prediction of their properties requires knowledge of the yarn geometry. The modelling of unit cells of biaxial and triaxial braids is investigated in several works as for instance [1], [2], [3], [4]. The unit cell provides enough information for the behaviour of the structure if mechanical computations for composites have to be done. Once the behavior of a braided structure at yarn or fiber level have to be investigated but on larger scale of the structure – for instance in order to see the behavior of different parts of braided profile during loading, one unit cell is not more enough. In such case is preferable the complete structure to be generated. Complete model of the structure has additional advantage in case of using combinations of different materials, where single conductive or with other functionality yarns are presented only on some places in the structure. In [5] is presented generalized geometrical model for generation of the structure of biaxial braids with arbitrary floating length and yarns in a group. Its implementation in software [6] allows visualization and export the geometry of the braids in several formats for mechanical and other computations.

This work presents an extension of the model, presented in [5], where additionally to the braiding yarns as well inlay yarns are included, so that triaxial braids can be modelled.
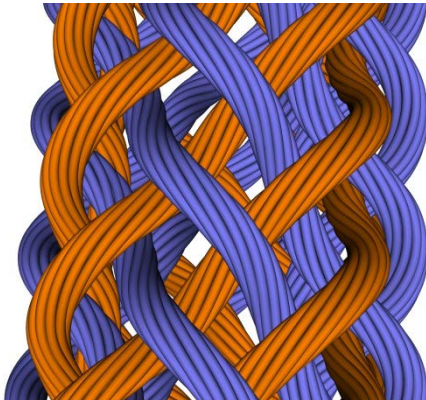

Figure 1. 3D Model of tubular braid of twisted yarns with S- and Z- Twist for the separated directions.

APPROACH

The triaxial braids are braids, where additional inlay yearns are placed between the yarns of the carriers (braiding yarns). The inlay yarns are inserted into the braiding area through a special opening of the each horn gear [7].

Thus, each horn gear can enter only one inlay yarn. In a geometry emulator software like the TexMind Configurator [8] the modelling of the inlay yarns is simple as it requires a placement of inlay yarn on the center of each horn gear (Fig. 2).
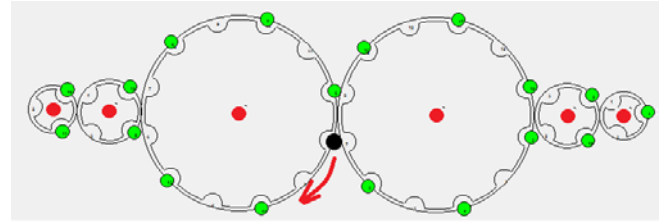

Figure 2. Custom (Fancy) flat braiding machine as basis for generalized model for the placement of inlay yarns in geometrical models. The green circles are the carriers with the braiding yarns, the red circles are the places, from where the inlay yarns are inserted.

More interesting is the question for the placement of the inlay yarns for generalized braids with arbitrary floating length for geometrical models, which are based not on the process emulation, but on the knowledge about the topology of the structure. For those structures the main braiding equation is first applied [Kyosev] for determination of the floating length of the structure:

$$Floating_{Length} = \left\lceil \frac{Slots \quad per \quad Horn \quad Gear}{Repeat \quad Length} \right\rceil$$

The repeat length of the carrier arrangement on the Figure 2 is two (1 Full + 1 Empty position = 2 carrier positions).
The structure will have six ridges, the first with floating length of 1, second two, third and fourth - six:

$$Floating_{Length} = \left\lceil \frac{12}{2} \right\rceil = 6$$

followed by two and one. During the time, where the black carrier goes around the half of the horn gear with twelve slots, its yarn will cross first the yarns of the three carriers, which are currently on its another (upper) half side, and after that the three carriers, which will come to this gear dining its rotation. In this meaning, during the floating of the yarn over the ridge with six yarns, only one inlay can be inserted through the horn gear and it is normally placed in the middle of the crossing area. For the braid with six ridges at all – six inlay yarns can be placed at all. The coordinates for the placement of the inlay yarn can be calculated as the middle distance between two yarn axes multiplied by the half of the floating length of the ridge.

RESULTS

Figure 3 presents simulated triaxial braids which can be produced on the machine, given on the figure 2. It is well visible, that in the large middle ridges only one inlay yarn per ridge is placed, because these areas are build during the motion of the carriers around only one horn gear per ridge. Thus, the possibility for including inlay yarns between each crossing point in some textile modelling software packages is from the braiding point of view not correct and can be used for better placement of think heavy tows, presented as several yarn pieces each only.
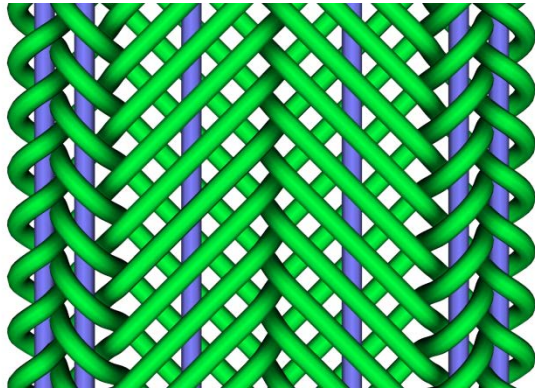
Figure 3. Triaxial flat braid with areas with different floating lengths – 1:2:6:6:2:1.

Figure 4 presents a triaxial flat braided structure with floating length of two (regular braid). Each ridge can adopt from the machine only one inlay yarn.
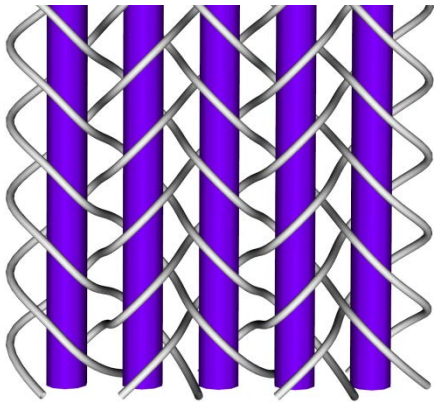

Figure 4. Triaxial flat braided structure with floating length of two.

The results of the implementation of the model for tubular braids is presented on figure 5, where models of triaxial braids with floating length of two and three, respectively, are presented.

CONCLUSION

Technological explanation about the number of the inlay yarns per ridge in triaxial braided structures is presented and used for determination of the placement position of the inlay yarns in geometrical models of braided structures. With its implementation the software Braider is extended with the possibility to create, evaluate and export the geometry of triaxial briads.
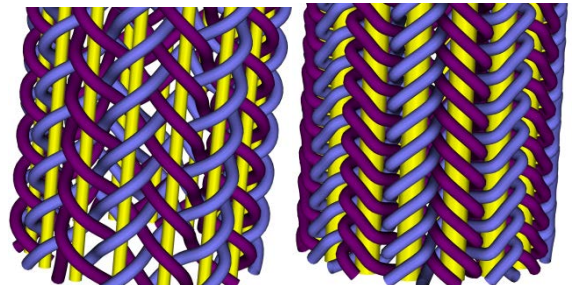
Figure 5. Triaxial tubular braid with floating length of two and three.

REFERENCES
[1] Pastore, C.M., Birger A., Clyburn, E. "Geometrical Modelling of textile reinforcements." In C.C. Poe, C.E. Harris (Eds.) *Mechanics of Textile Composites*. Virginia: Hampton, 1995. 597-623.
[2] Mungalov, D., Bogdanovich, A.E. US Patent 6,439,096. 27 August 2002.
[3] Bogdanovich, A.E., Pastore, C.M., Birger A. "Analysis of Composite Shallow shell structure reinforced with textiles." In P. Hamelin, G. Verchery (Eds.). *Textile Composites in Building Construction*, Part 2. Paris, 1991. 35-44.
[4] Lomov, S., Parnas, R., Bandyopadhyay Ghosh, S., Verpoest, I., Nakai, A. "Experimental and Theoretical Characterization of the Geometry of Two-Dimensional Braided Fabrics." *Textile Research Journal*, 2002, 72(8), 706-12.
[5] Kyosev, Y.K. "Generalized geometric modelling of tubular and flat braided structures with arbitrary floating length and multiple filaments." *Textile Research Journal*. Accepted 2015.
[6] Kyosev, Y.K. "TexMind Braider" www.texmind.com, Mönchengladbach, 2012.
[7] Kyosev, Y.K. *Braiding Technology for Textiles: Principles, Design and Processes*. Woodhead Publishing Series in Textiles No. 158, 1st Editon, Woodhead Publishing Limited, 2014.
[8] Kyosev, Y.K. "Machine configurator for braided composite profiles with arbitrary cross section." In *Proceedings from 16th European Conference on Composite Materials ECCM 16*, Seville, Spain, 22-26 June 2014.

Polymers and
Smart Applications

Nanocellulose-based Textile Coatings for Smart Textiles

Yungsang Kim, Suraj Sharma, Sergiy Minko
Nanostructured Materials Lab, University of Georgia, Athens, GA, USA
sminko@uga.edu

OBJECTIVES

The objective of this research is to develop a nocellulose based platform for functionalization of textile materials to add valuable properties including those associated with stimuli-responsive behavior and electronic devices. The specific focus is on the stability and robustness of the textile coatings that could survive in multiple washing cycles.

INTRODUCTION

Development of textiles that provide adjustable comfort, monitoring human body and its environment, aesthetic effects, protective properties, energy harvesting and storage, etc. is attractive if combined with resiliency and robustness. Many functional properties of textiles can be approached by making functional fibers and surface treatment of fabric. However, retaining the properties after multiple washing remains quite challenging. Water, surfactants and abrasive action in washing cycles degrade the surface of textiles and fibers resulting in a partial or complete loss of the functional properties when they are related to the structure and composition of the fiber surface.

APPROACH

Here we use nanocellulose hydrogel for the creation of a fibrous coating on the surface of fibers and textiles. The coating forms a 3D-network of nanoscopic cellulosic fibers with a very high specific surface area and a small mesh size in a submicrometer range. The coating can be loaded with functional particulates that are hold and reserved by the 3D-cellulosic network. Nanocellulose is obtained from widely available cellulose in wood and in cellulosic waste products generated in farms and industry. In essence, the nanocellulose is cellulose fibrils with widths in the nanometer range of dimensions (from micrometers to 20-30 nm in diameter). Fibrillated NC is produced in the form of a hydrogel of cellulosic nanofibers. Nanocellulose has very high specific surface area with concomitant extremely large concentrations of OH functional groups available for reaction and hydrogen bonding with functional molecules and particulates. We propose the use of nanocellulose structures as carriers for functional molecules, particles and as a "gluing agent" to adhere the functional species to fibers and fabrics.

RESULTS AND DISCUSSION

Cross-sections of the NC coated fabric are visualized with SEM (Fig. 1a,b) demonstrating the formation of a dense few micrometer thick nanocellulose "skin" on the fabric surface. The skin is capable to trap submicrometer particles, and nanowires. We developed several methods for enhancing the interaction between cellulosic fibrils in the 3D-network and approached a high stability and resistance of the coating to typical washing conditions.
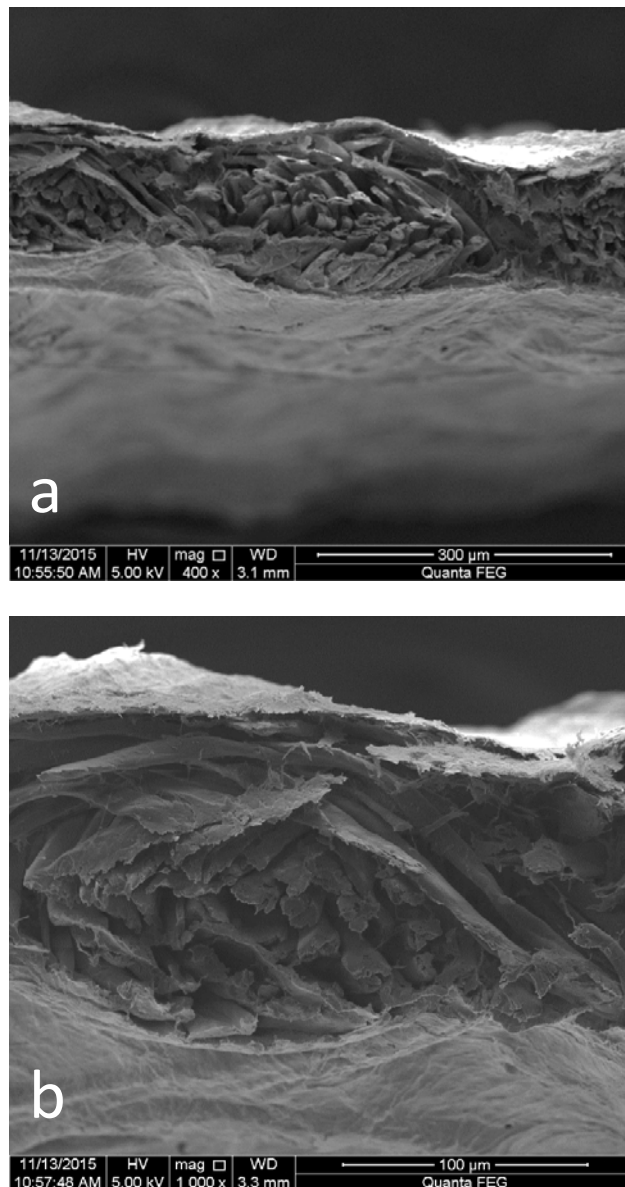

Figure 1. SEM images of cross-sections of a cotton fabric coated with nanocellulose thin "skin."

In this presentation we discuss several examples of applications of the naocellulose skin for making stimuli responsive textile coatings, textile dyeing and making electroconductive textiles.

ACKNOWLEDGMENT

Cellulose Dissolution: Promising Approach for the Preparation of Composite Materials

Noureddine Abidi, Sanjit Acharya, Poorna Wansapura, Niwanthi Dissanayake, Yang Hu, Rohan Dassanayake

Fiber and Biopolymer Research Institute, Department of Plant and Soil Science, Texas Tech University, Lubbock, Texas, USA

noureddine.abidi@ttu.edu

INTRODUCTION

Cellulose is the most abundant natural polymer on earth. Cotton fiber is composed of 95% of cellulose after scouring and bleaching. The dissolution of cellulose represents the first key step for most applications of cellulose and it is highly affected by the degree of polymerization (DP) of cellulose. Due to the high DP (9000-15000), the dissolution of cellulose is difficult to achieve under a relatively mild condition.

Cellulose is a very stable polymer as it plays a crucial role in the structural soundness of plants. This stability makes it particularly difficult to deconstruct. The degree of insolubility of cellulose is due to its chemical and physical structure. In order for dissolution to occur, a solvent must be able to insert itself between microfibrils and cellulose chains. The extent of the use of cellulose to develop an economically sustainable renewable bioproducts industry is limited due to its inefficient and incomplete dissolution in most common solvents. In this paper, we report on the dissolution of cellulose in three solvent systems: NaOH/urea, DMAC/LiCl and 3-butyl 1-immidazolum chloride ionic liquid (BmimCl)).

APPROACH

Microcrystalline cellulose and cotton fibers were used as source of cellulose. Cellulose was dissolved in NaOH/urea, DMAC/LiCl, and ionic liquid (3-butyl 1-immidazolum chloride) followed by regeneration in water. Films and aerogel materials were formed from the cellulose gel.

Cellulose and chitin were also dissolved and combined to form hybrid biomaterials. The resulting bio-composite was tested for its antimicrobial properties.

Electron scanning microscopy, Fourier transform infrared spectroscopy, BET, wide angle X-ray diffraction, were used to characterize the morphology, functional groups, surface porous morphology, and crystallinity.

RESULTS AND DISCUSSION

The results showed that films with good mechanical properties can be prepared up to 15% concentration of MCC. However, the films prepared from 5% MCC solutions were more homogenous. Hydrogen bonding and structural of the cellulose was greatly impacted in the regenerated films of 5% MCC concentration. The crystallinity of the films was decreased and the analysis of variance showed significant effect of the drying method and the concentration of MCC on the crystallinity of the film. The thermal stability of the films was reduced compared to the starting material. The adsorption of water by the films was significantly higher than MCC. In steady state flow measurements, 5% MCC solution exhibited resemblance to Newtonian flow while solutions with higher concentration showed pseudoplastic behavior.

The regenerated hybrid cellulose-chitin material obtained exhibits amorphous structure and degrades at low temperature compared to pure cellulose and chitin. The films exhibit excellent antimicrobial properties.

Development of Composite Filament by Conventional Melt Extruder

Ali Afzal[1], Jean-Yves Drean[1], Nabyl Khenoussi[1], Sheraz Ahmad[2], Niaz-Ahmad Akhtar[3]

[1]ENSISA, Université de Haute Alsace, France; [2]National Textile University, Pakistan; [3]University of Engineering and Technology Taxila, Pakistan

aliafzalch89@gmail.com

ABSTRACT
A composite filament was developed using polyethylene terephthalate as resin matrix and monofilament of copper wire as core of the filament. The lab scale conventional melt extruder machine was modified to introduce the copper filament into the resin matrix for the development of composite filament. The lab magnifier was used for morphological analysis of the filament.

INTRODUCTION
A material composed different materials having peculiar form at macroscale level with distinct recognizable interfaces between them is called as composite material (Akovall and Uyanik). The filament developed with two different materials having distinctive interfaces between them is called as composite filament. The materials which can be used for the development of such filaments includes metals, piezoelectric polymers, conductive polymers, high performance fibers and different coatings (Martins et al.; Bedeloglu et al.; Bedeloglu, Sunter, and Bozkurt; Morris et al.). The composite filaments are used for wide spread of applications including UV protection, electrical conductivity, thermal conductivity, flame retardancy, self-cleaning and antimicrobial etc. Composite technical filaments are multifunctional filaments which can be used as smart materials in functional textiles. These filaments have considerable importance in smart and functional textiles. The use of metals in shape of coating or filament and piezoelectric materials bring these structures in class of smart textiles. Composite coaxial filaments are used for technical applications like sensors, actuators, signal transmission, and electromagnetic shielding as well as for other potential applications like reinforcement filaments etc.

Different researchers worked on the development of composite filaments using different methods and materials. In a study, a complete setup was designed for the manufacturing of composite filament using PVDF(TrFE) polymer with copper filament (Kechiche, Bauer, et al.). In another study the composite filament was developed using specialized spinneret for keeping the core at the center of the filament (Kechiche, Khoffi, et al.).

In this study, a modification has been made in the conventional melt extrusion machine for the development of composite filament.

MATERIALS AND METHOD
In this study a coaxial composite filament was developed using the core of copper monofilament produced by Goodfellow with 99.9% purity having diameter of $50\pm5\mu m$. The virgin polyethylene terephthalate polymer was used as resin matrix in shape of pallets for the development of the composite filament.

The lab scale melt extrusion machine marketed by FilaTech GmbH was used for the development of composite filaments. It comprised of spinneret head, winding section and control section which controls the whole process. The machine is designed for the manufacturing of monofilaments with various controlling parameters including the extrusion speed at range from 0.1 mm/min to 20 mm/min, oven temperature selected up to 350°C and winding speed can be varied up to 200 rev/min. The piston extrusion mechanism made it possible to use hollow piston for the passage and delivery of copper monofilament through it. Considering the friction perspective, the hole in the piston couldn't be made very small. The internal diameter of piston is 05mm and outer diameter is 9.5mm. Three layered structure of aluminum foil having thickness of 16µm was used to create a head on the end of piston. A hole of 200µm was made in the foil structure using a paper pin for passage of copper filament though a hole (Figure 1).
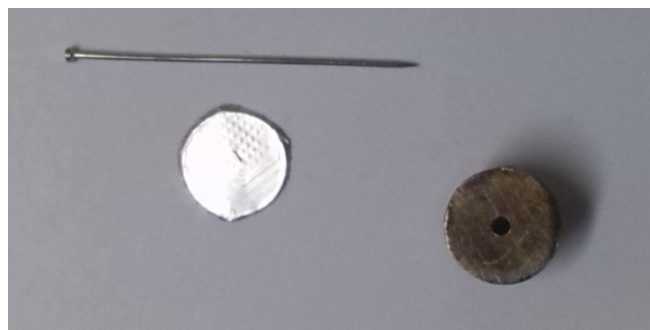

Figure 1. Spinneret with aluminum plied structure used on the head of piston.

The coaxial composite copper/polyester filament was extruded by melting the polyester in the oven at temperature of 300°C with resident time of 5 minutes after drawing in the copper monofilament through the spinneret head of 1mm inner diameter. The extrusion speed was set at value of 10mm/min. The drawing speed was set at value of 60rev/min. The coaxial composite filament was developed having the outer diameter in range of 01±0.25mm. The copper filament along with the molten polymer was extruded through the spinneret head followed by stretching and then cooling with air at ambient temperature. The cooled stretched filament was wound on the package with the help of winding system.

A graduated lab magnifier for the analysis of fibers and filaments was used for the morphological analysis of the filament.

RESULTS AND DISCUSSION

The successful modification in machine allows to develop the composite filament without chocking the hollow piston by melt polymer. Furthermore, the frictional affect was also resolved by successful development of the composite filament. The morphological study revealed that the developed filament have core at the center which satisfy the requirements of composite filament. The longitudinal view of the composite filament is shown in Figure 2. The copper filament was observed as dark black line in the center of the composite filament. The modification also allowed the core filament to move at limited tolerance which helped to better positioning of the core in the composite filament.
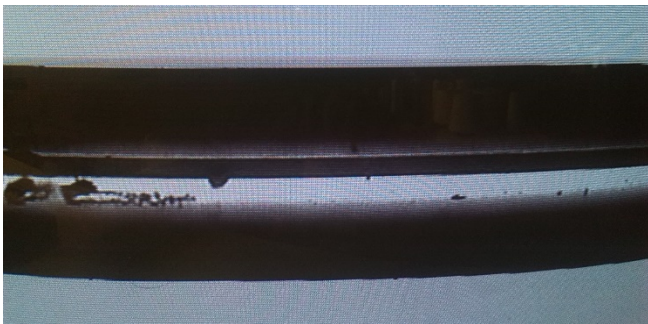

Figure 2. Longitudinal view of the developed composite filament.

CONCLUSION

It was concluded that the modified conventional machine design can be successfully employed for the manufacturing of the composite filaments. In addition, the morphological study also revealed the good positioning of core filament at the center of the composite filament due to low tolerance in movement of the core by the piston head.

KEYWORDS

Composite filament, Copper wire, Melt extrusion, Polyester

REFERENCES

Akovall, Gunerl, N. Uyanik. "Introduction." *Handbook of Composite Fabrication*. Ed. Gunerl Akovall. UK: Rapra Technology Ltd., 2001. 3-20.

Bedeloglu, Ayse, et al. "Bending and Tensile Properties of Cotton/metal Wire Complex Yarns Produced for Electromagnetic Shielding and Conductivity Applications." *Journal of The Textile Institute*, 2012, 103.12: 1304-11.

Bedeloglu, Ayse, Nilsen Sunter, Yalcin Bozkurt. "Manufacturing and Properties of Yarns Containing Metal Wires." *Materials and Manufacturing Processes*, 2011, 26.11: 1378-82.

Kechiche, Mohamed Bouraoui, Francois Bauer, et al. "Development of Piezoelectric Coaxial Filament Sensors P(VDF-TrFE)/copper for Textile Structure Instrumentation." *Sensors and Actuators A: Physical*, 2013, 204: 122-30.

Kechiche, Mohamed Bouraoui, F. Khoffi, et al. "Mechanical Characterization of Composite Polyethylene Terephtalate / Copper Filaments." *Proceedings of the Spring 2012 Fiber Society Conference*: 238-39.

Martins, Rui S., et al. "Piezoelectric Coaxial Filaments Produced by Coextrusion of Poly(vinylidene Fluoride) and Electrically Conductive Inner and Outer Layers." *Journal of Applied Polymer Science*, 2014, 131.17: 8749-60.

Morris, S E, et al. "High-Strength, Metalized Fibers for Conformal Load Bearing Antenna Applications." *Antennas and Propagation, IEEE Transactions on* 59.9, 2011: 3458-62.

Flexible Solar Textiles with Style for Future Smart Clothing System

Youngjin Chae, Hyowon Lee, Poon King Wang
Lee Kuan Yew Centre for Innovative Cities, Singapore University of Technology and Design
youngjin_chae@sutd.edu.sg

OBJECTIVE

A flexible solar textile based on Dye-Sensitized Solar Cell (DSSC) will be presented as a power source for future wearable electronics and smart clothing system. Along with the optimum physical characteristics of light weight and flexibility, DSSC will be fabricated into a textile geometry (Dye Sensitizes Solar Textiles, DSST) by considering the characters in different type of sensitizers. Moreover, style effects of different DSSTs created by the different types of color arrangement, will be compared and discussed in terms of its overall conversion efficiency, lifetime and visual aesthetic for future user environment.

INTRODUCTION

Thanks to various emerging technologies today, a number of approaches have been proposed and explored in wearable computing to provide all-time, full-scale and ambient interface to end users. By allowing a wearer to seamlessly interact with the user environment, *smart clothing* has been considered as the ideal game player in future wearables. However, to run the all-day carried-on multifunctional system, it is essential to find a relevant power device to support enough amount of energy to support its various sensors, actuators and other computing units. Additionally, in order to enhance mobility and convenience to the wearing condition, light and flexible rechargeable battery is being widely discussed. Along with the functional characteristics, the design aspects (i.e., form factors & colors) in wearable technology has become increasingly important. As a communicating medium throughout the system, design factors is known to represent the user identity, emotions and feelings during its daily usage. Various design aspects can be effectively converged on to the smart clothing system, by adopting the concept of second skin, viewed as a physical extension of the user.

DSSC is a third generation photovoltaic device, easily applied on flexible substrates for flexible, compact and light application. By mimicking the photosynthesis process, it has an additional advantage of low cost, simple fabricating procedure, higher efficiency under weak light conditions. Also known as a light harvester in DSSC system, sensitizers (dyes) absorb photons at their respective wavelengths and generates an excitation of electrons and hole pairs. The sensitizer is an important element, which affects the power conversion efficiency and the stability of the DSSC system. Additionally, due to its different optical properties resulting from its molecular design, dyes can be used as an attractive color factor for further applications in DSSCs.

Inspired by the textile industry, recognizable achievement has been made in the field of electronic textiles (E-textile). By weaving fiber-shaped solar cells, textile-based solar cells with sufficient photovoltaic performance has been developed. Compared to planner solar cells, textile-based solar cells are well known for its flexible, bendable and scalable advantages. Additionally, it can be easily integrated into various fabrics or other flexible substrates. Considering both functional and aesthetic needs for power devices in future wearable systems, a multi-color based DSST with satin weave structure was fabricated in this research. Fibrous stainless wire was selected as a base material for photo and counter electrodes. Directly grown ZnO nanorod (NR) was suggested as the semiconducting layer of photo electrode, to meet the property of the bendable wire substrates. A number of ZnO-grown Stainless Still (SS) wires were respectively immerged in to 3 different organic dyes to utilize its various colors as a decorative factor for future smart clothing system. Color loaded photo electrodes were then assembled into satin structure with the same number of Platinum (Pt)-coated counter electrodes to achieve the planner textile geometry structure, taking into account the flexibility, scalability and mechanical stability, for its final usage as a garment material. Lastly, a solid type electrolyte was prepared by synthesizing a graft copolymer to enhance its physical stability and long-term efficiency of DSSTs. By using the 3 different types of dye sensitizers in a single DSST, color as an additional design factor to initiate different styles for future wearable power source in a smart clothing was made possible. Its panchromatic effect and the impact of the overall performance were further evaluated, in accordance to the color arranging ratio and the main color on 6 different types of DSSTs.

EXPERIMENT

Fabrication of counter electrode

After the ultra-sonication with deionized (DI) water, SS wires (0.1mm diameter) were spin coated with Pt for 30s and sintered at 450 ◦C for 30 min.

Fabrication of photo electrode

ZnO NR arrays were prepared onto the SS wire template. Wires were sintered at 450 ◦C for 30 min in order to remove the remaining salts and polymers. To achieve different sensitizing characteristics, ZnO NR SS wires were selectively immersed into respective dyes of D102, D131 or D149 (0.5 mM) in an acetonitrile/tert-butyl alcohol mixture (v/v ¼ 1: 1) solution (65°C).

Fabrication of DSSC

Six types of satin structure DSSTs were assembled by using different color arrangements. Using a handloom, 5 colored photo electrodes and 5 platinum-coated counter electrodes, as warp and weft, were woven into a satin structure. A solid-state polymer electrolyte was prepared by dissolving PVC-g-POEM in THF and MPII, LI and I_2 solution in acetonitrile. Finally, the DSSTs was coated with two layers of PET film in a sandwich structure, to maximize its durability. 6 different types of single/ multi-color flexible solar textile was fabricated by the different arranging ratio of ZnO NR SS wires with different colors. Each DSST were named by their predominant color (i.e., D102, D131 and D149) and single or multi-color arrangement (i.e., 102S, 131S, 149S, 102M, 131M, and 149M).

Measurement of performance

Characteristics of ZnO NR arrays on SS wires were examined by Scanning Electron Microscope (SUPRA 55VP, NICEM, Carl Zeiss) images and X-ray diffraction (XRD) measurements (Rigaku RINT2000 wide-angle goniometer). To evaluate the characteristics of the sensitizers in 6 different DSSTs, the lifetime and the color fading characteristics of 3 indoline dyes on ZnO NRs SS were observed before and after the exposure under continuous light. The photostability of sensitizers loaded on ZnO NRs-SS was evaluated, after being exposed under continuous irradiation followed by the American Association of Textile Chemists and Colorists (AATCC) Test Method (16-2004b, option 3). UV-visible spectrophotometer (Hewlett Packard, Hayward, CA, USA) and Portable Sphere Spectrophotometer SP60 was used to observe the lifetime and color fastness of the dye loaded ZnO NRs SS which was further evaluated by the the Commission International d'Eclairage (CIE) LAB color value. To analyze the panchromatic effect, the efficiency of 6 solar textiles with different color arrangements was compared. Short-circuit current density (Jsc, mA), open-circuit voltage (Voc, V) were measured by a solar simulator with an irradiance of 100mW/cm^2 at AM 1.5 by a 50-500 W Xe Lamp (Thermo Oriel, 91193, USA).

RESULTS AND DISCUSSION

The results of photochemical stability and color fastness of 3 different dyes on ZnO NR-SS sample show respective peak indicating that the genuine characteristics of the dyes were consistently maintained while decreased total amount of dyes was observed in an opposite order to their molecular size of D131<D102<D149. This shows that the dyes with smaller molecular sizes have faster degradation phases because they are more exposed to air and light. The color difference of two samples (ΔE) before and after irradiation was calculated by the following equation:

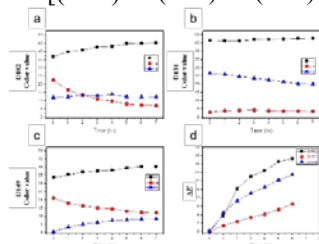$$\Delta E = [(\Delta L^*)^2 + (\Delta a^*)^2 + (\Delta b^*)^2]^{1/2}$$

Figure 1. L*, a*, b* and Δ E curves of indoline dye loaded ZnO NR SS samples.

The results of the change in color value (change in ΔE: D131 (6.7) < D149 (14.4) < D102 (17.8)) seems to correlate with the molecular size of each indoline dye and the shape of the fading rate curve, which represents the physical state of the dye on a fibrous material and the color factor lightening rate, respectively (see Figure 1 and Figure 2). Performances of 6 different DSST with single or multi-color DSSTs have shown the order of efficiency 131M > 131S > 102M > 102S > 149M > 149S. 1.16% of maximum overall energy conversion efficiency of was achieved for multi-color-based DSSTs with D131 as the main color (131M DSST, ratio = D102: D103: D149= 1: 3: 1). The order of the highest to lowest efficiency and Jsc values was identical to

the order of the band gap size and the adsorbed amount of each dyes (D131 > D102 > D149) for both single and multi-color systems (see Table 1). This further indicates that higher conversion efficiencies were mainly influenced by a stronger binding force between the semiconducting layer and the sensitizer. With the same main color, both efficiency and Jsc of multi-color DSSTs was always higher than the single DSSTs. This shows a strong evidence that the higher efficiency was led by the panchromatic effects of multi-color systems by expanded light absorption spectra of DSSTs.
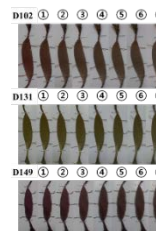

Figure 2. Color changes of indoline dye-loaded ZnO NR SS samples from 1 to 7 irradiation hours.

Table 1. Table 1. Performance of indoline dye-based DSSCs with ZnO NRs at 100 mW/cm^2.

Type	Jsc (mA/cm^2)	Voc (V)	FF	Efficiency (%)
102 single	10.66	0.281	0.306	0.92
131 single	14.4	0.261	0.303	1.15
149 single	9.80	0.246	0.275	0.65
102 multi	13.77	0.254	0.286	1.00
131 multi	14.75	0.262	0.300	1.16
149 multi	13.22	0.242	0.28	0.93

CONCLUSION

By comparing the different types of DSSTs based on its color arrangement in in a single DSST, it was found that the multi -color arrangement in photoelectrods had both increased levels of efficiency and of circuit current density, through a panchromatic effect. The color values of DSSTs were observed by CIE value enabling the visual design factor and increased life-time of DSSTs, through dye stability and color fastness of each sensitizer. The enhanced performance and aesthetic possibility for flexible DSST experimented in this study is a promising prototype of future solar cells which can be further integrated into clothing material or wearable devices.

REFERENCES

1. Chae, Youngjin, et al. "Metal-free organic-dye-based flexible dye-sensitized solar textiles with panchromatic effect." *Dyes and Pigments*, 2014.
2. Chae, Youngjin, et al. "All-solid, flexible solar textiles based on dye-sensitized solar cells with ZnO nanorod arrays on stainless steel wires." *Materials Science and Engineering B*, 2013, 178.17: 1117-23.

Functional Fibers
and Structures

Enhancing the Efficiency of Diesel Fuel Filters by the Usage of Bicomponent Fibers with Water-guiding Channels

I. Noll, G. Seide, T. Gries

Institut für Textiltechnik der RWTH Aachen University, Otto-Blumenthal-Str. 1, Aachen, Germany

inga.noll@ita.rwth-aachen.de

KEYWORDS

Diesel fuel filter, Water separation ability, Bicompo- nent fiber

BACKGROUND

To current state, more than 40 million passenger cars and over 2 million trucks are registered in Germany. About one in four passenger cars and the total number of trucks are powered with diesel fuel and have a respective fuel filter. [1] Among others, diesel fuel filters fulfill two functions, the separation of particles and the separation of water from the fuel. Due to governal restrictions based on discussions on the climate change, mineral diesel shall gradually be substituted by bio diesel. At current, mineral diesel contains 7% of bio diesel. [2]

The separation of water is a major challenge in the filtration of diesel fuels. Especially through legislative decrees on the rising content of biodiesel in regular diesel, the increase of the efficiency of diesel fuel filters has been subject of research throughout the past ten years. Due to its chemical structure, biodiesel exhibits a higher level of affinity to water than mineral diesel. Water in the fuel may lead to corrosion of engine components or to a hydrolytic decomposition of the diesel fuel [3].

AIM AND METHOD

In order to solve these technical challenges, a bicomponent fiber with water-guiding channels is developed within a research project to increase the water separation ability of filters. Therefore, a spinning package for the extrusion of such bicomponent fibers is designed by using simulation-based approaches. Hereinafter, an application-related material combination and a new cross-sectional shape of the bicomponent fiber are investigated. The fibers are processed to form a nonwoven, which undergoes an endurance test to validate its filtration efficiency. The new development may contribute to increase the water separation ability of diesel fuel filters and to meet legal decrees.

MAIN RESULTS

Investigations in the field of climate-physiology have shown that the fiber geometry has a major impact on the absorption of water. In specific, the capillary activity is increased by grooves. [4] Hereinafter, a new bicomponent fiber has been designed at the Institut für Textiltechnik of RWTH Aachen ITA). Its cross-sectional shape and the effect on the water separation ability are demonstrated in Figure 1.
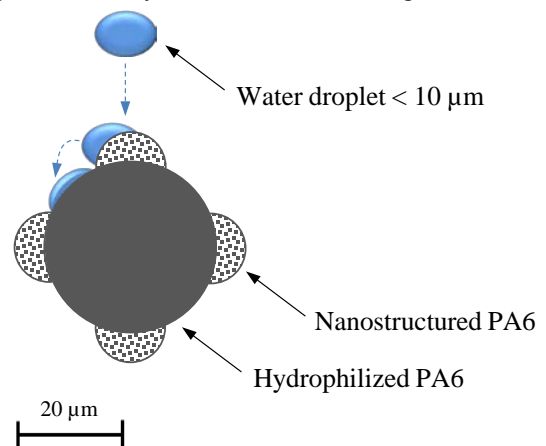

Figure 1. Cross-sectional shape of a bicomponent fiber with a water-guiding channel.

The bicomponent fiber is based on Polyamide 6 due to its resistance towards diesel fuel and its hydrophilic character. [5] The water-guiding channel is hydrophilized by adding antistatic-agents at 10 wt%. Four bulges are nanostructured with silicon dioxide in order to increase the surface roughness. There is a gradient in the water contact angle from 85° (nanostructured PA6) to 50° (hydrophilized PA6). Thus, the water – separated from the diesel fuel – is likely to be transported along the water-guiding channel.
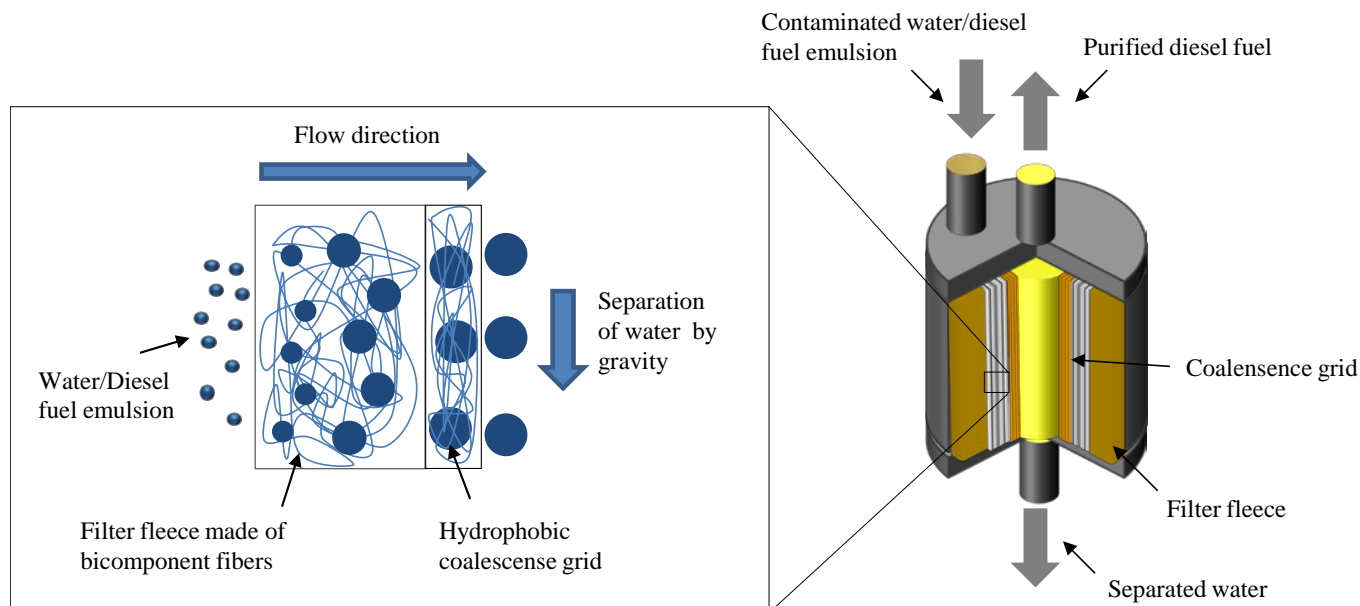
Figure 2. Principle of water separation in newly designed filter fleece.

Water droplets with a critical size of less than 10 µm can hardly be separated from diesel fuel by using existing filters. Through the cloverleaf-shape of the bicomponent fiber a capillary effect is reinforced. Once the water/diesel fuel emulsion flows through the filter fleece, water droplets are separated when impinging on a nanostructured bulge. Decisive physical mechanisms are the difference in the Laplace pressure as well as the Wenzel model. [6] Hereinafter, the curvature of the surface of the nanostructured bulge causes a separation of the water droplet from the diesel fuel. [7] The droplet flows along the bulge to the water-guiding channel of the fiber. Due to the greater hydrophilicity of the channel, the water droplet is transported along the fiber and coalesces into larger droplets at intersection points of the nonwoven, Figure 2. The large water droplets are transported in the bicomponent fiber in the flow direction and end up in the coalescence grid. The grid consists of a hydrophobic nonwoven, at which the water droplets are separated by gravity as known from conventional diesel fuel filters.

CONCLUSION
This research work represents an approach to increase the filtration efficiency of diesel fuel filters while meeting the demands as set by legal decrees.

FUTURE WORK
Future work includes the completion of the simulation-based design of the spinneret as well as an extrusion of the bicomponent fibers. A validation of the research approach is made by forming needle-punched nonwovens, which are exposed to diesel fuel in an endurance test. The newly developed fibers are proneto show a four times higher separation efficiency for dispersed water droplets with a size of less than 10 µm.

REFERENCES
[1] http: // www.hydac.com /de / produkte /filtration-und pflege / diesel Kraftstofffilter. Accessed 17 December 2015.
[2] Bundesrepublik Deutschland: Gesetz zur Einführung einer Biokraftstoffquote durch Änderung des Bundes-Immissions-schutzgesetzes und zur Änderung energie- und stromrechtlicher Vorschriften, Commencement: 01.01.2007.
[3]Bockey, D. Biodiesel—Situation und Entwicklungsperspek-tive, Union zur Förderung v. Öl- u. Proteinpfl. e.V., FVS Tagung, 2003.
[4] M. Tascan, E. Vaughn, K. Stevens, P. Brown. "Effects of total surface area and fabric density on the acoustic behavior of traditional thermal-bonded highloft nonwoven fabrics." *The Journal of The Textile Institute*, 2011, Volume 102, Issue 9.
[5] Kuhnke Automation GmbH & Co. KG. Chemische Beständigkeit von Kunststoffen, Kuhnke Technologies Know-how Medizintechnik. Editor: Bürkle GmbH, Rheinauen, 2003.
[6] S. Agarwal. *Nanoskalig struktrurierte Textilfiltermedien für die Tr. v. Öl-Wasser-Emulsionen.* Diss., Universität Stuttgart, 2012.
[7] J. Ju, Y. Zheng, T. Zhao, R. Fang, L. Jiang. "A multi-structural and multi-functional integrated fog collection system in cactus." *Nature Communications*, 2012.

Luminescent and Glucose-sensitive Hybrid Biofiber Based on Bactaerial Nanocellulose

Jingjing Yao, Shiyan Chen,Yan Ge , Huaping Wang

State Key Laboratory for Modification of Chemical Fibers and Polymer Materials, Key Laboratory of Textile Science & Technology (Ministry of Education), College of Materials Science and Engineering, Donghua University, Shanghai, China

1149132@mail.dhu.edu.cn; wanghp@dhu.edu.cn

INTRODUCTION

Sustainable alternatives for high-performance and functional materials based on renewable resources are intensely needed as fossil-based materials become exhausted and serious environmental issues[1]. Bacteraisl cellulose (BC) is internationally recognized as a type of natural bio-nanomaterial with highly crystalline, large specific surface area and excellent mechanical properties[2]. Functionalized BC-based nanocomposites such as flexible magnetic and electroactive aero-gels[3] and photochromic film[4] have recently been shown since nanoreactor effects of the BC nanofibers. However, functionalized fibers based on bacterial nanofibers, a more promising application of smart textile[5] for knittability were not reported. In this paper, we fabricated macrofibers based on bacterial nanofibers, which were fabricated by wet-extrusion of the the suspensions containing TEMPO-oxidized bacterial nanofibrils into acetone coagulation. We further obtained luminescent fibers by wet-spinning of CdTe-loaded bacterial nanofibers. Effect of pH on the fluorescence of luminescent fibers and quantitative analysis of glucose after enzymatic treatment was investigated.
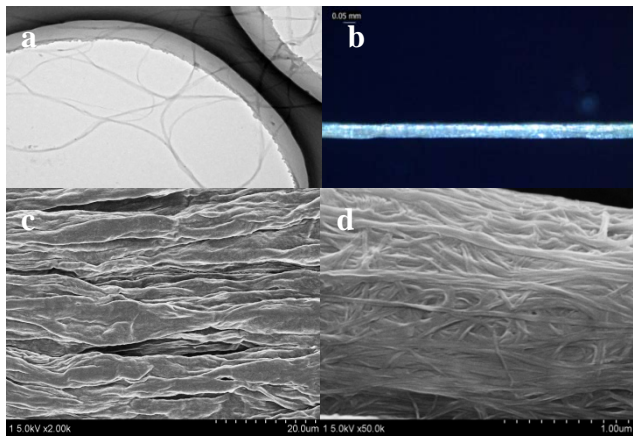
RESULTS AND DISCUSSION

Figure 1. (a) TEM images of individual bacterial nanofibrils. (b) optical micro-scopy images of macrofiber with crossed polarizer. (c, d) SEM images showing the surface structures from the micro to the nanometer scale.

TEM in Figure 1 a shows morphologies of the individual bacterial nanofibrils prepared by the TEMPO-mediated oxidation method. The width of the nanofibers was in the range of 20~50nm and their length was observed to be >5 μm, which reveals large aspect ratio. The spinning suspension of nanofibrils was dehydrated by acetone, leading the cellulose nanofibers to aggregate into macrofiber with ca. 60 μm diameter. The spun fibers of the nanofibers had rough surfaces (Figure 1 c, d) and the individual nanofibrils show moderate orientation, as also indicated by the birefringence when observing the macrofibers between crossed polarizers (Figure 1 b).
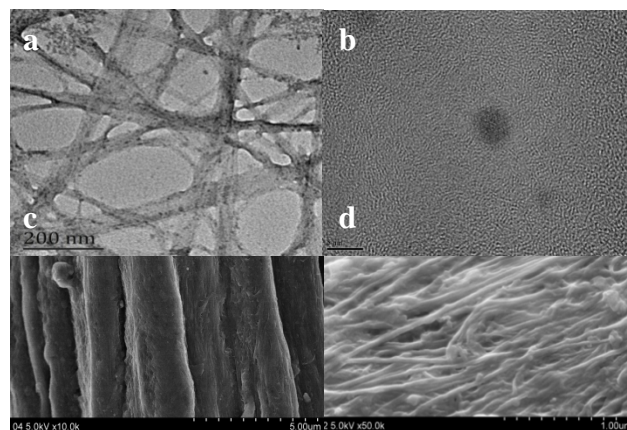

Figure 2. (a) TEM image of CdTe QDs loaded bacterial nanofiber (b) TEM image of TGA-capped CdTe QDs. (c) SEM images showing micro and nanometer scale structures of the macrofiber from CdTe-loaded bacterial nanofiber.

TEM image in Figure 2a shows morphologies of the bound to the surface of the nanofibers by situ synthesis. CdTe were anchored onto BC nanofibers through the hydrogen bonds between the carboxylate anion of TGA and the hydroxyl groups of BC. The size of TGA-capped CdTe QDs was distributed centered at diameters of 4~8 nm (Figure 2 b). Figure 2 (c, d) shows surface structures of the macrofiber from CdTe-loaded bacterial nanofiber. The nanoparticle-loaded nanofibers had rougher surfaces and larger diameter than neat bacterial nanofibers result from distribution of CdTe .
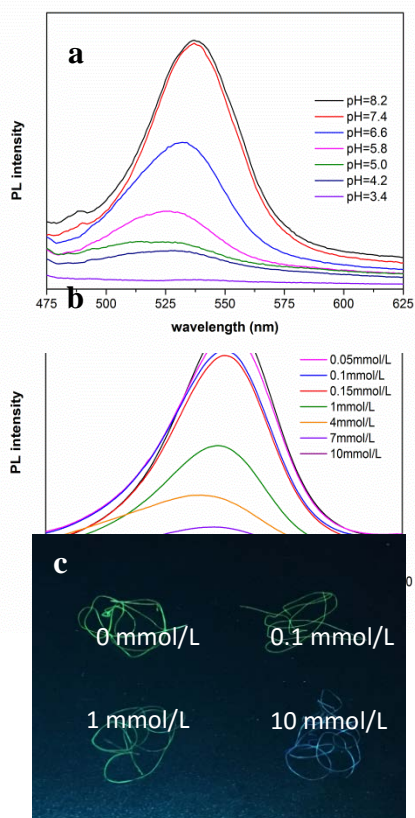
Figure 3. (a) Effect of media pH on the fluorescence intensity of hybrid macrofibers. (b) Fluorescence emission spectra of the hybrid macrofibers in the presence of different concentrations of glucose. (c) Response of hybrid macrofiber to glucose with different concentrations.

As shown in Figure 3 a, the fluorescence intensity of the TGA-capped QDs was highly sensitive to the pH. The fluorescence intensity of QDs changed dramatically with decreasing pH because the capping agents are removed from the surface of the QDs. Gluconic acid (H$^+$) was produced after oxidation of glucose catalyzed by GOD. Therefore, the fluorescent fibers were attempted to quantitative analysis of glucose. As shown in Figure 3 b, fluorescence intensity gradually decreases with increasing glucose concentration. An obvious decrease of PL intensity can still be observed when concentration of glucose was reduced to 0.05 mM. Changes of fluorescence of hybrid macrofiber with different concentrations of glucose can be observed under 365nm UV-lamp excitation (Figure 3 c).

CONCLUSION
We fabricated macrofibers based on bacterial nanofibers and further obtained luminescent fibers by wet-spinning of CdTe-loaded bacterial nanofibers, applying to quantitative analysis of glucose after enzymatic treatment. This method provides a green, effective, stable and glucose sensitive macrofiber, which are promising for potential applications of smart textile for glucose detection in future studies.

REFERENCES
[1] Das, P., Heuser, T., Wolf, A., et al. "Tough and catalytically active hybrid biofibers wet-spun from nanochitin hydrogels." *Biomacromolecules*, 2012, 13(12): 4205-12.
[2] Moon, R.J., Martini, A., Nairn, J., et al. "Cellulose nanomaterials review: structure, properties and nanocomposites." *Chemical Society Reviews*, 2011, 40(7): 3941-94.
[3] Pääkkö, M., Vapaavuori, J., Silvennoinen, R., et al. "Long and entangled native cellulose I nanofibers allow flexible aerogels and hierarchically porous templates for functionalities." *Soft Matter*, 2008, 4(12): 2492-99.
[4] Ge, Y, Chen, S., Yang, J., et al. "Color-tunable luminescent CdTe qu.antum dot membranes based on bacterial cellulose (BC) and application in ion detection." *RSC Advances*, 2015, 5(69): 55756-61.
[5] Lee, J., Kwon, H., Seo, J., et al. "Conductive Fiber-Based Ultrasensitive Textile Pressure Sensor for Wearable Electronics." *Advanced Materials*, 2015, 27(15): 2433-39.
[6] Walther, A., Timonen, J.V.I., Díez, I., et al. "Multifunctional high-performance biofibers based on wet-extrusion of renewable native cellulose nanofibrils." *Advanced Materials*, 2011, 23(26): 2924-28.

How to Flame Retard Polyamide-6 Fibers

Mathilde Casetta[1,2,3], Mathieu Coquelle[1,2,3], Jun Sun[4], Sophie Duquesne[1,2,3], Xiaoyu Gu[4],
Sheng Zhang[4], Serge Bourbigot[1,2,3]

[1]Univ Lille Nord de France, Lille, France; [2]ENSCL, ISP-UMET, Villeneuve d'Ascq, France; [3]CNRS, UMR 8207, Villeneuve d'Ascq, France; [4]Beijing Key Laboratory on Preparation and Processing of Novel Polymeric Materials, Beijing University of Chemical Technology, Beijing, China

mathilde.casetta@univ-lille1.fr

INTRODUCTION

Polyamide (PA) fibers are among the most used technical fibers. For some applications like in the home textile industry or transportation field, materials have to comply with strict fire safety standards to limit the flammability risks. Among the different existing methods to achieve fire performance, the incorporation of additives directly in the melt during extrusion was chosen as this process is easy, relatively inexpensive and allows avoiding the durability issues generally encountered with surface treatment methods [1]. However, the choice of the FR additives is rather limited as they must be stable at the processing temperature of PA6 (around 250°C). Moreover, low loadings (< 10wt.%) and reduced particles size (generally < 10µm) must be used to keep the spinnability of the filled material. Thus, the aim of this work is to design a flame retardant system allowing to develop fibers with improved fire performance.

APPROACH

On the basis of Lewin's work [2] who showed that the combination of ammonium sulfamate and dipentaerythritol improved the reaction to fire of PA6 at low loadings (< 2.5wt.%), sulfamate salts were selected as potential flame retardants (FR) for PA6 fibers. A preliminary study at the laboratory scale showed that ammonium sulfamate (AS) and guanidine sulfamate (GAS) were efficient at a loading as low as 5wt.%. However, processing issues occurred for larger scale production due to the thermal instability of the formulations around 240-265°C [3]. Thus, the objective of the present work is to substitute partially the sulfamate salt by melamine polyphosphate (MPP) to limit the risks of matrix degradation but also to develop a synergistic effect between the two additives. After finding the ratio giving the best fire performance, the mechanism of action of the whole system was investigated analyzing both the gas and the condensed phases.

RESULTS AND DISCUSSION

Selection of the optimum sulfamate/MPP ratio

Different PA6/sulfamate/MPP formulations were prepared by microextrusion (DSM X-plore micro 15 device) at 245°C and 100rpm under a nitrogen flow. Then, micro-scale combustion calorimetry (MCC) (FAA micro calorimeter, Fire Testing Technology) was used to assess the flammability of the formulations. Table I summarizes the data extracted from the MCC curves for the PA6/GAS/MPP formulations.

Table I: MCC results for PA6 and PA6/GAS/MPP formulations.

Formulation	pHRR (W/g)	ΔpHRR/ PA6 (%)	T_{pHRR} (°C)
PA6	588	-	456
PA6/GAS5%	500	-15	449
PA6/GAS4%/MPP1%	429	-27	420
PA6/GAS2.5%/MPP2.5%	411	-30	428
PA6/GAS1%/MPP4%	498	-15	395
PA6/MPP5%	530	-10	391

It can be observed that the most important decrease of the peak of heat release rate (pHRR) is obtained with the 50/50 GAS/MPP ratio. Thus, this formulation was selected to scale up the process and the mode of action of this FR system was studied more precisely.

Fire properties of the PA6/GAS2.5%/MPP2.5% formulation extruded at large scale

The reaction to fire of the selected formulation (PA6/GAS2.5%/MPP2.5%) was first evaluated by mass loss calorimetry (MLC) (Mass Loss Calorimeter, Fire Testing Technology) and compared to pure PA6. Contrary to what was previously observed for MCC, similar values of pHRR, of time to pHRR and total heat release rate (THR) were obtained for pure PA6 and for the FR formulation. However, the burning behavior during the MLC experiment is different for these two formulations as, contrary to the pure PA6, a carbonaceous residue is obtained at the end of the test for the FR formulation (Figure 1).

Figure 1: Cross-section of the PA6/GAS2.5%/MPP2.5% formulation at the end of the MLC test.

Other fire properties like the limiting oxygen index (LOI) and the UL-94 ranking were also determined, giving respectively 37 vol.-% and V0 for the FR formulation compared to 28 vol.-% and V2 for pure PA6. This improvement was attributed to a change in the melt viscosity of the matrix due to the incorporation of the FR additives. The lower viscosity allows:

- the removal of the material from the flaming zone and thus a rapid extinction during the LOI test.
- the decrease of the size of the flaming drops, allowing their extinction during the fall, leading to a V0 ranking at the UL-94 test.

Degradation mechanism of the PA6/GAS/MPP formulation

The previous investigations allowed demonstrating that the combination of GAS and MPP was leading to improved FR properties in terms of MCC, LOI and UL-94. In order to understand the influence of the FR additives on the degradation process of the PA6 matrix, thermogravimetric (TG) analyses were done under air on the PA6, PA6/GAS 5% and PA6/GAS2.5%/MPP2.5% formulations. The derivative TG curves are given in Figure 2 and show that the main decomposition step occurs at lower temperature when MPP is incorporated in the formulation, suggesting that MPP promotes PA6 decomposition.
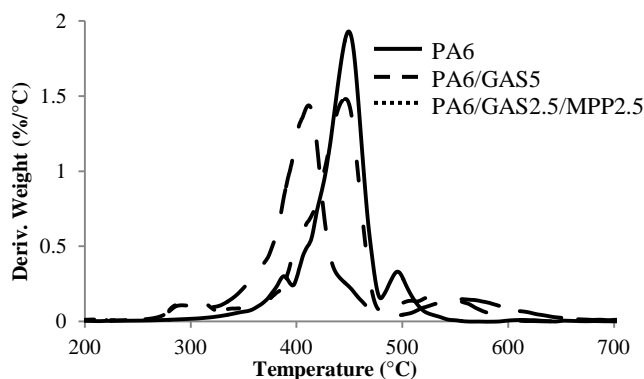
Figure 2: Derivative TG curves of the formulations with and without FR additives.

To understand the exact role of MPP in the formulation, the mechanisms of degradation were investigated analyzing the gas phase through the coupling of thermogravimetric analysis (TGA) and Fourier Transform Infrared spectroscopy (FTIR) and also through pyrolysis-gas chromatography-mass spectrometry (py-GC/MS). It was shown that GAS and MPP modify the degradation pathway of PA6 as they promote the formation of molecules of higher molecular weight. As these compounds are less easily flammable, it could explain the enhancement of the MCC results using the FR additives.

In order to go further into the investigation of the mode of action of the GAS/MPP system, the degradation products of the condensed phase were then analyzed to detect potential chemical reactions between, PA6, GAS, MPP and/or their degradation products. Solid state NMR was used to study the condensed phase and allowed showing that GAS promotes char formation at high temperature and the presence of MPP enhances this process.

CONCLUSION

The incorporation of a 2.5% GAS/ 2.5% MPP mixture into PA6 allows obtaining a LOI of 37vol.%, a V0 ranking at the UL-94 test and a 30% decrease of the pHRR at the MCC compared to pure PA6. It is proposed that a higher dripping and a lower viscosity are responsible for the better LOI and UL-94 results. The mechanism of action of the FR system was also investigated and it was shown that compounds of higher molecular weight were found as degradation products in the presence of GAS and MPP. Moreover, these two additives promote char formation at high temperature, as demonstrated by solid-state NMR.

KEYWORDS

Polyamide, flame retardancy, fibers, sulfamate

REFERENCES

[1] A.R. Horrocks. *Polymer Degradation and Stability*, 1996, Vol. 54 (2-3): 143-54.
[2] M. Lewin, J. Brozek, M.M. Martens. *Polymer for Advanced Technologies*, 2002, Vol. 13 (10-12): 1091-1102.
[3] J.B. Dahiya, B.K. Kandola, A. Sitpalan, A.R. Horrocks. *Polymer for Advanced Technologies*, 2013, Vol. 24 (4): 398-406.
.

Mechanical and Functional Characterization of Basalt Woven Structures

Hafsa Jamshaid[1,2], Rajesh Mishra[1] , Jiri Militky[1], Zuzana Hrubošová[1]

[1]Technical University of Liberec Chech Republic; [2]National Textile University, Faisalabad Pakistan

hrntu@hotmail.com

INTRODUCTION

The history of textiles can be traced back to the prehistoric times. Fabrics made from both natural and manufactured fibres have been extensively used for clothing, decoration and industrial applications. Current applications of textiles have crossed many barriers and reached limits beyond expectations. Fields like sports and leisure, healthcare and wellness, energy generation and storage, electronics and IT, automotive and aerospace, just to give a few examples, are using hi-tech textile reinforced composite materials. Fibres are frequently used for improving the strength and rigidity of polymers [1]. Incorporation of several different types of fibres into a single fabric has led to the development of hybrid structures. The behaviour of hybrid structure is a weighted sum of the individual components in which there is a more favourable balance between the inherent advantages and disadvantages. Also, using a hybrid structure that contains two or more types of fibre, the advantages of one type of fibre could complement with what is lacking in the other. As a consequence, a balance in cost and performance can be achieved through proper material design [2].

The aim of doing this research is to analyse the mechanical and functional properties like electrical, acoustic properties and thermal stability of structures on the basis of fiber properties and weaves. An attempt has been made to measure the electrical resistance of different hybrid fabrics in order to understand the effect of fabric structure on the resistance of fabric. It will help to design technical textiles from fabrics where electrical resistance property is required during use. Such fabrics could be incorporated into prepreg systems used for composite manufacture.

APPROACH

Basalt is a fibre originated from rocks and having excellent properties Polypropylene is a by-product of oil refining processes. It has the lowest density among all synthetic fibres. Polyester is also thermoplastic polymer and it most commonly refers to polyethylene terephthalate (PET). Polyester is the most versatile, most cost effective and most widely used fiber in various applications. Jute is one of the most affordable natural fibres and is second only to cotton in amount of production in the whole world Jute is a thermoset polymeric fibre. The idea was to use these common polymeric fibres in the weft along with basalt warp so as to create hybrid woven structures. The fabric samples produced are,: Plain weave, matt weave and twill weave with Basalt-PP, Basalt-PET, and Basalt-Jute. Pure non hybrid fabrics were made for the comparison purposes.
Shear properties of all fabrics were measured on tensile testing machine by picture frame method. Shear test was performed on TIRA machine.

Measurement of thermal conductivity by C-Therm TCi Thermal conductivity analyzer is performed. Electrical resistance measurement was done on a measuring device (ohmmeter) 4339B High Resistance Meter. Acoustic property was measured by using two-microphone impedance tube according to ASTM E1050-08.Thermal stability is checked by TGA.

RESULTS AND DISCUSSION

It is observed that effect of weave have strong influence on shear property of all fabrics.It is observed that with the use of jute yarn in weft direction, the hairiness in the fabric increases thus increasing the content of air pores. İt can also observed that matt weaves have highest resistance followed by twill and plain respectively. The fabrics investigated are characterized by different thicknesses depending on the weave and different fibre composition. The thermal resistance is correlated with thickness in present study.The thermal properties are also co realted with theoratical model .
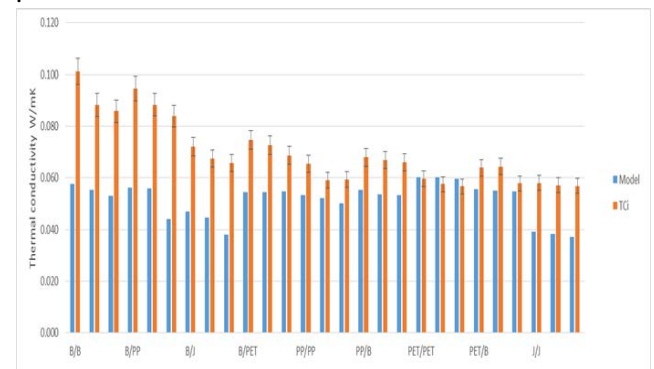

Fig.1: Thermal property.

It is visible that the highest electrical resistance had 100 % basalt samples with twill and matt structure. There is no statistically significant difference between resistances of twill and matt weave of B/B samples. On the other hand statistically significant difference can be observed between samples with different material composition preserving the same weave pattern. It can also be observed that in all the hybrid structures highest electrical resistance is in B/J structures due to properties of material used**.**
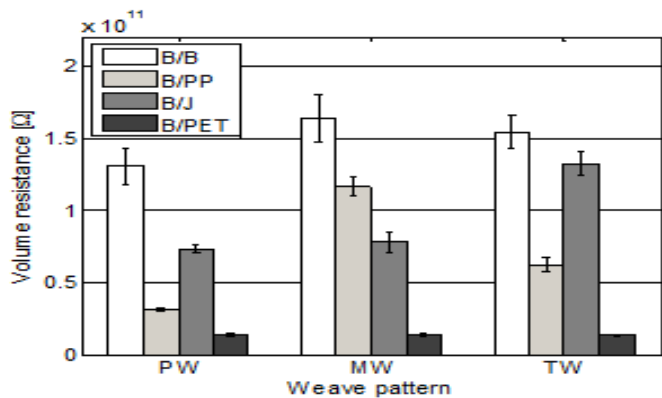
Fig. 2: Volume resistance of structures.

It can be seen that fabrics with polyester fiber have better SAC .The reason for better SAC of polyester fabrics may be finer fibers which results in higher number of fibers per unit weight of the material. This leads to higher total fiber surface area, and greater possibilities for a sound wave to interact with the fibers and ultimately dissipate inside the structure. 100% Jute and Basalt fabric shows lowest SAC values in both frequencies. With the use of basalt fiber for hybrid structures SAC improves for all fabrics.

Thermal stability of structures is greatly improved by addition of basalt.

CONCLUSION

It is concluded that the mechanical property depend on fibre and weave. Thermal resistance and electrical resistance depends mainly on fabric thickness and is directly proportional to it.. B/J structures has higher thermal and electrical resistance. With the use of basalt fiber for hybrid structures SAC improves for all fabrics. Thermal stability is also affected by material content. So overall properties improved by the uses of hybridization.

KEYWORDS: woven fabric, Basalt, Shear Moduli, Thermal resistance, Electrical resistance, Acoustic properties, GA.

REFERENCES
1. Mallick, P. *Composites Engineering Handbook*. New York: Marcel Dekker, Inc., 1997.
2. Dorigato, A., Pegoretti, A. "Fatigue resistance of basalt fibres-reinforced laminates." *Journal of Composite Materials*, 2012, 46(15): 1773-85.

.

Fabric Processes, Structures, and Properties

Artificial Finger for Textile Fabrics

Brigitte Camillieri, Marie-Ange Bueno

Laboratoire de Physique et Mécanique Textiles, Ecole Nationale Supérieure d'Ingénieurs Sud Alsace, University Haute Alsace
marie-ange.bueno@uha.fr

STATEMENT OF PURPOSE

The goal is to design an artificial finger to replace the human finger during friction test on textile surfaces. In this study, four different kinds of textile fabrics are chosen because they represent a wide range of textile fabrics for clothing industry. Then alternative friction tests are carried out by humans on these fabrics. The evolution of the coefficient of friction during a displacement cycle are compared for the four fabrics. This helped to select the fabric used to develop the artificial finger. Then the artificial finger is designed by mimicry by studying the influence of the main morphological and mechanical criteria of the finger (shape, texture, Young's modulus) on the friction signal. Finally, the developed artificial finger is validated by comparing the results obtained for the four kinds of fabrics with the artificial and human fingers.

APPROACH

The four investigated fabrics are:
o A plain woven fabric with a low surface pile.
o A knitted polar fleece with a pile over the two sides of the fabric. The bristles have variable lengths and their orientation is random on the fabric surface.
o A knitted velvet. The bristles are parallel and of equal lengths (about 2 mm).
o A knitted artificial fur which bristles are parallel and of equal lengths (about 5 mm).

For pile fabrics as velvet or fur, the pile has a preferred direction for laying down as with the fur of an animal. This preferred direction is called further along pile and the other against pile main direction.

Two reciprocating linear tribometers have been used to measure the friction: a tribometer for fabrics equipped with a slider (artificial finger) and a tactile tribometer where the slider is a human finger. In both cases, the fabric sample is fixed on an oscillating table and the normal and tangential forces are measured.

A preliminary study showed that the touch exploration of textiles is carried out under a pressure of about 3 kPa with a sliding nominal speed of 20 mm/s (Breugnot). For both tribometers, the chosen sliding distance is 50 mm. For human finger, the choices are: using the index of the dominant hand with a finger tilt angle of 25 relative to the horizontal (Bueno et al.). Several cycles are performed but only the second one is exploited.

In addition, each artificial finger has an apparent contact area of 1.5 cm^2, which corresponds to the surface of the finger in contact when the pressure is 3 kPa (Breugnot). Consequently, the nominal normal force is 0.5 N.

RESULTS AND DISCUSSION

First study

The first study with a panel of seventeen people allowed to see each fabric presents a specific evolution of the coefficient of friction (COF).
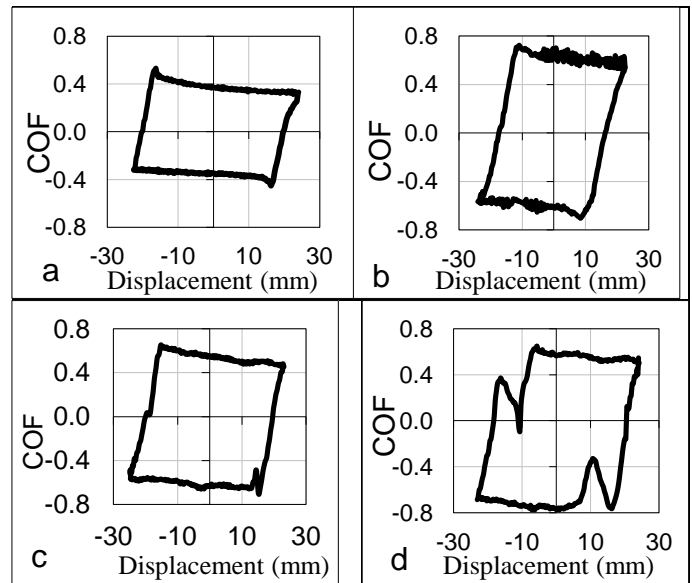

Figure 1: Typical evolution of the COF between a human finger and the four fabrics investigated a) plain woven fabric b) polar, c) velvet fabric and d) artificial fur. For velvet and artificial fur, the COF is positive along pile and negative against pile main direction.

From Figure 1, because of the specific and complex COF evolution, the velvet has been chosen to develop the artificial finger.

Slider design

To design the slider used as an artificial finger for textile fabrics, the chosen approach is to study in a tribological point of view the influence of different characteristics of a finger: its rounded shape, the texture of the fingertips, i.e. the dermatoglyphics and its hardness. In that purpose, different shapes of slider have been investigated (Fig. 2) and two materials.
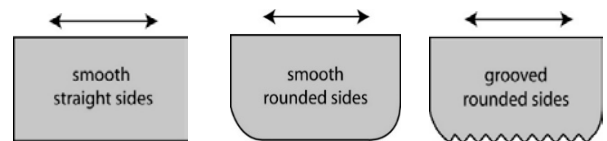

Figure 2: Different shapes of the slider used.

The selected slider is made of silicone and presents a grooved sole and rounded leading edges and covered with a specific fabric. Figure 3 shows the evolution of the COF for this slider.
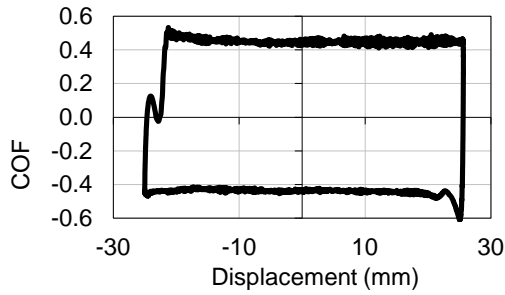
Figure 3: Evolution of the COF on velvet obtained with the artificial finger selected.

Validation of the artificial finger

For all the fabrics investigated, the curves obtained with a human finger or with the artificial finger have very similar appearance except in the transitory slopes. Therefore, qualitatively the artificial finger has the same behaviour as a real finger.

Table I gathers COF values obtained between the four investigated fabrics and the artificial finger or a human finger. For fabrics with oriented pile (velvet and fur fabrics), the COF along and against pile main direction are considered separately.

Fabric	Artificial finger		Human fingers		
	COF		COF		Panel size
plain	0.34		0.43 ± 0.12		40
polar	0.59		0.70 ± 0.21		40
	COF along	COF against	COF along	COF against	
velvet	0.45	0.44	0.58 ± 0.23	0.61 ± 0.16	17
fur	0.50	0.64	0.60 ± 0.13	0.85 ± 0.24	17

Table I: Values of COF for the four fabrics obtained with the artificial finger and the human fingers.

Quantitatively the artificial finger gives a value of COF that is included in the range of COF obtained by our panel of subjects. The values obtained with the artificial finger are consistently lower than those obtained by the human fingers; an explanation of this difference will be given.

DISCUSSION

There are some differences between the curves obtained by the two experiments and especially the transitory slopes. This can be explained by a different displacement of real and artificial fingers relative to the fabric in both directions.

CONCLUSION

This study shows the influence of each morphological and mechanical human finger features on the friction behavior with textile fabrics: rounded shape, finger texture and hardness. The rounded shape of the finger is not really relevant in this case but the finger texture is fundamental. In fact, the results obtained with smooth and grooved sliders allow us to bring some conclusions:

✓ With a smooth sole, the friction cycle depends on the length of the slider as the pile at the ends of the sliding region is not stressed in both directions.
✓ With a grooved sole, the pile is forced in both directions because the bristles interlock into the grooves.

The grooves, that is to say the dermatoglyphics, thus play an important role in the friction behavior of the finger against pile surfaces.

The influence of finger hardness has been evaluated with the help of rigid (made of aluminum) and soft (made of silicone) sliders. With the soft slider made in silicone, the adhesion is too important with textile fabrics. Therefore it has to be covered by a chosen material. A specific fabric has been identified.

The results obtained with the grooved rigid slider and the grooved soft slider covered with a suitable fabric are closed together in qualitative and quantitative points of view.
However, the artificial finger made of silicone and covered with a structured fabric gives with velvet, a friction cycle closest to that obtained with a real finger, in particular as regards the transient due to changes of fabric direction. In addition, the coefficients of friction obtained with a real finger and with this slider are of the same order of magnitude.

The artificial finger developed gives good results qualitatively and quantitatively for all the different fabrics tested representing a wide range of textile fabrics.

REFERENCES

Breugnot, Cécile. "Contribution À La Caractérisation Mécanique Du Toucher Des Surfaces Textiles À Partir De Critères Neurosensoriels." PhD Thesis. Université de Haute Alsace, 2005.

Bueno, Marie-Ange, et al. "Costam: Tool Design for a Controlled Tactile Stimulation." *AMSE JOURNALS-AMSE IFRATH Modelling* C, 2015, 75.2: 31-42.

KEYWORDS

Tactile, artificial finger, friction, textile fabrics

Sound Absorption Properties of Spunmelt Multilayer Nonwovens

Osman Babaarslan[1], Dilan Canan Çelikel[2]
[1]Çukurova University, Textile Engineering Department, Adana, Turkey
[2]Vocational School of Technical Sciences, Gaziantep University, Gaziantep, Turkey
celikel@gantep.edu.tr

OBJECTIVE

The aim of this research is to determine sound absorption performance of spunmelt multilayer nonwovens. Nonwoven samples in 7 different fabric weights with two different fiber cross-section shapes of round and trilobal, were tested at impedance tube and sound absorbtion coefficients obtained. It has been observed the effect of fiber cross-section shapes and fabric weight on sound absorbtion properties of spunmelt multilayer nonwoven fabrics.

INTRODUCTION

Noise is unwanted, undesired sound that effects human health and comfort negatively. There are two main methods for noise control as active noise control and passive noise control. Modifying and canceling sound field by electro-acoustical approaches is called active noise control. Passive noise control refers to those methods that aim to suppress the sound by modifying the environment close to the source [1]. Sound insulation is the basic passive noise control method and depends on sound absorbtion. Sound absorbtion is the reduction and converstion of sound energy to another type of energy, mostly heat energy.

Nonwoven fabrics with their porous, fibrous structures are one of the most commonly used sound absorbing materials for many technical applications (building and automotive insulations, machine insulations etc.). When a sound wave enters into a porous structure, the air molecules at the surface of the material and within the pores of the material are forced to vibrate resulted with loose of their original energy. This is because part of the energy of the air molecules is converted into heat due to thermal and viscous losses at the walls of the interior pores and tunnels within the material [2].

APPROACH

In this research sound absorbtion performance of spunmelt multilayer nonwovens has been investigated. Spunmelt nonwovens with the advantages of economical and short production line, with lower fabric weights will create lighter alternatives in the sound absorbers market, compared with bulky and heavy needle- punched nonwovens weights reaches to 1000 gr/m^2.

Castagnade et all reported that the sound absorption properties are decreasing during the compression of a fibrous mat and Yilmaz et all reported the decrease in sound absorption coefficient has been detected with increasing compression [3, 4]. Therefore, it is clear that the bonding under the pressure creates a denser and thinner structure and reduces porosity, so the sound absorbtion is effected negatively. Based on this approach bonding has not been applied to the nonwovens produced under this research. Unbonded three layers compose spunmelt multilayer nonwoven fabrics. As the outer layers are spunbond nonwovens; middle layer, sandwiched between spunbond layers, is the meltblown nonwoven. Fabric design of nonwoven samples has been illustrated in Figure 1.
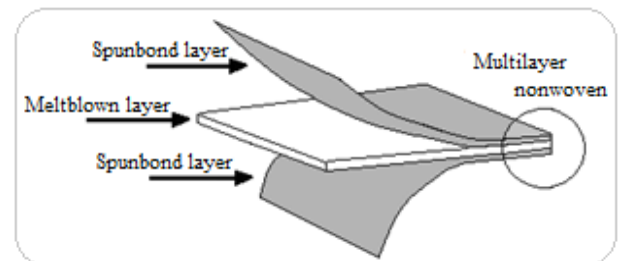

Figure 1. Spunmelt multilayer fabric design.

Raw material of all layers is polyester fiber with the same specifications for each layer. Spunbond layers composed of two types of fibers cross-section of round and trilobal and weight of layers is 40 g/m^2; meltblown layers have 7 weight ranges of 50 g/m^2, 75 g/m^2, 100 g/m^2, 125 g/m^2, 150 g/m^2, 175 g/m^2 and 200 g/m^2; multilayer nonwoven fabrics' weights range from130 g/m^2 to 280 g/m^2.

Acoustic insulation performance of nonwoven fabrics has been determined with impedance tube, according to the the standart 'ISO 10534-2 Determination of sound absorption coefficient and impedance in impedance tubes– Transfer Function method'. Impedance tube method is most widely used and significant method owing to short test times with small sample sizes and simple, accurate measurement. The basic principle of the measurement is shown in Figure 2 schematically.
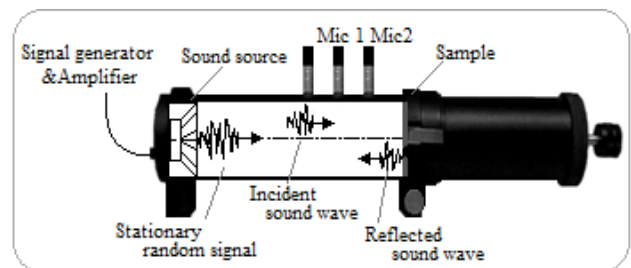

Figure 2. Impedance tube for the two microphone transfer function method [5].

RESULTS AND DISCUSSION

In Figure 3 the sound absorbtion coefficients of spunmelt multilayer nonwovens can be observed for increasing fabric weights.
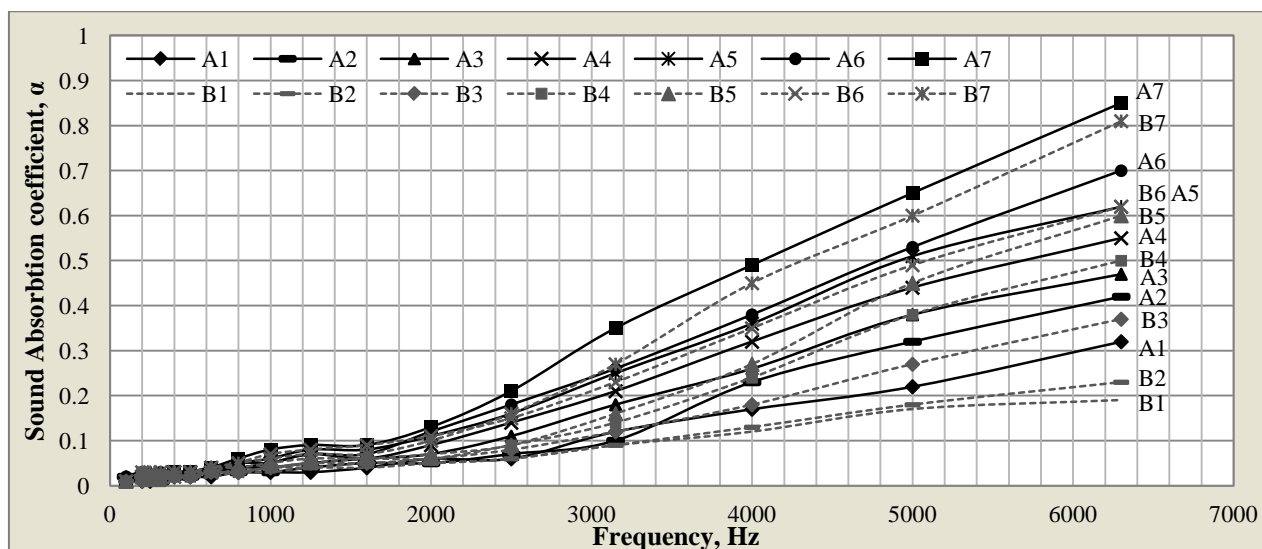
Figure 3. Sound absorbtion coefficients of spunmelt multilayer nonwovens.

The performance of sound absorbing materials is evaluated by the sound absorption coefficient(α), ranges between 0- 1, and is defined as the ratio of acoustic energy that is absorbed by the material. Sample code A represents multilayer nonwovens' spunbond layers containing round cross-section shaped fibers; sample code B represents containing trilobal cross-section shaped fibers. Each range of fabric weight has been numbered from 1 to 7, where 1 represents the lightest fabric as 130 gr/m^2 and 7 is the heaviest one as 280 gr/m^2.

As shown in Figure 3, higher sound absorbtion coefficients have been obtained for all samples as the increase of the fabric weight. This is because when fabric weight increases, more fibers interaction in the structure composes more paths for the sound wave to move, resulted with the frictional losses and absorbtion of sound energy, so sound absorbtion performance becomes better.

B samples have lower sound absorption coefficients than A samples for each range of fabric weights. The reason of this may be because different pore structures and fiber surface area of between A and B samples. Fibers of round cross-section have larger fiber surface area and less cavities creates smaller connected pores which improves sound absorbtion. Furthermore it should be noted that the correlation between A and B samples are not regular. For example the sound absorbtion coefficient of A5 and B6 equals 0.62 for the frequency of 6300 Hz and higher absorbtion than B5. This means that the lighter fabrics containing fibers with the cross-section of round have better sound insulation performance than the heavier fabrics containing fibers with the cross-section of trilobal.

CONCLUSION
In this research spunmelt multilayer nonwovens have been examined to investigate the sound absorption properties. As the variation of the fibers cross-section shape of round and trilobal at the outer layers, it has been observed that sound

absorbtion performance has been effected. All samples had low sound absorbtion coefficients range between 0.0– 0.3 up to the frequency of 3000 Hz. The highest sound absorbtion coefficient 0.85 (85% sound absorbtion) has been observed at A7 for the frequency of 6300 Hz at the maximum range of fabric weight of 280 gr/m^2. The results show that sound insulation can be performed by spunmelt multilayer nonwovens for high frequencies and compete with commercially used bulky and heavy needle-puched nonwovens.

FUTURE WORK
In the future, porosity and air permeability performance of spunmelt multilayer nonwovens will be examined and the results will be associated with sound absorbtion properties obtained from this research. Also all results will be analysed statistically.

KEY WORDS
Noise control, sound absortion, impedance tube, spunmelt, multilayer nonwovens.

REFERENCES
[1] *Engineering Acoustics*, Accessed March 1, 2016. h*ttp:/en.wikibooks.org/wiki/Engineering_Acoustics.*
[2] Arenas, J.P., Crocker, M.J. "Recent Trends in Porous Sound Absorbing Materials." *Journal of Sound and Vibration,* 2010, July: 12-17.
[3] Castagnede, B., Aknine, A., Brouard, B., Tarnow, V. "Effects of Compression on the Sound Absorption of Fibrous Materials." *Journal of Applied Acoustics*, 2000, 61: 173-82.
[4] Yilmaz, N.D., Michielsen, S., Banks-Lee, P., Powell, N. "Effects of Material and Treatment Parameters on Noise-Control Performance of Compressed Three-Layered Multifiber Needle-Punched Nonwovens." *Journal of Applied Polymer Science*, 2011, 123: 2095-2106.
[5] Ryu , Y. "Test Procedure for Determination of the Acoustic Properties of Materials Using the Two-Microphone Transfer Function Method." *Journal of Building Acoustics*, 2002, Volume 9, 1: 73-79.

Electromagnetic Characterization of Textile Materials for the Design of Wearable Antennas

Caroline Loss[1,2,3], Rita Salvado[1], Ricardo Gonçalves[3], Pedro Pinho[3,4], Sam Agneessens[5], Hendrik Rogier[5]
[1]FibEnTech Research Unit–University of Beira Interior; [2]CAPES Foundation; [3]Instituto de Telecomunicações–Aveiro;
[4]Instituto Superior de Engenharia de Lisboa; [5]Department of Information Technology, Ghent University/iMinds
carol@ubi.pt

ABSTRACT

Wireless communication systems are made up of several electronic components, which over the years have been miniaturized and made more flexible, such as batteries, sensors, actuators, data processing units, interconnectors and antennas. In the context of wearable systems, the antennas have been challenging because they are conventionally built on rigid substrates, hindering their efficient and comfortable integration into the garment.

Considering the flexibility and dielectric intrinsic properties of textile materials, the development of textile antennas may boost wearability and enlarge the domain of applications of such wireless communication systems, aiming purposes such as tracking and navigation, mobile computing, energy harvesting and storage [1]–[7]. Moreover, wearable antennas and clothing with antennas embedded on them emerge as potential interfaces of the human-technology-environment relationship, enhancing the interaction of the end user with some electronic devices, making them less invasive and more discrete.

To obtain good results, wearable antennas have to be thin, lightweight, of easy maintenance, robust, and moreover, must be low cost for manufacturing and commercializing. In this way, planar antennas, the microstrip patch type, have been proposed for garment applications, because this type of antenna presents all these characteristics, and also are adaptable to any surface [2].

The knowledge of the electromagnetic properties of the materials is essential to a good design of the antenna. Many criteria should be considered, as several characteristics of the textile materials directly affect the behavior of the antenna [8]. Specific electrically-conductive textiles are available on the market and have been successfully used in the radiating components. Conventional textile fabrics have been used as substrates. However, little information can be found on the electromagnetic properties of these regular textiles. Indeed, woven, knits and nonwovens are inhomogeneous, highly porous, compressible and easily influenced by the environmental hygrometric conditions, making their electromagnetic characterization difficult [9].

In this context, the main objective of this paper is to present an experimental characterization of the electromagnetic properties of some textile materials, aiming the selection of textiles well suited as dielectric substrates for the development of wearable antennas. The Resonator-Based Experimental Technique was used. It is based on the theory of resonant methods and consists in calculate the electromagnetic parameters of the material under test, at a single frequency, by measuring the shift in frequency and the value of Q-factor of one resonator board with a microstrip patch antenna.

The resonant methods generally give higher accuracies than non-resonant ones and do not require a complex sample preparation [10]. Other advantage of this method is that the measured values are not influenced by the condition of some variables, as for example, the type of glue/adhesive sheet, the connector and the manufacturing technique of the probe, which can lead to non-repeatability of the measurements and introduce errors in the final values.

In order to understand the influence of some mechanical properties, such as thickness and surface roughness, on the electromagnetic behavior of the textile materials, this paper also correlates the permittivity values (measured with the Resonator-Based Experimental Technique) with the mechanical properties. The thickness and surface roughness of the textile fabrics were measured using the KES – Kawabata Evaluation System [11]. It was found that materials with higher roughness have higher permittivity values, due to the augmented presence of air in the superficial porosity.

To validate the experimental characterization method, the measured permittivity values were considered for the dimensioning of wearable antennas, which performance was further tested. These antennas were designed to resonate around 2.45 GHz covering the Industrial, Scientific and Medical (ISM) band, between 2.4 and 2.45 GHz. This bandwidth also supports the WLAN (Wireless Local Area Network), Bluetooth and SRCS (Short Range Communication Systems 802.15.4) applications. The results of the antennas supported the validation of the method.

Therefore, the characterization of the electromagnetic properties of textile materials to apply as dielectric substrates in wearable antennas   may be easily performed with the resonator-based experimental technique used in this paper. This technique proved to be an efficient, simple, easy and quick technique to find suitable dielectrics for textile antennas.

KEYWORDS
Electromagnetic characterization, dielectric materials, textile antennas, wearable technologies.

REFERENCES

[1]   T. Kaija, J. Lilja, P. Salonen. "Exposing textile antennas for harsh environment." *Proceedings of the 2010 Military Communications Conference*, 2010: 737-742.

[2]   I. Locher, S. Member, M. Klemm, S. Member, T. Kirstein, G. Tröster, S. Member. "Design and Characterization of Purely Textile Patch Antennas." *IEEE Transactions on Advanced Packaging*, 2006, Vol. 29, No. 4: 777-88.

[3]   S. Agneessens, H. Rogier. "Compact Half Diamond Dual-Band Textile HMSIW On-Body Antenna." *IEEE Antennas Propag. Mag.*, 2014, Vol. 62, No. 5: 2374-81.

[4]   C. Hertleer, H. Rogier, S. Member, L. Vallozzi, L. Van Langenhove. "A Textile Antenna for Off-Body Communication Integrated Into Protective Clothing for Firefighters." *IEEE Trans. Antennas Propag.*, 2009, Vol. 57, No. 4: 919-25.

[5]   F. Declercq, A. Georgiadis, H. Rogier. "Wearable aperture-coupled shorted solar patch antenna for remote tracking and monitoring applications." *5th European Conference on Antennas and Propagation*, 2011.

[6]   R. Gonçalves, N. Carvalho, P. Pinho, C. Loss, R. Salvado. "Textile antenna for electromagnetic energy harvesting for GSM900 and DCS1800 bands." *Antennas and Propagation Society International Symposium (APSURSI) 2013*, 2013: 1206-07.

[7]   A. Dierck, F. Declercq, H. Rogier. "A Wearable Active Antenna for Global Positioning System and Satellite Phone." *IEEE Trans. Antennas Propag.*, 2013, Vol. 61, No. 2: 532-38.

[8]   R. Salvado, C. Loss, Gon, P. Pinho. "Textile materials for the design of wearable antennas: A survey." *Sensors (Switzerland)*, 2012, Vol. 12, No. 11: 15841-57.

[9]   S. Sankaralingam, G. Bhaskar. "Determination of Dielectric Constant of Fabric Materials and Their Use as Substrates for Design and Development of Antennas for Wearable Applications." *IEEE Trans. Instrum. Meas.*, 2010, Vol. 59, No. 12: 3122-30.

[10]   L.F. Chen, C.K. Ong, C.P. Neo, V.V. Varadan, V.K. Varadan. *Microwave Electronics: Measurement and Materials Characterization*. Chichester: John Wiley & Sons, Ltd, 2004.

[11]   S. Kawabata. "Measurement of the Mechanical Properties of Fabrics." *The Standarization and Analysys of Hand Evaluation*, Second Ed., Osaka: The Textile Machinery Society of Japan, 1980: 28-57.

Natural Fibers

Composite Processes, Properties, and Modeling

Characteristics and Prospective Applications of Powders Derived from Natural Fibers

Rangam Rajkhowa[1], Mehdi Kazemimostaghim[1], Xungai Wang[1,2]

[1]Australian Future Fibres Research and Innovation Centre, Deakin University, Geelong, VIC, Australia

[2]School of Textile Science and Engineering, Wuhan Textile University, Wuhan, China

rangam@deakin.edu.au

OBJECTIVES

Objective is to utilize unspinnable natural fibers in new applications.

INTRODUCTION

Ultrafine particles can be fabricated by a top down approach of milling from natural fibers or fabrics. Innovative applications of such particles will benefit the textile life cycle by utilization and value addition of waste fibers. Prospective applications of products from powders via traditional and additive manufacturing routes include textile surface treatment, ion separation, cosmetic and biomedical applications. It is important to understand the size, morphology, structure, surface and bulk properties of particles to design appropriate products. This paper discusses some of these properties and associated advantages for new applications.

APPROACH

Particles of different sizes were prepared from cellulosic and protein fibers using cutter milling, wet attritor milling, spray drying and air jet milling without any pre-treatment and use of chemicals. Particle size distribution was measured using laser light scattering and scanning electron microscopy. Change in microstructure during production was analysed by FTIR and XRD. Surface area was determined using nitrogen adsorption. To understand biomedical application prospects of silk particles, their in-vitro degradation kinetics, cell and tissue growth supporting properties, and loading and release properties of model drugs were investigated. To understand application potential for ion separation applications, binding and release of different ions from particles were measured by atomic absorption spectroscopy. For use in textile surface treatments, particles were used in screen printing formulations. Particles were also produced from naturally coloured fibers such as alpaca hair to prepare printing formulations.

RESULTS AND DISCUSSIONS

Size, morphology and structure: A combination of wet attritor milling and spray drying produced particles from natural fibers with a volume average particle size of about 5 µm and a surface area up to 20 m^2/g. As shown in the magnified image (Fig.1), a particle appears to be an aggregate of submicron primary particles. The particle size could be reduced to less than 1 µm by de-aggregating such aggregates using jet milling or bead milling. The required time of milling varied depending on the nature of fiber but the limiting particle size remained nearly the same. These particles are insoluble in water and the natural crystalline structure of native fibers is retained during the fabrication process as revealed by FTIR and XRD results.

Figure 1: Wool powder and SEM image of a wool particles.

Bulk properties: The bulk properties such as cohesiveness, flowability, compressibility, and aggregation behaviors were analyzed. Such properties depend primarily on the fabrication methods. For example, Fig.2 shows that after air jet milling (AJM) powder compressibility increased. Increase in cohesiveness and reduction in powder flow index after AJM were revealed through power rheometer measurements. Inverse gas chromatography was used to measure the surface energy and the results showed that increase in surface energy due to size reduction was responsible for increasing cohesiveness and reduction of powder follow. These results are important to designing particles for 3D printing and cosmetic applications.
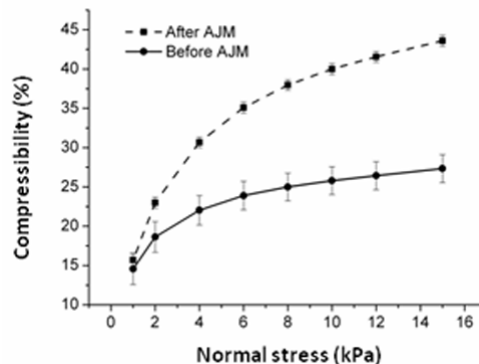

Figure 2: Compression properties of wool powder.

Sorption properties: Increase in surface area of particles allowed rapid adsorption of dyes and various ions. For example, wool powders could be dyed even at room temperature in 5-10 minutes depending on size whereas parent fibers could take hours even at an elevated temperature. Similarly, loading capacity of various ions was significantly increased when fibers were converted to fine particles. Fig.3 shows the influence of silk particle size on absorption of Cr^{6+} ions. Adsorbed ions were released if pH was changed. Fig 4 shows percentage desorption of Cr^{6+} by different fibers and powders. The reversible binding speed of powders was much faster than the fibers. Our studies also

show that particles can be efficiently used for loading of drugs. For example, equilibrium loading of model drugs *Orange G*, *Azophloxine, Rhodamine B*, and *Crystal Violet* on silk particles could be achieved in less than 10 min at room temperature compared to 2-3 days needed for fibers. Loading and release of these chemicals depended on the size of the particles, pH, and the structure and properties of model drugs. Both fibers and particles could slowly release the drugs over many days at pH 7.4 at 37°C without a significant initial burst.
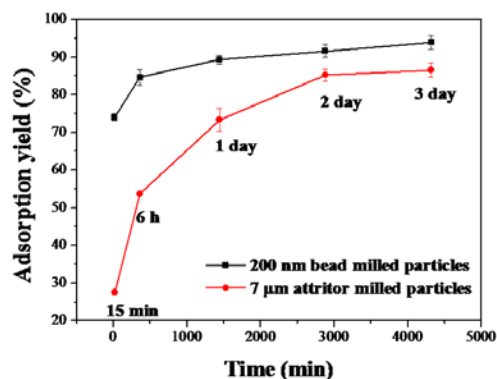
Figure 3: Adsorption of Cr^{6+} by silk powders of different size.
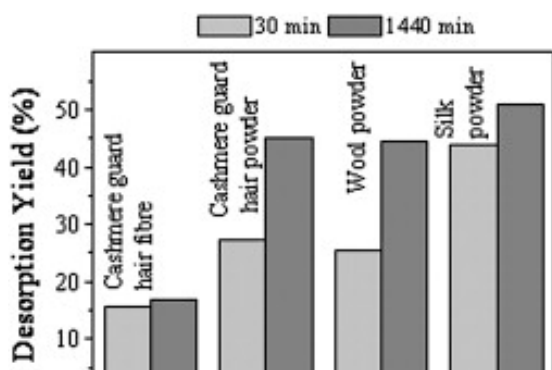
Figure 4: Cr^{6+} desorption from cashmere guard hair fiber and different powder.

Biocompatibility: Biocompatibility of particles from protein fibers was investigated by in-vitro cell culture studies. Fig.5 shows results of cell count when silk particles were used in the cell culture media. Particles prepared from different silk varieties were able to support the adhesion and migration of mouse fibroblasts. Particles could be effectively used to reinforce scaffolds used for tissue engineering with improved mechanical properties and better differentiation of bone marrow cells. Biodegradability of the particles is enhanced due to increase in surface area and roughness. Degradation of silk particles by protease XIV was about three-fold faster compared to silk fibers.

Surface treatment: Particle size was controlled to meet the need for screen printing. Up to 20% particles could be added in the printing paste for screen printing. Fig.6 shows the results of printing from waste colored cashmere coarse hairs
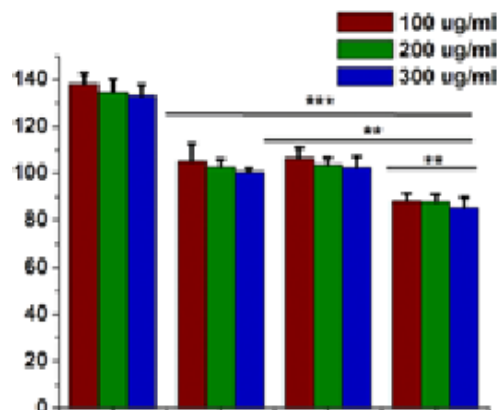

Figure 5: Relative Viability of cells in the presence of micro-particles of silk derived from four varieties of silk.

Figure 6: Cashmere guard hair and a screen print from powder prepared from the hair.

CONCLUSION

Good scope exists for application of particles from natural fibers for textile surface treatment, biomedical applications such as drug delivery, skin care and tissue scaffolds and separation of ions. Particles can be designed with adequate size, flow and bulk properties for various applications. As no pre-treatments are needed and chemical free manufacturing process can be used for fabricating ultrafine particles, this approach can be useful for large scale production of fiber powders and utilization of wastes for novel applications. We are currently exploring such new applications and also use additive manufacturing approaches to develop products from fiber powders.

REFERENCES

1. Bhardwaj, N., et al. *International Journal of Biological Macromolecules,* 2015, 81: 31-40.
Kazemimostaghim, M. et al. Powder Technology, 2015, 281: 321-27.
2. Rajkhowa, R., Wang, X. "Silk Powder for Regenerative Medicine." *Silk Biomaterials for Tissue Engineering and Regnerative Medicine*. Cambridge: United Kingdom, 2014. ISBN 9780857096999.
3. Rajkhowa, R., et al. "Ultrafine wool powders and their bulk properties." *Powder Technology*, 2012, 224: 183-18.

The Effect of Titanium Dioxide on the Processing Time of Composites Made of Commingled Glass and PA 6 Fibres

Robert Brüll, Karolina Jaksik, Gunnar Seide, Thomas Gries
Institut für Textiltechnik der RWTH Aachen University
robert.bruell@ita.rwth-aachen.de

INTRODUCTION

The importance of light weight construction in the mobility sector has increased throughout the recent years. Both the automotive industry as well as the aerospace industry aim to achieve the lowest possible weight at maximized mechanical properties (Witten, Kraus & Kühnel 2014). Reduced weight leads to higher energy efficiency thus decreasing operating costs. In order to achieve the mentioned efficiency while staying profitable, fibre reinforced thermoplastic composites (FRTCs), are being developed (Renault 2014). These can be produced by commingling thermoplastic fibres with reinforcement fibres to hybrid yarns and weaving these into fabrics. The textile structures are subsequently heated and consolidated through compression moulding. For an optimal consolidation, the temperature distribution needs to be homogenous throughout the organic sheets. Excessive temperatures can lead to degradation of the polymer. A low temperature leads to consolidation constraints. However, the heating and cooling times of the organic sheets are the cycle-time determining factors. Shorter cycle times lead to higher outputs, thus reducing the costs per part. In the course of the BMBF-project "NanoOrgano" the shortening effect of nanoscale fillers on the heating and cooling times of hybrid yarn based thermoplastic composites was observed at the Institute for Textile Technology, Aachen (Kravaev, Seide, Gries 2012). The goal of the follow-up project "VIP Organo" is the validation of the innovation potential of this effect. The corresponding technology chain is pictured in Figure 1.

APPROACH AND METHODS

As a first step Polyamide 6 compounds containing different concentrations of titanium dioxide are being investigated. The most promising compound is chosen for further processing and investigation. With regard to previous results stated by Brüll et al. (Brüll et al. 2015), this work will focus on the influences of the investigated particles on the processing of Polyamide 6 and the resulting cycle times for the production of FRTCs. The material chosen is a Polyamide compound with the addition of nanoparticles of titanium dioxide. This modification of the Polyamide compound has several effects. A small increase in the concentration of titanium dioxide (TiO2) leads to an increase in the heat conductivity and decrease in the heat capacity (Kravaev, Seide, Gries 2012). This leads to shorter heating and cooling times which in turn have a significant effect on the cycle-time during the consolidation process. In addition, the macro particle orientation is lowered which decreases the characteristic thermal shrinking of the thermoplastic compound and thus enables an easier thermal processing of the material. The concentration can't be increased indefinitely however. The TiO2 particles while having the positive effects mentioned also lower the strength of the compound (Kravaev, Seide, Gries 2012). Therefore, a compromise needs to be made. The results of Brüll et al. (Brüll et al. 2015) show that the most promising concentration of TiO2 is 5 wt.-%.

In order to properly assess the effect on the cycle-time the process needs to be twofold. Firstly, the two production methods need to be compared regarding their actual cycle-times. This means that the industrial standard method of filmstacking needs to be reproduced as well as the method using a hybrid roving. Secondly, the mechanical properties need to be examined. This is achieved by comparing the two differently produced FRTC with an industrially produced FRTC. With the intention of achieving comparability, the materials used are kept as similar as possible. With the modified Polyamide compound being the only exception.

In order to produce a FRTC the modified Polyamide compound is turned into a hybrid roving using the commingling method. This process involves mixing the different Polyamide yarn and a glass fibre yarn together using air turbulences. Ideally the resulting hybrid roving has

Material Level

Nano-particle/PA Process Level · Nano-compound · Nano-PA/Glass · Hybrid yarn · 2D-fabrics · Prototype

Compounding · Filament spinning · Commingling · Textile production · Consolidation · Testing
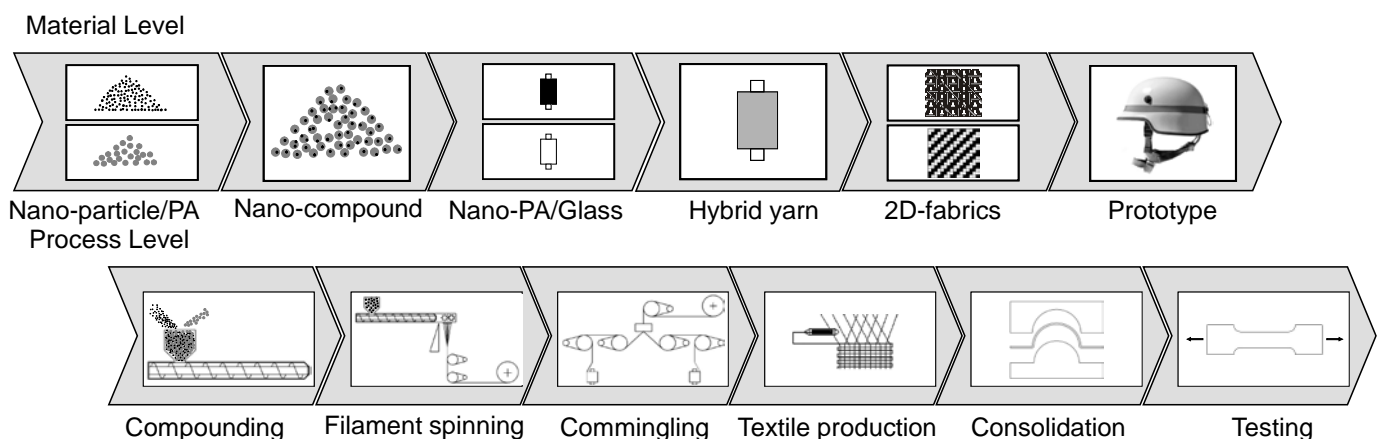
Figure 1: Technology chain of the BMBF project NanoOrgano.

an even distribution of the two components. This significantly decreases the flow path of the Polyamide compound during the consolidation process from half the diameter of the glass fibre yarn to half the diameter of a single glass fibre. The optical microscopic examination of the hybrid roving shows that the idealistic distribution can't be reached. An analysis of the tensile test and the optical microscopic examination results after the commingling process however show an interesting correlation. The better the fibres are mixed the lower is the strength of the hybrid roving. This shows that the reinforcement fibres are damaged by the air turbulences involved which will affect the strength of the FRTC. Due to the structure of the hybrid roving produced by the commingling process the tensile test has its limitations. The hybrid roving structure shows loops, knots and straight patches of parallel fibres. This means that the reinforcing fibre can't be tested as one entity. The tensile test after the consolidation process gives a more accurate assessment of the damage. Finally, the hybrid roving is woven into a twill 2x2 fabric which is layered to achieve the right thickness and consolidated in a heating press.

RESULTS AND DISCUSSION
The Results show the positive effects of the increased heat conductivity, decreased heat capacity and reduced flow path on the cycle time of the consolidation process. The cycle time of the FRTC made out of the hybrid roving is up to 20 % shorter than the cycle time of the FRTC made using the filmstacking method. This underlines the potential for a more efficient chain of production. However, the tensile and bending tests of the FRTC show a decrease in the mechanical properties of the composite by 5 - 10 %. This underlines the afore mentioned limitations of the commingling process. The loss in mechanical strength is the result of the damages to the glass fibres during this process. However, it is noticable that the loss in strength after the consolidation process is less than before. This can be due to the shrinking polyamide compound during the consolidation

process which can straighten the fibres. Or be due the inconsistencies in the structure of hybrid roving caused by the random nature of the mixing process. This should be further investigated.

KEYWORDS
Fibre reinforced thermoplastic composites, heat pressing, commingling, nanoscale fillers, thermal conductivity.

REFERENCES
1. Witten, E., Kraus, T., Kühnel, M. *Composites-Marktbericht 2014: Marktentwicklungen, Trends, Ausblicke und Herausforderungen.* Bayreuth, Frankfurt: AVK, CCeV, 2014.
2. Renault, T. "Latest Developments in Thermoplastic Composites for Automotive Applications." *2nd International Conference & Exhibition on Thermoplastic Composites, Conference Proceedings.* Hubert Borgmann. Bremen: MESSE BREMEN, WFB Wirtschaftsförderung Bremen GmbH, 27-28 October 2014: 17-20.
3. Kravaev, P., Seide, G., Gries, T. *Drapierfähige Halbzeuge aus nanomodifizierten Hybridgarnen für die Herstellung von faserverstärkten thermoplastischen Bauteilen Abschlussbericht.* Aachen, Hannover: RWTH, 2012.
4. Brüll, R., Hütten, A., Seide, G., Gries, T. "Using nanoscale fillers to improve the thermal properties of fibre reinforced thermoplastic composites regarding processing times." *CAMX Conference Proceedings, Society for Advancement of Material and Process Engineering, Composites and Advanced Materials Expo*, Dallas, Texas, October 26-29, 2015: 1609-23.

Mechanical and Structural Characteristics of a High-performance, Fully-thermoplastic, Fiber-reinforced Composite

Andres Leal[1], Joshi C. Veeramachaneni[1], Felix A. Reifler[1], Martin Amberg[1], Dominik Stapf[2],
Gion A. Barandun[2], Dirk Hegemann[1], Rudolf Hufenus[1]

[1]Empa, Swiss Federal Laboratories for Materials Science and Technology, Switzerland
[2]University of Applied Sciences Rapperswil, Institute for Materials Technology and Plastics Processing, Switzerland
andres.leal@empa.ch

OBJECTIVE

The objective of this work has been to develop an ultra-light, fully thermoplastic composite material with enhanced fiber-matrix interfacial characteristics and tensile property retention of the reinforcing UHMWPE fibers.

INTRODUCTION

The use of UHMWPE fibers as a reinforcement of composite materials has been historically hindered by their poor interfacial properties. Previous attempts to develop fully thermoplastic composites based on continuous UHMWPE yarns have shown that aside from their limited adhesive properties, the thermal processes used to make the composite significantly degrade the mechanical properties of the reinforcing fiber [1]. In an attempt to overcome the observed limitations, the present study focuses on the development of a novel semi-finished product which consists of a continuous UHMWPE-based hybrid yarn produced in a two-step process. First, the UHMWPE yarn is subjected to a continuous plasma polymerization in order to deposit an adhesion-promoting polar functional film on its surface, followed by an overjacketing extrusion consisting of a modified wire coating process in which the functionalized UHMWPE yarn is coated with a polymer melt which will subsequently serve as a matrix in the final composite component.

APPROACH

Materials

A MirAcle® Minu γ multifilament UHMWPE yarn with a linear density of 16 g/km and the Versify® 4200 polyolefin plastomer (POP) have been used to develop the fully-thermoplastic composite.

Plasma Polymer Deposition

The plasma polymerization process in which the surface of the UHMWPE yarn is functionalized was performed using an in house pilot plant device where a reel-to-reel operation allows to activate the yarn at a winding speed of 44 m/min.

Overjacketing Extrusion

The plasma-activated UHMWPE yarn was subjected to an overjacketing extrusion (OE) in which a single screw extruder feeds the polymer melt to a melt pump which in turn supplies the molten material at a fixed throughput of 5.25 g/min to the wire coating die illustrated in Fig. 1.
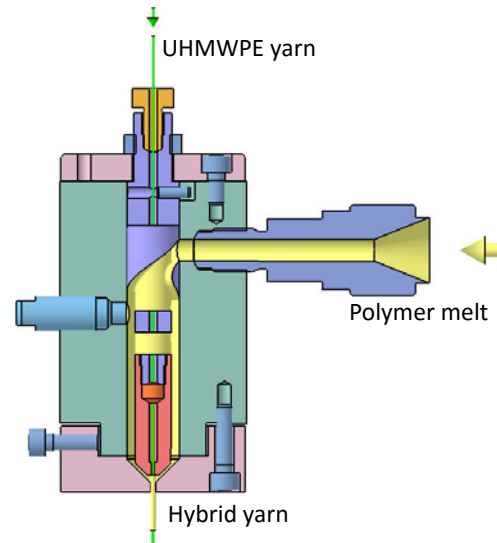

Figure 1. Schematic of wire coating die used for the overjacketing extrusion of an UHMWPE yarn.

Fiber-reinforced Composite

In order to make composite plates, the hybrid yarn resulting from the OE process was woven into a 4/1 twill fabric, and layers of woven hybrid yarn were then stacked with layers of commercially available UHMWPE fabric in an alternate fashion in order to construct lay-ups consisting of 16 to 20 layers. The fabric lay-up was hot compacted with a hydraulic press following a predefined pressure ramp at a temperature of 120 °C. The theoretical fiber volume fraction of the resulting fully thermoplastic composite is 0.54, which corresponds to a laminate density of 0.93 g/cm^3.

RESULTS AND DISCUSSION

A processing window for uniform UHMWPE yarn coating during OE was established in terms of two variables: winding speed of the hybrid yarn and overjacketing die temperature. Fig. 2 shows the range of temperatures and speeds for which a uniform coating is obtained, along with the amount of sheathing material applied to the UHMWPE yarn during OE.
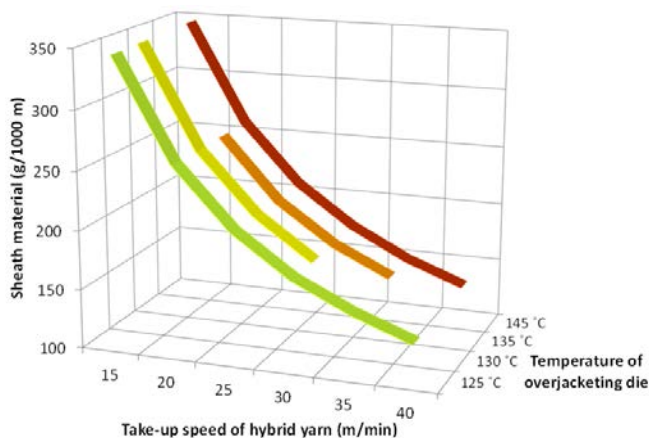
Figure 2. Effect of take-up speed and processing temperature on the resulting linear mass density of applied sheathing polymer [2].

The mechanical properties of the UHMWPE yarn after the different processing steps are reported in Table I. Its tensile strength is maintained constant, while Young's modulus undergoes a reduction of 10% after OE. The observed reduction might well be coupled to the measured increase of 14% in strain to break [2]. Wide angle X-ray diffraction patterns of the different yarns have been acquired. The equatorial profiles indicate that with respect to crystalline structure, all yarns are highly oriented with FWHM values of 2.4° to 3.9° (Fig. 3). Nevertheless, the varying relative intensities of the non-orthorhombic phase peak at $2\theta = 19.9°$ show that the molecular structure of the UHMWPE is slightly affected by the processing conditions associated with the fabrication of the hybrid yarn [2].

Table I. Mechanical properties of UHMWPE yarn after various processing steps [2].

Treatment	Strength (GPa)	Strain to break (%)	Young's modulus (GPa)
As-received	2.5 ± 0.1	3.6 ±0.2	77 ± 4
After hexane cleaning	2.4 ± 0.1	3.6 ±0.4	75 ± 4
After plasma polymerization	2.4 ± 0.1	4.2 ±0.2	72 ± 4
After OE	2.4 ± 0.1	4.1 ±0.2	69 ± 1

The tensile properties of the fully thermoplastic composite produced by hot compaction are displayed on Table II along with the properties of other types of composite materials reported in the literature. The advantage of using the UHMWPE yarn in combination with a discrete matrix system with enhanced interfacial behavior becomes apparent as the good tensile properties and low density of the yarn are successfully reflected in the properties of the laminate.

Table II. Tensile properties of selected fiber-reinforced composites [2].

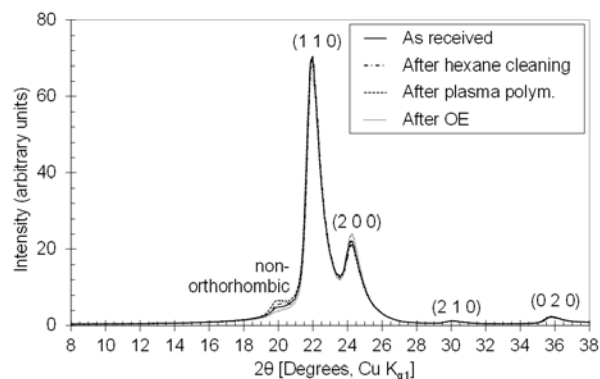| Composite	Density (g/cm^3)	Modulus (GPa)	Strength (MPa)
UHMWPE-POP	0.93	24 ± 5	317 ± 17
100% self-reinforced PP (Curv®)	0.82	4.2	120
100% hot compacted woven Dyneema®	0.97	7.0	250

Figure 3. Equatorial profiles (2θ scans) of WAXD patterns of UHMWPE fibers after various processing steps [2].

CONCLUSION
The feasibility of developing a hybrid yarn which can be used as a basic building block for the manufacture of an ultra-light, continuous fiber fully thermoplastic composite has been shown. The inert surface of the UHMWPE filaments is successfully activated by means of a continuous plasma polymerization process which enhances the fiber's adhesive behavior up to five times. The use of a stiffer matrix system is expected to significantly improve the observed out-of-plane properties of the composite laminates.

KEYWORDS
UHMWPE; Thermoplastic composite; plasma polymerization; extrusion.

ACKNOWLEDGMENT

REFERENCES
[1] Ward, I.M., Hine, P.J. "The science and technology of hot compaction." *Polymer*, 2004, 45:1413-27.
[2] Leal, A.A., Veeramachaneni, J.C., Reifler, F.A., Amberg, M., Stapf, D., Barandun, G.A., et al. "Novel approach for the development of ultra-light, fully-thermoplastic composites." *Materials and Design*, 2016, 93: 334-42.

Fibers for Medical Applications

Antibacterial Activity and Washing Durability of Bamboo Fabrics Treated with Different Metal Salts

Oğuz Demiryürek, Mustafa Tutak, Tuğba Tulunay
Erciyes University, Textile Engineering Department
demiryurek@erciyes.edu.tr

ABSTRACT

In this study, the antibacterial properties of bamboo fabric treated with three different metal salts (Cu, Zn and Ag) and the washing durability of treated with/without silicone were studied. Bamboo fabric were treated with zinc, silver and copper metal salts and softened/unsoftened by silicone with exhaustion technique. The treated fabric samples were washed 10 times to determine the durability of antibacterial properties. All fabric samples were analyzed by XRF for amount metal ions on the fiber. The ASTM E2149-01 and TS EN 1149-1 test methods were used to determine the bacteriodynamic activity and antistatic performance of the treated fabrics. All metal ions treatment on the fabrics enhanced the antibacterial properties which were durable to repeated washing.

KEYWORDS: Ag/Zn/Cu metal salts, antimicrobial activity, bamboo fabric, silicone

INTRODUCTION

Fibers which provide large surface area and absorb humidity generate suitable medium for microbial proliferation. Damaging textiles by micro-organisms can occur at almost all stages from manufacturing to end-use. This often gives rise to objectionable odor, product degradation, dermal infection, allergic responses and risks associated with transfer of microbes [1]. If bacteria form a parasitic association with other organisms, they are classified as pathogens [2]. In order to meet the consumer demands, different finishing chemicals, especially silver, zinc and copper have been applied to textile materials for their antibacterial properties [3-7]. There are different studies in the literature about antibacterial treatments of bamboo fabrics. Yang et al. investigated the antibacterial efficiency of bamboo charcoal/silver biological protective material [3]. Tang et al. used silver and gold nanoparticles to enhance the bamboo pulp fabrics [4]. Zheng et al. investigated the antimicrobial activity of silver nanparticle loaded viscose fabrics. Zhang et al. investigated the antibacterial activity of zinc oxide (ZnO) nanoparticle loaded bamboo pulp fabrics [6]. Yu et al. investigated the surface functionalization of bamboo with nanostructured ZnO [7]. The all above treatments enhanced the antibacterial property of bamboo fabrics. Afrin et al. investigated the origin of the antibacterial propert of bamboo charcoal fibers. They conclude that the antibacterial agents are located in lignin, not in hemicelluloses or other water-soluble chemical components [8]. Yang et al. carried out a comparative study of bamboo lyocell and other regenerated fabrics. They concluded that the antibacterial activity of bamboo lyocell fiber is higher than that of wood lyocell fibers.

The literature focused on enhancing the antibacterial property of bamboo fabrics with different metal salts. In this study different metal (copper, zinc and silver) salts were applied on bamboo fabrics with and without silicone in order to improve the antibacterial property of bamboo fabrics. The fabrics were washed ten times in order to see the durability of the treatment. Amounts of metal additives on the treated fabrics have been determined according to XRF analysis method.

MATERIALS AND METHODS

The single-jersey knitted bamboo fabric (80 g/m^2) was supplied by Boyteks, Kayseri-Turkey. The fabric samples were treated with 0.1 M of CuSO$_4$, Zn(NO$_3$)$_2$ and AgNO$_3$ in glass bottles at 95 ^{o}C for 30 min. For softening, after the application of metal salt, fabric samples were finished with softening agent (Silicone softener: Setasoft 1640, Setas chem.) at 50 ^{o}C for 20 min. Dyeing, metal salts treatment and softening diagram have been shown as an example in Figure 1.
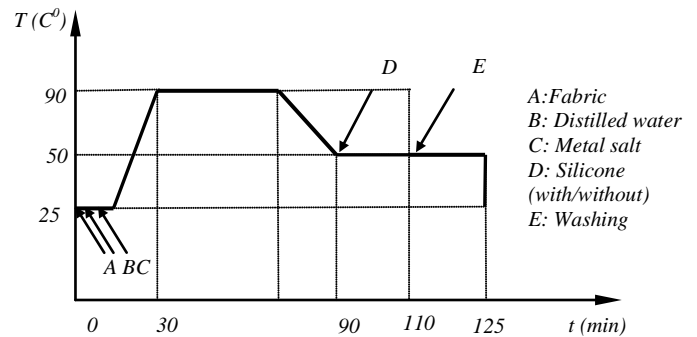

Figure 1: Metal salt application to bamboo fabrics with or without silicone softener.

Cultures of *Escherichia coli* (ATCC 11229) and *Staphylococcus aureus* (ATCC 25923) bacteria were used in the study: Before the antimicrobial tests, all bacteria from the fresh culture were grown in nutrient broth at 37 ^{o}C for 18 hours. ASTM E2149-01 test method was used for the bacteriodynamic activity bactericidal (killing of bacteria) of treated bamboo fabrics against selected bacterial species. The 0.5 g of sterile fabric sample was introduced into the 10 ml nutrient broth inoculated with the desired microbe during 3 hours and incubated at 37 ^{o} C overnight. The number of colonies in the tubes was counted serial diluting process at 0 and 3 h. The reduction per cent caused by each concentration of the samples on selected test bacteria was expressed as Equation 1:

$$R(\%) = \frac{c_0 - c}{c_0} x100 \qquad (1)$$

where C_o (cfu) is the number of microbial colonies on the treated fabric at zero time and C (cfu) is the number of microbial colonies on it after three hours. R (%) is the reduction in bacterial population [10]. The antibacterial activity results for bamboo fabrics treated with metal salts with or without silicone softeners is shown in Table-I.

Table-I. Antibacterial activity results for bamboo fabrics treated with metal salts with or without silicone softeners.

Metal Salt	Treatment	*Escherichia coli*			*Staphylococcus aureus*		
		Bacteria count (count/ml)		Decrease	Bacteria count (count/ml)		Decrease
		Initial	After 3 h.	(%)	Initial	After 3 h.	(%)
CuSO4	No treatment	9.200.000	14.600.000	Increase	10.200.000	17.500.000	Increase
	%1 Cu	6.700.000	0	100	8.100.000	0	100
	%1 Cu+10 times washed	8.100.000	1.000.000	88.75	7.000.000	500.000	92.85
	%1 Cu+ silicone	7.600.000	0	100	9.100.000	0	100
	%1 Cu+ silicone+ 10 times washed	8.000.000	4.000.000	50	9.200.000	4.048.000	44
Zn(NO$_3$)$_2$	No treatment	9.200.000	14.600.000	Increase	10.200.000	17.500.000	Increase
	%1 Zn	8.200.000	0	100	6.900.000		100
	%1 Zn+10 times washed	7.900.000	3.500.000	43.03	6.700.000	3.500.000	47.76
	%1 Zn+ silicone	11.000.000	0	100	9.000.000	0	100
	%1 Zn+ silicone+ 10 times washed	9.600.000	4.500.000	53.12	8.500.000	5.600.00	34.1
AgNO$_3$	No treatment	9.200.000	14.600.000	Increase	10.200.000	17.500.000	Increase
	%1 Ag	8.200.000	0	100	6.900.000	0	100
	%1 Ag+10 times washed	7.900.000	0	100	6.700.000	0	100
	%1 Ag+ silicone	11.000.000	0	100	9.000.000	0	100
	%1 Ag+ silicone+ 10 times washed	9.600.000	0	100	8.500.000	0	100

CONCLUSIONS

As a result of experimental study according to ASTM E2149 on the antibacterial activity of bamboo fabrics treated with different metal salts with or without silicone softener, following conclusions can be drawn:

• Raw regenerated bamboo fabrics did not show antibacterial property.

• The washing decreased the metal ion count and antibacterial efficiency of fabrics. However, fabrics still have shown antibacterial effect.

• Silicone treatment does not contribute to the antibacterial efficiency of the fabrics.

• The best metal salt was found as AgNO$_3$ for maximum antibacterial effect with or without silicone.

ACKNOWLEDGMENT

REFERENCES

1. U.C. Hipler, P. Elsner. *Bifunctional Textiles and the Skin*. Basel: Karger, 1995. 15-44.
2. J. Wearing. *Bacteria*. USA: Crabtree Pub., 1991. 5-58.
3. Yang, F.C., Wu, K.H., Liu, M.J., Lin, W.P., Hu, M.K. "Evaluation of the antibacterial efficacy of bamboo charcoal/silver biological protective material." *Materials Chemistry and Physics*, 2009, 113(1): 474-79.
4. Tang, B., Sun, L., Li, J.L., Kaur, J., Zhu, H.J., Qin, S., Yao, Y., Chen, W., Wang, X.G. "Functionalization of bamboo pulp fabrics with noble metal nanoparticles." *Dyes and Pigments*, 2015, 113: 289-98.
5. Zheng, J., Song, F., Wang, X.L., Wang, Y.Z. "In-situ synthesis, characterization and antimicrobial activity of viscose fiber loaded with silver nanoparticles." *Cellulose*, 2014, 21(4): 3097-3105.
6. Zhang, G.Y., Liu, Y., Morikawa, H., Chen, Y.Y. "Application of ZnO nanoparticles to enhance the antimicrobial activity and ultraviolet protective property of bamboo pulp fabric." *Cellulose*, 2013, 20(4): 1877-84.
7. Yu, Y. Jiang, Z.H. Wang, G., Tian, G.L., Wang, H.K., Song, Y. "Surface functionalization of bamboo with nanostructured ZnO." *Wood Science and Technology*, 2012, 46(4): 781-90.
8. Afrin, T., Tsuzuki, T., Kanwar, R.K., Wang, X. "The origin of the antibacterial property of bamboo." *Journal of the Textile Institute*, 2012, 103(8): 844-49.
9. Yang, G.S., Zhang, Y.P., Shao, H.L., Hu, X.C. "A comparative study of bamboo Lyocell fiber and other regenerated cellulose fibers." *Holzforschung*, 2009, 63(1): 18-22.
10. Tutak, M., Gun, F. "Antimicrobial Effect of Ci Basic Red 18:1 and Ci Basic Yellow 51 on Some Pathogenic Bacteria." *Fibers and Polymers*, 2011, 12: 457.

Development of Antibacterial Braided PET Suture

Faten Debbabi[1], Mohamed Adnene Haj Ayed[2], Saber Ben Abdessalem[3]

[1]Textile Engineering Laboratory, Monastir University, Tunisia
[2]Laboratory of Chemical, Pharmaceutical and Pharmacological Development of Drugs, Monastir University, Tunisia
[3]Textile Materials and Processes Research Unit, Monastir University, Tunisia
debbabi_faten@yahoo.fr

INTRODUCTION

The aim objective of this study is the development of new non absorbable antibacterial PET braided using chitosan as antibacterial product and citric acid as crosslinking agent.

Today, sutures are widespread in the world and are widely used in all surgical interventions. They are the most implanted biomaterials (Chu et al.). They have physical and chemical properties quite different from each other. Non-absorbable sutures have undergone several improvements in their mechanical properties. However, there are no new significant improvements in their physiological properties since their first use.

Chitosan is one of many antibacterial products. It is also biocompatible, immunostimulant, regenerate cells and hydrophilic. The modification of the suture surface, which promote hydrophilicity, has a great influence on the development of the antibacterial barrier (Khulbe et al. ,Werner et al.). Chitosan is resistant to sterilization with ethylene oxide (EO) and keeps its antibacterial properties after this treatment. Therefore, it is suitable for the treatment of polyester suture sterilized with EO (Juan et al.,Marreco et al.). For all these reasons, chitosan was chosen to develop our antibacterial sutures.

Most proposed methods generally used to apply the chitosan on textile materials require a chemical modification of the fiber typically using toxic products. The technique proposed in this study does not require any modification in the macromolecular chains and only biocompatible products are used.

APPROACH

Preparation of coating solution (chitosan-CA)

Appropriate amount of Chitosan is dissolved gradually in a solution of 1% acetic acid with stirring and gradually heating to 60 °C. After complete dissolution of chitosan, citric acid is gradually added. Citric acid is used as crosslinking agent. Finally, hypophosphite sodium was added as catalyst of the crosslinking reaction. The resulting solution (chitosan -AC) is used for suture coating.

Manufacturing of PET antibacterial braided sutures

Braided suture made of 16 non-texturized PET yarns with 49 dtex count and 16 filaments per yarn was fabricated. Then suture was scoured. Because PET is a hydrophobic polymer, hydrolysis treatment of PET by NaOH is used to improve hydrophilicity of PET by creating new carboxylic groups on the suture fiber surface. Finally, before coating, suture is hot stretched under 200 °C.
For suture coating, PAD Day process is used to avoid gluing between sutures and to ensure a uniform import rate of chitosan. The alkalized PET suture passes in a coating bath containing the coating product prepared previously (Figure 1), then through a heat chamber. Consequently, coating solution is polymerized under heating effect and biofilm is formed on the suture surface. Multilayers of coating solution are applied on suture surface by multiple passes throw the coating bath followed by polymerization in heat chamber. The suture is then neutralized in a 0.1 N NaOH solution followed by a washing in water bath before being dried at a temperature of 80 °C.

Chitosan concentration, citric acid concentration, temperature, residence time in the thermal chamber and the passage number are the five factors considered during coating treatment. The temperature is selected between 120 and 160 °C. Temperature of 120 °C is the minimum needed temperature for drying the coating material. The maximum temperature supported by the coating product is 160 °C. The residence time was defined in the technological limits of the machine between 0.45 min and 4.5 min. The number of passages in the coating bath and in the heating chamber was selected between 1 and 3. To study the impact of each solution component present in the coating solution on the effectiveness of the coating process, 9 coating solutions were prepared with different component concentrations. The chitosan concentrations were 1% (minimum viscosity), 2 % and 3% (maximum solubility of chitosan). The citric acid concentrations were between 3% and 10% according to several studies reported in the literature (Gawish et al. ,Wang et al.). Sodium hypophosphite is used for proportional concentrations (1/3) at citric acid concentration according to the work of Wang et al.
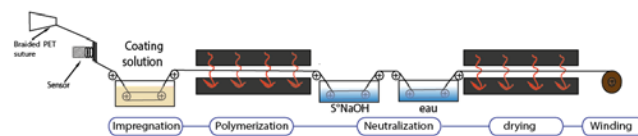

Figure 1. Suture coating process.

RESULTS AND DISCUSSION

The main effects of coating conditions respectively on the maximum force at break and the PET suture friction coefficient are studied. We note that the maximum force at break is not affected by the coating conditions and still meet the USP requirements. A slight increase of the friction coefficient versus the number of passes is noticed. It can be justified by an accumulation of the coating film to the PET suture surface.

The ATR-IF spectrum prove the existence of the coating product on suture surface (Figure 2). In fact, the appearance of large band from 3600 to 2400 cm^{-1} indicates the existence of -OH and -NH groups in the suture surface. This band covers the peaks related to the -OH groups of the PET

surface which become less pronounced after the coating. The fixation of the film to the suture surface can be attributed primarily to the adhesion of the polymerized product by hydrogen bond between the -NH2 groups of chitosan and the -COOH groups of PET (Figure 3, bonds I). Other hydrogen bonds-linkages are also possible between the OH groups of the citric acid and the C=O groups of PET (Figure 3, bond II) and between the carboxylic groups C=O of the complex chitosan-CA and -OH groups of PET created on the surface of suture following alkalization treatment (Figure 3, bond III).
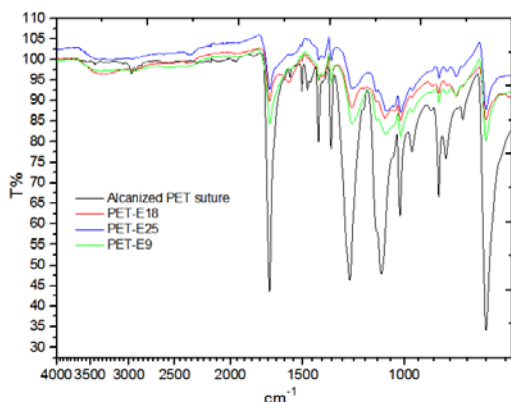
Figure 2. ATR-IF spectrum of coated sutures.
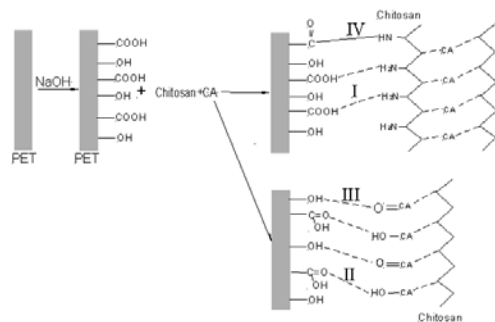
Figure 3. Possible reactions between chitosan-CA film and alkalized PET.

Best antibacterial sutures are obtained by coating the suture with coating solutions containing various concentrations of chitosan and the same concentration of citric acid (10%). The needed number of passage in the bath depends on the concentration of chitosan in the solution. In fact, in the case of coating solutions containing 1% chitosan (PA-E9) and 2% (E18-PA) three passages were required to have a film on the surface of the wire. In the case of the coated suture with a solution containing 3% of chitosan (PA-E25), one passage was sufficient to have film on surface.

Sutures coated with a solution containing 2% and 3% of chitosan show irregular surfaces. They have higher friction coefficient values than that of the suture coated with a solution containing 1% chitosan. Sutures coated with a multi-layer coating solution containing 1% chitosan have a smooth surface. This is due to the progressive application of the coating product on the suture surface. The SEM images shown in Figure 4 prove the existence of a uniform layer of biofilm Chitosan-CA on the suture surface.

The antibacterial effects against S.epidermis and S. aureus are tested. The test results are presented in Table I. The best antibacterial effects against the two bacterial strains are obtained in the case of suture coated with 1 % of chitosan applied progressively in three passages.
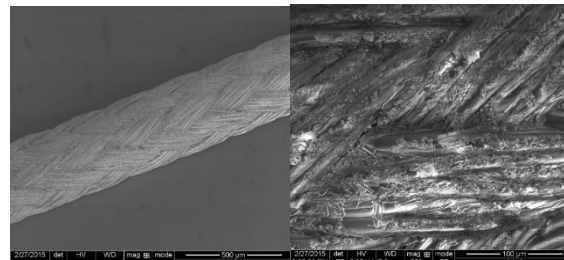

Figure 4. SEM images of coated suture PET-E9.

Table I. Antibacterial inhibition distance of PET sutures.

Inhibition distance (mm)	Staphylococcus epidermis G(+)	Staphylococus aureus G(+)
No coated PET	0	0
PET-E9	2,5±0,7	4,5±0,7
PET-E18	2,75±0,3	2,75±1,0
PET-E25	0	3,75±0,3

CONCLUSION

The aim objective of this study is to develop new process for producing antibacterial PET braided suture. The optimum conditions to have an antibacterial effect and a smooth surface are determined. The best suture is obtained by applying multilayers of chitosan-CA solution containing 1 % of chitosan.

REFERENCES

Chu, Chih Chang, Howard P. Greisler, J. Anthony von Fraunhofer. *Wound Closure Biomaterials and Devices.* United States: CRC-Press, 1997.

Gawish, S. M., et al. "Citric Acid Used as a Crosslinking Agent for the Grafting of Chitosan onto Woolen Fabric." *Journal of Applied Polymer* Science, 2012, 123.6: 3345-53.

Juan, A. San, et al. "Degradation of Chitosan-Based Materials after Different Sterilization Treatments." *IOP Conference Series: Materials Science and* Engineering, 2012, 31: 012007.

Khulbe, K.C., C. Feng, T. Matsuura. "The Art of Surface Modification of Synthetic Polymeric Membranes." *Journal of Applied Polymer* Science, 2012, 115.2: 855-95.

Marreco, P.R., et al. "Effects of Different Sterilization Methods on the Morphology, Mechanical Properties, and Cytotoxicity of Chitosan Membranes Used as Wound Dressings." *Journal of Biomedical Materials Research Part B: Applied* Biomaterials, 2004, 71.2: 268-77.

Wang, Yun Li, et al. "Morphology and Properties of Pet Fabric Finished by B-Cyclodextrin and Citric Acid." *Advanced Materials* Research, 2011, 331: 412-15.

Werner, Carsten, Manfred F. Maitz, Claudia Sperling. "Current Strategies Towards Hemocompatible Coatings." *Journal of Materials* Chemistry, 2007, 17.32: 3376-84.

KEYWORDS

PET braided suture, antibacterial effect, chitosan, biofilm.

Wearable Sensors and Therapy Devices Based on Photonic Textiles

Brit Maike Quandt, Marek Krehel, Marisa Pfister, Luciano F. Boesel, René M. Rossi

Empa, St. Gallen, Switzerland

rene.rossi@empa.ch

INTRODUCTION

Flexible sensors based on incorporating polymer optical fibers (POF) or fluorescent moieties into textiles possess several advantages in the medical and chemical fields. POFs have become more and more popular for sensing applications due to increased homogeneity. E.g., in the medical area, POFs have been used for measuring various vital parameters, such as heart rate, oxygen saturation, and respiratory rate. [1] Optical fibers show great potential for usage in combination with other medical diagnostic machinery as they are immune to electromagnetic interference, are resilient to harsh environmental conditions, and show high sensitivity. [1,2] The flexibility has often been a bottleneck for integration of POFs into textiles. To that aim, POFs more flexible than the current gold-standard of PMMA are needed, since high deformation and deformation rates are present during textile integration, e. g, stitching. [2]

In this work we report our recent developments on textiles incorporating flexible POFs developed at our institute. These fibers are either core/cladding POF [2], which can be used for logging heartbeat or blood oxygenation [2], or core-only fibers, used as pressure or strain sensors. [3,4] These fiber applications combine to be used in pressure ulcer research for increased understanding of tissue changes under load. At the same time, the integrated, flexible textile options ensure that no additional detrimental pressure points are created. Optimized versions of the core/cladding POFs were also used for the creation of a flexible fabric by weaving. With these textiles, homogeneous side light-emission was intended by varying the weaving production parameters. With such a photonic clothing, one could potentially perform phototherapy on neonates suffering from jaundice. It would allow direct contact with its mother as well as improved insulation.

APPROACH

Photoplethysmograph: The optical fibers used in this study were produced using a melt-spinning process. The core of the optical fibers were made of cycloolefin polymer (Zeonor 1020R, Zeon, Düsseldorf, Germany) and as cladding material a fluorinated polymer (THVP 2030GX, Dyneon, Burgkirchen, Germany) was used. The optical fiber was embroidered on the carrier fabric using an embroidery machine ERA TM 0625 (Saurer AG, Switzerland) which can achieve speeds of up to 500 rpm. Pulse wave signals were analyzed with a near infrared tissue spectrometer Oxiplex provided by ISS (Champaign, USA), the same apparatus providing the light sources. The measurements were performed by locating the PPG-fabric on the middle finger of the right hand. Further details on the production of the optical fibers and the final PPG patch, and on the PPG measurements are found in [2].

Phototherapy: The woven textile was produced with a non-automatic loom, with PES as warp and the previously described POF as weft yarn. Varied parameters were the warp thread thickness as well as weaving pattern. With these variations, the bending curvatures of the POF were changed to control side light out-coupling.

Pressure and strain sensor: The pressure-sensitive POFs were extruded from a single-screw extruder equipped with a 2 mm-diameter die. Production parameters were the temperature at both extruder and heating collar as well as the pull-off speed. The latter reached up to 30 meters per minute. The optical fibers consist only of a core (a commercial siloxane block co-polymer: Geniomer, Wacker, Germany), utilizing air as the cladding and thus reaching a critical angle of total reflection of 44.8 ° with the materials' refractive index being 1.42. The deflection of light by pressure was analyzed during load cycles in respect to the siloxane chain length with varying loads. Additionally, long-term signal output was investigated. From these results, a calibration of our sensor is possible with the well-known linearity of response of POFs. Further details may be found in [3].

RESULTS AND DISCUSSION

Photoplethysmograph: The stitched textile PPG-setup contains 4 lines of stitched optical fibers, 2 for out-coupling the incoming red (692 nm) and infra-red (834 nm) light, and two for in-coupling the light reflected back by the tissue. Heart rate and blood oxygenation values were compared with a standard commercial product (Nellcor). It is clear that the values of our experimental textile PPG-setup agree with those of a commercial product.

Another important property of our setup is the high comfort levels, as demonstrated by friction measurements against synthetic skin models (PUR). As shown in Fig. 1, the coefficient of friction of the optimized setup (inset on the right) is well below those of typical hospital bedsheets, either cotton or cotton/polyester. Therefore, we do not expect any discomfort when the setups will be used for extended periods of time.
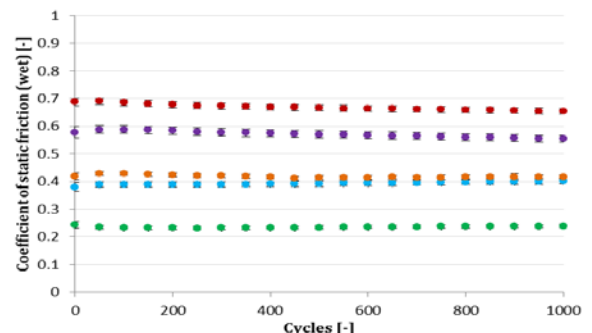

Figure 1: Friction of PPG-setup (orange/blue) with a skin model compared to hospital bedsheets (red/purple) and low-friction textile (green).

Phototherapy: Various weaving patterns were analyzed. The side emission of light from the textile was then logged with several repetitions. The most suitable pattern was chosen, with a theoretically lowest standard deviation over the entire length of the fabric when illuminated from both sides, hence rendering a constant light emission. Simplicity of production played a role in choosing the optimum pattern. An exemplary sample can be seen in Figure 2, showing the illumination from the right side.
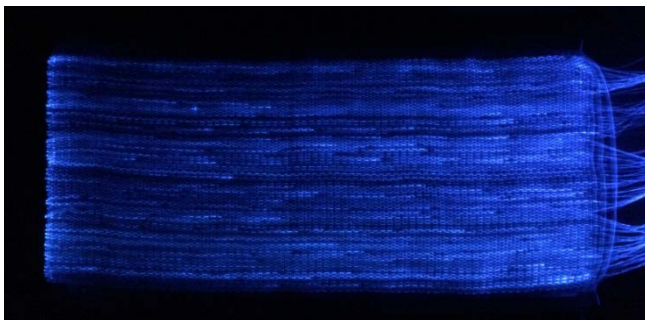

Figure 2: Weave illuminated by LEDs from the right side, decrease in light intensity towards the left can be observed.

Pressure and strain sensor: The pressure-sensitive fibers show good reproducibility as can be seen in Figure 3. Responses vary with production parameters and material grade, varying in siloxane chain length. Such, fibers can be chosen depending on their application's needed sensitivity. Linearity of the response has been shown for different fibers. Data from such sensors could then allow for better understanding of tissue changes under load with a flexible sensor option.
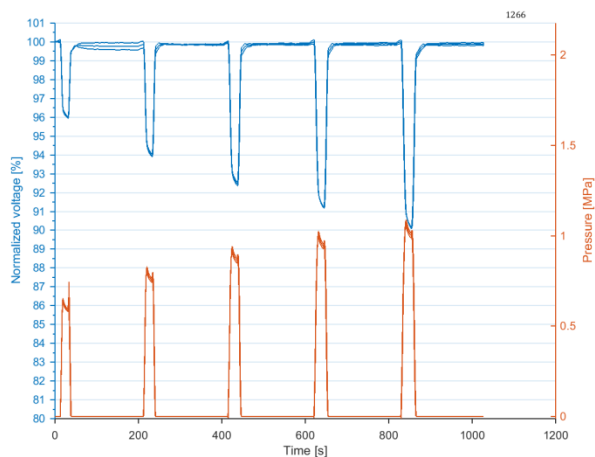
Figure 3: Pressure cycles on a block copolymer fiber, as the pressure is increased, the normalized voltage decreases as a response. Standard deviations are indicated in both load application and response.

Additionally, these fibers have been used for respiration measurements. [4] The fibers are strain sensitive and their extension with, e.g., the expansion of the thoracic region upon respiration may be logged (Figure 4). The good agreement with a commercial respiration sensor shows the versatility of the clad-less fibers. [4]
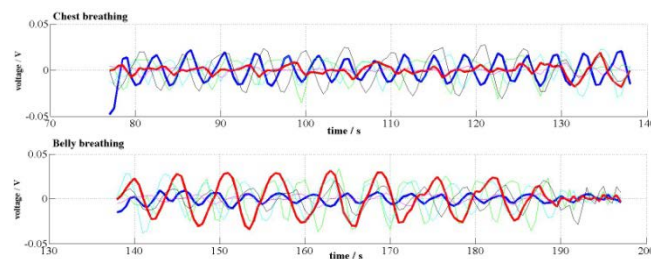
Figure 4: Chest and belly breathing with the strain sensor located at the heart (blue), and upper belly (red), as well as sternum, side of the belly, side of the back and shoulder blade (turquoise, purple, cyan, black).

CONCLUSION AND OUTLOOK

In this work, we presented three examples of the use of polymer optical fibers as wearable sensors or therapy devices. These photonic textiles are very versatile for wearable long-term monitoring and allow for measurements at different parts of the body, most notably not only on thin body parts. Furthermore, the presented fabrics have the haptic and comfort of conventional fabrics (or even better) and thus enhance the acceptance of the wearer, which is necessary for long-term monitoring purposes. Future work will concentrate on increasing the signal response and signal/noise ratio of the different systems. Generally speaking, the real potential of wearable photonic sensors is seen in applications and fields in which electronic counterparts are unsuitable, such as diagnostic means (e.g., MRI) but also other biomedical appliances (e.g., pace maker). Wearable and comfortable monitoring devices will allow for an improvement in the quality of life of elderly patients.

REFERENCES
[1] Quandt, B. M., et al. *Advanced Healthcare Materials*, 2015, 4: 330.
[2] Krehel, M., et al. *Biomedical Optics Express*, 2014, 5: 2537.
[3] Krehel, M., et. al. *Sensors*, 2012, 13:11956.
[4] Krehel, M., et al. *Sensors*, 2014, 14: 13088.

Sustained Release of VEGF from Silk Fibroin Nanoparticle-modified, Bacterial

Cellulose-based Scaffold for Tissue Engineering

Baoxiu Wang[1], Shiyan Chen[1], Zhe Li[1], Xiangguo Lv[2], Chao Feng[2], Huaping Wang[1]

[1]State Key Laboratory for Modification of Chemical Fibers and Polymer Materials, Key Laboratory of Textile Science & Technology (Ministry of Education), College of Materials Science and Engineering, Donghua University, Shanghai, China

[2]Department of Urology, Affiliated Sixth People's Hospital, Shanghai Jiaotong University, Shanghai, China

2130305@mail.dhu.edu.cn

OBJECTIVE

Inadequate vascularization is one of the barriers limiting the effectiveness of tissue reconstruction. To develop scaffolds that are capable of inducing angiogenesis, we developed a vascular endothelial growth factor (VEGF) loaded silk fibroin nanoparticle-modified bacterial cellulose based scaffolds for sustained release of VEGF to induce angiogenesis. In this work, the VEGF-loaded nanoparticles were prepared via self-assembling of silk fibroin molecular chains with average diameter of 205 nm and then the nanoparticles were immobilized to the scaffolds. Results of in vitro release study indicated that the nanoparticles modified scaffold exhibited sustained release of VEGF for several weeks.

INTRODUCTION

Tissue engineering has been a promising strategy to repair complex urethral stricture in urinary system. Scaffold materials, cells and growth factors are the key factors for tissue engineering. Bacterial cellulose (BC) produced by Gluconacetobacter xylinus has recently received extensive attention as an excellent nanofibrous scaffolds candidate for tissue regeneration due to their refined 3D nanofibrils network architecture which successfully mimics the native ECM. And it has been studied for urinary[1], artificial skins[2], blood vessels[3]. However, inadequate vascularization of tissue-engineered scaffolds limits its effectiveness, resulting in insufficient nutrient and oxygen supply to the cells[4]. Therefore, formation of new blood vessels is critical to urinary reconstruction.

Previous research has proven that the administration of growth factors can promote tissue revascularization. Vascular endothelial growth factor (VEGF) which is one of the most important and widely studied angiogenic growth factors has been shown to be useful for enhancing regeneration of scaffolds[5]. However, the short half-life (~50 minutes) of VEGF makes excessive amounts of it required, leading to induce severe side effects. And sustained release of VEGF is crucial to the development of mature blood vessels. Therefore, it is particularly important to deliver VEGF continuously to the scaffold and control its release during tissues reconstruction.

In this study, our main objective is to develop a scaffold with a sustained local release of VEGF to enhance the vascularization of bacterial cellulose based scaffolds. The local release of VEGF was achieved by application of silk fibroin nanoparticles (SFNPs) prepared via self-assembling of silk fibroin molecular chains. The incorporation of VEGF into SFNPs stabilizes growth factor, protects it from denaturation and proteolytic degradation and subsequently prolongs its sustained release. Then the VEGF-loaded nanoparticles were combined with bacterial cellulose based scaffolds.

RESULTS AND DISCUSSION

Morphology of SFNPs and the scaffold with immobilized nanoparticles

The morphology of silk fibroin particles observed by FE-SEM is shown in Fig. 1. Fibroin formed spherical nanoparticles with average diameters of 205 nm as shown in Fig. 1a. The diameters of SFNPs could be modulated by changing the formulation conditions such as the ethanol amount and the silk fibroin concentration. The scaffold with highly interconnected micropore (171 ± 71 μm) has high affinity with SFNPs. As shown in Fig. 1c, the SFNPs are closely attached to the nanofibers of BC, which means the large loading capacity of SFNPs. It is obvious that the amount of VEGF introduced into scaffold is greater with more SFNPs in scaffold, leading to induce angiogenesis.

In vitro release of VEGF from SFNPs and the scaffolds

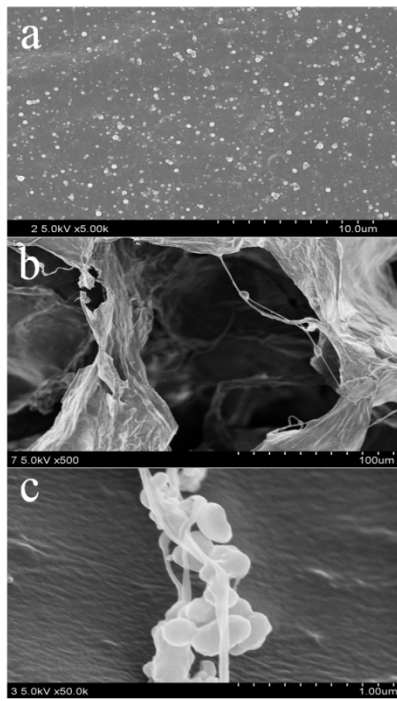As shown in Fig. 2, the scaffold incorporating VEGF-loaded

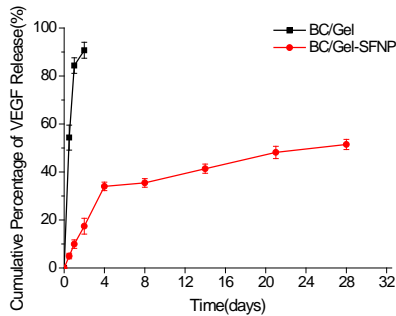Fig. 1: FE-SEM images of (a) SFNPs, (b) the scaffold containing SFNPs, (c) SFNPs embedd in scaffold.

Fig. 2: Cumulative release of VEGF from the scaffolds (■ the scaffold containing adsorbed VEGF and ● the scaffold modified by VEGF-loaded SFNPs).

nanoparticles with 0.05 μg of VEGF/mg fibroin, showed an initial burst release with more than 10% of protein being released during the first two days, which might be due to the free VEGF on the surface of SFNPs. As we can see from the tendency of the curves, the release profiles of VEGF evidently increased with time and have continued for more than 28 days. This indicates a successfully sustained release of VEGF. However, more than 80% of the VEGF was released within 2 days from the VEGF adsorbtion group. That means SFNPs and

scaffold could provide a dual release condition for VEGF which contributed to the sustained release for a long time.

CONCLUSION

The nanoparticles were easily prepared under mild condition, which protect activity of VEGF and provides a sustained release of it. Furthermore, results of in vitro release indicate that bacterial cellulose based scaffold incorporating VEGF-loaded silk fibrion nanoparticles have shown to work as a carrier that provides a sustained release of VEGF in a timewise manner that could be used in urinary regenerative applications. Our next work is to perform the animal experiment to investigate the potency of this bacterial cellulose based scaffold for induced angiogenesis in vivo.

REFERENCES

1. Bodin, A., Bharadwaj, S., Wu, S., et al. "Tissue-engineered conduit using urine-derived stem cells seeded bacterial cellulose polymer in urinary reconstruction and diversion." *Biomaterials*, 2010, 31(34): 8889-901.

2. Kucińska-Lipka, J., Gubanska, I., Janik, H. "Bacterial cellulose in the field of wound healing and regenerative medicine of skin: recent trends and future prospectives." *Polymer Bulletin*, 2015, 72(9): 2399-419.

3. Bodin, A., Ahrenstedt, L., Fink, H., et al. "Modification of nanocellulose with a xyloglucan–RGD conjugate enhances adhesion and proliferation of endothelial cells: implications for tissue engineering." *Biomacromolecules*, 2007, 8(12): 3697-704.

4. Kaushal, S., Amiel, G.E., Guleserian, K.J., et al. "Functional small-diameter neovessels created using endothelial progenitor cells expanded ex vivo." *Nature Medicine*, 2001, 7(9): 1035-40.

5. Lü, W.D., Zhang, M., Wu, Z.S., et al. "Decellularized and photooxidatively crosslinked bovine jugular veins as potential tissue engineering scaffolds." *Interactive Cardiovascular and Thoracic Surgery*, 2009, 8(3): 301-05.

Functionalization and Biocompatibility Evaluation
of Drawn Fibers for Neural Tissue Implants

Kateřina Strnadová[1], Jan Lukášek[2], Ilona Krabicová[1], Lukáš Stanislav[3], Michal Řezanka[2], Věra Jenčová[1],
Šárka Beranová[4], Ivan Stibor[2], David Lukáš[1]

[1]Department of Nonwovens and Nanofibrous Materials, Technical University of Liberec; [2]Institute for Nanomaterials, Advanced Technologies and Innovation, Technical University of Liberec; [3]Department of Manufacturing Systems and Automation, Technical University of Liberec; [4]Institute of complex systems, CENAKVA, FFPW, University of South Bohemia in České Budějovice, Nové Hrady

katerina.strnadova2@tul.cz

ABSTRACT
Our study focuses on the development of aligned fibers for neural tissue implants. Therefore, we prepared highly oriented fibers coated with polypyrrole. The novelty of this study is the use of drawing technique for the fiber fabrication instead of electrospinning. Drawing enables us the fabrication of scaffolds with highly oriented microfibers. These scaffolds were subjected to basic in vitro experiments and the results are presented in this article.

INTRODUCTION
The healing of nervous system injuries and disorders is of great interest because these pathologies represent a great health risk for patients and affect their quality of life and the incorporation of the patients back into society. Each year 250 000 to 500 000 people in the world suffer from spinal cord injuries (WHO, 2013). Therefore, enormous efforts are being made to enable neural regeneration. Neural tissue engineering offers a promising approach to treating nervous system injuries. Currently, there is no effective treatment for spinal cord injuries. In the literature, there are studies into the implementation of various types of scaffolds, neither of which has been successfully introduced into practice so far. The main reason for this is the failure of neural cells to proliferate and to extend their neuritis, the cells forming glial scars instead [1]. This problem should be in the future overcome by the combination of methods for scaffold fabrication with surface functionalization and drug release [2]. It has been shown previously that the neural cells prefer aligned scaffolds that guide their neurite outgrowth [3] and that microfibers promote the neurite extension better than nanofibers [4]. And there are many other factors that can influence neuron proliferation and neurite extension, such as the use of conductive polymers [5, 6], and the addition of growth factors and other signal molecules [2]. Nowadays, electrospinning is mainly used to prepare scaffolds for neural tissue engineering [5, 7, 8], which are further functionalized by polypyrrole or polyaniline or others [5, 6].

EXPERIMENTAL APPROACH
Scaffold fabrication
Materials: For fabrication of our scaffolds we used ε-polycaprolactone (PCL; Sigma Aldrich, Mw 80,000). We prepared 12% (*w/w*) solution in chloroform. The fibers were drawn on Micromanipulator (Technical University of Liberec) and were fixed within the supporting ring (PMMA; Technical University of Liberec) for better manipulation (Fig. 1).

Drawing: The mechanical drawing was used to prepare the scaffolds for biological experiments. The motion program of Micromanipulator consisted of circular interpolation with S – curve acceleration and deceleration profile (2000ms).

Top speed of drawing element was 6 m/min with 500 fibres per sample. In the first step the droplet of a PCL solution is placed on an underlay. A movable element, in this case a needle, touches the droplet and erodes its surface. In the next step, the needle starts moving away and due to a surface tension of the polymer, it forms a fibre. The PCL solution solidifies as a result of the evaporation of the solvent, so finally the length of the fibre is extended partially by using the core still-liquid material and partially by stretching the surface [9]. The process ends when the needle lays the fibre down on the underlay in the defined distance.

Fig. 1. Immobilized fibers within the supporting ring.

Functionalization
Prepared PCL scaffolds were subsequently functionalized by a thin conductive polypyrrole (PPy) layer . The polymerization reaction of pyrrole (Sigma-Aldrich) was maintained for three days at room temperature in the presence of $FeCl_3$ and *p*-toluenesulfonic acid.

Scaffold characterization
Polypyrrol coated and uncoated fibers were analyzed by scanning electron microscope (Tescan, VEGA3 SB Easy Probe) (Fig. 2) and NIS Elements software (Nikon). The fiber diameter was counted from 100 meassurements (Fig. 3). The average of fiber diameter of PCL and PPy-PCL were 12,4 ± 4,1 µm and 12,1 ± 5,2 µm, respectively, with the minimal value 5,5 µm and maximal value 24,9 µm of fiber diameter for PCL and with the minimal value 3 µm and maximal value 29,8 µm of fiber diameter for PCL-PPy.
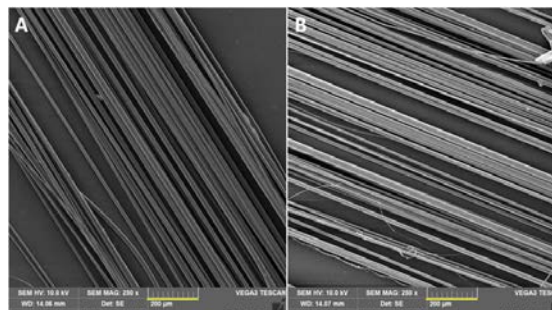

Fig. 2. SEM of drawn PCL fibers. A: PPy uncoated; B: PPy coated. Scale bar: 200 µm. Magnification: 250 x.

In vitro experiments

In the *in vitro* experiments we compared our PPy-coated and PPy-uncoated drawn fibers. We tested both scaffolds for cell adhesion and proliferation with MTT assay, fluorescence and electron microscopy. For all experiments we used 3T3 mice fibroblasts. We tested both scaffolds at day 1, 7 and 14 after cell seeding.

In vitro cell culture: 3T3 mice fibroblasts (3T3 Swiss Albino, ATCC) were cultivated in Dubelcco's modified Eagle's medium (DMEM, Lonza) with 10% (*v/v*) of fetal bovine serum (Lonza) and 1% (*v/v*) of penicillin / streptomycin / amphotericin B (Lonza). Cells were maintained at 37 °C, 5 % of CO_2. The medium was changed three times a week. 6th passage was used for the experiments.

Samples: The immobilized fibers were sterilized for 30 minutes in 70% ethanol and washed three times with sterile phosphate buffered saline (PBS, pH 7,4). After wash, the scaffolds were seeded with cells in the concentration of $1 \cdot 10^5$ per well in 24-well plates.

RESULTS AND DISCUSSION

Our results reveal that our scaffolds are capable for cell adhesion and proliferation. The fluorescent microscopy also reveals that the cells grow in the direction of fibers and that they prefer to grow on the PPy-coated scaffolds (Fig 3). This result was also confirmed by the MTT assay (data not shown).
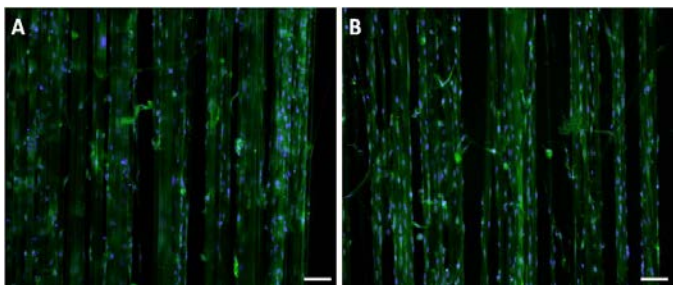
Fig. 3. Fluorescent microscopy of cells seeded on aligned fibers 7 days after cell seeding. A: PCL; B: PCL-PPy. Staining: Phalloidin-DAPI; Scale bar: 100 μm; Magnification: 100x.

Also the data from the SEM suggest better cell proliferation on the PPy-coated fibers, since the cells cover the whole surface of the scaffold in comparison to PPy-uncoated fibers (Fig. 4).
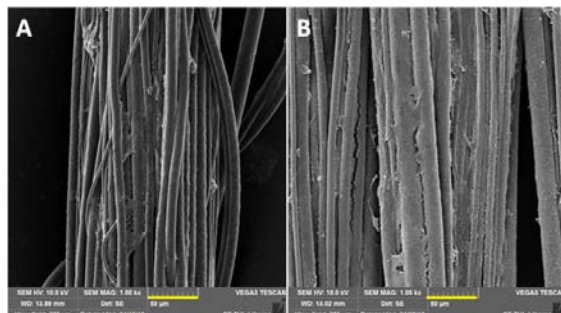

Fig. 4. SEM of drawn PCL fibers. A: PPy uncoated; B: PPy coated. Scale bar: 200 μm. Magnification: 250 x.

CONCLUSION

Our experimental data show that our scaffolds are capable for cell adhesion and proliferation and are biocompatible. Our results reveal that the cells prefer polypyrrol coated fibers. The fluorescent microscopy also indicates the oriented growth of the cells. These features of our scaffolds will be beneficial for further studies and functionalization of aligned drawn fibers.

STATISTICS

All statistical analyzes were performed with Statistica 12 software.

REFERENCES

[1] Li, J., Lepski, G. "Cell transplantation for spinal cord injury: A systematic review." *Biomed. Res. Int.*, 2013. DOI: 10.1155/2013786475.

[2] Chudickova, M., Bruza, P., Zajicova, A., Trosan, P., Svobodova, L., Javorkova, E., Kubinova, S., Holan, V. "Targeted neural differentiation of murine mesenchymal stem cells by protocol simulating the inflamatoy site of neural injury." *J. Tissue Eng. Regen. Med.*, 2015. DOI: 10.1002/term.2059.

[3] Corey, J.M., Lin, D.Y., Mycek, K.B., Chen, Q., Samuel, S., Feldman, E.L., Martin, D.C. "Aligned electrospun nanofibers specify the direction of dorsal root ganglia neurite growth." *J. Biomed. Mater. Res. A,* 2007, 83(3): 636-45. DOI: 10.1002/jbm.a.31285.

[4] Wang, H.B., Mullins, M.E., Cregg, J.M., McCarthy, C.W., Gilbert, R.J. "Varying the diameter of aligned electrospun fibers alters neurite outgrowth on Schwann cell migration." *Acta Biomater.*, 2010, 6: 2970-78. DOI: 10.1016/j.actbio.2010.02.020.

[5] Lee, J.Y., Bashur, C.A., Goldstein, A.S., Schmidt, C.E. "Polypyrrole-coated electrospun PLGA nanofibers for neural tissue applications." *Biomaterials*, 2009, 30, 4325-35. DOI: 10.1016/j.biomaterials.2009.04.042.

[6] Guimard, N.K., Gomez, N., Schmidt, CE. "Conducting polymers in biomedical engineering." *Prog. Polym. Sci.*, 2007, 32: 876-921. DOI: 10.1016 / j.progpolymsci.2007.05.012.

[7] Yang, F., Murugan, R., Ramakrishna, S., Wang, X., Ma, Y.X., Wang, S. "Fabrication of nano-structured porous PLLA scaffold intended for neural tissue engineering." *Biomaterials*, 2004, 25, 1891-900. DOI: 10.1016/j.biomaterials.2003.08.062.

[8] Novikova, L. N., Petterson, J., Brohlin, M., Wiberg, M., Novikov, L.N. "Biodegradable poly-β-hydroxybutyrate scaffold seeded with Schwann cells to promote spinal cord repair." *Biomaterials*, 2008, 29, 1198-1206. DOI: 10.1016/j.biomaterials.2007.11.033.

[9] McKinley, G.H., Sridhar T. "Filament-stretching rheometry of complex fluids." *Annu. Rev. Fluid Mech.*, 2002, 34, 375-415. DOI: 10.1146 / annurev.fluid.34.083001.125207.

High-modulus, Melt Spun Polycaprolactone Fibres for Biomedical Grafts

Tom O'Haire, Stephen J. Russell, Parikshit Goswami
School of Design, University of Leeds, United Kingdom
t.ohaire@leeds.ac.uk

INTRODUCTION

The mechanical requirements for a graft or regenerative tissue scaffold can vary depending on the expected load and healing time for such a device. For synthetic tendon repair the graft should have mechanical properties that facilitate its surgical introduction and fixation and be capable of withstanding high tensile loading with limited extension during the recovery phase. Tendons have a tensile strength of 50 to 150 MPa and an elastic modulus of 550 MPa and upwards [1-3]. Finding a suitable synthetic material is often a compromise between mechanical performance and biocompatibility. Polycaprolactone (PCL) is known to have excellent properties as a biomaterial due to the favorable cytotoxic and cell growth response observed *in vitro* and *in vivo*. In addition, the biological breakdown time for PCL is acceptable for applications where the graft is expected to bear load for an extended period of healing [3]. However, the measured tensile properties of as-spun PCL is insufficient for high tenacity and high modulus applications [4, 5]. The post-spinning drawing of polycaprolactone is one option for increasing the mechanical properties of PCL.

APPROACH

Partially oriented multifilament yarns of PCL were produced using a mixing extruder with a multi-filament die. The fibres were then formed in to fully drawn filaments through a continuous multi-stage cold drawing process (Fig. 1) designed to elongate and orientate the polymer chains.
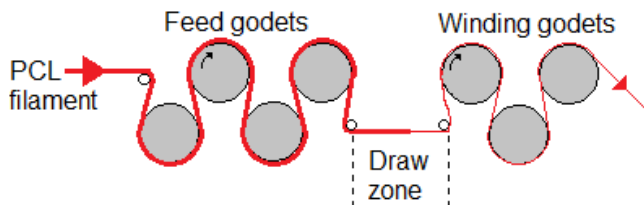

Figure 1. The cold drawing of polycaprolactone.

The tensile properties, including the modulus and elastic recovery of filaments subjected to cyclic loading was measured. The mechanical properties of undrawn and drawn filaments were compared.

RESULTS AND DISCUSSION

Fibre properties

The mean diameter of as-spun PCL filaments was 85 µm as determined by cross sectioning. After the multi-stage drawing process the mean filament diameter reduced to 30 µm.

Tensile properties

The stress strain curves for the as-spun PCL indicated low molecular chain orientation which resulted in a high level of plastic flow (> 500 %) and a relatively low tensile strength (63 MPa) and Young's Modulus (315 MPa). Through drawing, the tensile strength and Young's modulus increased to 700 MPa and >1000 MPa respectively (Fig. 2).
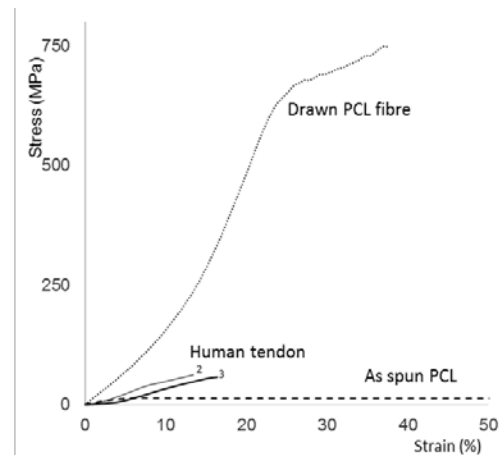

Figure 2. Typical stress strain curves for as-spun and drawn PCL with human patellar tendon [2, 3].

CONCLUSIONS

PCL multifilament yarns were melt spun and drawn to a final diameter of 30 µm and were found to have a tensile strength and Young's modulus that exceeds the mechanical properties of tendons and substitute vascular and non-vascular grafts. The mechanical properties of the filaments were found to be tunable creating the possibility of engineering 2D/3D woven/knitted or unidirectional assemblies with appropriate performance for a range of biomedical applications.

This presentation will discuss additional data on the cyclic loading behavior as a function of drawing conditions, along with other relevant data on PCL fibre properties.

REFERENCES

1. Maganaris, C.N., Paul, J.P. "In vivo human tendon mechanical properties." *J. Physiol.*, 1999, 521(Pt. 1): 307-13.
2. Johnson, G,A., et al. "Tensile and viscoelastic properties of human patellar tendon." *J. Orthop. Res.*, 1994. 12(6): 796-803.
3. Hashemi, J., Chandrashekar, N., Slauterbeck, J. "The mechanical properties of the human patellar tendon are correlated to its mass density and are independent of sex." *Clin. Biomech.*, 2005, 20: 645-52.
4. Mochizuki, M., et al. "Hydrolysis of polycaprolactone fibers by lipase: Effects of draw ratio on enzymatic degradation." *J. App. Polym. Sci.*, 1995, 55(2): 289-96.
5. Ratcliffe, A., et al. "Scaffolds for tendon and ligament repair and regeneration." *Ann. Biomed. Eng.*, 2015, 43(3): 819-31.
6. Lowery, J.L., Datta, N., Rutledge, G.C. "Effect of fiber diameter, pore size and seeding method on growth of human dermal fibroblasts in electrospun poly(ε-caprolactone) fibrous mats." *Biomaterials*, 2010. 31(3): 491-504.

Mechanical Behavior of Rat Tendons Under Cyclic Tensile Loadings

Gilles Arnold[1], Rodrigo Labat Marcos[2], Rachid Rahouadj[3]

[1]Université de Haute Alsace, Laboratoire Physique et Mécanique Textiles (LPMT), Mulhouse, France
[2]University of Nove de Julho, Biophotonics Applied to Health Sciences, São Paulo, Brazil
[3]Université de Lorraine, Laboratoire d'Energétique et de Mécanique Théorique et Appliquée (LEMTA),
Vandœuvre-lès-Nancy, France
gilles.arnold@uha.fr

OBJECTIVE

A tendon is a multiscale microstructure made of helical collagen molecules, microfibrils, fibrils, fibers and fascicles (Fig. 1a). It results a complex mechanical behavior (which is also coupled with bio-chemical phenomena). Tendinitis is a common disease of the tendon which if untreated can result in serious long-term complications. It is generally treated using nonsteroidal anti-inflammatory drugs (NSAID) which give good results against pain. An alternative to drugs is Low Level Laser Therapy (LLLT). The aim of this study is to compare the effect of LLLT and NSAID treatment on the mechanical properties in the case of acute inflammation of tendon. In a first step, indicators of the mechanical performance of tendons are proposed. In a second step the link with the microstructure is discussed to find more pertinent indicators of the general mechanical properties of tendons.

INTRODUCTION

To characterize the mechanical behavior of the tendon, the current literature refers primarily to the strength and elongation at rupture and to the stiffness measured in the linear region of the tensile curve (Sahin et al., 2012). These mechanical properties correspond to the behavior under monotonic loading which doesn't reflect adequately the in vivo conditions. In this study, cyclic loading have been performed on rats tendons after different treatments. Numerous mechanical properties were extracted from each test. There modifications were evaluated and linked to the acute inflammatory process and treatments. The correlations between mechanical properties and biochemical indicators have been analyzed (Marcos et al., 2013).

APPROACH

The experimental protocol was conducted as described in a previous paper (Marcos et al., 2013).

Samples Preparation

Tendinitis was induced in a group of male Wistar rats using collagenase, an enzyme that degrades collagen and induces an acute inflammatory process. The same procedure was used for a control group (CTL) without collagenase. A first group (DIC) was treated using diclofenac sodium (Voltaren injectable® – Novartis 2.5 mg/kg). Two other groups (L1J and L3J) were treated by laser irradiation with doses of 1 J and 3 J respectively. The last group (TEN) was not subjected to any treatment of tendinitis. The animals of the DIC, L1J and L3J groups were treated in the same conditions for 6 days. On day 7, animals were sacrificed with halothane. Achilles tendons were dissected and immediately used for biomechanical analysis.

Biomechanical Analysis

Musculotendinous junction (MTJ) was fixed in the lower grip as osteotendinous junction (OTJ) was fixed in the upper one using a universal tensile test machine (zL2.5 Zwick-Roell – Germany). The distance L_0 between the grips (Fig. 1b) was measured before each test, its mean value was approximately 2 mm. Displacement u was controlled following loading and unloading cycles at a constant velocity of 1 mm/min. At each cycle, maximal displacement applied to tendon was increased of 10% of L_0 and tensile force F was released until 0.1 N. The sequence was repeated until rupture (Fig. 2).
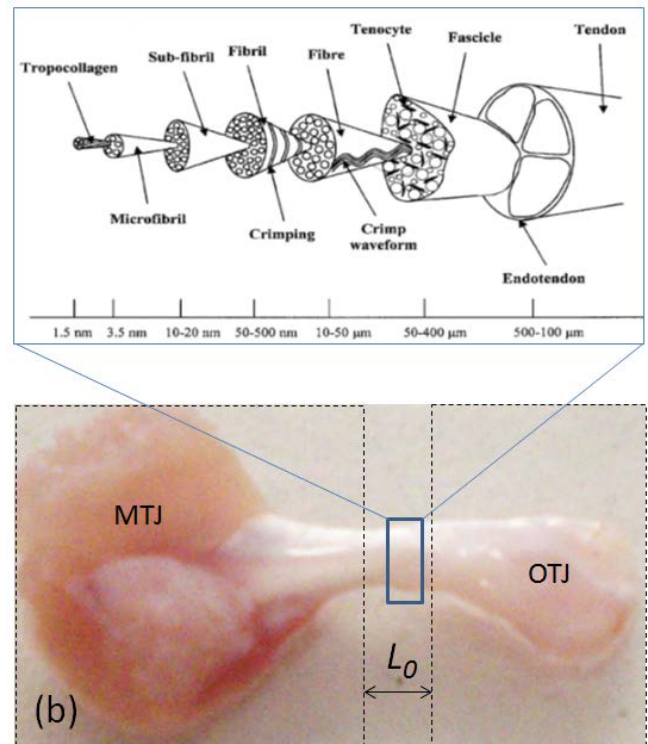

Figure 1: (a) Multiscale microstructure from tendon (from Screen, et al., 2005); (b) Rat Achilles tendon.

Several mechanical characteristics were extracted from the force – displacement curves obtained from cyclic loadings of each tendon. The consideration of numerous characteristics enables description of tendon mechanical behavior without to prejudge the choice of a particular set of parameters. Three stiffnesses were measured at each loading – unloading cycle (indexed i) as illustrated in Fig. 2: secant stiffness k_s as the load / displacement ratio; tangent stiffness k_t as the local slope of the envelope of the loading curve; unloading stiffness k_u as the slope of the curve immediately after a maximum point M_i (F_i , u_i):

$$k_s{}^i = \frac{F_i}{u_i}$$

$$k_t{}^i = \frac{F_i - F_{i-1}}{u_i - u_{i-1}} \text{ with } i = \{1 \ldots n\} \text{ and } (F_0 = 0, u_0 = 0)$$

$$k_u{}^i = \left.\frac{\partial F}{\partial u}\right|_{dF<0} \left(M_i{}^+\right)$$

The stretch λ was defined as the ratio L / L_0 where L and L_0 are respectively the current and initial distances between the two grips of the loading device ($L = L_0 + u$). The maximum value of the force F_{max} and the corresponding value of the stretch λ_{Fmax} characterize the mechanical strength in term of load and elongation. The maximum of each stiffness was measured: $k_{s\ max}$, $k_{t\ max}$ and $k_{u\ max}$, as well as the corresponding force and stretch values: ($F_{ks\ max}$, $\lambda_{ks\ max}$), ($F_{kt\ max}$, $\lambda_{kt\ max}$) and ($F_{ku\ max}$, $\lambda_{ku\ max}$) respectively. Finally 11 measured values were considered for each tested tendon.
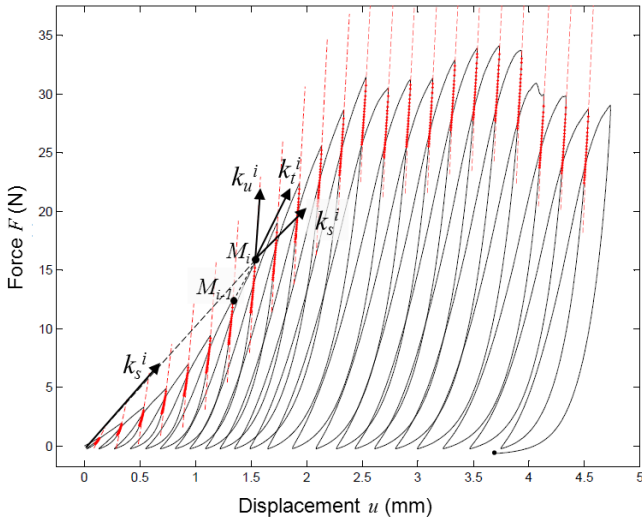
Figure 2: Definition of the 3 different stiffnesses at each cycle.

RESULTS AND DISCUSSION

Representative load – displacement curves are shown in Fig. 3 for the DIC and L1J groups as examples. Envelope curves exhibit the typical response obtained for tendon under monotonic loading: *i.e.* a "toe" region, followed by a "linear" part up to a maximum (λ_{Fmax}, F_{max}) beyond which the force decreases. This evolution is commonly explained by the helical shape of the collagen molecules (Grytz et al., 2009) and by the well-known phenomena of gradual recruitment of collagen fibers. Large differences of load levels were also observed. Because of the shape of the load – displacement envelope curves, the evolution of stiffnesses k_s and k_t with displacement u (Fig. 3) exhibited an increasing phase, a maximum and a final decreasing phase where k_t reached negative values. If the initially increasing evolution of k_t was linked to the reorientation of the fibers, the suddenly decreasing evolution of k_t could be explained by a gradual fracture of the fibers that could be described using a damage variable (Weisbecker et al., 2012). The evolution of the unloading stiffness k_u with displacement

was different but could also be partially explained by damage: it increased linearly up to saturation close to the maximum load. One can note that the maximum value of the secant stiffness k_s was reached when the secant was tangent to the envelope curve, corresponding to the maximum global stiffness of the tendon. Tangent stiffness k_t and unloading stiffness k_u describe the response of the tendon under an increasing or a decreasing load, respectively. The tangent stiffness k_t reveals the ability of the tendon to resist to a force increment at a given force level. The unloading stiffness values were much higher than the values of secant and tangent stiffnesses. This difference could be related with the viscoelastic behavior that was not assessed in this study.
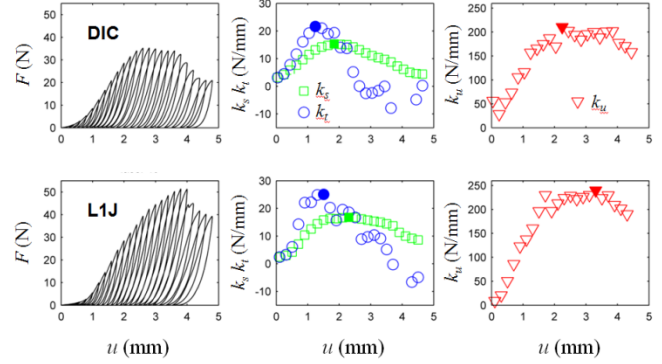

Figure 3: Representative F-u curve, k_s, k_t and k_u evolution for DIC and L1J groups.

CONCLUSION AND FUTURE WORK

In the framework of this study, the definition of different stiffnesses has enabled to describe the evolution of the mechanical properties of the tendons under cyclic loading. In a future work, models of the literature could be adapted and identified using these results in order to assess more accurate information on the behavior like viscosity and damage.

KEYWORDS

Tendon, LLLT, stiffness, tensile behavior.

REFERENCES

1. Elias, P.Z., Spector, M. *J. Mech. Behav. Biomed. Mater.*, 2012, 12: 63-73.
2. Grytz, R., Meschke G. *J. Mech. Behav. Biomed. Mater.*, 2009, 2: 522-33.
3. Marcos, R.L., Arnold, G., Magnenet, V., Rahouadj, R., Magdalou, J., Lopes-Martins, R.Á.B. *J. Mech. Behav. Biomed. Mater.*, 2013, 29: 272-85.
4. Sahin, H., Tholema, N., Petersen, W., Raschke, M.J., Stange, R. *J. Ortho. Res.*, 2012: 1952-57.
5. Screen, H.R.C., Shelton, J.C., Chhaya, V.H., Kayser, M.V., Bader, D.L., Lee, D.A. *Annals of Biomed. Eng.*, 2005, 33-8: 1090-99.
6. Weisbecker, H., Pierce, D.M., Regitnig, P., Holzapfel, G.A. *J. Mech. Behav. Biomed. Mater.*, 2012, 12: 93-106.

Textile Prosthetic Heart Valve Designs
to Reduce Reynolds Shear Stress

Antoine Vaesken[1], David L. Bark, Jr.[2,3], Atieh Yousefi Koupei[2], Marcio Forleo[3], Frederic Heim[1], Lakshmi P. Dasi[1,2]

[1]Laboratoire de Physique et Mecanique Textiles EA 4365, LPMT-ENSISA, Mulhouse, France; [2]Department of Biomedical Engineering, Ohio State University, Columbus, Ohio, USA; [3]School of Biomedical Engineering, Colorado State University, Fort Collins, Colorado, USA
antoine.vaesken@uha.fr

INTRODUCTION

A series of studies have demonstrated that textile valves may provide flexible leaflets, allowing hemodynamics that mimic the native valve and these valves can be tuned for durability. Polyester textiles have been most widely investigated for this purpose so far[1]. It has been especially demonstrated that polyethylene terephthalate (PET) textile material can be durable to withstand up to 200 Mio cycles without any sign of rupture if the fabric design is defined in a proper way[2].

Although textile valves are promising, the hemodynamics resulting from their design remain undefined. Hemodynamics are important in design as high shear stress, stagnant flow, and turbulence can all contribute to thrombosis, which can lead to heart attack or stroke[3]. It could be interesting to know if the textile fabrication can be controlled to manipulate the generation of turbulence. Owing to spatiotemporal fluctuations in stress, turbulence is a prominent factor that may result in blood damage either through hemolysis or platelet activation. It takes an important part in inducing platelet activation relative only to shear stress[4]. We aim to reduce turbulence, while providing adequate hemodynamic performance. In order to optimize the hemodynamics of a textile valve, we will explore in this study: (1) The effect of different aspect ratios between heart valve inner diameter and its height; (2) the influence of textile processing techniques on hemodynamic performance.

MATERIAL AND METHOD

Figure 1: Textile valve.

Valve manufacturing & textile characterization

The methods used to fabricate the textile valves are previously described[5]. Valves were made with a low profile and a high profile corresponding to a height to diameter ratio (h/D) of 0.5 and 0.7 respectively, where h is the height, and D the diameter of 23 mm. To study characteristics of a low profile valve, we considered four different textiles (non-woven, monofilament, multifilament non calendared and calendared).

Durability, stiffness, and surface roughness all vary with the different weave and yarn conditions. The effect of the stiffness and surface roughness on flow is crucial to determine the construction that provides the best hemodynamic performance.

Table I: Characteristics of the valve materials used.

Sample	A	B
Yarn structure	Multifilament calendared	Multifilament non calendared
Thickness (µm)	73	134
Surface density (g/m^2)	52.2	73.7
Yarn count (tex)	50	50
Bending stiffness (mg.mm)	0.0077	0.0119
Surface roughness (SMD µm)	4.8	10.7
Sample	C	D
Yarn structure	monofilament	Non-woven
Thickness (µm)	60	152
Surface density (g/m^2)	45.2	73.9
Yarn count (tex)	10	NA
Bending stiffness (mg.mm)	0.0165	0.0097
Surface roughness (SMD µm)	1.6	13.3

In-Vitro testing

Constant flow was applied across valves of various constructions to investigate the role of surface roughness and design on turbulences[6]. A flow loop was designed with a submersible pump that provided a flow rate of 30 and 60 L/min. The valve was inserted into a mounting chamber, which was in line with PVC piping that returned flow to a reservoir containing the submersible pump. The mounting chamber was a transparent, rigid, acrylic cylindrical tube with an axisymmetric sinus. A blood analog of a water/glycerin mixture was used for experiments with a viscosity of 3.5 cP and a density of 1080 kg/m^3.

This mixtures were seeded with 1-20 micron sized polyamide tracer particles. A Photron Fastcam SA3 high-speed video was used to capture positions of illuminated particles. The camera was set into a double-frame mode with each frame separated by 250 µs.

RESULTS AND DISCUSSION
Influence of the valve profile
Reynolds Shear Stress (RSS) contours for flow across a high profile and a low profile multifilament valve are shown in figure 2. RSS scales with the average velocity, as demonstrated by similar normalized RSS scales between studies at 30 and 60 L/min. At the valve edge there is little quantitative difference in RSS values between the two valve designs. However, downstream of the valve RSS values increase by approximately a factor of 2.
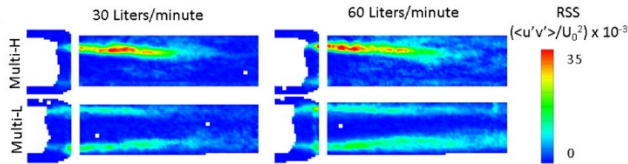

Figure 2: RSS contour for high (top) and low profile (bottom).

The low profile valve model seems to reduce turbulences compared to the high profile valve. It appears that the high profile causes a larger ripple in the fabric and results in turbulences. Conversely, with a lower profile, the valve appears to limit the RSS.

Influence of the fabric construction
Contour plots of RSS for the four textile structures are shown in figure 3.
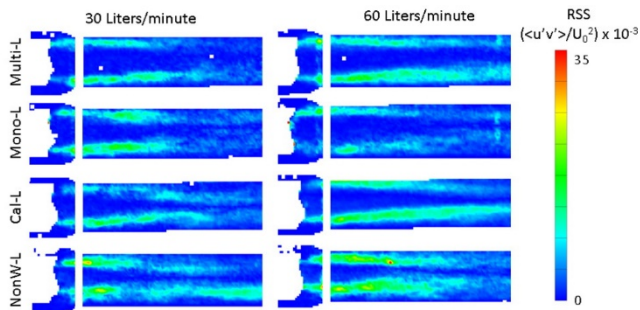
Figure 3: RSS contour for different textile.

Although the valve profile impacts RSS in general, the textile construction exhibit globally minimal influence on turbulence. The results show only minimal correlation between the roughness of the textile surface and the turbulence produced by the valve.

CONCLUSION
This work demonstrates that textiles can be engineered to provide favorable hemodynamic conditions to be employed as prosthetic heart valve.

KEYWORDS
Textile valve, turbulence, surface roughness.

ACKNOWLEDGMENT

REFERENCES
[1] Frederic Heim, Bernard Durand, Nabil Chakfe. "Textile heartvalve prosthesis: Manufacturing process and prototype performances." *Textile Research Journal*, 2008, 78(12): 1124-31.

[2] Antoine Vaesken, Foued Khoffi, Frederic Heim, Florence Dieval, Nabil Chakfe. "Fiber heart valve prosthesis: Early in vitro fatigue results." *Journal of Biomedical Materials Research Part B: Applied Biomaterials*, 2015.

[3] Khandakar Niaz Morshed, David Bark, Jr., Marcio Forleo, Lakshmi Prasad Dasi. "Theory to predict shear stress on cells in turbulent blood flow." *PLoS ONE*, 2014, 9(8): e105357.

[4] Marina V. Kameneva, Greg W. Burgreen, Kunisha Kono, Brandon Repko, James F. Antaki, Mitsuo Umezu. "Effects of turbulent stresses upon mechanical hemolysis: experimental and computational analysis." *ASAIO Journal: 1992*, 2004, 50(5): 418-23.

[5] Frederic Heim, Bernard Durand, Nabil Chakfe. "Textile heart valve: Novel shaping process and material performances." *Materials and Manufacturing Processes*, 2011, 26(10): 1303-09.

[6] Marcio Forleo, Lakshmi Prasad Dasi. "Effect of hypertension on the closing dynamics and lagrangian blood damage index measure of the b-datum regurgitant jet in a bileaflet mechanical heart valve." *Annals of Biomedical Engineering*, 2014, 42(1): 110-22.

Posters

Surface Morphologies of Nylon Knitted Textiles Coated with Different Zeolites

Alenka Ojstršek, Karin Stana Kleinschek, Darinka Fakin
University of Maribor, Faculty of Mechanical Engineering, Institute of Engineering Materials and Design, Maribor, Slovenia
alenka.ojstrsek@um.si

OBJECTIVE

The aim of this research was to apply four different types of zeolites in the form of a very fine powder together with different chemicals and auxiliaries on nylon knitted fabric according to industrially-acceptable exhaustion procedure in order to select the most appropriate zeolite regarding the changes in fabrics' morphologies (SEM) and in molecular-chemical level (FTIR).

INTRODUCTION

Fabrication of multi-functional textiles by various strategies of surface modification with different (nano- or micro-) particles offers excellent potential either for improving some undesired properties or to impart special functionalities developing high-added value products, i.e. textiles for protection, medical and sport activities, technical textiles, etc. [1]. Zeolites of numerous types have received increased interest over recent years on account of their superior heat resistance, high surface area, exchangeable cations, and high chemical stability [2,3]. Because they are non-toxic and non-absorbable by the humans, zeolites would be highly promising for the fabrication of multifunctional textiles that are constantly in direct contact with the skin.

EXPERIMENTAL PART

Materials

Four different industrially-synthesized zeolites (Silkem Kidričevo, Slovenia) were used in the form of very fine powder, i.e. 4A, 13X, ZSM-5 and a mixture of those three zeolites in a ratio 60:30:10. A series of experiments were carried-out using a light grey 100% polyamide (PA) knitted fabric, which was industrially-manufactured by Julon, Ljubljana (Slovenia).

Zeolites Coating Procedure

Eight previously-optimized initial baths were composed of: i) 3% owf (of weight of fabric) of individual zeolite 4A, 13X, ZSM-5 or zeolites mixture, and ii) 3% owf of individual zeolite 4A, 13X, ZSM-5 or mixture of zeolites together with additives (add.) suitable for PA treatment, i.e. 0.3% owf of amphoteric levelling agent, 0.5 ml/L of pH-regulator and acetic acid (80%) for pH 5.5-6.5 adjustment.

The application of individual treatment bath was accomplished according to the exhaustion procedure at a temperature of 98°C for 60 min using liquor-to-fabric weight ratio of 30:1 in a sealed stainless-steel treatment-pot, housed in a Labomat (W. Mathis) laboratory device.

Analytical Methods

The surface morphologies of different zeolites as well as zeolite-coated knitted textiles were observed by a scanning electron microscope FE-SEM-ZEISS Gemini Supra 35 VP (Carl Zeiss NTS GmbH, Germany).

Infrared absorbance spectra of different zeolites as well as zeolite-coated fabrics were obtained using a spectrophotometer FTIR System Spectrum GX (Perkin Elmer) with a Golden Gate ATR attachment and a diamond crystal. The measurements were taken in the range of 4000-650 cm^{-1} wavenumber using 16 scans and a resolution of 4 cm^{-1}.

RESULTS AND DISCUSSION

Characterization of Zeolites

With an aim to study the surface morphologies of four different zeolites for the subsequent surface modification of PA knitted textile, SEM micrographs of zeolites were taken, and presented in Figure 1. Additionally, ATR-FTIR spectra of zeolites powder were recorded (Figure 2) in order to elucidate the difference between three types of zeolites a well as its combinations.
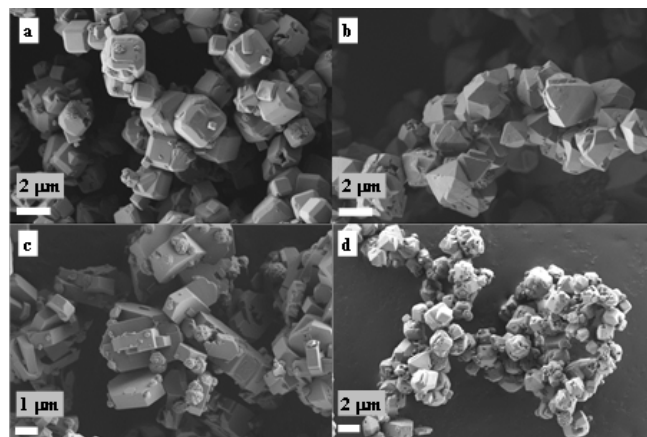

Figure 1. SEM images of selected zeolites: a) 4A; b) 13X; c) ZSM-5; d) mixture.
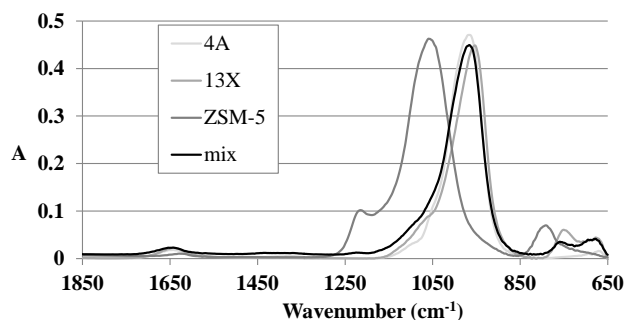

Figure 2. ATR-FTIR spectra of used zeolites.

SEM images in Figure 1 show structural/formational differences between used zeolite, namely cubic crystals of zeolite A (a), octahedral crystals of zeolite X (b) and pentasil building blocks of zeolite ZSM-5 (c), which was all present in mixtures of those zeolites (d) as expected from

the producer information. Moreover, examined zeolites are different sizes ranging from 1 up to 3 μm.

From FTIR spectra of selected four zeolites in Figure 2, it can be seen that the intensive bands appear in the area of low frequency at a wavenumber of ca. 970 cm-1 (4A, 13X and ZSM-5) and at 1067 (mixture of zeolites) and correspond to the stretching vibrations of Si–O(Si) and Al–O(H) functional groups, respectively.

Morphological and Molecular-Chemical Analyses of Zeolites-Coated Nylon Knitted Fabrics

SEM images in Figure 3 demonstrated the different coating morphologies regarding the zeolites type, i.e. 4A, 13X, ZSM-5, and zeolites mixture as well as the employed baths composition, i.e. aqueous dispersions of individual zeolite (1st row), and slightly acidic aqueous dispersions of individual zeolite together with proper additives - add. (2nd row). In the case of aqueous dispersions of zeolite A and 13X, exceedingly low content of micro-particles could be observed over complete fibers' surfaces as compared to the samples treated with the same zeolites, but in the combination with additives upon the acidic conditions.
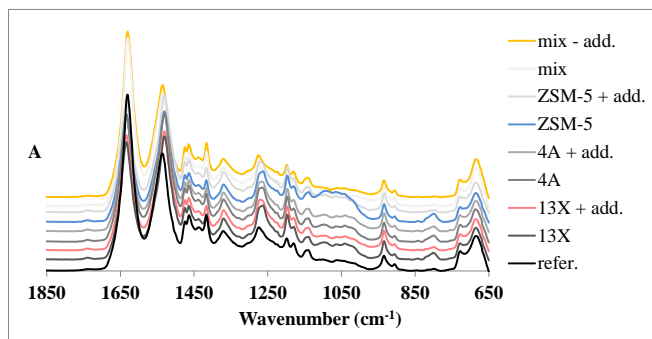
Figure 4. FTIR spectra of (refer.) and coated PA using aqueous dispersions of different zeolites and zeolites together with additives (add.)

In infrared spectra in Figure 4, typical peak positions for polyamide were depicted, irrespectively of treatment type, including amide I (C=O stretching vibrations) at ~1631 cm^{-1} and amide II (N–H bending and C–H stretching vibrations) at 1531 cm^{-1} as also fully interpreted [4]. In addition, some

characteristic absorption bands are evidently recognized for the zeolite modified PA fabrics, i.e. the peaks around 1000 or 1060 cm^{-1} (regarding the zeolite used) corresponded to stretching vibrations and at 799 cm^{-1} to the bending Si–O vibrations of Si–O–C [3,4]. Meanwhile, some peaks became lower like peaks at 1631 cm^{-1} and 3298 cm^{-1} due to the reduced amino groups or intensified like peaks at 1275 cm^{-1} on account of presence of C–H symmetric bending vibrations of Si–CH2–CH2–.

CONCLUSION

The results obtained by surface morphology observation and identification of specific molecular vibrations of zeolite coated polyamide knitted fabrics proven the suitability of employed exhaustion procedure regarding the type of zeolite used as well as composition of treatment bath.

KEYWORDS

Nylon Knitted Fabric; Zeolites; Coatings; Surface Morphology;

REFERENCES

[1] A. Ojstršek, K. Stana Kleinschek, D. Fakin. "Characterization of nano-sized TiO2 suspension for functional modification of polyester fabric." *Surface & Coatings Technology*, 2013, 226: 68-74.

[2] S. Liu, X. Cao, L. Li, C. Li, Y. Ji, F.S. Xiao. "Preformed zeolite precursor route for synthesis of mesoporous X zeolite." *Colloids and Surfaces A: Physicochemical and Engineering Aspects*, 2008, 318 (1-3): 269-74.

[3] R.S. Carran, A. Ghosh, J.M. Dyer. "The effect of zeolite molecular sieve based surface treatments on the properties of wool fabrics." *Applied Surface Science*, 2013, 287: 467-72.

[4] A. Monteiro, B. Jarrais, I.M. Rocha, M.F.R. Pereira, C. Freire. "Efficient immobilization of montmorillonite onto cotton textiles through their functionalization with organosilanes." *Applied Clay Science*, 2014, 101: 304-14.
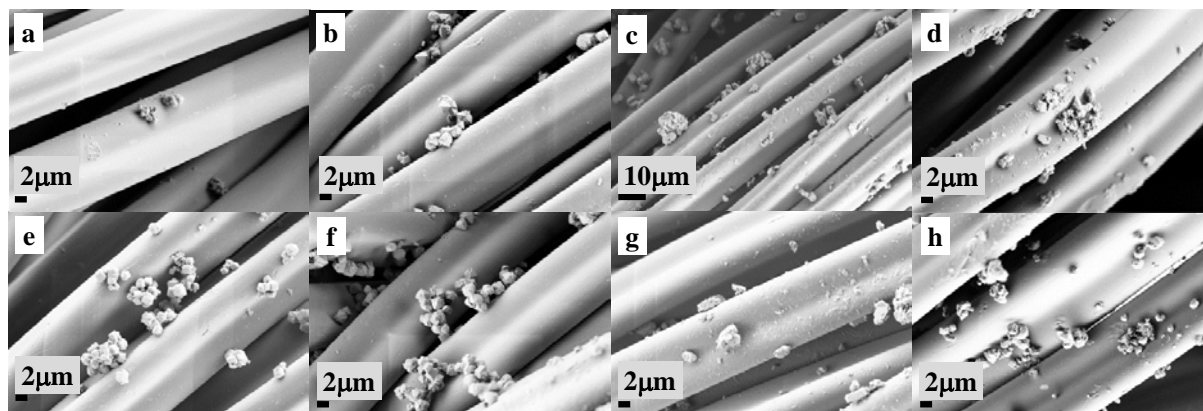
Figure 3. SEM images of PA fabrics coated with 3% owf of: a) zeolite 4A; b) zeolite 13X; c) zeolite ZSM-5; d) zeolite mix.; e) zeolite 4A + add.; f) zeolite 13X + add.; g) zeolite ZSM-5 + add.; h) zeolite mix. + add.

Applicability of Porous, Three-dimensional Aluminosilicates for Cellulose Surface Modification

Darinka Fakin, Silvo Hribernik, Alenka Ojstršek

University of Maribor, Faculty of Mechanical Engineering, Institute of Engineering Materials and Design, Maribor, Slovenia

alenka.ojstrsek@um.si

OBJECTIVE

The main objective of the presented research was to study the applicability of selected porous three-dimensional aluminosilicates in combination with crosslinking agent for cellulose surface modification without compromising the mechanical performance.

INTRODUCTION

Three-dimensional aluminosilicates known as zeolites consist of corner-sharing AlO_4 and SiO_4 tetrahedra with channels' and cavities' size ranges between 0.3 and 1.2 nm, which are classified as micro pores and are filled by cations (alkali and alkaline earth metals: K, Na, Ca, Mg) and water molecules (Liu et al., 2008). A variety of forms (A, Y, X, beta, ZSM-5, etc.) can be synthesized from aqueous basic aluminosilicate precursor gels under hydrothermal conditions at elevated temperatures within the laboratory. Due to the zeolite's particular characteristics (high thermal and hydrothermal stability, high surface area, exchangeable cations, and uniform internal channels and cavities), the technology of zeolite coatings is convenient for a variety of potential applications that are related to membrane separation, industrial ion exchange, adsorption, solid-acid catalysis process, etc. (Bastani et al., 2013, Meng et al., 2009). Because they are non-toxic and non-absorbable by humans, and due to the above-listed properties, zeolite particles would be highly promising for the fabrication of multifunctional textiles. In addition, the principle of fibers coating with particles' colloidal dispersions could easily be adapted to existing textile finishing processes, thus making them industrially viable.

EXPERIMENTAL PART

Materials

Trials were conducted using an industrially-bleached 100% cellulose fabric (Co) in plain weave with a mass of 110 g/m2, warp density of 41 threads/cm and weft density of 38 threads/cm, and warp/weft fineness of 20 tex. The zeolites used during this study were synthesised and supplied by Silkem Kidričevo, Slovenia in the form of very fine powder; with average particle sizes of 3.45 μm, composed of 18.08 wt.% Na_2O, 29.24 wt.% Al_3O_3, 43.73 wt.% SiO_2.

Pad-Dry-Thermofix Process

Zeolites (Z) in three concentrations (5, 10, or 30 g/L) with or without the additions of 40 g/L modified dimetylol dihydroxy ethylene urea (crosslinking agent - cr.a) were applied onto cotton fabric during the pad-dry-thermofix procedure. Samples were padded twice with a pad-liquor, by using a laboratory pad-mangle with 80% wet pick-up, dried for 3 min at a temperature of 100°C, and then treated at 150°C for 5 min.

Characterization Techniques

For the morphological analysis the samples were placed on an adhesive carbon band attached to the brass holder of a Zeiss Gemini Supra 35 VP Scanning Electron Microscope (Carl Zeiss NTS GmbH, Germany), and then the SEM images were taken. X-ray powder diffraction (XRD) measurement of zeolites was performed at room temperature in a XRD diffractometer PANalytical X'Pert PRO, using CuKα1 radiation (λ1 = 1.5406 Å) over 2θ range of 5 do 50° per 100 sec and a step size of 0.016°. Fourier transform infrared spectroscopy (FTIR) of the samples was accomplished using a FTIR System Spectrum GX spectrophotometer (Perkin Elmer) with a Golden Gate ATR attachment and a diamond crystal. The absorbance spectra were obtained within the range of 4000-650 cm^{-1}, with 32 scans and a resolution of 4 cm^{-1}. Selected mechanical properties (elongation at break, tensile strength and breaking tenacity) of modified fabrics were determined according to standard ISO 13934-1 using a Textechno statigraph M test machine.

RESULTS AND DISCUSSION

Zeolite Analysis

SEM image of selected zeolite particles was taken with the intention of studying zeolite surface morphology for the subsequent modification of cellulose fabric (Figure 1). In addition, the crystalline nature of zeolites was investigated by XRD analysis, as shown in Figure 2.
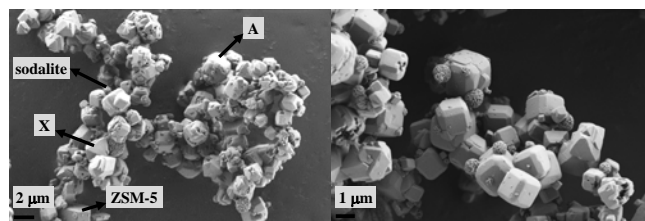

Figure 1. SEM images of used zeolite at different magnifications.

From SEM micrographs in Figure 1, it could be unequivocally perceived the mixture of three different types of zeolites in sizes between 2 and 6 μm. Notably, the examined sample shows different ratio of the cubic crystals of zeolite A in the largest amount, followed by the octahedral crystals of zeolite X, and the pentasil building blocks of zeolite ZSM-5 in the moderate amount, which was also confirmed by X-ray powder diffraction measurement (Figure 2).
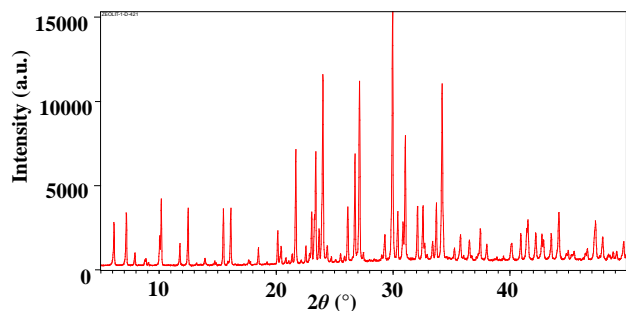
Figure 2. X-ray diffractogram of zeolites.

The XRD pattern in Figure 2 exhibited strong peaks characteristic for three different types of zeolites (A, X, and ZSM-5) with high crystallinities as previously disclosed by SEM micrographs in Figure 1.

Zeolite-Treated Fabrics Analyses
The gained SEM micrographs are shown in Figure 3, the infrared spectra in Figure 4 and mechanical properties in Table I.
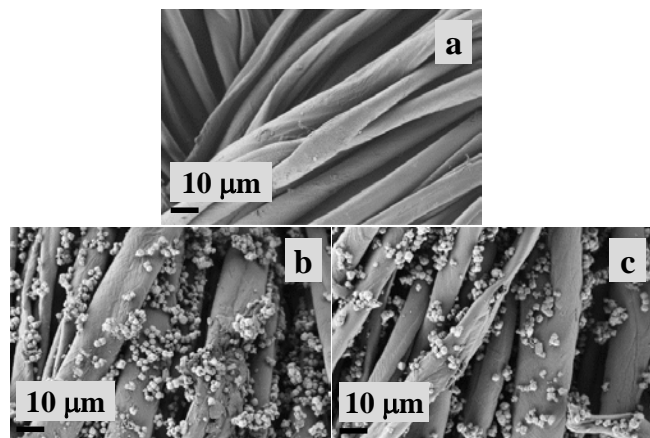

Figure 3. Selected SEM images of: a) untreated; b) 30 g/L zeolite; c) 30 g/L zeolite + crosslinking agent.
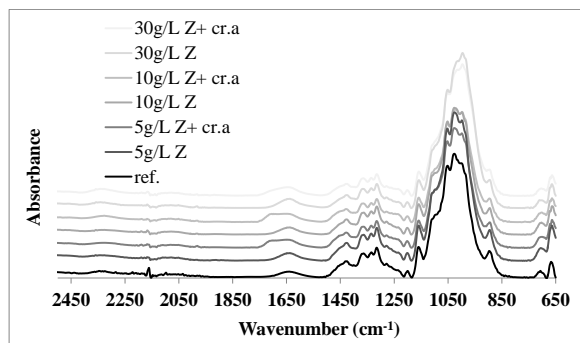
Figure 4. Infrared spectra of modified cellulose.

The SEM micrograph in Figure 3(a) showed the clear and clean cellulose fibers' surface of untreated (reference) sample that was efficiently (but not ideal) modified with zeolites, thus changing the surfaces' morphologies - Figure 4(b,c).

Table I. Selected mechanical properties.

Sample	Elongation at break (%)	Tensile strength (N)	Break. tenacity (cN/tex)
Reference			
warp	8.65 ± 0.37	421 ± 22	441 ± 22
weft	14.31 ± 0.38	354 ± 18	371 ± 19
5 g/L Z			
warp	9.24 ± 0.71	494.63 ± 33	517.93 ± 34
weft	13.80 ± 2.20	388.82 ± 15	407.14 ± 16
30 g/L Z			
warp	8.51 ± 0.26	504 ± 36	528 ± 37
weft	11.91 ± 1.08	414 ± 17	434 ± 18
5 g/L Z +cr.a			
warp	7.49 ± 0.59	435.15 ± 18	455.66 ± 18
weft	10.19 ± 1.60	363.13 ± 28	380.24 ± 29
30 g/L Z+cr.a			
warp	8.31 ± 0.68	501 ± 28	524 ± 29
weft	10.30 ± 0.81	372 ± 33	389 ± 34

From Table I it could be perceived that after zeolite particles application, the elongation at break was moderately decreased, and on the other hand, tensile strength and breaking tenacity were significantly intensified in both directions as also reported by (Carran et al., 2013).

CONCLUSION
Selected zeolite particles in water dispersion are shown to be an effective material for functional modification of cellulose fabric achieving acceptable surface coatings. Moreover, the tensile strength, breaking strength and elongation at break are enlarged regarding the concentration of zeolites as well as the crosslinking agent employed.

KEYWORDS
Cellulose Fabric; Zeolite; Pad-Dry-Thermofix Process; Surface Morphology; Mechanical Properties.

REFERENCES
1. D. Bastani, N. Esmaeili, M. Asadollahi. "Polymeric mixed matrix membranes containing zeolites as a filler for gas separation applications: A review." *Journal of Industrial and Engineering Chemistry*, 2013, 19 (2): 375-93.
2. R.S. Carran, A. Ghosh, J.M. Dyer. "The effects of zeolite molecular sieve based surface treatments on the properties of wool fabrics." *Applied Surface Science*, 2013, 287: 467-72.
3. S. Liu, X. Cao, L. Li, C. Li, Y. Ji, F.S. Xiao. "Preformed zeolite precursor route for synthesis of mesoporous X zeolite." *Colloids and Surfaces A: Physicochemical and Engineering Aspects*, 2008, 318 (1-3): 269-74.
4. X. Meng, F. Nawaz, F.S. Xiao. "Templating route for synthesizing mesoporous zeolites with improved catalytic properties." *Nano Today*, 2009, 4 (4): 292-301.

Effect of Electrospinning Parameters on Air and Water Vapour Permeability of PP Nonwoven Substrate Coated With PA-6 Nanoweb

Ahsan Nazir[1,2], Nabyl Khenoussi[1], Tanveer Hussain[2], Dominique Adolphe[1], Laurence Schacher[1]

[1]Université de Haute-Alsace – ENSISA – Laboratoire de Physique et Mécanique Textiles (EA 4365) Mulhouse – France
[2]Department of Textile Processing, National Textile University, Faisalabad, Pakistan
ahsan.nazir@uha.fr

OBJECTIVES

Electrospinning is one of the most viable techniques to produce nanofibers, and finds many technical applications including protective textiles. For such uses as protective clothing, performance and comfort are both important aspects for safety and performance of the wearer. Current study focuses on the effects produced by coating of nanofibrous web on air and water vapor permeability of Polypropylene nonwoven that may be used to produce various types of protective clothing..

INTRODUCTION

Electrospinning is a simple technique that allows producing nanofibers with customized properties at much higher rate and using a large number of fiber forming materials (Wang, Fu and Li; Greiner and Wendorff). Amongst countless potential applications of electrospinning, different protective products have received a great attention from researchers. Many technical products like medical gowns and different respiratory protective products are valuable addition in field of electrospun materials (Vitchuli et al.). Comfort is the key parameter that describes the potential end-use and value of all such wearable protective products. Needle based electrospinning has long been developed and being investigated for development of such products. However, Needleless Electrospinning recently gained importance for commercial production of such products (Niu, Lin and Wang). The needleless setup employed in this work is based on generation of nanofibers by electrostatic force between two wire electrodes. The polymer solution is coated on one of the wire electrodes through a solution carrier (coater) that moves on to and fro manner along the wire electrode. The electrostatic force pulls the polymer toward the opposite electrode and fibers move towards it. At end of their flight towards the opposite electrode, they are deposited on a collector that may be selected on base of the specific end use.

MATERIALS AND METHOD

PA-6 was produced by dissolving it in formic acid in three different concentrations, C (18%, 19% and 20% w/w) and was electrospun on a spunbond nonwoven substrate (100% Polypropylene) using Elmarco's Nanospider NS 1WS500 (Elmarco). Other than solution concentration, the input parameters included the applied potential difference, V (at 35, 45 and 55 KV), the distance between electrodes (at 260, 275, 290 mm), the polymer solution carriage speed, Cs (at 290, 340 and 390 mm/sec), substrate speed (15, 20 and 25 mm/min) and air flow (at 120, 130 and 140 m^3/h). The experiments were designed using Taguchi method, which was also used for analysis of results. The diameter of

nanofibers was determined using scanning electron microscope. The air permeability of nanofiber coated nonwoven webs was determined according to ASTM D737 using SDL Atlas air permeability tester. The water vapor permeability of samples was tested according E96-95.

RESULTS AND DISCUSSION

Effect of input variables on Air Permeability

From analysis of variance it was observed that concentration and voltage produced strong significant impact on air permeability while other factors have less significant effect. This is due to their lower impact on fiber diameter (which is main contributor to permeability) as compared to concentration and voltage. The effect of concentration, voltage and ultimately the fiber diameter has been discussed in following paragraphs.

As shown in figure 1, increasing concentration has an overall increasing impact on air permeability. This is due to the fact increasing concentration normally results in thicker fibers with higher standard deviation (Nazir et al.). Both these factor lead to increased air flow because of larger inter-fibre spaces. Similarly, increasing voltage was found to decrease the air permeability. This is due to production of thinner fibers at higher voltages thus reducing the pore size and resultant air flow.

The fact that higher diameter and variation in diameter increases the air permeability has also been depicted in figure 2, that shows a contour plot of air permeability against mean diameter and SD in diameter (Nazir et al.). The presence of dark areas at top right column shows that air permeability is higher for thicker fibers with larger standard deviation.
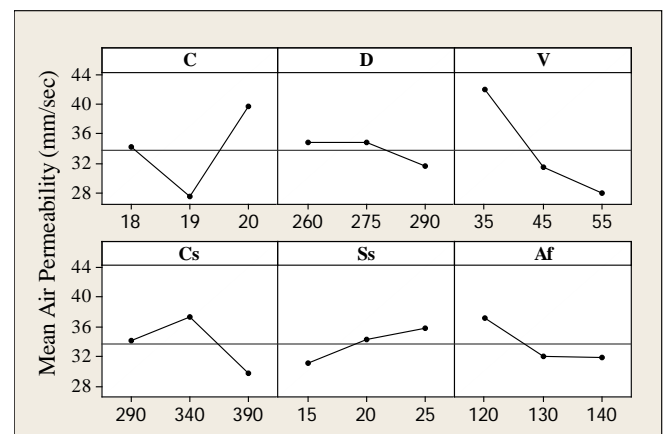

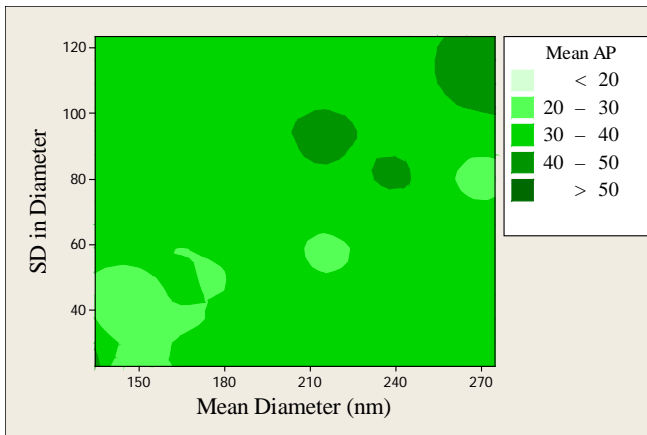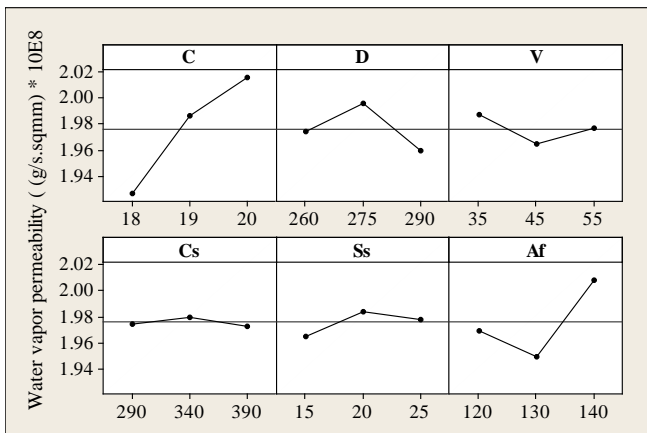Figure 1: Effect of input variables on air permeability.

Figure 2: Effect of diameter and standard deviation in diameter on air permeability.

Effect of input variables on Moisture Vapor Permeability

For moisture vapor permeability, similar trends were observed as for air permeability. The statistically significant factors (from ANOVA) included the solution concentration only even though other factors also posed some impact on the water vapor permeability. From figure 3, it could be observed that increasing concentration, almost linearly, increased the water vapor permeability of nanofiber coated nanowebs. Amongst other factors, P-value for air flow was found to be 0.075 that shows that its effect is close to the highly significant effect of concentration. Increasing air flow was increased the moisture vapor permeability. This was due to the fact that higher air flow leads to higher fiber loss thus leading to thinner web as compared to that formed at lower air flow.

The effect of fiber diameter and its variation on water vapor permeability has been depicted in figure 4. The figure shows that increasing the fiber diameter and standard deviation in diameter increased the permeability of water vapors through the nanofiber coated nonwoven web.

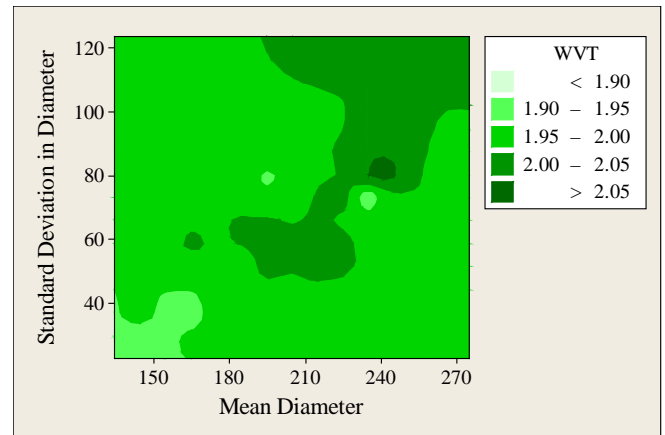Figure 3: Effect of input variables on water vapor permeability.

Figure 4: Effect of diameter and standard deviation in diameter on water vapor permeability.

CONCLUSIONS

The current study focused on effect of coating nanofibers web on air and water vapour permeability of nonwoven polypropylene. It was observed that coating the nonwoven with nanofibers significantly impacted the permeability of the structure produced thereafter. It was also observed that the input parameter that affect the diameter and thickness of web i-e concentration, voltage and air flow are the basic factors that must be controlled to control the permeability of the resulting composite web. Finally, the diameter and variation in diameter nanofibers coated on composite web has been confirmed to affect the permeability of this structure.

REFERENCES

Elmarco. "Ns 1ws500u; Most Versatile Electrospinning Equipment." Web. 2015/06/14.

Greiner, A., J.H. Wendorff. "Electrospinning: A Fascinating Method for the Preparation of Ultrathin Fibers." *Angew Chem Int Ed Engl* 46.30 (2007): 5670-703.

Nazir, A., et al. "Using the Taguchi Method to Investigate the Effect of Different Parameters on Mean Diameter and Variation in Pa-6 Nanofibres Produced by Needleless Electrospinning." *RSC Advances* 5.94 (2015): 76892-97.

Niu, H., T. Lin, X. Wang. "Needleless Electrospinning: Developments and Performances." *Nanofibers—Production, Properties and Functional Applications*. INTECH Open Access Publisher, 2011: 17-36.

Vitchuli, Narendiran, et al. "Electrospun Ultrathin Nylon Fibers for Protective Applications." *Journal of Applied Polymer Science* 116.4 (2010): 2181-87.

Wang, H.S., G.D. Fu, X.S. Li. "Functional Polymeric Nanofibers from Electrospinning." *Recent Pat Nanotechnol* 3.1 (2009): 21-31.

In Vitro Biodegradability of Bacterial Cellulose by Cellulase and Compatibility In Vivo

Shiyan Chen[1], Baoxiu Wang[1], Xiangguo Lv[2], Chao Feng[2], Huaping Wang[1]

[1]State Key Laboratory for Modification of Chemical Fibers and Polymer Materials, Key Laboratory of Textile Science & Technology (Ministry of Education), College of Materials Science and Engineering, Donghua University, Shanghai, China

[2]Department of Urology, Affiliated Sixth People's Hospital, Shanghai Jiaotong University , Shanghai, China

chensy@dhu.edu.cn; wanghp@dhu.edu.cn

Bacterial cellulose (BC) have great potential in tissue scaffold due to its unique structure and properties including high tensile strength and good biocompatibility.[1-4] However, poor biodegradability of BC in human body may be one of the most disadvantages limiting its applications in the field.[3,4] In this paper, we developed a simple absorption method to prepare biodegradable cellulase/BC materials. Cells incubation and subcutaneous implantation demonstrated that the cellulase/BC materials had good in vitro and in vivo biocompatibility.

The purified BC pellicles were cut into 3×3 cm sheet with the same thickness (about 2 mm) and under a brick to remove free water. Then the BC pellicles were put into flasks containing enzyme solutions with the optimal concentration (5 mg/mL) for 30 min under magnetic stirring. The cellulase/BC composites were rinsed with water to remove cellulases that have poor absorb abilities to BC.

Fig. 1 shows the FE-SEM images of cellulase/BC composites for different time during degradation process in simulated body fluid. The 3D nanofibrous network is maintained just along with some tiny holes on the surface of BC for the first 2 weeks. As the extension of the degradation time from 2 to 8 weeks, shown in Fig. 1e-f, although the 3D nanofibrous network still can be observed, the degradation obviously increase and the hole become larger than those in the initial stage. After degradation for 8 weeks later (Fig. 1g), the 3D nanofibrous network of BC almost disappear with fracture of many fibrils and fall into pieces. It is indicated that the cellulose chains were randomly broken by cellulase and BC were gradually degraded. This kind of degradation is necessary for scaffold materials to provide interspace for growth of new tissue.
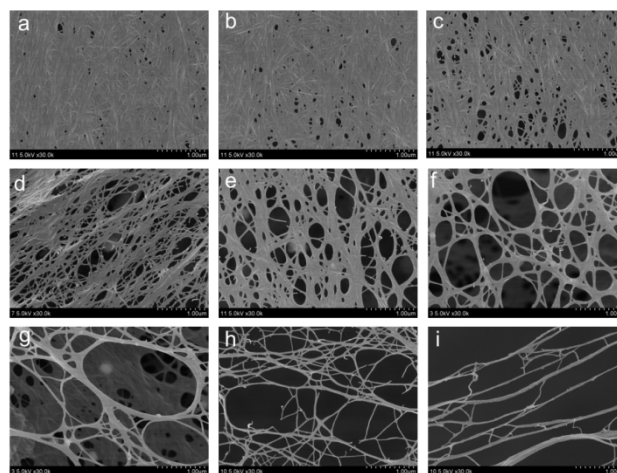

Figure 1: FE-SEM images of cellulase/BC composite for different degradation time: (a) 12 h, (b) 24 h, (c) 48 h, (d) 2 w, (e) 4 w, (f) 6 w, (g) 8 w, (h) 12 w and (i) 16 w (The enzyme concentration and absorption time: 5 mg/mL, 30 min).

Muscle-derived cells were seeded the on the surface of pure BC and cellulase/BC composites scaffold to observe the cell propagation for 4 weeks and the H&E staining images are shown in Fig. 2. Good cell proliferation on the surface of samples is observed, which indicates good biocompatibility of samples (Fig. 2a-h). However, few cells migrate into pure BC due to its compact fibrous network and non-degradability (Fig. 2a-d). For cellulase/BC composites, along with the degradation, some cellular infiltration of the sample was evident, this is because the degradation of BC makes it porous which is favorable to cell ingrowth (Fig. 2e-h).
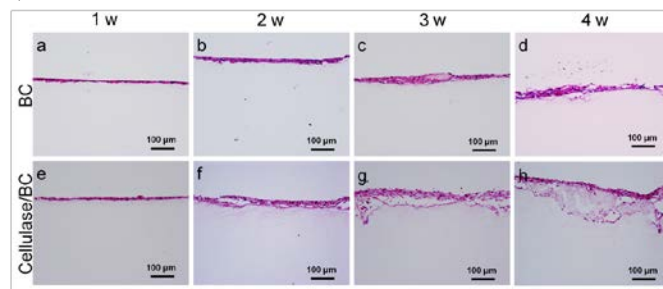

Figure 2: HE staining images of BC and cellulase/BC composite (the enzyme concentration and absorption time: 5 mg/mL, 30 min) after 1 w, 2 w, 3 w and 4 w of in vitro incubation.

Subcutaneous implantation is an international method to evaluate the safety of materials. Fig. 3 shows the HE staining images of in vivo evaluation of the biocompatibility

of pure BC and cellulase/BC composites under different periods. As shown in Fig. 3a-h, no tissue degeneration, necrosis and hyperplasia are observed and a large number of macrophages accumulation phenomenon does not appear, only slight inflammation is found around the tissue. It can be found that only a few cells are observed in the BC section, and the boundary is obvious between BC and the tissue (Fig. 3a-d). However, no boundary can be found between materials and tissue in the cellulase/BC composites which indicates better biocompatibility of the cellulase/BC composite scaffold (Fig. 3e-h). Moreover, a large number of cells ingrowth into implanted material could be seen, especially in Figure 3 h, which might benefited from the degradation of BC. It showed the degradation of BC makes cell penetration very easy. The phenomena demonstrated that the cellulases still kept their function to degrade the cellulose in vivo and the degradation products have no effect on the biocompatibility of the cellulose. Both pure BC and cellulase/BC composites have good biocompatibility, which is consistent with previous reports.[5] It is indicated that introduction of cellulase into BC may be a good method to modulate and realize the degradation of cellulose, and further applied in tissue engineering applications.[5]
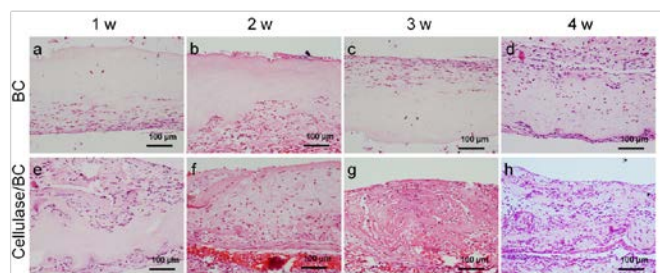

Figure 3: HE staining images of BC and cellulase/BC composite (the enzyme concentration and absorption time: 5 mg/mL, 30 min) after 1 w, 2 w, 3 w and 4 w of hypodermic implantation.

In conclusion, biodegradable BC incorporating cellulase content was prepared by absorption method. Results show that BC material could be degraded in SBF. An obvious cell adhesion and growth on cellulase/BC composite was observed, which indicates the good in vitro biocompatibility of material. In vivo evaluations showed there were no tissue degeneration, necrosis phenomenons in the tissue section which indicated the implanted material was degraded along with the cells ingrowth into it. The cellulase/BC composite prepared by absorption method not only shows good degradation behavior, but also has good in vitro and in vivo biocompatibility, which could be an ideal candidate for bioabsorbable tissue scaffold material.

KEYWORDS
Bacterial cellulose·Cellulase·Biodegradation·Tissue scaffold

REFERENCES
1. Petersen, N., Gatenholm, P. "Bacterial cellulose-based materials and medical devices: current state and perspectives." *Applied Microbiology and Biotechnology*, 2011, 91 (5): 1277-86.
2. Svensson, A., Nicklasson, E., Harrah, T., Panilaitis, B., Kaplan, D., Brittberg, M., Gatenholm, P. "Bacterial cellulose as a potential scaffold for tissue engineering of cartilage" *Biomaterials*, 2005, 26 (4): 419-31.
3. Wang, J., Zhu, Y., Du, J. "Bacterial cellulose: a natural nanomaterial for biomedical applications." *Journal of Mechanics in Medicine and Biology*, 2011, 11 (02): 285-306.
4. Huang, Y., Zhu, C., Yang, J., Nie, Y., Chen, C., Sun, D. "Recent advances in bacterial cellulose." *Cellulose*, 2014 21 (1): 1-30.
5. Bodin, A., Bharadwaj, S., Wu, S., Gatenholm, P., Atala, A., Zhang, Y. "Tissue-engineered conduit using urine-derived stem cells seeded bacterial cellulose polymer in urinary reconstruction and diversion." *Biomaterials*, 2010, 31 (34): 8889-8901.

The Application of Chitosan/Cotton Blend Yarn for Addressing Functional Clothing Needs of Patients Suffering from Epidermolysis Bullosa

Ngan Yi Kitty Lam, Li Li

Institute of Textiles and Clothing, The Hong Kong Polytechnic University, Hung Hom, Hong Kong
kitlamny@hotmail.com

ABSTRACT

Epidermolysis Bullosa (ab. EB) is a hereditary skin disease which increases the risk of death in new born babies or young children in 20 out of 1 million live births [1]. They require special wound dressing to protect their skin from friction and scratching, because these will cause painful blisters. Since there is no cure for this skin disease and there are no specific clothing guidelines. To enhance the recovery rate of skin would help to reduce pain and discomfort of patients [2]. Parents of the patients claimed that they were not satisfied with function, material and comfort of clothing that they have purchased for their children. Chitosan is a functional material and it is well known of its antimicrobial properties. This material could provide moistening and deodorizing, assisting immunity and protection by adsorption. In order to enhance the wound healing rate by inhibiting the growth of bacteria on skin and to provide soft clothing with comfortable fabric for enhancing the wearing comfort to patients, the application of yarn and fabric composited by chitosan/cotton fibre with different blending ratio was purposed for addressing the functionality of their needs and offering the fabric comfort to EB patients. Therefore, a pilot study was conducted for investigating the actual needs of functional clothing from EB patients and their parents.

KEYWORDS

Epidermolysis Bullosa, Wound Healing, Functional Clothing, Chitosan/Cotton Blend Yarn.

REFERENCES

[1] Fine, Jo-David. "Epidermolysis bullosa: a genetic disease of altered cell adhesion and wound healing, and the possible clinical utility of topically applied thymosin beta4." Annals of the New York Academy of Sciences, 1112, 2007: 396-406.
[2] Diem, Anja. "Living with EB-Impact on Daily Life." Life with Epidermolysis Bullosa (EB): Etiology, Diagnosis, Multidisciplinary Care and Therapy. New York: Springer, 2009, 313-33.

Sewing Thread Consumption of Overegged Three-thread Stitch Type 504

Jaouachi Boubaker[1], Aouine Sana[2], Khedher Faouzi[1]

[1]Textile Engineering Laboratory; [2]National Engineering School of Monastir, University of Monastir, Tunisia
boubaker.jaouachi@gmail.com

ABSTRACT

This work deals with the consumption behaviour of overegged three-stitch type 504. Indeed, using its geometrical shape based on Taguchi analysis technique, the amount value of sewing thread to sew garments is accurately estimated. In fact, the obtained models are derived statistically taking into account different variables: number of fabric's layers, material thickness and woven fabric mass. The results show that good relationships between the tested inputs and the thread consumption value were founded and proved. In addition, the high coefficient of regression values ranged from 0.847 to 0.904, reflect the effectiveness of the analysis results. Therefore, influence of the studied influential fabric parameters on the sewing thread consumption of woven fabric samples was investigated. Indeed, it may be concluded that the number of stitched thicknesses of studied woven fabrics affect enormously the consumption of sewed thread than the other studied inputs.

INTRODUCTION

Although the majority of garments contain different parts, which are seamed using the overegged stitch types, there are few studies dealt with the consumptions basing on these stitches. Regarding the literature survey, different works related to consumption behaviours were conducted excepting those basing on the overegged stitches. Carvalho et al. (2004) were studied the possibility of an innovative device for bobbin thread consumption measurement on industrial lockstitch sewing machines. Hence, in their study they depicted an overview of the used technique was given within particular interest to the quantification of bobbin thread consumption in lockstitch machines. Sheraz et al. (2014) were studied geometrical modelling to calculate the consumption of sewing thread for lockstitch (301) and an experimental investigation of the effect of two different type of stitches viz., lockstitch (301) and chain stitch (401) at the seat seam of trouser for military armed forces respectively. Recently, the consumption was studied using different methods as function of some sewing parameters and their impacts on the consumed thread (Sai Krishnan & Ashok Kumar (2010), Jaouachi et al. (2012), Jaouachi & Khedher (2013 and 2015) and Khedher & Jaouachi, 2015). However, until today, there are no statistical models giving exactly the consumption of sewing thread in the garment companies except the compared regression and theoretical modelling of the consumption using the fuzzy theory conducted by Jaouachi's work (Jaouachi & Khedher, 2013). In this present work, we studied the consumption of sewed thread using the three-thread overegged stitch (504) as function of fabric inputs: the thickness and number of fabric layers parameters.

APPROACH

Four denim fabrics (F3-F6) within different properties and two other woven ones (flat and lining) are tested in order to accurately evaluate their consumptions in specific zones inside sewed popular garments (pants, jackets, etc.). Table I shows these fabrics and their principal physical characteristics used in our experimentation.

Table I: Studied denim fabrics and their characteristics.

Fabric / Characteristics	F1	F2	F3	F4	F5	F6
	lining	flat	denim	denim	denim	denim
Blend	65%PES+ 35%CO	100% CO	100% Chanvre	100% CO	100% CO	100% CO
M (g/m²)	157	231	320	370	422	413
T_{hf} (mm)	0.33	0.42	0.53	0.68	0.81	0.88
Ends/cm	31	35	39	32	27	26
Picks/cm	42	33	22	22	19	18

To evaluate objectively the sewed consumed thread (C_{st}), the number of fabric layers (N_L) and the thickness of woven fabric sample (T_{hf}) represent our tested inputs in this work. To evaluate each input contribution when level is changed (see Table II), a mixed Taguchi analysis was elaborated using Minitab software.

Table II: Studied inputs using mixed Taguchi design and their levels.

Inputs \ Levels	T_{hf} (mm)	N_L
I	0,33	1
III	0,42	2
III	0,53	3
IV	0,68	-*
V	0,81	-
VI	0,88	-

T_{hf}: thickness of fabric (mm); N_L: number of layers of fabric, *- : no level.

Before and after stitching the specimens, all experimental conditions are regulated and adjusted as recommended by Brother FB-N110-3020-05-S3F industrial 3 thread overlock sewing machine manufacturer instructions to obtain good sewing quality appearance. In addition, each stitch length can be adjusted from 2mm to 4mm within a width ranging from 2.3mm to 7mm. It is notable that, the sewing thread to sew woven fabric samples within length equals to 100mm as well as the sewing machine adjustments are kept constant to guarantee the same experimental conditions for overall tested specimens. Each combination was performed and repeated 10 times to obtain objective results. Experimentally, the consumption of sewing thread (C_{st}) value is measured after unstitching carefully all assembled layers of fabric specimen lengthening 100mm and then the sewed thread lengths are evaluated.

RESULTS AND DISCUSSION

To investigate the effect of the sewn thickness variations of the unstitched fabric and seamed layers of the same fabric samples on the consumption of sewing thread, the experimental Taguchi design was applied. The obtained findings using Minitab software show that there is a good relationship between the consumption value and the studied input parameters for the all woven fabric samples. Nevertheless, to improve the obtained findings, the regression analysis yielded coefficients of each parameter as well as the constant term, from which we obtained the Taguchi design analysis within the coded and uncoded forms respectively. Hence, in the selected experimental design of interest, the consumption of sewing thread can be predicted following the high coefficient of regression (close to 1) obtained. In addition, it is used in hypothesis tests to help decision whether to reject or fail to reject a null hypothesis. A commonly used cut-off value for the P-value is 0.05. Regarding the high values of R^2 (equal to 0.904), it may be concluded that good correlations between experimental results and those using elaborated models proved the effectiveness of the established relationship mentioned above.

$$C_{st} = 86,6 + 3,41 T_{hf} + 7,98 N_L$$

The quantity of sewing thread to sew garments is widely decreased. Basing on the high coefficient of regression value, which reflects the good relationship between C_{st} and the tested inputs the consumption evolution is sufficiently explained.

Relationships between number of layers and the consumption of overegged three-thread type 504

The variations of the consumption values as function of fabric thicknesses corresponding to different layers (ranged from 1 to 3 layers) are discussed. The linear regression given by the equation below shows that a good relationship was founded between the thickness and the consumption value. Furthermore, all evolutions presented high coefficients of regression proving an accurate prediction of the consumed thread. However, for comparative two assembled layers of seamed fabrics, the increase of their thicknesses seems widely correlated with the consumed thread. Indeed, the results show that the correlation between the thickness and the consumed sewing thread was encouraged enormously when layer's number increased too (the regression coefficient increased widely for 1, 2 and 3 layers respectively $R^2(C_{st1}) = 0.847$, $R^2(C_{st2}) = 0.86$ and $R^2(C_{st3}) = 0.915$). In the experimental design of interest, thickness seems in a good agreement with the thickness except for the two last fabric samples where we saved the contrast. Due to these fabrics present thicknesses value, which are not correspondent to their mass, this contrast can be sufficiently explained.

Relationships between mass of woven fabric and the consumption behaviour

In the other hand, the obtained findings confirmed that there are accurate relationships between the mass of fabric samples and the consumed thread behaviour. Indeed, Figures 4-6 show the effects of the different tested fabrics and their consumption values using different layer numbers for each fabric specimen tested. However, the inputs presented high contributions which differ as function of the seamed woven fabrics. Basing on our findings, the contributions are ranged from 6.94% (for lining fabric) to 17.17% (for denim fabric) which seem important on the consumption sewing thread using three-thread overegged stitch type (504). These differences of contributions may be explained by the fabric characteristics as compressibility, yarn-to-yarn friction, etc. In this study, the overall calculated contributions relative to the tested fabrics are carried out. Hence, the increase effects for F1, F2, F3, F4, F5 and F6 when input's levels changed are 6.94%, 11.81% and 12.87%, 14.25%, 16.57%, 17.17% respectively. Regarding the linear regression results obtained, it is undoubtedly remarkable, that high correlations (ranged from 0.933 to 0.961) tie the mass within the woven fabric consumptions. Therefore, possible predictions in the specific design of interest are fruitful and the consumption behaviour has high correlation values with mass of the woven fabrics based on its tremendous influence on the consumed thread.

CONCLUSION

Two most influential inputs have been investigated and discussed basing on their significant influences on the sewing thread consumption behaviour of overegged three-stitch type 504. The application of the statistical method using Taguchi analysis and linear regression techniques proved the effectiveness of their contribution values. Indeed, in this study, the coefficient of regression obtained are very close to 1 which reflecting, firstly, the good relationships between the inputs parameters and the sewing thread consumptions and secondly the prediction possibility of the consumed amount.

KEYWORDS

Sewing thread, consumption, overegged stitch, linear regression, Taguchi analysis.

REFERENCES

1. Carvalho, H., Rocha, A., Monteiro, J.L., Silva, L.F. "An innovative device for bobbin thread consumption measurement on industrial lockstitch sewing machines." *IEEE International Conference on Industrial Technology (ICIT)*, 2004: 1034-39.
2. Jaouachi, B., Khedher, F., Mili, F. "Consumption of the sewing thread of jean pant using Taguchi design analysis." *Autex Research Journal*, 2012, 12(4): 81-86.
3. Jaouachi, B., Khedher, F. "Evaluating sewing thread consumption of jean pants using fuzzy and regression methods." *Journal of the Textile Institute*, 2013, 104 (10): 1065-70.
4. Jaouachi, B., Khedher, F. "Evaluation of Sewed Thread Consumption of Jean Trousers Using Neural Network and Regression Methods." *Fibres & Textiles in Eastern Europe*, 2015, 23, 3(111): 91-96.
5. Sai Krishnan, A.N., Ashok Kumar, L. "Design of sewing thread tension measuring device." *Indian Journal of Fibre & Textile Research*, 2010, 35: 65-67.
6. Sheraz, A.R., Mohsin, M., Ahmed, F., Afzal, A. "Geometrical model to calculate the consumption of sewing thread for 301 lockstitch." *Journal of the Textile Institute*, 2014, 105 (12): 1259-64.

Structure and Properties of Polytetrafluoroethylene (PTFE) Fiber

Ruiliu Wang, Guangbiao Xu

College of Textiles, Donghua University, Shanghai, China

guangbiao_xu@dhu.edu.cn

INTRODUCTION

Polytetrafluoroethylene (PTFE) served as engineer material has excellent physical and chemical properties, such as high thermal stability, extremely low coefficient of friction (Biswas and Vijayan). These performances could be attributed to composition and structure of PTFE, which is helical linear polymer made up of carbon and fluorine and carbon chain tightly surrounded by fluorine atoms acted as protective layer (Biswas and Vijayan). Correspondingly, PTFE fibers used to fabricate filter cloths were considered to still own the same outstanding features as that of PTFE. However, until now there were few comprehensive studies on PTFE fibers and its properties. In this present study, the performances of PTFE fibers were characterized thoroughly by some methods.

RESULTS AND DISCUSSION

Morphological structure

Longitudinal and Cross-section SEM images of PTFE fibers were presented in Fig. 1. The longitudinal surface of the fiber was full of grooves, which would largely increase the specific area of fiber, and the cross section was sheet-like, irregular and with rough edge.
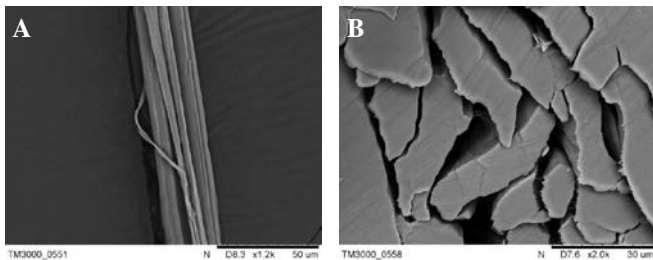
Fig. 1. SEM images of PTFE fibers: A) longitudinal surface morphology and B) cross-section morphology.

Chemical structure

Fig. 2 showed the infrared spectrum of PTFE fibers, three apparent peaks can be seen at 1207, 1151 and 636 cm^{-1}, respectively. The 1207 and 1151 cm^{-1} bands were assigned as the symmetric and asymmetric CF_2 and CC stretching vibrations (Oshima et al.) . The doublet at 638-626 cm^{-1} in the spectrum of PTFE film (Masetti et al.) was not found in that of PTFE fibers except the peak at 636 cm^{-1}. We learned that

636 cm^{-1} band was assigned to a regular helix and 626 cm^{-1} band was associated to the helix-reversal defect (Quarti, Milani and Castiglioni). Then we speculated that there were no conformations transitions. All these possibilities could be explored further through a study of temperature controlled infrared spectra.
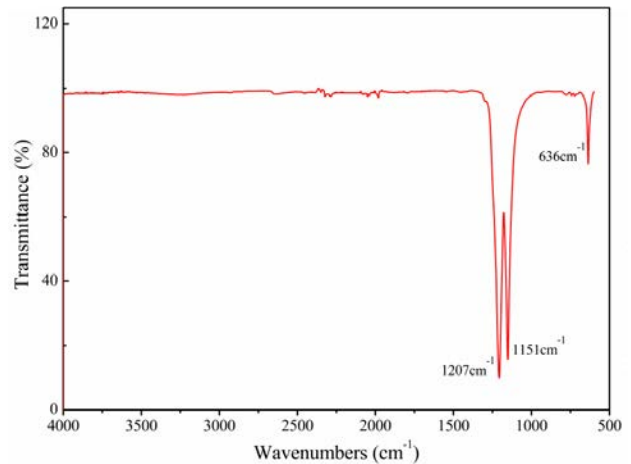

Fig. 2. FT-IR infrared spectrum of PTFE fibers.

Fiber fineness

The fineness distribution and linear density of PTFE fibers were shown in Fig. 3 and Table I respectively. It was approximately normal distribution and the distribution range was so wide, the fineness under 5 dtex accounted for 60%, and all this would bring difficulties for spinning and weaving.
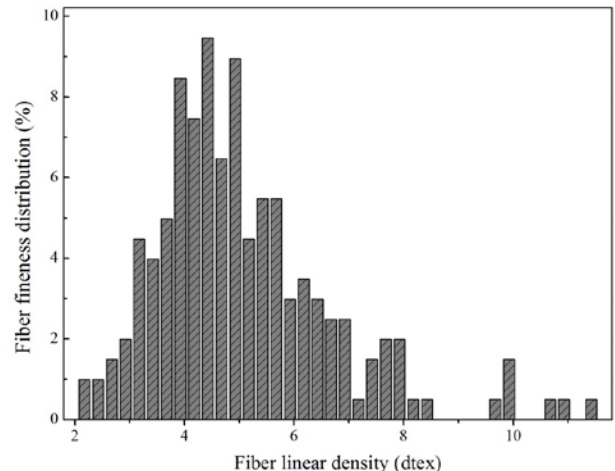

Fig. 3. Fineness distribution of PTFE fibers.

Table I. Linear density and tensile properties of PTFE fibers.

PTFE fibers	Linear density (dtex)	Tensile strength (cN)	Elongation at break (%)
Min	2.09	3.57	2.96
Max	11.50	15.59	14.06
Ave	5.07	6.92	6.38
CV (%)	32.58	38.07	30.66

Tensile properties

As shown in Table I, the average strength (1.37 cN/dtex) was calculated. As seen from the unflat fractured cross-section, there were some filamentous protrusions, so low strength may be ascribed to non-simultaneous breaking of macro-fibril.

Thermal properties

TG analysis and DSC curve of PTFE fibers were presented in Fig. 4. The melting point (T_m), crystallization temperature (T_c) and the decomposition temperature (T_d) which was defined as the point at which the mass loss was 5% were noted on the DSC and TG curve, respectively. The T_m of PTFE fibers was 329.1^{o}C, which was consistent with that of PTFE film (329°C), and the T_d of PTFE fibers was 508.6^{o}C, which was a little lower than that of PTFE film (525°C) (Chen et al.). All these indicated that excellent thermal stability was preserved completely though the percent of crystallinity (shown in Table II) was reduced.
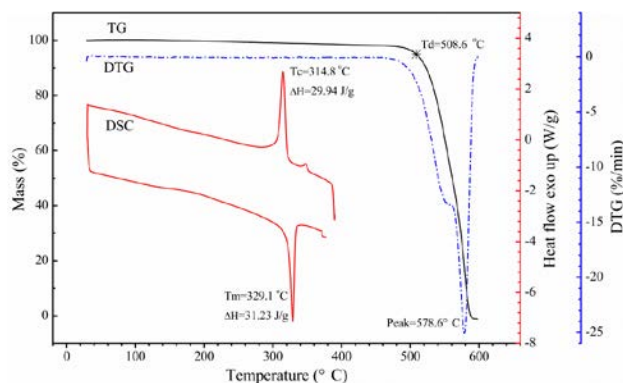
Fig. 4. TG analysis and DSC curve of PTFE fibers.

Table II. Partial physical properties of PTFE fibers.

Sample	Crystallinity (%)	Water contact angle (^{o})	Friction coefficient	
			μ_s	μ_k
PTFE fibers	74.85	119.93	0.19	0.17

Surface properties

The contact angle and the shape of water droplet on the surface of the fibers layer were shown in Table II and Fig. 5,

around 120° indicated that it was hydrophobic surface, and which coule be used for self-cleaning surface. Friction coefficient of fibers (0.17-0.19) was lower than that of hydrocarbon polymers, and a little higher than that of PTFE films (0.14) (Oshima et al.) which may result from the rough surface full of grooves.
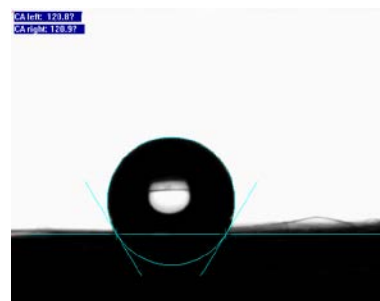

Fig. 5. Water contact angles of PTFE fibers.

CONCLUSION

The structure and properties of PTFE fiber were studied by various tests in this paper. It has been found that the longitudinal surface of the fibers was full of grooves and the cross section was sheet-like and irregular. The infrared spectrum of PTFE fibers was same as that of films except 626 cm^{-1} bands associated to the helix-reversal defect. The excellent thermal stability and the low friction coefficient of PTFE were preserved completely. The contact angle test showed that the fibers were hydrophobic.

REFERENCES

Biswas, S.K., Kalyani Vijayan. "Friction and Wear of PTFE—A Review." *Wear,* 158.1 (1992): 193-211.

Chen, Jinhua, et al. "Preparation of Sulfonated Crosslinked Ptfe-Graft-Poly(Alkyl Vinyl Ether) Membranes for Polymer Electrolyte Membrane Fuel Cells by Radiation Processing." *Journal of Membrane Science,* 256.1-2 (2005): 38-45.

Masetti, G., et al. "Conformational Order and Disorder in Poly (Tetrafluoroethylene) from the Infrared Spectrum." *Macromolecules,* 6.5 (1973): 700-07.

Oshima, Akihiro, et al. "Chemical Structure and Physical Properties of Radiation-Induced Crosslinking of Polytetrafluoroethylene." *Radiation Physics and Chemistry,* 62.1 (2001): 39-45.

Quarti, Claudio, Alberto Milani, Chiara Castiglioni. "Ab Initio Calculation of the Ir Spectrum of Ptfe: Helical Symmetry and Defects." *The Journal of Physical Chemistry B,* 117.2 (2013): 706-18.

Correlation of Polyethylene-based Precursor Properties on the Sulfonation for Stabilisation

Gisa Wortberg, Inga Noll

Institut für Textiltechnik, RWTH Aachen University, Aachen, Germany

inga.noll@ita.rwth-aachen.de

INTRODUCTION

Carbon fibers have excellent properties with a low density at the same time. Due to the complex manufacturing process, the production costs of polyacrylonitrile-based carbon fibers are at a high price of 15 to 25 €/kg. This is the reason why carbon fibers for mass application in the automotive or renewable energy industry are not widespread [1]. The production of the polyacrylonitrile (PAN) precursor is the main cost factor (50 - 65 %) [2]. These costs are due to the use of the complex solvent spinning process. The solvent, the solvent recovery and the raw material PAN are the main cost drivers [2]. Using new raw materials instead of PAN can be an option to reduce the costs. One of those materials is polyethylene. Advantages of polyethylene are the high availability of the material, the low material price (1 - 1.5 €/kg) and the good suitability as precursor [3].

STATEMENT OF PURPOSE

Polyethylene (PE) is processible in the economic melt spinning process. These precursors are prepared for the subsequent process step of carbonisation by using chemical stabilisation (sulfonation). The strategy is to adjust these precursor properties by the melt spinning process, thus resulting in a precursor, which can be stabilised sufficiently by sulfonation. The results of the sulfonation are brought in correlation with the precursor properties. The filament diameter and the polymer structure, e.g. the crystallinity, of the precursor have an influence on the sulfonation process.

APPROACH

For the melt spinning experiments a high density PE (HDPE) was used, provided by the company Saudi Basic Industries Corporation. The melt flow index (190 °C, 2.16 kg) is 20 g/10 min. The use of HDPE can be explained by the fact that carbon fibers based on HDPE achieved the highest tensile strength among carbon fibers based on other polyolefin precursors [4]. The idea is that the precursor properties have an impact on the sulfonation. Precursors with different single filament diameters and crystallinity were spun. The crystallinity and the single filament diameter were controlled by the spinning process. Filament diameter was determined by optical light microscopy, crystallinity was measured by wide angle x-ray diffraction (WAXD). The data of the spun precursor are listed in table I.

Table I: Properties of polyethylene precursors.

Sample	Filament diameter [µm]	Crystallinity [%]
No. 1	16.4	66
No. 2	19.1	59
No. 3	22.2	57
No. 4	32.8	35
No. 5	49.7	41

There is a major difference between the conversion of PAN-based precursors and PE-based precursors to carbon fibers. The stabilisation of PAN-based precursors is a thermal stabilisation. PE has to be stabilised in another way because of its relatively low melting point (130 - 135 °C). PE would stay inert and melt by using thermal stabilisation, whereas for PAN cyclisation takes place. For this reason an artificial interconnection of the molecules within the fibers is required [4]. A chemical stabilisation (sulfonation) is needed [5] which is the most common method for the stabilisation of polymers [6]. The long molecules are linked by the addition of sulfonic acid groups ($-SO_2OH$) and an SO_3-bridging effect during sulfonation process. The size of the sulfonic acid group is the reason for the torsion of the polymer chain around its carbon capture axis. Every fifth to seventh carbon atom is substituted with a sulfonic acid group, in the case of a completed sulfonation [7].

A high concentration sulfuric acid (96 %) as sulfonation material was used for the sulfonation experiments. The experiments were carry out in a double walled reaction vessel (capacity: 1 litre) heated up with a temperature control unit (Huber CC-K5 with Pilot ONE) by the company Huber Kältemaschinenbau GmbH, Offenburg, Germany. One part of the double walled reaction vessel are borosilicate glass with an inlet and outlet for thermo fluids. The reaction vessel is filled with sulfuric acid where the precursor samples are put in. The acid is heated up to 120 °C and hold at this temperature for 6 h (sampling point after each hour). Then the sulfonated samples are washed acid free and dried. To investigate the melting enthalpy of the stabilised samples the method of differential scanning calorimetry (DSC) is used.

RESULTS AND DISCUSSION

During the sulfonation of HDPE, an increase of the sulfonation time causes a colour change of the fibers from white to brown and black. The colour change however, is - analogue to the thermal stabilisation of PAN - no indication for a complete sulfonation. This is proven by the thermal analysis. Furthermore with increasing sulfonation time and temperature depending on the degree of crystallinity an increase of the filament diameter can be observed.

In figure 1 the specific change of state enthalpies of all samples from table I are plotted against the sampling points during the 6 h sulfonation.

In the diagram a significant decrease of the specific change of state enthalpy against the sulfonation time can be observed. The biggest difference of potential show sample no. 1. Whereby sample no. 5 shows the lowest change of melting enthalpy.
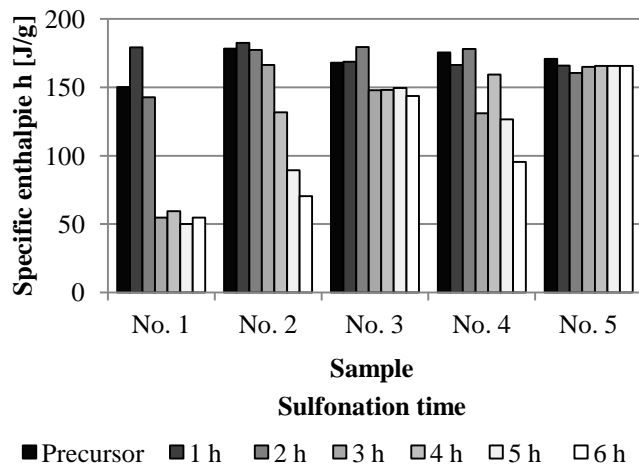
Figure 1: Change of melting enthalpy over sulfonation time.

Figure 1 shows that the sulfonation reaction is highly depending on the filament diameter and the degree of crystallinity of the precursor. Due to the fact that the sulfonation is a diffusion controlled process, smaller filament diameters lead to a faster sulfonation. This phenomenon can be observed in figure 1 from sample no. 1 to no. 3. Furthermore bigger filament diameters create a skin-core structure while sulfonation. Whereby the sulfonated skin of the fiber prevents the penetration of acid into the filament core. Sample no. 4 shows a domination of the influence by the degree of crystallinity on the sulfonation ability. Where sample no. 4 is a more amorphous material, what provides a better penetration of the sulfuric acid into the fiber core and leads to a faster sulfonation.

The comparison between the melting enthalpies and density measurements of sulfonated samples in figure 2 indicates that small filament diameter leads to faster and more efficient sulfonation reaction.
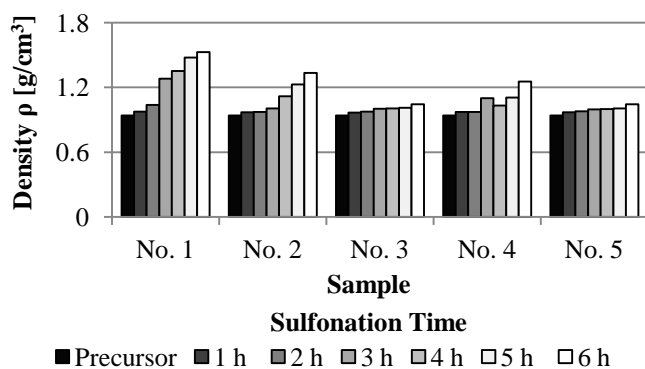
Figure 2: Results of density measurements of sulfonatee HDPE sample.

This is especially recognizable by sample no. 1. If the samples no. 3 to no. 5 are considered, it can be seen that the influence of the diameter decreases to the effectiveness of the sulfonation and the influence of crystal structure increases from sample no. 3 to sample no. 4. The reason

why sample no. 4 sulfonated better, what can be seen in faster increase of density, than sample no. 3 and no. 5 is that in sample no. 3 a skin-core structure is formed and only a portion of the fiber is sulfonated. Sample no. 5 shows, compared to no. 4, a much higher diameter and higher crystallinity, what leads to a lower increase of density due to a longer diffusion way in the fiber.

CONCLUSION AND FUTURE WORK

Sulfonation was conducted in a high concentrated sulfuric acid (96 %) at 120 °C up to 6 h. After thorough analysis by using different methods, like differential scanning calorimetry and pycnometry, the influence of fiber diameter and crystal structure on sulfonation reaction efficiency can be shown. This leads to the conclusion that filaments with small diameters sulfonate as well as amorphous fibers with larger filament diameters. Whether one of the parameters (diameter and crystallinity) has a lower or higher influence than the other, or if they are equal, has not yet been determined. It is also possible that the crystal size has an influence on the sulfonation of PE. The orientation of the polymer chains may also be important for the sulfonation process and on the final carbon fibers. These unsolved issues will be investigated in the next steps.

REFERENCES
[1] Leon, Y., Leon, C.A., Schimpf, S. "Low cost carbon fiber (LCCF) for automotive and aerospace applications Part I: Review of existing and emerging technologies." Midwest Advanced Materials and Processes Conference. Dearborn, Michigan, USA. 12-14 September 2000: 12-23.
[2] Wilms, C. "Cost-efficient production method for the manufacture of carbon fiber precursors." ("Kosteneffizientes Produktionsverfahren zur Herstellung von Carbonfaser-Precursoren.") PhD Thesis, Institut für Textiltechnik der Rheinisch-Westfälischen Technischen Hochschule, Aachen, 2013.
[3] Platts. *Polymerscan*. McGraw Hill Financial: New York, USA, Vol. 36 (25).
[4] Zhang, D. "Carbon Fibers from Oriented Polyethylene Precursors." *Journal of Thermoplastic Composite Materials*, 1993, 6: 38-48.
[5] Noeske, H., Roelen, O. "Process for the chloro-sulfonation of polyethylene." US Patent 2889259. 1959. Available online (accessed on 24 June 2015): http://www.freepatentsonline.com/2889259.pdf.
[6] Kaneko, M., Sato, H. "Sulfonation of Poly(propylene) Films with Fuming Sulfuric Acid." *Macromolecular Chemistry and Physics*, 2005, 206: 456-463.
[7] Younker, J., M., Saito T., Hunt, M.A., Naskar, A.K., Beste, A. "Pyrolysis Pathways of Sulfonated Polyethylene, an Alternative Carbon Fiber Precursor." *Journal of the American Chemical Society*, 2013: 6130-41.

Meltspun Polyamide 6-Graphite Fibres: Manufacturing and Analysis with Additional Comparison of Pre- and Inline Compounding

Karolina Jaksik[1], Robert Brüll[1], Philip Minnmann[2], Felix Schmidt[2], Gunnar Seide[1], Thomas Gries[1]

[1]Institut für Textiltechnik (ITA) der RWTH Aachen University, Aachen, Germany
[2]RWTH Aachen University, Aachen, Germany
karolina.jaksik@ita.rwth-aachen.de

INTRODUCTION

The past years have seen a steady increase of fibre composite materials used in the automotive and aviation industries. Due to the minimized weight and maximized mechanical properties, a higher efficiency is attained resulting in lower operating costs. Thermoplastic composites, so called organic sheets, have been used to great effect in various applications. They are produced by commingling thermoplastic fibres with reinforcement fibres to form a hybrid yarn which can be weaved into fabrics. By heating the fabric the thermoplastic fibres are melted to create the matrix around the reinforcement fibre. Because of the low heat conductivity of most thermoplastic materials, the melting process requires large amounts of energy and time and is therefore expensive. By increasing the heat conductivity within the thermoplastic fibres, higher efficiency can be achieved, reducing production costs. Past experiments have shown that embedding particles with high heat conductivity, such as graphite or carbon nanotubes, are an appropriate method of increasing the heat conductivity of fibres. A test of the industrial application of melt-spinning thermoplastic fibres with embedded graphite was done at the Institute for Textile Technology, Aachen. The focuses of the investigation were the mechanical and thermal properties, with cost and economic feasibility also bearing importance.

APPROACH

Compounds of different graphite concentrations were created using graphite (*TIMREX synthetic Graphite,* Timcal Deutschland GmbH) and PA6 (*Ultramid B24 N03,* BASF SE, Ludwigshafen, Germany). A range of mixtures with 3, 5, 7, and 10 wt% graphite was created using the *Lab-Compounder KETSE 20/40* of Brabender GmbH & Co. KG, Duisburg, Germany for compounding. The string was then granulated again using a *Granulator S* of Brabender GmbH & Co. KG, Duisburg, Germany. A multifilament was then spun on a *Pilot high temperature bi component melt spinning plant* of Fourné Polymertechnik GmbH. A microscope of the type *DM400M* of Leica Mikrosysteme GmbH, Wetzlar, Germany was used to get a qualitative measure of the particle distribution as well as a quantitative measure of the diameter of the filaments. The mechanical properties were measured carrying out tensile strength tests on a *Zwick Z2.5* machine of Zwick GmbH & Co. KG, Ulm, Germany. A gravimetric examination to determine the relative concentration of graphite after the spinning was also done using the *STAR TGA/DSC 1 SF 1100* machine of Mettler-Toledo GmbH, Gießen, Germany.

RESULTS AND DISCUSSION

The increase in graphite concentration resulted in a linear increase (slope 0.0117) in the thermal conductivity of the fibre, as shown in the diagram below, Fig. 1.
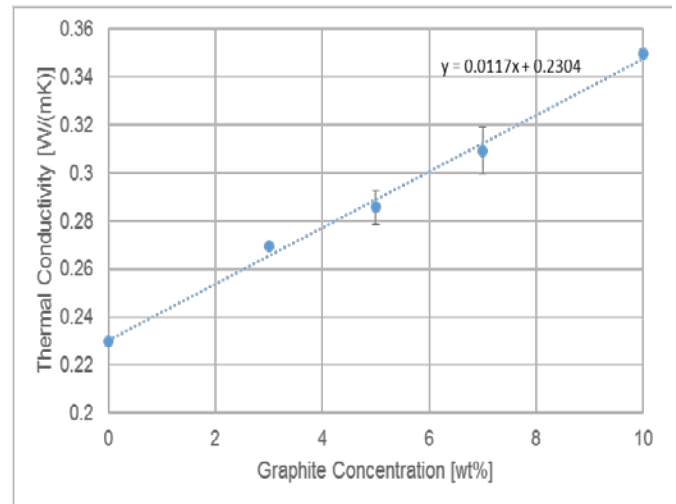

Fig. 1: Thermal conductivity at different concentrations, (Minnmann 2015).

However, with the increase in concentration of graphite the mechanical properties were reduced to a certain extent. While a fibre with a concentration of 3 wt% could withstand an elongation of ~250 %, fibre breakage occurred for 7 wt% at ~150 %. The elongation at break also showed a major decrease as the concentration increased. In particular, a concentration of 10 wt% graphite meant it was no longer suitable for further processing as a fibre., rendering higher concentrations ineffective in increasing efficiency.
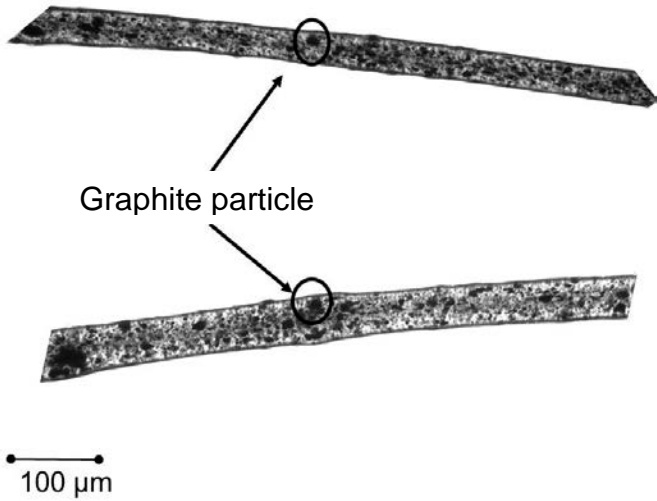
Fig. 2: Comparison of fibres with a nominal concentration of 3 wt% under a light microscope. Top: Pre compounded, bottom: inline compounded, (Minnmann 2015).

A difference was made between pre and inline compounding. Pre compounding means the master batch was mixed with the PA6 to the appropriate concentration on a twin screw extruder and processed into pellets, before being melt spun into a fibre. Inline compounding mixes the master batch with the PA6 during the melt spinning process with the master batch being mixed in the extruder attached to the spinning machine. The use of inline and pre compounding made a significant difference in the distribution of the particles and therefore the conductivity. Fibres that used inline compounding tended to have a lower concentration than anticipated, while the pre compounded fibres showed higher concentrations. The distribution in the pre compounded fibres was also better.

As seen in Fig. 2, despite using the same light intensity for both pictures the pre compounded fibre is much darker due to a higher concentration and better distribution of the particles. This was also shown in the gravimetric measurements where the actual values for the concentration differed up to 27.80 % for a concentration of 3 wt% compounded inline from the nominal value, as seen in Tab. I. For both fibres comparatively large agglomerates can be found, which become more frequent with higher concentrations. The homogeneity of the fibres therefore decreases with higher concentrations as the graphite agglomerates.

While it was possible to melt spin the fibres using a pre-industrial melt spinning plant, the filters did clog much quicker with higher graphite concentrations. This made it impossible to spin for longer than 60 minutes even at 3 wt%, with the machine being completely blocked at 10 wt% before reaching a stationary state.

CONCLUSION

The use of polyamide 6 with embedded graphite particles has proven to be possible on industrial melt spinning plants. Concentrations of 3 and 5 wt% graphite were particularly effective, reaching an increase in thermal conductivity of 30 % with 5 wt% graphite. As the concentration of graphite increases, the thermal conductivity also increases proportionally. The mechanical properties were slightly reduced with the compound being rendered unsuitable for processing above a concentration of 10 wt% graphite. There is still potential to improve the spinning parameters to increase the spinning duration above 1 hour. Possibilities to increase homogeneity and thermal conductivity include increasing the number of compounding steps or increasing crystallinity within the thermoplastic. In the future, dispersing additives in the master batch could be a solution to being able to spin higher concentrations of graphite without as much loss of mechanical properties and processability. Using graphite as a filler for fibres used in organic sheets is therefore an effective way of reducing the cost of production by increasing its efficiency of the melting process.

KEYWORDS

Polyamide 6, graphite, melt spinning, inline-compounding.

REFERENCES

Minnmann, P. *Herstellung und Untersuchung schmelzgesponnener Polyamid 6—Graphit Filamente mit Vergleich von Vor- und Inline-Compoundieren.* B. Sc. Thesis, RWTH Aachen University, 2015.

Spool	Nominal [wt%]	Actual 1 [wt%]	Actual 2 [wt%]	Actual 3 [wt%]	Ø [wt%]	Variance [wt%]	Deviation [%]
3 Pre	3	3,39	3,53	4,22	3,71	0,44	23,78
3 Inline	3	3,03	1,33	3,83	2,74	1,29	8,67

Table. I: TGA results for various fibres at a concentration of 3 wt% (Minnmann 2015).

Effect of Concentration on Hydrophobicity of Polydimethylsiloxane Fiber Mat by Electrospinning

Seon Ah Jeong, Tae Jin Kang

Department of Materials Science and Engineering, Seoul National University, Seoul, Republic of Korea

taekang@snu.ac.kr

INTRODUCTION

Among the various soft matrices, polydimethylsiloxane (PDMS) is an inert, non-toxic, highly flexible, mechanically stable, and inexpensive hydrophobic polymer. During the past decade, there have been several reports on the fabrication of the superhydrophobic PDMS surfaces. Carbon nanotube (CNT)/PDMS composites were fabricated for superhydropho bic coatings [1]. Superhydrophobic surfaces were prepared by casting PDMS on a textured templates by Stanton et al.[2]. Ke et al. [3] prepared a PDMS-based superhydrophobic surface by self-assembly of the modified-SiO_2 micro-particles on the PDMS. However, the complicated steps, special apparatus for preparation or expensive costs of the process may still face some challenges for commercial applications.

Superhydrophobic surfaces can be produced in many ways: layer-by-layer deposition, template synthesis, phase separatio n, crystallization control, spraying, and electrospinning, et al. Recently, the electrospinning technique has been widely utilized to fabricate superhydrophobic surface with electrospun fibers since the small fiber diameters contribute to superhydrophobicity by the resultant uniquely formed surface roughness or texture.

In this study, the PDMS prepolymer solution with TEOS crosslinker were prepared by sol-gel process and used as spinning solution for electrospinning process. To investigate the effect of the concentrations of the polymer solution on the hydrophobicity of the electrospun PDMS fiber mat, the solutions with the four different concentrations, 25, 15, 5, 0.5 wt%, were prepared. The morphological and water repellent properties of the electrospun fiber mat were examined.

EXPERIMENTAL

Preparation of PDMS Prepolymer Solution

A PDMS prepolymer solution was prepared by sol-gel precess. PDMS (Mn=50,000, Aldrich®.) was dissolved in 30 mL of tetrahydrofuran(Samchum) solvent and 5mL of TEOS crosslinker (Junsei Co.), 200 µL of nitric acid (60%, Samchun) were added. Nitric acid was used as the catalyst for the hydrolysis of TEOS. The polymer solution with the different concentrations (25, 15, 5, 0.5 wt%) were prepared to investigate the effect on the electrospun fiber's morphology and its water-repellent properties. The mixed solution was magnetically stirred for 1 hour and aged at the temperature 353 K. During aging process, the crosslinking reaction between PDMS and TEOS was induced, resulting in a viscous transparent PDMS sol for the electrospinning process and evaporation of the THF solvent.

Electrospinning Process

As-prepared PDMS prepolymer solutions were used for the eletrospinning process shown in Fig.1. The flow rates of sol was 15 mL/h and the applied voltage was in the range of 10 kV to 11 kV. The electrospun fibers were collected on a aluminium foil placed 15 cm from the syringe tip.
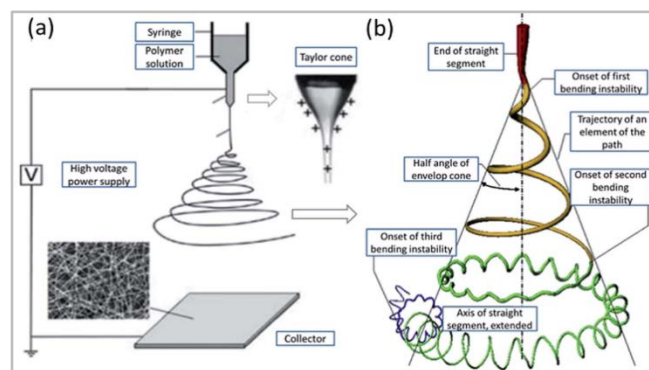

Fig. 1: (a) Schematic illustration of a typical basic electrospinning setup. (b) A diagram that shows the prototypical insta ntaneous position of the path of an electrospinning jet that contained three successive electrical bending instabilities.[4]

Characterization

The fiber morphologies of the electrospun PDMS mat were examined by Scanning Electron Microscopy (SEM) (JSM-7600F, JEOL). The fiber diameters and bead sizes were determined by analyzing the SEM images using a custom code image analysis program. The CAs of water droplets on the samples were measured using a contact angle meter (Attension, KSV Instruments). After dropping the 3.6±0.2 µL of water droplets onto the samples, the average contact angle was obtained by measuring at four different positions of the sample.
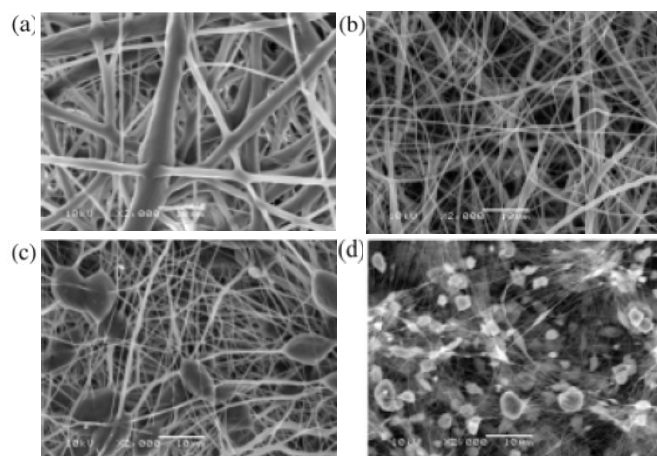
RESULTS AND DISCUSSION

Fig. 2: SEM micrograph of the electrospun PDMS fibers at a concentrations of (a) 25 wt%, (b) 15 wt%, (c) 5 wt%, and (d) 0.5 wt% of the polymer.

Figure 2 shows the SEM images of the electrospun PDMS fibers with the different concentrations of polymer solutions. It was observed that with the change in the concentration of the polymer solution, the electrospun fiber mat showed the different fiber morphology and diameter. As the concentration of the PDMS solutions decreased, the fiber diameter decreased and beads strung along the fiber were formed. The differences in the surface structures is due to the influence of viscosity of the polymer solution. The electrospun fibers of the dilute solution tend to form beaded structures due to the high surface tension and the low viscosity and electrical conductivity of the solution.

Table I: The fiber diameters and bead sizes of electrospun PDMS fibers.

Concentration (wt%)	Fiber Diameter (nm)	Bead Size (nm)
25	2200	No bead
15	580	No bead
5	590	7350
0.5	110	2650

Table I indicates the fiber diameters and the bead sizes of electrospun PDMS fibers at the different concentrations. The concentrated solutions (25 wt%) generated the very thick fibers with a broad size distribution of a diameter was obtained with the average fiber diameter of 2200 nm. When the solution concentration decreased, at a 15 wt%, the fiber diameters decreased and the uniform fibers were obtained with the average fiber diameter of 580 nm. At the lower concentration of 5 wt%, it can be found that the comparative large bead structures were generated. In further dilution of the polymer solution (0.5 wt%), the bead size decreases and the bead density increases with decreasing the fiber diameters about 110 nm.
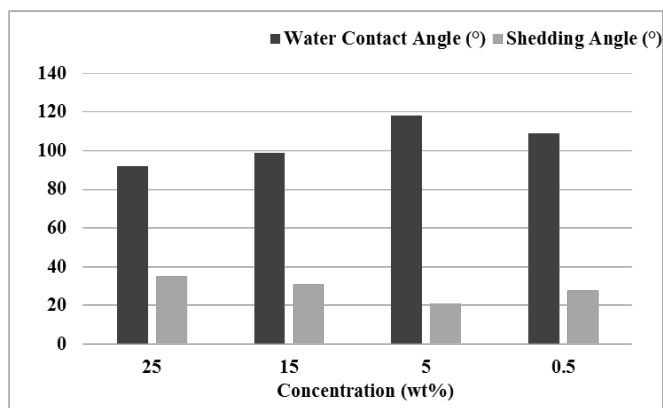
Fig. 3: The water contact angles and sliding angles of the electrospun PDMS fiber mat at a concentrations of 25 wt%, 15 wt%, 5 wt%, and 0.5 wt%, respectively.

The electrospun PDMS fiber mat were compared for their hydrophobicities by their water contact angels and shedding angles (Fig. 3). All of the electrospun fiber mat have the contact angles higher than 90°. Because the PDMS is a very hydrophobic material, the eletrospun fiber mat showed the hydrophobic properties as well without any further treatment. It is well known that the water-repellent property is governed by the surface energy and the surface roughness. Because the surface energies of the electrospun PDMS fiber mat in all of the concentrations were same, the surface morphology would affect the hydrophobicity of the surface. According to Figure 3, with the decrease of the concentrations from 25wt% to 5 wt%, the contact angle values increased and the shedding angles decrease. Especially, in 5wt%, there were a large increase of the CA. Based on the previous study[5], it is due to the presence of the bead structures. This is, the micro-sized bead structure enhanced the hierarchical morphology and contribute to the increase of the hydrophobicity of the electrospun mat. However, in the lower concentration of 0.5 wt%, the CA slightly decreased and the SA too. To increase the hydrophocity, the nano-sized fiber diameter and micro-sized bead structures has proven to be effective.
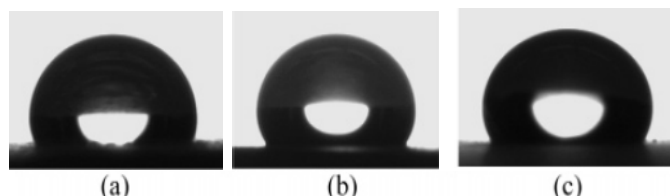

Fig. 4: Captured images of the water droplets placed on each electrospun PDMS nanofibers at a concentrations of (a) 25 wt%, (b) 5 wt%, and (c) 0.5 wt%. The contact angles are 92°, 118°, and 109°, respectively.

CONCLUSION

It has been shown that the electrospinning of the PDMS without any treatment can produce the hydrophobic fiber mat. Also, it has been proven that the morphology can be well controlled by changing the PDMS concentrations in spinning dope. As the surface morphology is a very important factor in the hydrophobicity of the surface of the mat, changing the PDMS concentrations can control the hydrophobicity of the fiber mat. To achieve the superhydrophobicity of the electrospun PDMS fiber mat, further treatment such as co-axial electrospinning and plasma treatment can be applied to enhance the hydrophobicity of the fiber mat.

REFERENCES
1. Z. Yuan, J. Bin, X. Wang, M. Wang, J. Huang, C. Peng, et al.. "Preparation of a polydimethylsiloxane (PDMS) /CaCO$_3$-based superhydrophobic coating." *Surf. Coat. Technol*., 2014, 254: 97-103.
2. M.M. Stanton, R.E. Ducker, J.C. MacDonald, C.R. Lambert, et al. "Super-hydrophobic, highly adhesive, polydimethylsiloxane (PDMS) surfaces." *J. Colloid Interface Sci,.* 2012, 367(1): 502-08.
3. Q. Ke, W. Fu, H. Jin, L. Zhang, et al. "Fabrication of mechanically robust superhydrophobic surfaces based on silica micro-nanoparticles and polydimethylsiloxane." *Surf. Coat. Technol,* 2011, 205(21-22): 4910-14.
4. D.H. Reneker, A.L. Yarin. "Electrospinning jets and polymer nanofibers." *Polymer*, 2008, 49(10): 2387-2425.
5. J. Zheng, A. He, J. Li, J. Xu, C.C. Han. "Studies on the controlled morphology and wettability of polystyrene surfaces by electrospinning or electrospraying." *Polymer*, 2006, 47(20): 7095-7102.

Carbon Yarn/Yarn and Fiber/Fiber Friction

Michel Tourlonias[1], Marie-Ange Bueno[1], Dominique Poquillon[2]

[1]LPMT, ENSISA, Mulhouse, France
[2]CIRIMAT, Université de Toulouse, Toulouse, France
michel.tourlonias@uha.fr

KEYWORDS: Carbon fiber, Friction, Yarn

INTRODUCTION
Carbon fiber reinforced composites (CFRC) are wildly been used in aeronautical industry. These carbon reinforcements are often weaved materials. During the process damaged occurred on carbon fibers that are due to friction phenomena and particularly fiber-to-fiber friction [1].

These friction phenomena occurred at different location during the weaving process during which the yarn geometrical configuration is specific. After a previous study about the friction between warp yarns [2], the present study is focused on two complementary aspects: on the one hand the friction between perpendicular yarns for reproducing the motion between warp and weft yarn during weaving process and, on the other hand, on the friction between two single fibers.

APPROACH

X_{max} = 1.76 mm
Rotation magnitude = 20°
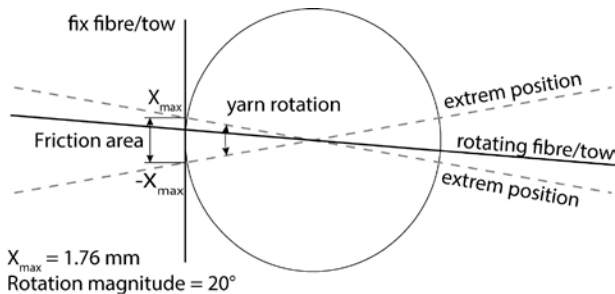
Figure 1: Schematic of friction experiment.

Material
For this study 3 types of carbon yarns are investigated. They are manufactured by Toho Tenax Europe GmbH with a count of about 800 tex. There have 12000 filaments or 24000 filaments of carbon per yarn section according to the fibre diameter (from 4.9 μm to 7 μm). The difference between these carbon fibres comes from the Young Modulus (from 240 GPa to 390 GPa).

Experimental device and measurements
Friction measurements are performed by means of a NTR2 nanotribometer (CSM Instrument Company, Peseux, Switzerland). This device is originally a pin-on-disk tribometer with reciprocating movement allowed. Specific sample carriers have been developed in order to position, maintain or move the carbon yarns or the carbon fiber.

According to the small friction angle as described on Figure 1, the motion between the two friction samples can be considered as perpendicular (the magnitude of the friction displacement is 3.4 mm for a lateral displacement of 0.15 mm). Measurements are realized at a constant distance between the sample carriers.
The experimental device allows to acquire friction and normal forces during each test which is composed of many rotation cycles. The coefficient of friction (COF) can then be computed as illustrated on Figure 2.

In order to understand the effect of different parameters, the same friction tests are realized (for a given carbon yarn or carbon fibre) in different experimental conditions (friction speed, normal load).

RESULTS AND DISCUSSION
In Figure 2, the typical average COF curve is plotted versus angular position. These curves represent the yarn-to-yarn and fibre-to-fibre friction. The shapes are close by considering fibre or yarn friction and are symmetrical between the two friction directions of the cycle. The evolution during a friction test of the COF is also studied.

It is interesting to note that the COF between yarns is higher than between the one measured between singles fibres. This phenomenon is probably due to the fibrous rearrangement during yarn-to-yarn friction test.
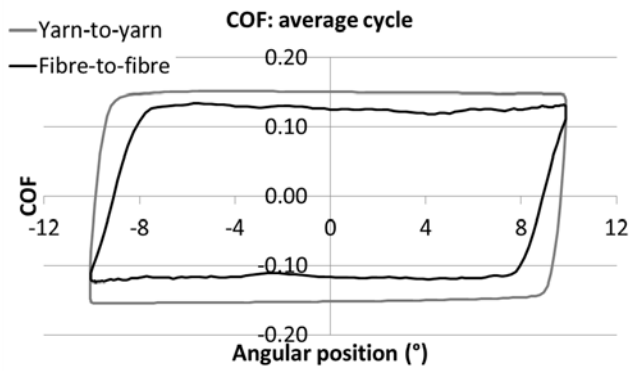
Figure 2: Average friction cycle in term of coefficient of friction for yarns and fibers.

Results show experimental conditions such as friction speed or normal load have only small influence on the friction properties. The significant roles of the Young Modulus of fibers and the sizing treatment have been highlighted.

REFERENCES
[1]   Archer, E., Buchanan, S., McLlhagger, A.T., Quinn, J.P. "The effect of 3D weaving and consolidation on carbon fiber tows, fabrics, and composites." *J Reinf Plast Compos.*, 2010, 29(20): 3162-70.
[2]   Tourlonias, M., Bueno, M-A. "Experimental simulation of friction and wear of carbon yarns during the weaving process." *Composites Part A: Applied Science and Manufacturing*, 2016, 80: 228-36.

Multicomponent Filaments Process for Use as Sensors

B. Glauß, B. Mohr, G. Seide, T. Gries

Institut für Textiltechnik der RWTH Aachen University, Otto-Blumenthal-Str. 1, Aachen, Germany
benjamin.glauss@ita.rwth-aachen.de

BACKGROUND

Aim of this research is to manufacture bicomponent filaments in a meltspinning process. A core-sheath geomatry is used. These fibres are, depending on further processing, suitable as sensor filaments. Based on the piezoelectric effect, they can sense movement and force and return an electrical, measurable signal. On the one hand, electrical conductivity in the core must be given. On the other hand, a certain polymer structure in the sheath material polyvinylidene fluoride (PVDF) must be created by drawing and subsequent poling in electrical fields. Poling and functionalisation of the sheath is described in detail in [1,2]. The focus of this work is the development of an electrically conductive core material for longterm extrusion.

AIM AND METHOD

State of the art for filament based sensors containing PVDF as an electrically functional material are mainly given by research carried out at ITA at Aachen University, the Swedish Universities Boras and Chalmers in Gothenburg in cooperation with SWEREA IVF in Mölndal as well as a group at University of Minho in Portugal. The ground-breaking fundaments were developed by Stephan Walter in his Ph.D. thesis at ITA [2]. There, he describes first the extrusion of bicomponent sensor fibres in a meltspinning process with subsequent contact poling in electrical fields. Further experiments showed the influence of spinning parameters on the PVDF structure [3.] The geometry used is given in Fig. 1. The function as a piezoelectric sensor could be shown; an electrical signal due to mechanical force was measured.

International state of the art is mainly given by the research of Anja Lund and Erik Nilsson. Lund explains the manufacture of sensor filaments in [3,4] including the formation of structures in PVDF, necessary for the piezoelectric effect. The material used for the core was polyethylene with 10 wt% of Carbon Black (CB). Precise information about core material conductivity was not given, however a conductivity of around 1 S/m can be deduced from graphs. The fibres application is shown in [6], where they are integrated into a glove for sensing motions of fingers. Further work is performed by the group around Rui S. Martins. A multicomponent monofilament is extruded with three layers. Inner and outer layer are based on a conductive polymer, in between these two layers there is the functional PVDF layer. By using a special spin pack and dye geometry, the same material can be used for the core and the outer layer, so that in general, two components are extruded into three layers.

The current deficit is the stability of the process, where only [1] and [3] give references of limited extrusion time. No extrusion can be held stable for more than 30 minutes. A rising pressure in the spin pack caused by the core component limits the extrusion time.
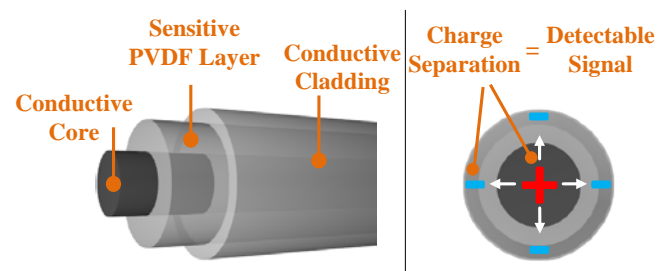

Figure 1: Geometry of sensor filament.

MAIN RESULTS

The material preparation for melt spinning is mainly focussed on the compounding of polypropylene (PP) with different content of CB as well as the dispersing agent BYK P4102 by BYK Additives & Instruments, Wesel, Germany. The materials are compounded in a twin-screw extruder by KEDSE 20/40 by Brabender, Duisburg, Germany. All three virgin materials are dry blended, compounded and granulated. Different specimens with CB content between five and ten wt% are the result. Aim of the different contents is to see the influence of different filler mass fraction on the process stability. Filter tests are carried out on the mono component filter tester A800 by Fourné Polymertechnik, Alfter-Impekoven, Germany. Results for pressure increase are shown in Fig. 2. Data show that using no dispersing agent already leads to a dramatic increase of spin pack pressure with 5 wt% CB only. For 6 wt%, experiments have to be terminated. With increasing use of dispersing agent, spin pack pressure develops less aggressive. Specimen G3 can be tested completely up to 10 wt% CB. G4 is stable concerning pressure increase. The constellation G4 of materials hence is best suitable within the experiments for the use as a core material in a

bicomponent spinning. Experiments with material Combination G5 lead to a steep pressure increase for higher concentrations of CB. Furthermore, experiments underlie large pressure fluctuations. As a consequence, it can be stated, that the positive effect of dispersing agent is limited. Process stability and pressure development suffer from too much dispersing agent. A possible explanation is that the different materials separate in molten state. After all, the amount of 3 wt% BYK P4102 shows a positive effect concerning process stability. The material G4 is used for further spinning experiments on the pilot scale machine by Fourné Polymertechnik.
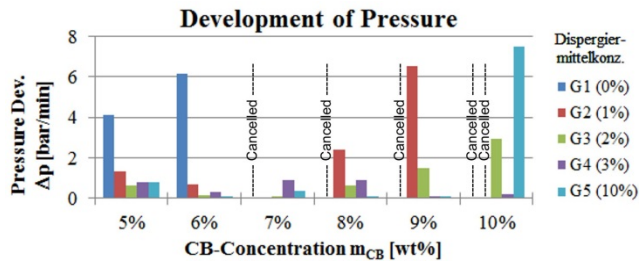
Figure 2: Development of spin pack pressure over the use of different mass content of Dispersing agent and carbon black content.

Subsequent bicomponent spinning trials confirm the results of filter testing. Bicomponent filaments are spun with the material combination PVDF Solef 1008 from Solvay-Solexis in the sheath and the material G4 as a core electrode. Spin pack pressure was constant over several hours and machine operation could be continued after cooling down and heating up again. Extrusion is carried out at 240 °C with a bicomponent-monofilament spinneret. Filaments could be drawn up to a draw ratio of 3.4, yielding 98% piezoelectric PVDF β-Phase and a conductivity of 0.17 S/m. According to [1,2,3], such fibres can be used after further functionalisation as sensor fibres.

CONCLUSION
This work shows the possibility to meltspin a bicomponent filament with conductive PP, CB and dispersing agent core and PVDF sheath. This kind of filament with according properties can, as shown in previous work, be used as a filament-based sensor. The use of a dispersing agent made it possible to continue extrusion over several hours.

FUTURE WORK
Future work includes the integration of such filaments into woven bands in order to form a textile which can subsequently be used as a force and movement sensor in textile applications. Furthermore, the continuous functionalization including poling in electric fields for endless filaments is yet unsolved.

KEYWORDS
Sensor filament, PVDF, Bicomponent filament

REFERENCES
[1] Glauss, B., et al.. "Poling Effects in Melt-Spun PVDF Bicomponent Fibres." *Key Engineering Materials*, Volume 644 (2014): 110-14.
[2] Walter, S.E.G. "Entwicklung Piezoelektrisch Wirksamer Sensorfasern auf Basis von Polyvinylidenfluorid."Aachen, RWTH Aachen, Diss., Zugl. Aachen: Shaker-Verlag, 2012.
[3] Glauss, B., et al. "Spinnability and Characteristics of Polyvinylidene Fluoride (PVDF)-based Bicomponent Fibers with a Carbon Nanotube (CNT) Modified Polypropylene Core for Piezoelectric Applications." *Materials*, 6 (2013): 2642-61.
[4] Lund, A., Hagström, B. "Melt Spinning of Poly(vinylidene fluoride) Fibers and the Influence of Spinning Parameters on β Phase Crystallinity." *Journal of Applied Polymer Science*, 116 (2010): 2685-93.
[5] Lund, A., Hagström, B. "Melt Spinning of β Phase Poly(vinylidene fluoride) Yarns With and Without a Conductive Core." *Journal of Applied Polymer Science*, 120 (2011): 1080-89.
[6] Akerfelds, M., et al. "Textile sensing glove with piezoelectric PVDF fibers and printed electrodes of PEDOT, PSS." *Textile Research Journal* (2015).
[7] Martins, R.S., et al. "Piezoelectric Coaxial Filaments Produced by Coextrusion of Poly(vinylidene fluoride) and Electrically Conductive Inner and Outer Layers." *Journal of Applied Polymer Science*, 131 (2014):131-48.

Numerical Analysis and Comparison of Airflow in Rotors with U and V Groove During Rotor Spinning Process

Ruihua Yang, Chao Liu, Yuan Xue, Weidong Gao

Key Laboratory of Science & Technology for Eco-Textiles, Education Ministry, Jiangnan University

Wuxi, Jiangsu, China

yangrh@jiangnan.edu.cn

INTRODUCTION

Rotor spun yarn is one of the most welcomed coarse yarns in textile market[1-3]. The key parts of rotor spinning consist of the rotor, feeding-combing mechanism, navel, torque up and yarn delivery system. All parts are composed into a box, called the 'spin box'. During rotor spun yarn spinning process silver were fed into feeding plate, and then fibers are gathered on the collection groove of the rotating rotor, inserting twist into the fibers. The yarn produced is then taken up onto a cross wound package, as illustrated by Fig 1, eliminating the need for a separate winding process, as in ring spinning. Rotors with different types of grooves are the most crucial devices deciding fiber type could be used and yarn thickness could be produced. U and V are most widely used and showing good adaptability both for fibers and yarn, as shown by Fig 2. In this paper, the statical pressure and air flow speed of rotors (Diameter 46 mm) with U and V grooves will be simulated and analyzed.
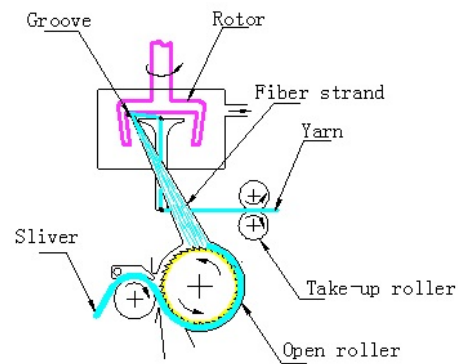
Fig. 1: Rotor spun yarn spinning process.
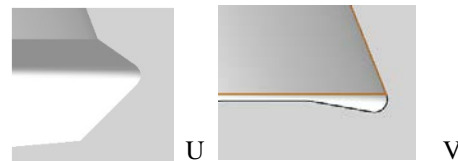
Fig. 2: Geometric sketch of collection grooves.

METHODS

Simple algorithm is used to solve the pressure and velocity coupled. Standard k-ε turbulent model is applied as the method of turbulent numerical simulation. As the development of turbulences is not sufficient, wall function method is used here. No slip boundary conditions are used in the wall. Geometric model of spin box was shown by Fig 3.
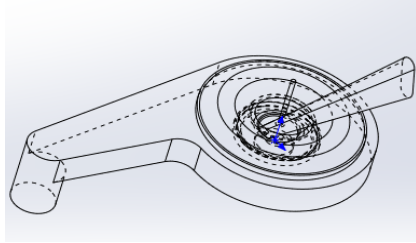
Fig. 3: Geometric model of spin box.
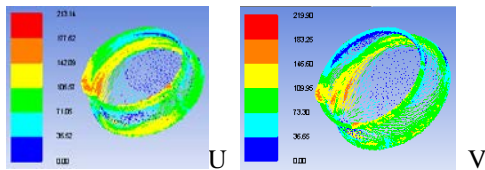
RESULTS AND DISCUSSION

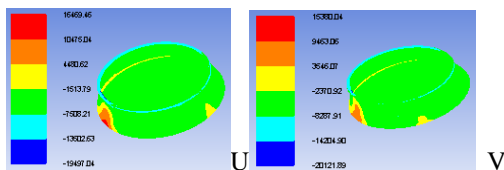Fig. 4: Airflow speed of rotor (U-type and V-type).

Fig. 5: Static pressure distribution of rotor (U-type and V-type).

Airflow speed and pressure of rotor and groove are illustrated by Fig 4-5. They demonstrates that airflow speed of rotor and groove of U-type is slower than that of V-type, 106-142m/s and 109-146 m/s separately, as a result, the static pressures of rotor and groove of U type are lower than that of V-type, -8287Pa and -7508Pa, separately. It can also been seen that airflow speed and static pressure is not steady in rotor or groove wall.

CONCLUSION

Airflow characteristics in rotors with U and V groove during rotor spinning process were simulated and analyzed. The highest airflow speed of V groove and U are 134.9 m/s and 113.6 m/s separately. While the lowest are 21.7 m/s and 35.7 m/s separately. The valley point of static pressure of V groove and U are -4431Pa and -4834.7 Pa separately. The results showed that airflow speeds of V groove at different angle are higher than that of U type, and as a result, the static pressures are lower than that of U. The trends of airflow speed and static pressure of different type of groove fits the experimental results that rotor yarn produced by V type rotor showed a better yarn evenness, higher breaking strength and evener twist than U type rotor.

ACKNOWLEDGMENT

REFERENCES

[1] Hasani, H., Semnani, D., Tabatabaei, S. "Determining the optimum spinning conditions to produce the rotor yarns from cotton wastes." *Ind Textila*, 2010, 61 (6): 259-64

[2] Huh, Y., Kim, Y.R., Oxenham, W. "Analyzing structural and physical properties of ring, rotor, and friction spun yarns." *Tex Res J*, 2002, 72 (2): 156-63.

[3] Chattopadhyay, R., Banerjee, S. "The frictional behaviour of ring-, rotor-, and friction-spun yarn." *J Text Inst*, 1996, 87 (1): 59-67.

Effect of the Proportion of Meta-aramid Fibers on Flammability of Meta-aramid/Wool-blended Yarn and Fabric

Tao Hua, Po Yee Ko, Yu Kun Zhu

Institute of Textiles and Clothing, The Hong Kong Polytechnic University, Hong Kong

tcthua@polyu.edu.hk

OBJECTIVE

This study aims to develop meta-aramid/wool blended yarns and fabrics through investigating the effect of the proportion of meta-aramid fibers on the blended yarn and fabric flammability. Five yarn and the resultant fabric samples with five proportions of meta-aramid fibers were produced by using worsted spinning system for yarn and flat knitting machine for knitted fabric, respectively. The flammability and other properties of the yarns and fabrics were evaluated. This study is expected to provide guide to the development of meta-aramid blended flame-resistance products.

INTRODUCTION

Burn injury is listed as one of the most devastating injuries and the fourth most common type of trauma in the world while over 40% fires are caused by textiles [1-2]. Prevailing fabrics for common professional garment and home furnishing fabrics are made of pure cotton, wool, man-made fibers or their blends that cannot provide sufficient protection to the growing environment hazards of heat injure. On the other hand, meta-aramid fiber is a high performance fiber featured with inherently flame resistance [3]. Besides, meta-aramid fiber has high thermal stability and insulation, non-melt drop characteristic, good anti-radiation performance, good moisture absorption and soft handle. However, its application is limited in areas requiring unusually high thermal and flame resistance such as firefighter clothing and high temperature filtration due to low yarn spinnability and relative high fiber cost. In the past, flame-resistance fiber blended fabrics have been developed and their properties were studied [4-7]. But there are very few cost-effective textiles made of meta-aramid fibers blending with other fibers for common functional garment and home furnishing fabrics such as workwear and bedding that only require low to medium level of flame resistance. Therefore, there is a high need for extending the application of meta-aramid fibers to be on furnishing and garment.

In this study, we tried to develop meta-aramid/wool blended yarns and fabrics via spinning and knitting trials. As the flammability of the aramid blended yarns and fabrics mainly depends on the proportion of meta-aramid fibers within the yarns and fabrics, the spinning trials were conducted to study the influence of aramid fiber proportion on the yarn properties. Furthermore, knitting trials were conducted and fabric performance was evaluated.

APPROACH

In this study, five yarn samples with five proportions of meta-aramid fibers were produced by using worsted spinning system. The detailed specifications of aramid/wool blended yarns are listed in Table I. Before the ring spinning on Zinser 451 frame, meta-aramid fiber slivers and wool fiber slivers were blended for 3-5 passages by using gilling box in order to achieve the designed blending ratios and even blending effect.

Table I: Specifications of aramid/wool blended yarns.

Yarn sample	Metric yarn count (Nm)	Metric yarn twist factor	Fiber blending ratio (%)	
			aramid	wool
100A			100	0
70A/30W			70	30
50A/50W	40	80	50	50
30A/70W			30	70
100W			0	100

After the yarn spinning process, the five blended yarn samples were evaluated in terms of yarn flammability and other yarn properties to investigate the effect of the proportion of meta-aramid fibers on the blended yarn properties. The yarn residue length was measured by using a modified yarn flammability vertical test referred to ASTM D 1230 and D 6413.

Using the five blended yarns, five single jersey fabrics were knitted by using CMS822 Stoll computerized flatbed knitting machine. The fabric flammability was also measured based on ASTM D1230. The influence of the aramid fiber proportion on the fabric flame-resistance was analyzed.

RESULTS AND DISCUSSION

Fig. 1 and Fig. 2 show the effect of aramid fiber proportion on blended yarn flammability and tenacity. As shown in Fig. 1, the flame resistance of aramid/wool blended yarns increases with the increase of the proportion of aramid fibers in the yarns in terms of yarn residue length after testing due to the excellent inherently flame resistance of meta-aramid fibers compared to wool fibers. The 100% meta-aramid fiber yarn can almost keep its original yarn length while for 100% wool yarn, there is no residue yarn left after the testing. Form Fig. 2, it can be seen that the yarn tenacity decreases when the proportion of aramid fibers in the blended yarn decreases. The possible reason is that the meta-aramid fiber strength is higher than that of wool fiber

and thus the increase of the proportion of aramid fibers within the blended yarn will increase the yarn strength.
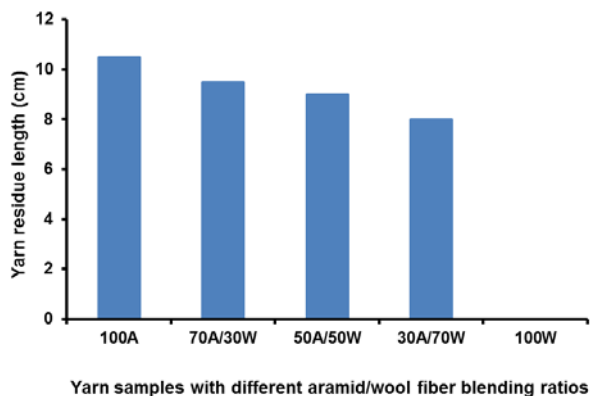

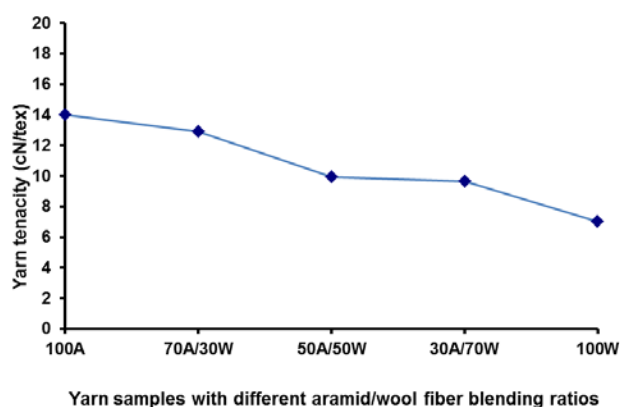Fig. 1: Effects of aramid proportion on yarn flammability.

Fig. 2: Effects of aramid fiber proportion on yarn tenacity.

After the fabric flammability testing, the appearance of five fabric samples by using aramid/wool blended yarns containing different ratios of aramid and wool fibers are presented in Fig. 3. As shown in Fig. 3, the flame resistance of wool fabric can be significant improved after blending with meta-aramid fibers. Among five fabric samples, the char area and damage level of the fabrics after testing decreases with the increase of the proportion of aramid fibers within the blended fabrics due to the higher flame resistance of meta-aramid fibers than that of wool fibers. The effect of the proportion of aramid fibers on the fabric flammability shows a similar trend to the effect on the blended yarn flammability.

| 100A | 70A/30W | 50A/50W | 30A/70W | 100W |
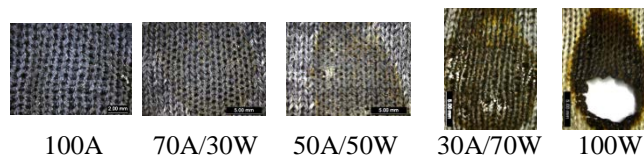
Fig. 3: Fabric appearance after flame-resistant testing.

CONCLUSION

In this study, meta-aramid/wool blended yarns and fabrics with different proportions of meta-aramid fibers were developed. The effect of proportion of meta-aramid fibers on the yarn and the resultant fabric flammability was investigated. The experimental results show that the flame resistance and tenacity of aramid/wool blended yarns increase with the increase of the proportion of aramid fibers in the yarns in terms of yarn residue length after testing due to the excellent inherently flame resistance and higher fiber strength of meta-aramid fibers compared to wool fibers. For the same reason, the char area and damage level of the fabrics decreases with the increase of the proportion of aramid fibers within the blended fabrics. The findings of this study will provide guide to the development of meta-aramid blended flame-resistance products.

REFERENCES

[1] FDA. Wound Healing Clinical Focus Group. "Guidance for Industry: Chronic Cutaneous Ulcer and Burn Wounds Developing Products for the Treatment." *Wound Repair Regen*, 2001, 9 (4): 258.
[2] Horrocks, A.R., Price, D. *Fire Retardant Materials*. Woodhead Publishing, Cambridge, England, 2001.
[3] Bourbigot, S., Flambard, X. "Heat resistance and flammability of high performance fibres: a review." *Fire and Materials,* 2002, 26: 155-68.
[4] Rengasamy, R.S., Kothari, V.K., Gotipamul, R.L. "Flame retardancy of Nomex/cotton ring-spun blended yarn fabrics." *Indian Journal of Fibre & Textile Research,* 2000, 25: 241-45.
[5] Gu, W. "Research on thermal properties of Nomex/Viscose FR fibre blended fabricz." *Materials and Design,* 2009, 30: 4324-27.
[6] Ndlovu, Lloyd N., Han, C.C., Yu, C.W. "Mechanical and FR properties of different ratios of cotton/polysulfonamide (PSA) core spun and blended yarns." *Journal of Engineered Fibers and Fabrics,* 2014, 9 (4): 24-31.
[7] Garvey, Samantha J., Anand, Suhhash C., Rowe, Trevor, Horrocks, A. Richard, Walker, David G. "The flammability of hybrid viscose blends." *Polymer Drgradatum and Stability,* 1996, 53: 413-16.

Lexicon for Sensory Evaluation of Tactile Textiles in Brazil

Rosimeiri Naomi Nagamatsu[1], Maria José Araújo Marques de Abreu[2], Cosmo Damião Santiago[1]
[1]Federal University Technology of Paraná, Apucarana, Paraná, Brasil
[2]Minho University, Azurém, Portugal
naomi@utfpr.edu.br; josi@det.uminho.pt; cosmo@utfpr.edu.br

INTRODUCTION

The space between clothing and the body is related to users comfort. Due to the priority to protect man from a particular hazard, the interaction between clothing and body comfort as well as structural properties of materials to be used in clothing manufacturing is often neglected. Indeed, comfort is one of the most important properties that influence the users decision when choosing a particular piece of clothing. [1].

Touch is one of the most used practice by the consumer to verify the comfort of the fabric. Thus, the touch is a tool to assess the quality of high sensitivity fabrics. [2] [3]

Investigations were carried out in France and Portugal in order to quantify the quality of touch textiles. The researchers used the sensory analysis method much exploited by the food industry and cosmetics and developed lexicons for tactile sensory evaluation in textiles. [3] [4]

The development of a lexicon for tactile sensory analysis is an important tool for tactile evaluation of products. For its development a selection of samples representing the product is performed and the development of protocols to be followed systematically by evaluators generate the terms and quantitative or qualitative validation. [5] Thus, this article presents the procedures used for the development of the Brazilian textile lexicon.

MATERIALS AND METHODS

Panelists

Fourteen assessors (five men and nine women) participated in these study. They were selected through triangular tests from ABNT NBR ISO 4120 [6]. In Brazil there are no sensory assessors in textiles, so it was necessary to select volunteers to form panelists.

Samples

20 samples of 57 collections of caps manufacturing industries in the Apucarana city were used. Each sample was cut into a dimension 20X20 centimeters and received a three digit numerical identification. They were fabric and knitted textures and different structures composed of natural and synthetic fibers such as linen, cotton, silk, viscose, polyester, polyamide, etc (Image 1)

Image 1: Fabric samples

Procedure

Procedures for the development of the Brazilian textile lexicon for tactile evaluation were adapted from ISO 11035 [7]. Sensory Assessors touched fabric samples arranged behind a cabin and an evaluation described the feelings to touch the samples. (Image 2)

Image 2: Assessment cabin

Assessors described the feelings at the first touch of the right side, then the reverse side and then lifted the sample holding the fabric with both hands. (Image 3)

Image 3: Samples touch

RESULTS AND DISCUSSION
299 terms were generated. After that evaluators were gathered to remove from the lexicon the irrelevant terms, leaving just 171 terms.

Again evaluators were gathered and grouped the terms of same meaning. The resulting terms were gathered in 21 representative groups shown in table 1

RELIEF	PLUSHY	FINE FABRIC
ROUGH	FRESH	THICK
HARSH	HOT	FLUIDUTY
CRUMPLED	RIGID	FIT
SMOOTH	ELASTICITY	SUAVE
HEAVY	SOFT	SLIPPERY
DRY	LIGHT	ICTCHES

Table 1: Initial lexicon

CONCLUSION
The lexicon in this study was made to assess the comfort of textile materials. The initial lexicon with twenty-one terms was generated by Brazilian panelists from textile samples collected in the city of Apucarana. This initial lexicon will still be validated by quantitative and qualitative methods.

After validation a panel of experts in textile sensory analysis will be used to quantify the tactile comfort of textile materials. Furthermore it can be used by other sensory panels.

KEYWORDS
Lexicon Textile. Sensory analysis. Hand feel.

REFERENCES
1. Abreu, M.J. *Contribuição para o Estudo da Parametrização dos Têxteis Hospitalares*. Guimarâes, 2004.
2. Kweon, S.-A.; Lee, E.-K.; Choi, J.-M. "A comparative study on the subjetctive fabric hand according to gender for winter sleepwear frabrics." *Fibers and Polymers*, 2004, Vol. 5, No. 1: 6-11.
3. Philippe, F., et al. "Tactile Feeling: Sensory analysis applied to textile goods." *Textile Research Journal*, 2004, Vol. 2004: 1066-72.
4. Nogueira, C.D.G.S. *Análise Sensorial de Produtos Têxteis*. Guimarães, 2011.
5. Lawlees, L.J.R., Civille, G.V. "Developing lexicons: a review." *Journal of Sensory Studies,* July 2013, Vol. 28: 270-81.
6. ABNT NBR ISO 4120, 2013. *Análise Sensorial-Metodologia-Teste Triangular*. Associa ABNT-Associaçao Brasileira de Normas Téchnicas. Rio de Janeiro, 2013.
7. ISO 11035. *Sensory Analysis-Idenification and Selection of Descriptors for Establishing a Seonsoru Profile by a Multidimensional Approach*. International Organization for Standardization. Genève, 1994.

.

Fabric Friction Sound Characterization in Dry and Wet State

F. Leclinche[1], K. Yosouf[1], E. Dréan[1], D. Adolphe[1], L. Schacher[1], V. Zimpfer[2]

[1]Laboratoire de Physique et Mécanique Textiles, Université de Haute-Alsace, France

[2]Institut franco-allemand de recherches de Saint Louis, France

floriane.leclinche@uha.fr

INTRODUCTION

The noise generated by fabric to fabric friction in the frame of military applications is essential to be studied in order to improve acoustic stealth. In this project, we used a set of fabrics and a system developed to simulate the human arm motion during walking or running. This system allows to record the friction sound generated and to extract acoustic imprints of fabrics. The set of fabrics is compared in two different conditions: dry state and wet state.

APPROACH

Nine fabrics with different weave pattern will be tested, 2 twills, 4 satins, 1 broken twill, 1 crepe and 1 plain. Each fabric sample is tested in dry and wet states. For the wet state a simple protocol is used. The sample is immersed in water during five minutes and then hung out during five minutes before testing. The fabrics were all conditioned during 24 hours in standard conditions (relative humidity HR%=65±5%, temperature T=20±2°C).

The mechanical properties of the fabrics are measured thanks to the Kawabata Evaluation System [1], especially the surface properties and the friction coefficient MIU. Acoustic measurement is achieved using an acoustic booth (figure 1) equipped with a system reproducing the human arm motion thanks to two samples rubbing together; one sample is fixed and the other one is mobile [2]. The fixed sample is placed above a silicone surface which reproduces human skin.
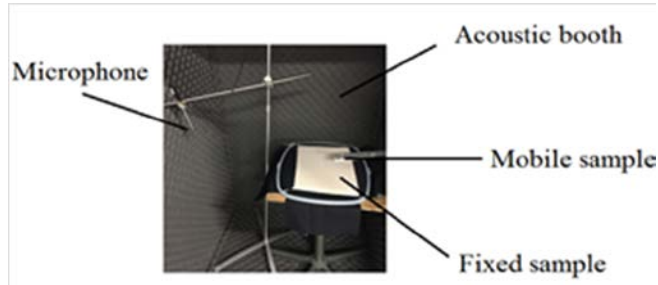
Figure 1: Acoustic booth.

A microphone Brüel & Kjaer ½ inch (type 4190) is used to detect the friction noise of the fabric specimen. The sound recording is performed thanks to a Sony recorder (PCM-M10) connected to a Brüel & Kjaer amplifier (type 2606). The microphone has been calibrated at 515 mV/Pa. The mechanical parts of the motion simulator, the recorder and the amplifier parts were placed outside the anechoic booth.

Duration of tests is around twenty seconds and some parameters, like the speed or the angle of scanning which were experimentally fixed, are constant.

The processing of the sound [3] is performed in three steps. Firstly, two or three seconds of the recording are selected using the Audacity® software. Secondly, the signal is processed by a weighting A filter. This filter will allow to reduce the background noise of the device and to amplify the perceptible range of the ear. Finally, the filtered sound signals are processed through FFT which allows to estimate the third octave band from 20 Hz to 20 kHz and to obtain noise level in dBA.

RESULTS AND DISCUSSION

As shown by K. Yosouf [3], the friction coefficient has an influence on the acoustic properties of fabrics.

Regarding the results presented in tables I and II, we can note for each fabric that the wet friction coefficient in the warp and weft directions is at least twice the dry friction coefficient. Therefore, the friction is more important and the abrasion will be quicker when the fabric is wet.

Tables I and II: Friction coefficients for warp and weft.

	Warp	
	dry	wet
plain	0.186	0.431
broken twill	0.256	0.682
satin 5	0.200	0.655
satin 12	0.261	0.587
twill 4	0.198	0.834
crepe	0.186	0.834

	Weft	
	dry	wet
plain	0.180	0.431
broken twill	0.208	0.624
satin 5	0.215	0.668
satin 12	0.191	0.726
twill 4	0.187	0.772
crepe	0.227	0.704

Moreover, in order to compare dry and wet sound spectra, a correlation coefficient is calculated for each sample using equation 1.

$$Cor(X,Y) = \sqrt{\frac{cov(X,Y)^2}{var(X) \cdot var(Y)}}$$ **Equation 1**

The calculation of this coefficient is made on an accurate frequency range, from 900 Hz to 10 kHz.

Table II: Correlation coefficient.

Fabrics	Correlation coefficient
plain	0.74
satin 12	0.88
broken twill	0.89
twill 4	0.93
twill 3	0.94
satin 6	0.94
crepe	0.94
satin 4	0.94
satin 5	0.97

Among samples, the results of two of them are presented: the plain weave which presents the lowest correlation and the satin 5 weave which has the highest correlation.

Figures 2 and 3 present the spectra in the dry and wet states for the plain and the satin after friction sounds processing.
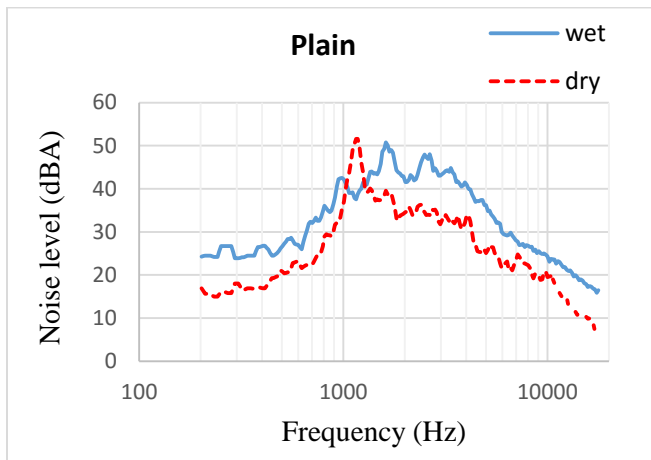
Figure 2: Plain spectra.
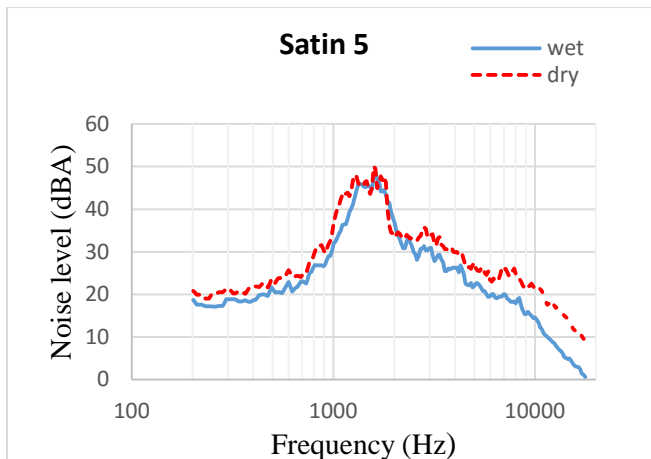
Figure 3: Satin 5 spectra.

Some differences can be noticed on the spectra shapes and the acoustic signature depending on the weaving pattern. For the plain, two different behaviors can be observed according to the test conditions. On the wet spectrum, the resonance is stronger and the frequency range is extended. Moreover, the wet spectrum is moved towards higher frequencies and the resultant sound is therefore higher pitched. As expected for the satin, no significant differences can be noticed between the two spectra; the high correlation indicates a similar behavior.

The frequency range of each textile sample was also represented. The frequency range corresponds to the intersection of the spectral density with the line which equals to the spectral maximum of the density less 10 dB. On figure 4, the dots represent the frequency of the spectral maximum of the density.
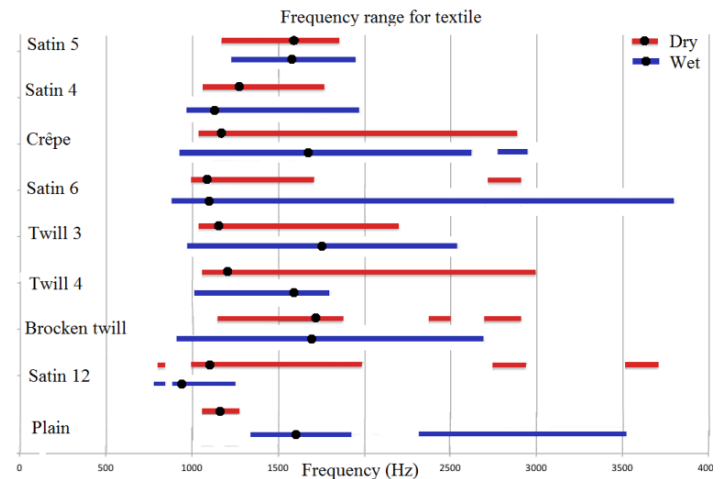
Figure 4: Frequency range in the dry and wet state.

This figure shows that the frequency ranges are different in the dry and wet states. The frequency of the spectral maximum is generally moved towards lower frequencies, the sound generated is therefore deeper and less audible.

CONCLUSION

The objective of the work was to compare the friction sound of fabrics in dry and wet states. Measurement showed that the acoustic behavior of fabrics and the friction coefficient are different for the two conditions depending on the weave pattern. For a military application, it seems more interesting to use satin 5 because there is no significant acoustic difference between wet and dry state and the frequencies are quite low. The next study will be to analyze the washing and frictional wear influence on the textile acoustic.

REFERENCES

[1] Kawabata, S. "The standardization and analysis of hand evaluation." *J. Text. Mach. Soc.,* Japan, 1980.
[2] Latroch, H. Doctoral Thesis, 2013, Mulhouse France. *Contribution au développement de nouveaux outils de caractérisation mécanique des étoffes: Etude et caractérisation de la signature sonore du frottement des étoffes*.
[3] Yosouf, K., Dréan, E., Schacher, L., Adolphe, D.C. Moukadem, A., Dieterlen, A., Zimpfer, V., Pellerin, V. "New method to characterize the sound generated fabric friction." *Conference Proceedings*, The Fiber Society, Spring 2014, Liberec, Czech Republic: 97-98.

Titanium Isopropoxide/Magnesium Acetate/PVP Composite Nanofibers via Electrospinning

Yakup Aykut

Uludág University, Engineering Faculty, Textile Engineering Department, Gorukle, Bursa, Turkey
aykut@uludag.edu.tr

INTRODUCTION

Ceramic nanofibers such as TiO_2, MgO and ZnO are produced via calcination of as-spun precursor nanofibers [1-4]. Since ceramic nanofibers are brittle, handling such fibers during fabrication is very challenge. In order to eliminate this weakness, firstly precursor materials are produced into nanofibrous form then ceramic fibers are obtained after a proper calcination process. Sol-gel electrospinning technology is a promising processing technique to produce ceramic precursor nanofiber structure. To produce precursor of TiO_2-MgO mix ceramic nanofiber system, we fabricated PVP/MgAc/Ti(IV) isopropoxide nanofibers via sol gel electrospinning technique. SEM, FTIR and TGA analyses were performed for morphology, chemical and thermal analysis of as-spun nanofibers.

EXPERIMENTAL

Schematic illustration of electrospinning process is demonstrated in Figure 1. In the process, simply, a suitable ceramic precursor(s)/polymers mix solution were prepared and subsequently electrospun into nanofibrous mat. In the procedure, first, a proper ratio of PVP was dissolved in ethanol. Then Ti (IV) isopropoxide was added into a polymer solution and magnetically stirred for 2 hours. Subsequently, the appropriate ratio of acetic acid and magnesium acetate (MgAc) were added into an alkoxide precursor solution for ageing. The stock solution is magnetically stirred in an ambient condition for 30 minutes to obtain a homogeneous electrospinning solution.
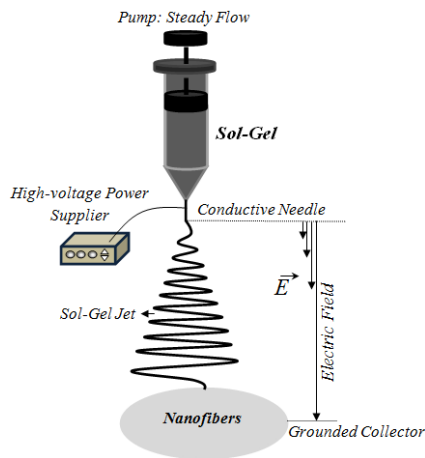
Figure 1. Schematic illustaration of *Sol-Gel* Electrospinning procedure.

After obtaining a desired viscosity, 1ml of the prepared stock solution is filled in a plastic syringe contains metal needle with 0.508 hole diameter. The solution is fed to needle with 0.5 ml/h flow rate. A power supplier (Gamma High Voltage Research, D-ES 30PN/M692) is connected to the metal needle, and 12 kV voltage is applied. A grounded collector covered with aluminum foil is located at 15 cm distance. Existence of the electrical field between the metal needle and collector causes ejection of solution droplet to the collector. The droplet is divided to pieces and each piece elongated during its journey from the needle to collector and collected as PVP/MgAc/Ti(IV) isopropoxide nanofiber form on the collector.
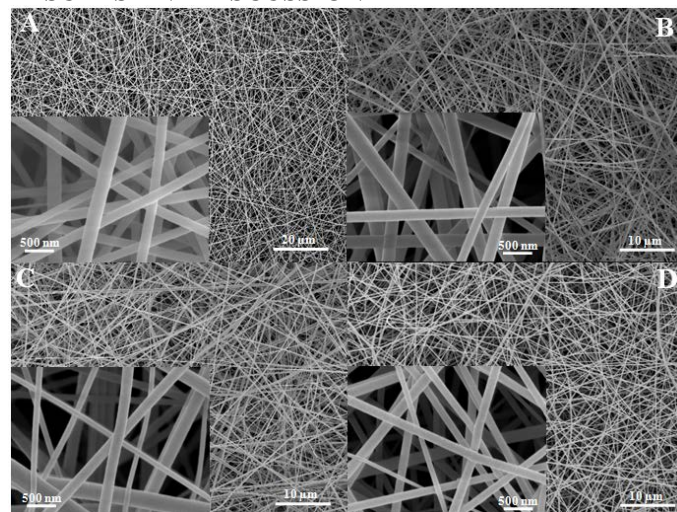
RESULTS AND DISCUSSION

Figure 2. Scanning Electron Micrographs of Ti (IV) isopropoxide/Magnesium Acetate/PVP composite nanofibers before calcinations with different MgAc contents respect to Ti (IV) isopropoxide: a)0 wt%, b)15 wt%, c) 30 wt%, and d)50 wt%.

Morphological and surface analysis of as-spun precursor Ti (IV) isopropoxide/ Magnesium acetate/ PVP nanofibers were investigated with a scanning electron microscopy (Figure 2A-2D). As shown by viewing the SEM images of as-spun nanofibers (Figure 2), nanofiber surfaces are smooth and all the nanofibers are randomly oriented by arranging 3D network structure in the mat. No defect structures such as bead-on-a-string morphology or fiber breakage is observed indicate the prepared electrospinning solutions has a homogeneity and appropriate viscosity, surface tension and electrical conductivity.

Chemical analysis of as-spun as-spun Ti (IV) isopropoxide/ magneisum acetate/ PVP nanofibers with different MgAc contents were conducted with FTIR spectra and demonstrated in Figure 3. As seen from the spectra, no big spectral change is observed with different ratio of Ti (IV) isopropoxide/magneisum acetate/PVP in the nnaofibers.

Broad band around 3600–3200 cm^{-1} in the spectrum demonstrated in (Figure 3) corresponds to O–H stretching vibration due to presence of water in the samples. The peaks present at 2965–2854 cm^{-1} corresponds to the asymmetric and symmetric C–H stretching vibrations of methyl groups comes from acetate and isopropoxide molecules [5-6]. The peaks at around 1740 and 1650 cm^{-1} correspond to stretching vibrations of C=O bonds in acetate and PVP molecules [6].
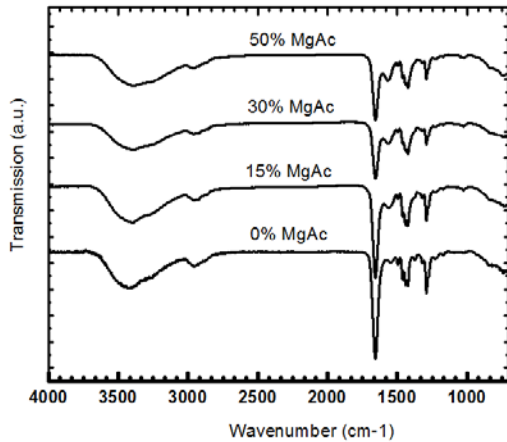

Figure 3. ATR-FTIR spectra of as-spun Ti (IV) isopropoxide/ magneisum acetate/ PVP nanofibers with different MgAc contents.

Weigth losses of as-spun nanofibers during the heat treatment processes were observed with TGA thermograms and given in Figure 4. Abrupt weight loss between 0-100°C is attributed to loss of water that are adsorbed on as-spun nanofibers. Second abrupt weight loss around 270°C is attributed to degratation of PVP molecules and combustional removal of by products (CO$_2$, H$_2$, etc.). Weight loss start at lower temperature with addition of MgAc in the system. The residual weight of all samples are around 20 wt % that corresponds to the final production of titanium magnesium oxide systems. No weight loss is observed and the slope reaches to balance at high temperatures indicate no more organic degrades and remove from the system and just phase transformation occurs.
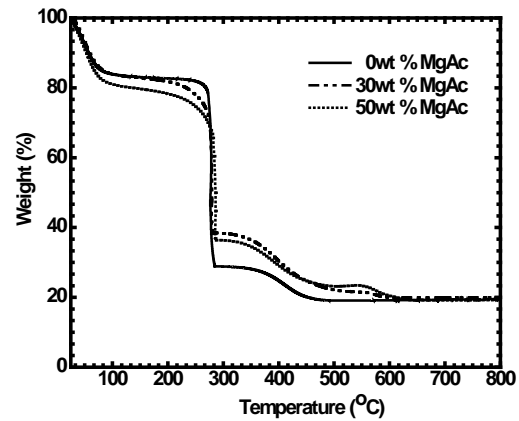

Figure 4. TGA thermograms of as-spun Ti (IV) isopropoxide/ magneisum acetate/ PVP nanofibers with different MgAc contents.

CONCLUSION

Ti (IV) isopropoxide/ magneisum acetate/ PVP nanofibers as precursors of calcined TiO$_2$-MgO mix crystalline nanofibrous structre were prepared via sol-gel electrospinning technique. SEM images of the precursor nanofibers with different Ti:Mg ration revealed that nanofibers are shown in 3D network structure and uniformityies are very high and stable even though changing the ration.

REFERENCES

1. Aykut, Y., Saquing, C., Pourdeyhimi, B., Parsons, G.N., Khan, S.A. *ACS Applied Materials and Interfaces*, 2012, 4 (8), 3837–45.
2. Li, D., Xia, Y. *Nano Letters*, 2003, 3: 555-60.
3. Shao, C., Guan, H., Liu, Y., Mu, R. *Journal of Materials Science*, 2006, 41(12): 3821-24.
4. Aykut, Y., Parsons, G.N., Pourdeyhimi, B., Khan, S. A. *Langmuir*, 2013, 29 (12): 4159-66.
5. Tian, H.Y., Luo, W.G., Pu, X.H., Qiu, P.S., He, X.Y., Ding, A.L. *Thermochim. Acta*, 2000, 360: 57-62.
6. Coates, J. "Interpretation of infrared spectra: a practical approach" in: R.A. Meyers (Ed.), *Encyclopedia of Analytical Chemistry*, Chichester: John Wiley & Sons Ltd, 2000, 10815-37.

Understanding Factors Influencing Cellular Response to Spider Silk

J. Catoe[2], K. Hafner[1], H. Maeser[1], O. Ross[1], L. Kays[3], C. Stoner[3], M. Ellison[3], D. Dean[1], M. Kennedy[3]

[1]Department of Bioengineering, Clemson University, Clemson, SC
[2]Department of Genetics and Biochemistry, Clemson, SC
[3]Department of Materials Science and Engineering, Clemson, SC
ellisom@clemson.edu

STATEMENT OF PURPOSE

The overall aim of this research program is to determine subtle differences in the surface properties of spider dragline silk. In the current phase, plating the dragline silk with various types of cells and observing their proliferation and alignment will aid in the elucidation of the variance in surface properties along the silk. Results also may provide insight into cell guidance by the silk, and also determine if cells could be utilized as rapid "sensors" to differentiate between varying silk surfaces

INTRODUCTION

Spider dragline silk mechanical properties and bulk properties have been tested and analyzed by many workers. However, more work needs to be done to characterize the surface properties of these fibers including the variations in charge distribution (by the amino acids) and surface morphology. Variations can be associated with different species and can be related to environmental conditions (e.g., spider habitat). Exploratory studies have used AFM to study the surface roughness and charge (Faugas, 2014). Other groups have studied cell growth on these native fibers and shown that the cells could adhere and align along with dragline fibers (Kuhbier, 2010). However, there apparently are no studies that quantify sensitivity of cells to silk surface variations.

APPROACH

The spiders, all females, were of the species *Nephila clavipes,* more commonly called Golden Orb Weavers. The spiders were housed in one 10' by 9' tent or in three individually sealed boxes, each box with a volume of approximately 1.5 ft^3. Webs were sprayed with distilled water daily and field crickets were fed to the spider approximately 3-4 times a week.

To collect the silk, a spider was removed from the habitat and cooled in a refrigerator (4°C) for one hour to partially incapacitate. The anesthetized spider was quickly fastened face up to a foam block. Using forceps, silk was then drawn (10 mm/sec) and wrapped onto a glass coverslip. Superglue was used to securely attach the silk to the coverslip. Initial tests were conducted by hand-wrapping the silk onto the coverslip. An improved reel system was devised that used two motors: one motor rotated the coverslip, allowing the silk to wrap around completely around the coverslip while the other motor moved the slip horizontally to create a grid with consistent spacing between strands.

Prior to the cell plating, the silk was treated using various amounts of UV exposure. Treated and untreated silks were then plated using two types of cells, fibroblasts and adipose stem cells. The silk-wrapped coverslips were placed in media-filled wells. Approximately 50,000 cells were plated and allowed to grow for a 3-day period. Silk and cells' actin fibers were fluoroscopically stained and microscopy images are taken throughout the trial to document how cell interaction with silk progressed.

RESULTS AND DISCUSSION

The initial results (Fig. 1) from plating the cells using the hand-wrapped silk it became evident that both a unified grid and a sterilization procedure was needed.
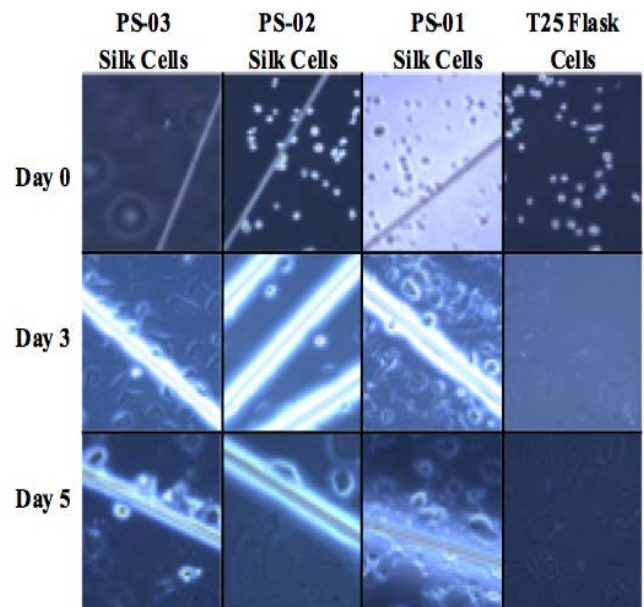

Figure 1: Preliminary tests of cells with dragline silk fibers showing cells interacting with silk surface and need for sterilization.

Figure 1 shows the progression of the cells for the duration of a five-day trial. The rightmost column is a control (slide without silk). The other images show

that the cells adhere to the silk and align along the fiber. Figure 1 also shows that slide contamination was in issue in the hand-wrapped trials.
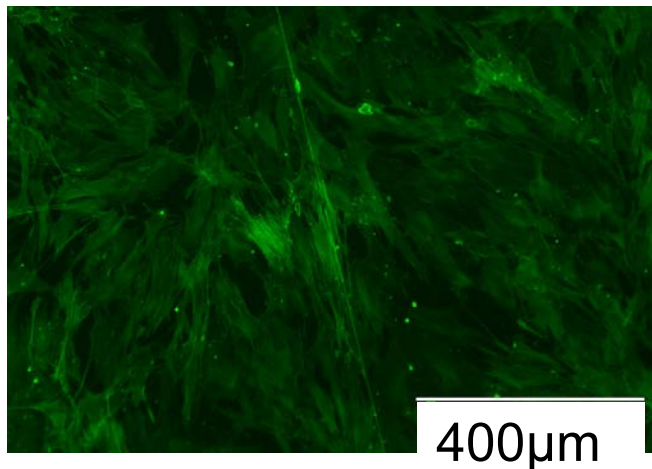

Figure 2: Actin staining of the cells and silk show the actin alignment along the silk fiber (longest fiber shown is silk).
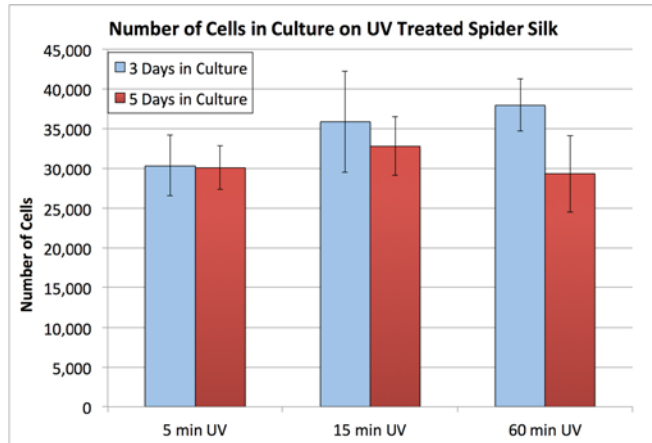

Figure 3: UV treatment proliferation results. Cell number between day 3 and 5 significantly decreased on 60 minutes UV treated silk (p=0.014, student t-test).

A second trial of cell plating was performed using the mechanized silking system. Fibroblasts were plated and are shown to align along the silk fiber (Fig. 2). Figure 3 shows how the varying amount of UV exposure affects the number of viable cells within the culture. It can be seen that longer UV exposure caused a larger percent of viable cell death between days three and five. A potential cause of this would be the cells response and reaction to the degraded surface properties of the silk exposed to 60 min of UV light.

CONCLUSIONS
Cells have been shown to align with the dragline silk fibers (both UV treated and untreated). Proliferation of cells was shown to be influenced by UV treatment duration.

REFERENCES
1) Bainbridge, P. *Journal of Wound Care*, 2013, Vol. 22 (8): 407-12.
2) Faugas, B., Ellison, M., Dean, D., Kennedy, M. *Journal of Surface Engineered Materials and Advanced Technology*, 2013, Vol. 3: 18-23.
3) Ko, F., Kawabata, S., Inoue, M., Niwa, M., Fossey, S., Song, J.W. "Engineering Properties of Spider Silk." Web. 2 Feb. 2016.
4) Kuhbier, J.W., Allmeling, C., Reimers, K., Hillmer, A., Kasper, C., Menger, B., Vogt, P.M. "Interactions between Spider Silk and Cells–NIH/3T3 Fibroblasts Seeded on Miniature Weaving Frames." *PLoS ONE*, 5(8). http://doi.org/10.1371/journal.pone.0012032.

GO/SiO$_2$ Ultrafiltration Composite Membrane Based on PAN Nanofibrous Substrate for Oil-Water Emulsions Treatment

Cheng Cheng, Lingdi Shen, Xuefen Wang

State Key Lab for Modification of Chemical Fibers and Polymer Material, Donghua University, Shanghai, China

chengcheng1519@126.com

INTRODUCTION

Recently, oil-water emulsions separation has been a worldwide challenge due to the increasing industrial oily wastewater and polluted oceanic waters, as well as the frequent oil spill accidents [1]. The demand for designing membranes with both high permeability and selectivity is urgent. The composite membranes, consisting of a porous supporting layer and a thin separation layer, have gained much attention. Owning to high surface area-to-volume, high porosity and fully interconnected structure, electrospun nanofibrous membrane used as a substrate could remarkably improve the drawback of low permeate flux for conventional support fabricated by phase inversion [2]. Graphene oxide (GO), the analogue of carbon nanotubes (CNTs) with a novel 2D carbon nanostructure, is an ideal film-forming material, which is attributed to its intrinsic properties of hydrophilicity and mono-atomically thick 2D structure [3]. However, the GO membrane with stacked layers often exhibits a compact and dense structure, which limits its application in ultrafiltration. Herein, a novel ultrafiltration composite membrane consisting a hydrophilic SiO$_2$ coated GO barrier layer and electrospun PAN nanofibrous substrate was fabricated for oil-water emulsions treatment.

APPROACH

PAN was dissolved in DMF to obtain a 8wt% homogeneous solution. PAN nanofibers were fabricated by electrospinning based on our previous work [4]. The thickness of the prepared PAN nanofibrous membrane is about 40 µm. The electrospun PAN nanofibrous membrane acting for supporting layers were cold-pressed at room temperature at 8 MPa for 30 s. The GO/SiO$_2$ composite was synthesized according to the report of a literature [5]. A vacuum-filtration assisted assembly technology was used for preparing the GO/SiO$_2$ nanofibrous composite membranes.

The surface morphology of the electrospun nanofibrous substrate and composite membranes were investigated by scanning electron microscopy. An image analyzer, namely, ImageJ 2X software were used to measure the PAN nanofiber diameters together with its distribution. Cross-flow measurements were carried out using oil/water emulsions to evaluate the filtration performance of the composite membranes.

RESULTS AND DISCUSSION

Figure 1 shows the typical SEM images of the as-prepared electrospun PAN nanofibrous membranes without treatment and the diameter distribution of PAN nanofibers. Obviously,
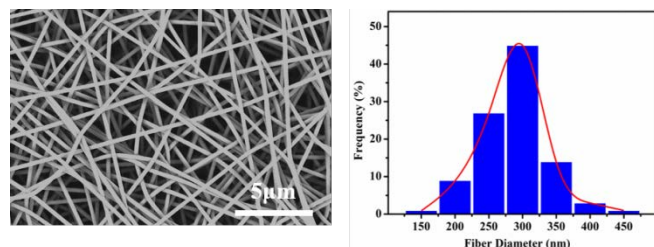

Fig. 1. Typical SEM image of electrospun PAN nanofibrous membrane and diameter distribution of nanofibers the average diameter of the PAN fibers was about 300 nm.
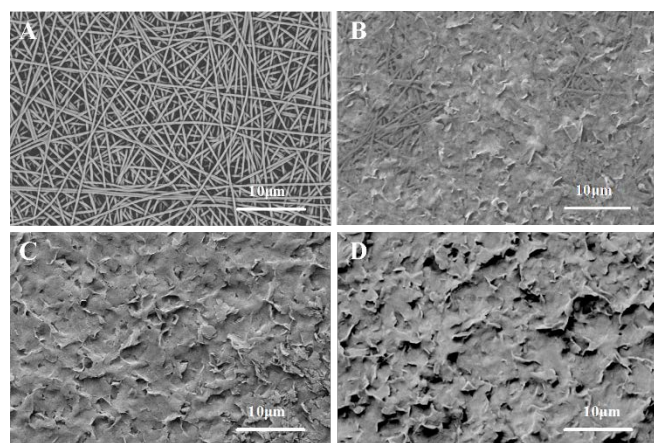

Fig. 2. Typical SEM images of electrospun PAN nanofibrous substrate and composite membranes with deposition amount of GO/SiO$_2$ composite.

To improve the mechanical strength of the substrate and to achieve a smooth surface for depositing GO/SiO$_2$ composite, the electrospun PAN nanofibrous membrane was cold- pressed at room temperature at 8 MPa for 30s, as shown in Fig. 2(A). With regard to the skin layer, the deposition amount of GO/SiO$_2$ composite should be optimized to obtain a defect-free barrier for the selectivity of the entire composite membranes. Fig. 2(B), (C) and (D) shows the typical surface morphologies of GO/SiO$_2$ top layer varied with different deposition amount, which was 0.03, 0.06 and 0.09 mg/cm^2 respectively. As the deposition amount increased, the bare nanofiber was gradually covered by GO/SiO$_2$ and an integrated GO/SiO$_2$ film formed when the deposition amount reached 0.06mg/m^2. In addition, the surface of skin layer was really rough, which was because the condensation of TEOS with the protic functional groups (e.g., -OH, -COOH) on the surface of GO led to the breeding of SiO$_2$ sol supported by GO, which gradually condensed and grow into bigger nanoparticles covered on the GO sheets [6]. It is worth mentioning that more fluidic

water channels formed between GO layers covered by SiO_2 are in favor of improving the separation efficiency.
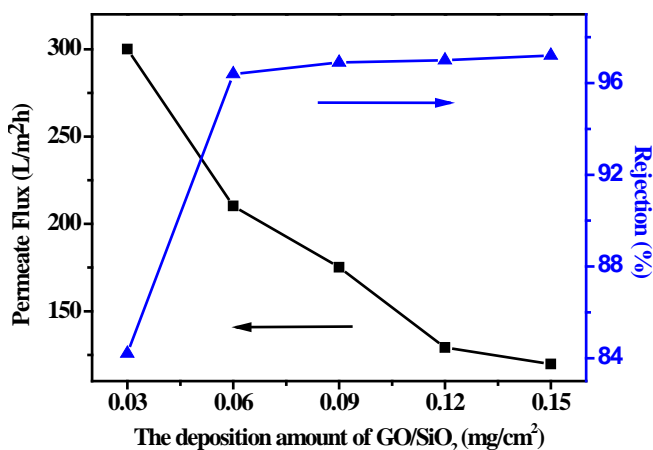

Fig. 3. The effect of GO/SiO_2 deposition amount on permeate flux and rejection rate of the composite membranes using oil-water emulsion as a feed solution (temperature: 25℃).

Fig. 3 illustrates the deposition amount dependence on permeate flux and rejection rate of the obtained nanofibrous membranes at low pressure (0.1MPa). With the increase of deposition amount from 0.03 to 0.06 mg/cm^2, the rejection exhibited a dramatical increase from 84.1% to 96.5% because low deposition amount of GO/SiO_2 was not enough to achieve an integrated skin layer and a defective barrier cannot obtain a high rejection. While the rejection remained the same when the deposition amount further increased, which was due to the formation of an intact separate layer. Moreover, as the deposition amount of GO/SiO_2 increased, the permeate flux significantly declined owning to the notably magnified mass transfer resistance. On the whole, the GO/SiO_2 nanofibrous composite membranes exhibited the optimum separation performance with permeate flux of 210.2 L/m^{2}h and rejection of 96.5% at 0.1MPa.

CONCLUSION
In summary, GO/SiO_2 ultrafiltration composite membrane based on PAN nanofibrous substrate prepared by using a simple vacuum-filtration assisted assembly method exhibited better performance for the separation of oil-water emulsion, which has the potential to be applied in the treatment of oily waste water.

KEYWORDS
Electrospun nanofibrous membrane, ultrafiltration composite membrane, graphene oxide, SiO_2, oil-water emulsions treatment

REFERENCES
[1] Shang, Y., Si, Y., Raza, A., Yang, L., Mao, X., Ding, B., Yu, *J. Nanoscale*, 2012, 4 (24): 7847-54.
[2] Wang, X., Fang, D., Yoon, K., Hsiao, B.S., Chu, B., *Journal of Membrane Science*, 2006, 278 (1-2): 261-68.
[3] You, H., Yang, Y., Li, X., Zhang, K., Wang, X., Zhu, M., Hsiao, B.S. *J. Membrane Sci.*, 2012: 241-247, 394-95.
[4] Liu, G., Jin, W., Xu, N. *Chem. Soc. Rev.*, 2015, 44 (15): 5016-30.
[5] Shang, Y., Si, Y., Raza, A., Yang, L., Mao, X., Ding, B., Yu, *J. Nanoscale*, 2012, 4 (24): 7847-54.
[6] Kou, L., Gao, C. *Nanoscale,* 2011, 3 (2): 519-28.

Thin-Film Nanofibrous Composite Hemodialysis Membranes with High Permeability and Great Selectivity

Xufeng Yu[1], Yadong Zhu[1], Xuefen Wang[1], Benjamin S. Hsiao[2]

[1]State Key Lab for Modification of Chemical Fibers and Polymer Material, Donghua University, Shanghai, China
[2]Department of Chemistry, Stony Brook University, Stony Brook, New York, USA
xf.yu@icloud.com

OBJECTIVE
To develop a new kind of thin-film nanofibrous composite (TFNC) membranes with high permeability and great selectivity for hemodialysis.

INTRODUCTION
Kidney disease is a significant cause of mortality in the world and its incidence rate has increased rapidly[1]. Hemodialysis is a vital clinical therapy for the patients with renal diseases. The core element of a hemodialysis equipment is the hemodialysis membrane, which can eliminate toxic metabolites and excess water from blood via diffusive and convective transport across the membrane and prevent loss of necessary proteins due to pore size exclusion of the membrane[2]. The characteristics of an ideal hemodialysis membrane can be defined[2]: (1) the porosity of support layer should be high and the separation layer should be as thin as possible to achieve a high permeability; (2) the separation layer should have a uniform pore-size distribution in order to achieve the greatest selectivity. Hence, we fabricated a novel nanocomposite hemodialysis membrane, which consisted of an ultrathin hydrophilic active separation layer and a scaffold-like nanofiber support layer.

APPROACH
Polyacrylonitrile (PAN) nanofibrous scaffold was prepared by electrospinning[3]. The solution (8 wt %) of PAN in N, N'-dimethylformamide (DMF) was prepared at 50 °C for 24 h. The electric voltage was 24 kV and the solution feed rate was 16 μL/min. The prepared PAN nanofibrous scaffold used as the supporting layer was cold-pressed at 5 MPa for 60 s.

The polyvinyl alcohol (PVA) solution (2 wt %) was prepared by dissolving PVA in water under stirring at 70 °C for 6 h. Then the glutaraldehyde (GA) was added to initiate the situ cross-linking reaction. The PVA/GA solution was cast onto the wet PAN supporting layer using an applicator. The resulting two-tier TFNC membrane was incubated for 6 h to complete the cross-linking reaction.

The morphology of membranes was examined via scanning electron microscopy (SEM). The membrane sieving coefficient (SC) was determined using the cross flow cell. And the lab-scale single layer dialysis test system utilized to evaluate the dialysis performance of membranes.

For comparison, the home-made conventional polysulfone (PSf) hemodialysis membrane as the control was prepared via phase inversion[4].

RESULTS AND DISCUSSION
Figure 1 showed the SEM images of the PAN nanofibrous scaffold before and after cold-pressed. The fiber diameter distribution was relatively uniform and the average diameter of the fibers was about 255 ± 30 nm. The nanofibrous substrate was more compact after being pressed and the morphology of nanofiber didn't change distinctly. It was found that the pores in an electrospun substrate were fully interconnected to form a three-dimensional network. Thus, the PAN nanofibrous scaffold was the excellent candidate as the supporting layer.
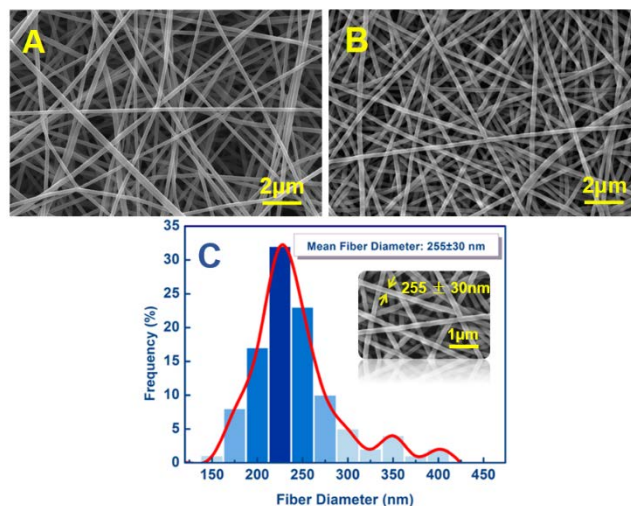

Figure 1. SEM images of PAN nanofibrous substrate electrospun from 8 wt% solution before (A) and after (B) cold-pressed, and the fiber diameter distribution (C).
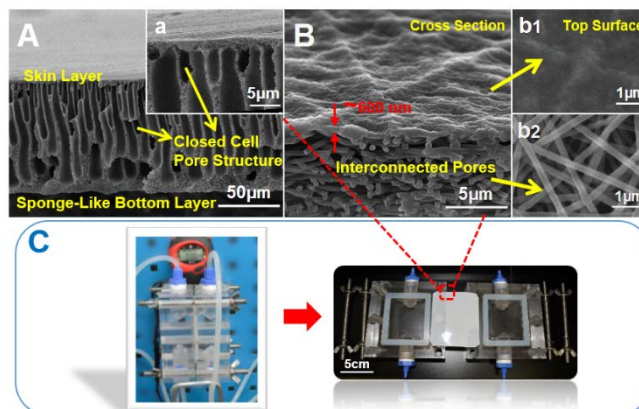

Figure 2. (A) A cross-sectional SEM image of a conventional PSf membrane using the phase inversion method (B) The cross-sectional SEM image of the PVA/PAN TFNC membrane. (C) Optical photographs of TFNC membrane and dialysis membrane cell assembly.

As shown in Figure 2A, the cross-sectional SEM image of the conventional PSf membrane showed the typical structure formation of a phase inversion membrane[5]. The closed cell porous structure and thick spongy bottom layer might block the toxic molecular substances through the membrane. In contrast, Figure 2B showed the cross-sectional SEM image of the PVA/PAN TFNC membrane. The nanofiber support layer showed porous structure with interconnected pores between individual nanofibers, so there were many paths along which the particles could move. The unique structure of the nanofiber support layer guaranteed direct paths for water and toxic metabolites excretion. The TFNC membrane had high porosity, interconnected pores supporting layer, and ultrathin coating layer.

Figure 3 presented the sieving curves of conventional PSf and PVA/PAN TFNC membranes. It was important to note that the TFNC membrane had a quite sharper separation curve than that of the conventional PSf membrane. It could be speculated that this might be due to a uniform pore-size distribution of TFNC membrane. The above result indicated that the PVA/PAN TFNC membrane provided great selectivity for hemodialysis.
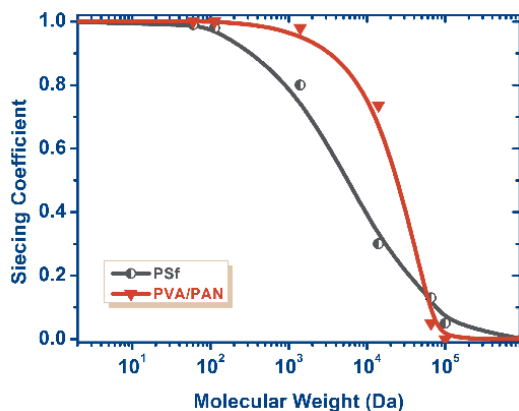

Figure 3. Sieving coefficients of molecular weight markers for the conventional PSf and PVA/PAN TFNC membranes. The following markers were used: urea (60 Da), creatinine (112 Da), vitamin B_{12} (1355 Da), lysozyme (14 kDa) and BSA (66 kDa).

The urea and lysozyme clearance, bovine serum albumin (BSA) retention of the conventional PSf and PVA/PAN TFNC membranes were measured to evaluate the hemodialysis performances. From Figure 4A, it could be figured out that 82.6 % of urea was cleaned by the PVA/PAN TFNC membrane after simulating dialysis for 4 h, which was higher than 76.2 % of the conventional PSf membrane. With respect to middle molecule toxic clearance, 45.8 % of lysozyme was cleaned out for the PVA/PAN TFNC membrane which was about 3.5 times higher than that of the conventional PSf membrane (12.8 %). As valuable blood protein was scarcely lost (almost ~ 100 % retention) during the dialysis process, while the BSA retention of conventional PSf membrane was about 91 % (Figure 4C).

CONCLUSION

A new type of high-performance hemodialysis membrane consisting of an ultrathin hydrophilic active separation layer and a scaffold-like nanofiber support layer was demonstrated. Naturally, the ultrathin hydrophilic PVA skin layer provided high selectivity (a narrow pore-size distribution) to remove uremic toxins and retain proteins, the nanofibrous support layer offered high permeability (a highly interconnected pore structure) to transfer the toxins during hemodialysis process.
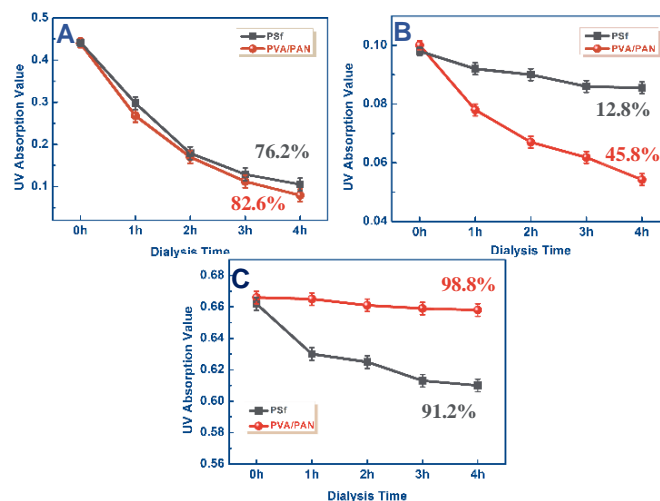

Figure 4. Comparison of the solute transmission efficiency for the conventional PSf and PVA/PAN TFNC membranes: (A) urea clearance percentage; (B) lysozyme clearance percentage; (C) BSA retention percentage.

FUTURE WORK

For the future development of TFNC membranes, the active layer could be modified to exhibit better hydrophilicity and blood compatibility.

KEYWORDS

Thin-film nanofibrous composite membrane, hemodialysis, selectivity.

REFERENCES

[1] S.S. Hayek, S. Sever, Y.A. Ko, et al. *N. Engl. J. Med.*, 2015, 373: 1916-25.
[2] C. Legallais, G. Catapano, B.V. Harten, et al. *J. Membr. Sci.*, 2000, 168: 3-15.
[3] L.D. Shen, X.F. Yu, C. Cheng, et al. *J. Membr. Sci.*, 2016, 499: 470-79.
[4] T. Xiang, L.S. Zhang, R. Wang, et al. *J. Colloid Interface Sci.,* 2014, 432: 47-56.
[5] A.L. Gao, F. Liu, H.Y. Shi, et al. *J. Membr. Sci.*, 2015, 478:96-104.

Co-deposition of Dopamine and Poly(ethyleneimine) Complex Nanofibrous Membranes for Dye Adsorption

Min Wang, Lingdi Shen, Xuefen Wang

State Key Lab for Modification of Chemical Fibers and Polymer Materials, Donghua University, Shanghai, China

wm910107@163.com

OBJECTIVE

To improve the dye removal performance of nanofibrous membrane by co-deposition poly(ethyleneimine) (PEI) and dopamine on the electrospun polyacrylonitrile (PAN) nanofibers.

INTRODUCTION

The removal of dyes from wastewater has become a critical issue because of their adverse effects on human health and environment [1]. The adsorption method could be the most cost-effective for dyes removal due to easy operation, high efficiency and low secondary pollution [2]. Over the past decades, affinity membrane has become an attractive and competitive separation medium in the field of dye removal [2]. Owning to the superior properties such as fine diameters, large specific surface area, environmentally benign nature and stability in liquid media, electrospun nanofibrous membranes have been widely used as affinity membranes [3]. PEI, an amino-rich polymer, has abundant adsorption sites for removing dyes and can be used as an adsorbent material [4]. As for dopamine, it not only could form strong adhesive interaction with various substrates during self-polymerization to adherent polydopamine (PDA), but also has a large number of active groups such as plenty catechol for further reactions with other molecules [5, 6]. Therefore, in this study, we combine electro- spinning with an improved one-pot approach of co-deposition of dopamine and PEI to fabricate PEI/PDA/PAN nanofibrous membranes for adsorption of dyes. Compared to the two-step method [6], the deposition time of the one-pot approach is greatly shortened, and the co-decorate membrane can be used without further cross-linking due to the covalent cross-linking reaction between PDA and PEI [7].

APPROACH

PAN powders were dissolved with DMF and stirred for 12 h in an oil bath at 50 °C to obtain 8.0 wt% homogeneous solutions. PAN nanofibrous membranes were prepared by electrospinning technique. The electrospinning parameters were as follows: the applied electric voltage was 22.0 kV, the distance between the spinneret and the grounded drum was 15.0 cm and the solution feed rate was 16.0 μL/min [8].

Dopamine hydrochloride and PEI were dissolved in Tris-HCl buffer solution (pH=8.0, 10.0 mM). The concentrations for dopamine and PEI were 0.5 g/L, 8.0 g/L, respectively; afterwards, the pH was adjusted to 8. The PAN nanofibrous membranes were immersed in fresh prepared solution after pre-wetted by Tris-HCl buffer solution and shaken at 30 °C for 8 h. Then the samples were taken out, washed with deionized water and dried in a vacuum at 40 °C overnight.

The morphologies of PAN and PEI/PDA/PAN nanofibers were observed by field emission scanning electron microscopy (FE-SEM).

All adsorption experiments were carried out by using 20 ml of Sunset Yellow FCF (SY FCF) dye solutions with different initial pH (1-7) and initial concentrations (50-450 mg/L). The concentrations of the SY FCF solutions were tested by UV–vis spectrophotometer. The amount of SY FCF dye adsorbed on the PEI/PDA/PAN nanofibrous membranes was calculated by the following equation:

$$q_e = \frac{(C_0 - C_e) \times V}{m}$$

RESULTS AND DISCUSSION

The PEI/PDA/PAN nanofibrous membranes were prepared by the combination of electrospinning and co-deposition of dopamine and PEI. Morphological changes of the membrane surfaces were characterized by FE-SEM, as shown in Figure1. As can be seen from Fig.1 A and B, PAN nanofibrous exhibited a smooth surface with average diameter of about 400 nm, while the surface morphology of PEI/PDA/PAN nanofibers became relatively rough after 8 h deposition (as displayed in Fig.1 C and D), indicating that some precipitates of PEI and dopamine deposited on the surface of PAN nanofibers.
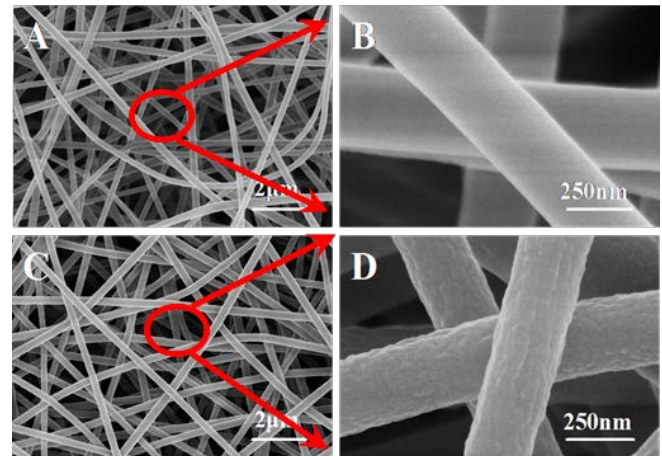

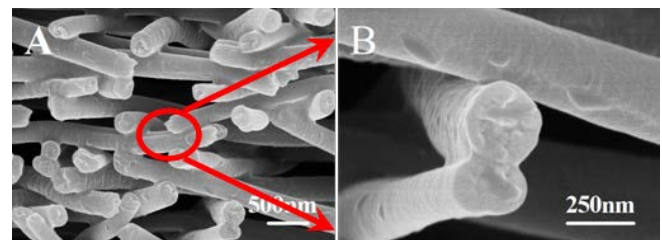Figure 1. Typical FE-SEM images of PAN (A and B) and PEI/PDA/PAN (C and D) nanofibrous membranes.

Figure 2. The cross-section FE-SEM images of the PEI/ PDA/PAN nanofibrous membranes.

Fig.2 showed the cross-section FE-SEM images of the PEI/ PDA/PAN nanofibers, and the junctions were observed

clearly among nanofibers, indicating that the product of dopamine and PEI reaction was attached to PAN nanofibers.

Fig.3A showed the relationship between the initial solution pH and the adsorption capacity of dye. As can be seen, the adsorption capacity of SY FCF dye increased with increasing the initial solution pH up to around 3, after that it began to decrease with further increase of pH. In general, a relatively high concentration of protons would be available to protonate amine and imino groups on PEI to form $-NH_3^+$ and $-NH_2^+-$ with low pH solution, which will enhance the strong electrostatic attractions between negatively charged dye anions and positively charged adsorption sites, resulting in an increased adsorption capacity of SY FCF dye [4]. Whereas, the extremely acid environment would destroy the surface structure of PEI/PDA/PAN nanofibrous membranes and reduced the adsorption capacity for SY FCF dye. Thus, the optimum pH value of SY FCF dye adsorption was around 3, and the adsorption mechanism of SY FCF dye adsorbed on the PEI/PDA/PAN nanofibrous membranes was electrostatic interaction. Furthermore, the effect of the dye concentration on the adsorption capacity of SY FCF dye was exhibited in Fig.3B. It was observed that the adsorption capacity of SY FCF dye increased with increasing the dye concentrations up to 300 mg/g, and then tended to approach a constant value of about 206.5 mg/g, attributing to the increase in the driving force of concentration gradient with an increase in the initial concentration [4]. As displayed in Figure.4, the adsorption amount of SY FCF dye increased with contact time and achieved equilibrium at 60 min.
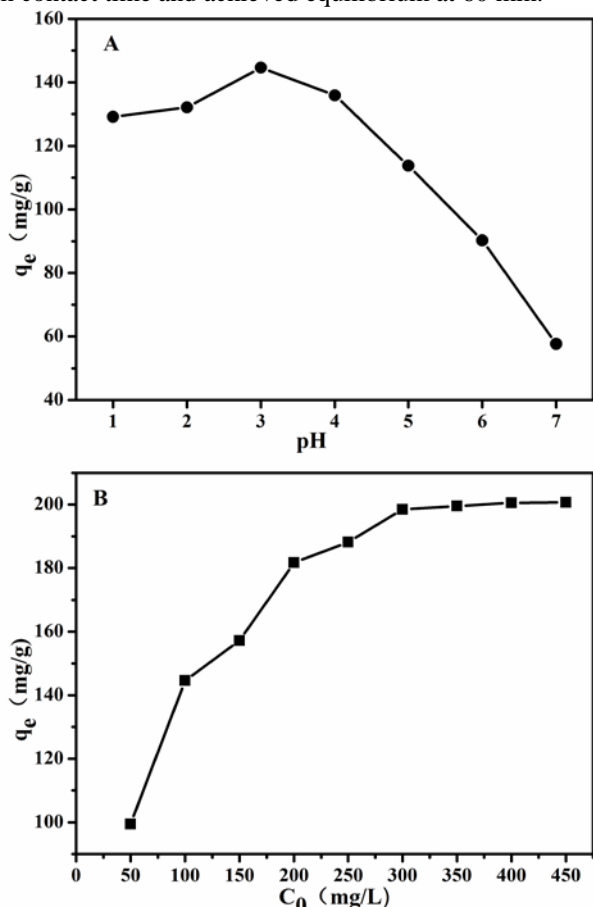

Figure 3. Effects of solution initial pH (A) and initial concentration (B) on the adsorption capacity of SY FCF dye on PEI/PDA/PAN nanofibrous membranes.
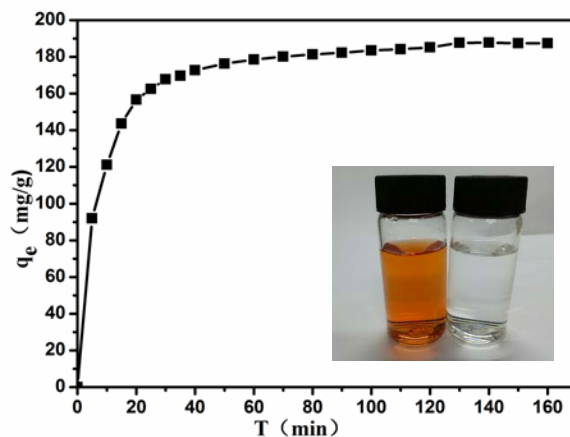

Figure 4. Effects of contact time of SY FCF dye adsorption on the PEI/PDA/PAN nanofibrous membranes.

CONCLUSION

In summary, we have demonstrated the fabrication of PEI/PDA/PAN nanofibrous membranes via co-deposition of dopamine and PEI on PAN nanofibers surface, in which PEI reacted with dopamine through Michael addition or Schiff base reaction between amino and quinine. This one-step strategy of co-deposition takes the advantages of universal, time-saving and easy operation. Then, the PEI/PDA/PAN nanofibrous membranes were used as an adsorbent for SY FCF dye removal. The results showed that the optimum solution pH for the adsorption was 3, and the adsorption mechanism of SY FCF dye on PEI/PDA/PAN nanofibrous membranes was dominated by electrostatic interaction. Additionally, the maximum adsorption capacity of SY FCF dye was about 206.5 mg/g. Therefore, the PEI/PDA/PAN nanofibrous membrane was considered as an effective and promising material for the removal of dye from wastewater.

KEYWORDS
Dopamine, PEI, co-deposition, nanofiber, adsorption

REFERENCES
[1] Lin, Y.F., Chen, H.W., Chien, P.S., Chiou, C.S., Liu, C.C. *J. Hazard. Mater.*, 2011, 185: 1124-30.
[2] Hong, G.S., Li, X., Shen, L.D., Wang, M., Wang, C., Yu, X. F., Wang, X.F. *J. Hazard. Mater.*, 2015, 295: 161-69.
[3] Nataraj, S.K.., Yang, K.S., Aminabhavi, T.M. *Prog. Polym. Sci.*, 2012, 37: 487-513.
[4] Min, M.H., Shen, L.D., Hong, G.H., Zhu, M.F., Wang, X.F., Hsiao, B.S. *Chem. Eng. J.*, 2012, 197: 88-100.
[5] Li, M.M., Xu, J., Chang, C.Y., Feng, C.C., Zhang, L.L., Tang, Y.Y., Gao, C.J. *J. Membr. Sci.*, 2014, 459: 62-71.
[6] Qiu, W.Z., Yang, H.C., Wan, L.S., Xu, Z.K. *J. Mater. Chem. A.*, 2014, 2: 10225-30.
[7] Yang, H.C., Liao, K.J., Huang, H., Wu, Q.Y., Wan, L.S., Xu, Z.K. *J. Mater. Chem. A.*, 2015, 3: 14438-44.
[8] Li, X., Wang, M., Wang, C., Cheng, C., Wang, X.F., *ACS Appl. Mater. Interfaces.*, 2014, 6: 15272-82.

Hierarchically Porous Carbon Black/Graphene Hybrid Fibers for High-performance Flexible Supercapacitors

Wujun Ma, Shaohua Chen, Meifang Zhu

State Key Laboratory for Modification of Chemical Fibers and Polymer Materials College of Material Science and Engineering, Donghua University, Shanghai, China

mawujun123456@163.com

INTRODUCTION

Due to the fast development of portable and wearable electronics in our society, it is critically important to develop matchable flexible and highly efficient energy storage devices [1-3]. Supercapacitors (SCs), which are superior in ultrahigh power density, exceptional cycle life, and fast charging/discharging capacity, are widely recognized as important candidates for wearable electronics [4-7]. In our daily lives, fiber is one of the most common flexible materials. If the SCs are made in a wire or fiber format, it can satisfy the development of flexible and wearable electronics. Graphene fiber formed by individual graphene nanosheets is one of the promising candidates as flexible electrodes, because they are light, highly conductive, bendable, even can be woven into wearable cloths. However, due to the strong π-π stacking interaction between individual graphene sheets, aggregation or restacking inevitably occurs in the fibers [8], which largely limits their application in supercapacitors that specifically require large surface areas and porous structure [9, 10].

Herein, low cost porous CB/rGO hybrid fibers were fabricated by a very simple, scalable wet-spinning method. Flexible solid-state SCs were assembled using these hybrid fibers and exhibited high capacitance of 97.5 F cm^{-3} and excellent cycling stability. Meanwhile, it maintained excellent physical and capacitive stability under bending deformation, indicating a good flexibility for flexible and wearable applications.

APPROACH

To obtain the hybrid fibers, CB (VXC-72R) and GO were mixed at weight ratios of 0:100, 10:90, 20:80 and 40:60 into distilled water. The mixtures (10 mg ml^{-1}) were sonicated for 2 h and then concentrated to 40 mg ml^{-1} by evaporation in 60 °C water bath. Continuous wet-spinning was carried out on a homemade apparatus. The CB/rGO fibers with 10%, 20%, 40% CB loading contents are respectively named as CB/rGO Fiber-10, CB/rGO Fiber-20, and CB/rGO Fiber-40 hybrid fibers.

RESULTS AND DISCUSSION

The morphology and microstructure of the neat and hybrid fibers were measured by SEM in Fig.1. It is obvious that for the neat rGO fiber without CB, the rGO sheets are packed very tightly due to the π-π interactions (Fig.1a-c). While for CB/rGO hybrid fiber, the rGO sheets were effectively separated apart by CB, forming a hierarchically porous structure (Fig.1d-f). Such an interconnected porous structure could largely increase the accessible surface areas and facilitate the electrolyte ions diffusion between rGO sheets when used as supercapacitor electrode.
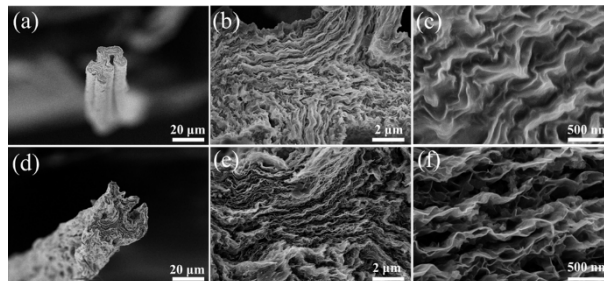

Fig. 1: SEM images of the cross-section of neat rGO fiber (a-c) and CB/rGO-40 hybrid fiber (d-f).
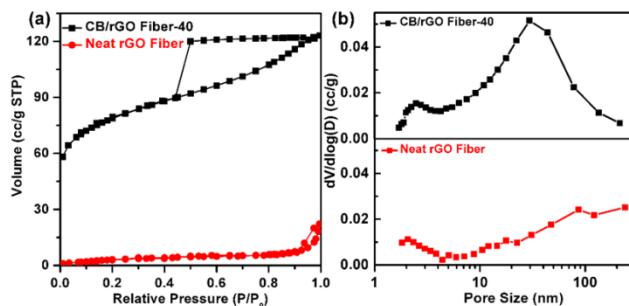

Fig. 2: (a) Nitrogen adsorption-desorption isotherms and (b) pore size distribution of the neat rGO fiber and CB/rGO-40 hybrid fiber.

The specific surface area and microstructures of the obtained fibers were measured using nitrogen adsorption–desorption technique (Fig.2a). The isotherm curve of CB/rGO-40 fiber shows type IV with a hysteresis loop, suggesting the presence of mesopores in the CB/rGO fiber [11], which is constructed by the stacked graphene sheets and CB. The Brunauer–Emmett–Teller (BET) surface area of the CB/rGO-40 fiber was as high as 254.6 m2 g−1. By comparison, the neat rGO fiber showed a lower specific surface area of 13.4 m2 g−1, indicating that the introduction of CB nanoparticles can efficiently prevent the agglomeration of the rGO sheets and form porous structure. The pore size distribution is shown in Fig.2b. Clearly, almost no obvious peaks of mesopores existed in the neat rGO fiber (Fig.2b), which is consistent with the low BET surface area, suggesting the serious restacking of the rGO sheets during drying. The CB/rGO-40 fiber shows a broad pore size distribution of 2-200 nm and two obvious peaks centered at 2.5 and 30 nm, suggesting the presence of mesopores and large pores in the fiber, which is consistent with the SEM images. Such hierarchical structure with high specific surface area and large fraction of mesopores could provide more favorable pathways for electrolyte penetration and more inner area for ion adsorption, thus facilitate the rapid charge-discharge and enhance the capacitance of the fiber electrode.

To explore the electrochemical performance of the porous fibers, all solid-state wire-shaped SCs are fabricated according to the schematic in Fig.3a. As shown in Fig. 3b, the maximum current density and integrated area of the CV curves increases definitely with the loading content of CB at the same scan rate. Fig. 3c shows that all GCD curves are nearly symmetric, demonstrating a typical behavior of double layer SCs. And the charge-discharge time obviously increases with the increasing CB content. The volumetric capacitances clearly increased with the increasing CB weight percentage (Fig. 3d) and the CB/rGO-40 fiber shows the highest capacitance of 97.5 F cm^{-3} at 2 mV s^{-1}, that is appropriately 7 times of the neat rGO fibers (15.3 F cm^{-3}) under the same condition. Furthermore, when the scan rate increases from 2 mV s^{-1} to 500 mV s^{-1}, the capacitance decreases to 48.7 F cm^{-3} corresponding to a retention rate of 50%, which indicates an excellent rate capability. This could be attributed to its small internal resistance (Fig. 3e).
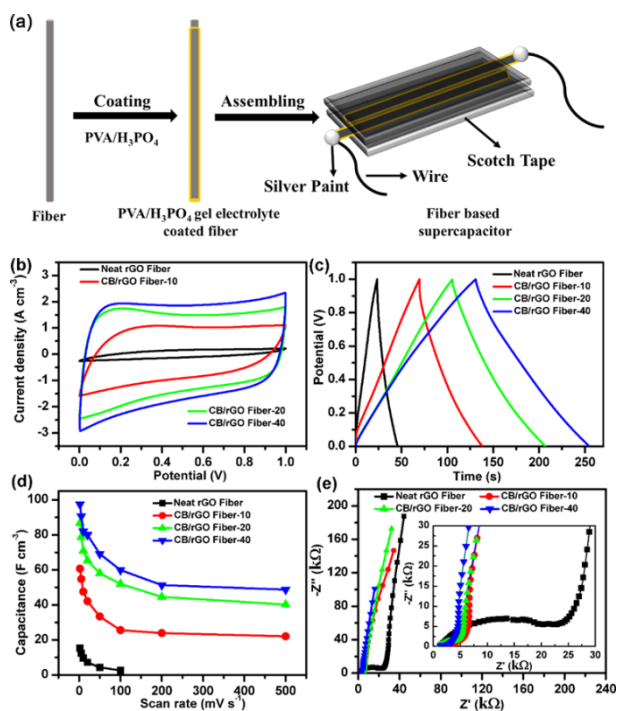

Fig. 3: (a) Scheme of the fabrication process of flexible solid-state supercapacitors based on the fibers. (b-e) Electrochemical performance of the SCs assembled from the neat rGO fibers and CB/rGO hybrid fibers. (b) CV curves at a scan rate of 50 mV s^{-1}. (c) GCD curves at a current density of 0.64 A cm^{-3}. (d) Volumetric capacitance of the SCs at different scan rates. (e) Nyquist plots of the SCs.

The SC based on CB/rGO-40 hybrid fibers was carefully investigated. The capacitance still remained at 95.9% of the initial capacitance after 2000 cycles, demonstrating excellent long-term performance durability (Fig.4a). Furthermore, this SC is high flexibility and electrochemical stability under repeated bending cycles. As shown in Fig.4b, it shows only 2% decay in capacitance after 1000 bending cycles between a bending angle of 0° and 180°.
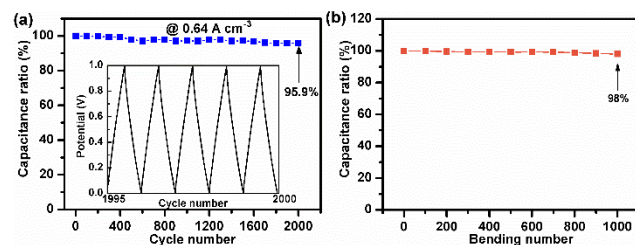

Fig. 4: (a) Dependence of capacitance ratio on the GCD cycle number. Inset: GCD curve after 2000 cycles at 0.64 A cm^{-3}. (b) Capacitance retention during 1000 bending cycles between a bending angle of 0° and 180°.

CONCLUSION

In summary, a very simple and scalable wet-spinning method was developed to fabricate porous CB/rGO hybrid fibers with low cost. By introducing CB as spacers, the restacking of rGO sheets was effectively hindered. The hybrid fibers possess very high surface area and a hierarchically porous nanostructure. A flexible solid-state SC assembled from the CB/rGO-40 hybrid fibers exhibited high single-electrode capacitance and excellent cycling stability. It also well maintained its physical shape and electrochemical performance under long-time periodical mechanical deformation.

ACKNOWLEDGMENTS

REFERENCES

[1] H. Nishide, K. Oyaizu. *Science*, 2008, 319: 737-38.
[2] F. Lufrano, P. Staiti, M. Minutoli. *J Power Sources*, 2003, 124: 314-20.
[3] Q. Cao, H.-S. Kim, N. Pimparkar, J.P. Kulkarni, C. Wang, M. Shim, K. Roy, M.A. Alam, J.A. Rogers. *Nature*, 2008, 454: 495-500.
[4] P. Simon, Y. Gogotsi. *Nat Mater*, 2008, 7: 845-54.
[5] P.J. Hall, M. Mirzaeian, S.I. Fletcher, F.B. Sillars, A.J.R. Rennie, G.O. Shitta-Bey, G. Wilson, A. Cruden, R. Carter. *Energ Environ Sci*, 2010, 3: 1238-51.
[6] C. Meng, C. Liu, L. Chen, C. Hu, S. Fan. *Nano Lett*, 2010, 10: 4025-31.
[7] G. Wang, L. Zhang, J. Zhang. *Chem Soc Rev*, 2012, 41: 797-828.
[8] X. Yang, J. Zhu, L. Qiu, D. Li. *Adv Mater*, 2011, 23: 2833-38.
[9] J. Hu, Z. Kang, F. Li, X. Huang. *Carbon*, 2014, 67: 221-29.
[10] A. Bello, F. Barzegar, D. Momodu, J. Dangbegnon, F. Taghizadeh, M. Fabiane, N. Manyala. *J Power Sources*, 2015, 273: 305-11.
[11] H.-F. Ju, W.-L. Song, L.-Z. Fan. *J Mater Chem A*, 2014, 2: 10895-903.

Fabric Waste Applied to Low-cost Subsurface Irrigation

Nicéa R. do Nascimento[1], Luísa R. B. S. Salvado[2], Francisco Fechine Borges[3], Giovanni M. de Holanda[4]
[1]UBI/Portugal; [2]UBI/Portugal; [3]IFPB/Brazil; [4]Independent Researcher
rita.salvado@ubi.pt

This paper abstract describes in general lines the PETI-BR Project: a very low-cost subsurface textile irrigation system based on reuse of PET bottles and synthetic textile waste. The solution proposed by this project aims at helping rural families in areas with problems of water scarcity and mitigating the indiscriminate disposal of PET bottles and textile waste, mainly synthetic ones.

INTRODUCTION

Throughout the rural area of the Brazilian semiarid region, it is very welcome a low-cost technology accessible to small farmers, which allows optimizing the use of water for irrigation. Such a possibility is specially important regarding food producing for family consumption and sale of surplus.

In addition to this scenario of serious scarcity, there is the indiscriminate disposal of PET bottles and textile waste. Despite it being a global problem, Brazil accumulates about two million tons per year of this waste material.

Companies of the clothing and textile industry located in the Northeast of Brazil face high costs and logistical difficulties for the reuse of synthetic textile waste, mainly due to the big distance to the recycling factories located in the South and Southeast of the country.

In this context, a new solution has been identified: the development of "tapes" for subsurface textile irrigation using synthetic textile waste. The idea is to provide a low-cost subsurface irrigation system based on reuse of PET bottle working as small water tanks connected to capillary "tubes" made with synthetic textile waste.

So, **PETI-BR** (**PE**T Subsurface **T**extile **I**rrigation—**BR**azil) was conceived by focusing on reuse of PET bottles and synthetic textile waste from the textile and clothing industry of Brazilian semiarid region that mostly end up in dumps and landfills. This solution allows building a very low-cost subsurface irrigation system, suitable mainly for the production of roots as cassava and sweet potatoes, which are fundamental for food and feed in semiarid regions. PETI-BR is inspired on Soda Bottle Wick Irrigation [1], with two major differences: the wick is based on fabric waste and the bottles are buried upside down, which allows to see the water level in the bottles at the ends.

THE BENEFICIARIES

There are innumerable groups worldwide which can be favoured by PETI-BR solution, including those located in arid regions and/or in countries affect by poverty. Although there is huge demand, we initially concentrate on the Brazilian semiarid region, which is affected by prolonged droughts and covers 980,000 km^2 of area, comprising 1,133 municipalities. It is considered the most populous semiarid region of the world – about 22 million people live there [2].

Regarding to social indicators, about 58% of the poor population of the country lives in semiarid. The Human Development Index (HDI) is considered low in 82% of its municipalities (below 0.65). Ten million people has no income or depend exclusively on government benefits.

In semiarid region, rains are very irregular, both temporally and spatially. In addition, there is a high rate of evaporation (about 3,000 mm/year), which greatly exacerbates the problem of water availability, causing the population need equipment for rainwater storage, such as tanks and reservoirs.

Sixty-seven percent of rural households in the semiarid region have no access to water supply network. Such a fact significantly reduces the possibility of production of food for consumption. This population needs, therefore, a method of irrigation for family farming that is efficient, use minimal water and has low implementation cost.

THE PETI-BR APPROACH

Essentially, PETI-BR is a solution for deploying a low-cost subsurface textile irrigation system. PETI-BR system is composed of reused PET bottles, buried upside down, interconnected by pieces of hose and having synthetic fabric strips placed between the inside part of the bottle and the ground to be irrigated. Figure 1 shows details of this assemblage.

Figure 1: PETI-BR's unit: a 2-litre PET bottle and fabric strips.

When filled with water, synthetic fabrics become a wet wick due to the capillary phenomenon, which allows wetting the soil around them. Thus, crops cultivated on these locations

will be irrigated with optimal amount of water, at the roots level, significantly reducing losses by evaporation.

The advantages of subsurface textile irrigation systems like PETI-BR are:

• Deposition of water and fertilizer directly in the root zone;
• Greater uniformity of moisture;
• Save in terms of water, fertilizer and energy;
• The lateral run-off and evaporation are almost null;
• Elimination of salt accumulation, reduction of superficial weeds proliferation and of system maintenance costs;
• Elimination of external agents influencing irrigation;
• And finally, facilitate handling and cooling the root zone [3].

The idea is that PETI-BR will be manufactured by rural or women's cooperatives in Brazilian semiarid region, like Women's Textile Cooperatives (WTCs) and Cooperatives of Garbage Collectors (CGCs), ensuring extra income for their families. Several cities in the interior of the Brazil's Northeast, a semiarid region, already have production centres of fabrics and clothing, often organized as WTCs. Thus, there is favourable conditions to recruit potential people to be trained to manufacture the PETI-BR system. Moreover, the textiles supply chain already exists and can be used in the devices production.

There are several cooperatives of garbage collectors that can provide the PET bottles and textile waste. The WTCs will be trained and may function as the organizational structure for production, coordinating the sewing women and handicrafters workforce, and organizing the distribution channels. These channels should provide/sell the product to the users as well as guidance for installation and use. Moreover, the end user may be trained to produce her/his own PETI-BR irrigation system.

The WTCs and CGCs should obtain funds for investments (only trainings) and for supporting the operative costs (production kits) and the production costs (materials and workforce). The funds may be obtained from financial institutions (with financing for appropriate and grassroot technologies) or preferentially as donation from companies with social programs. In this manner, the devices might be subsidized or gratuitously distributed to the population.

RESULTS
The Project has successfully completed the design and functionality examination phases, and validation in field has started. Initial tests conducted at the city of São Raimundo Nonato (Piauí – Brazil) and at the city of João Pessoa (State of Paraíba – Brazil) during the last 3 months of 2015 showed promising results for the production of cassava, as shown in Figure 2.

The variable costs per standard unit of PETI-BR (10 meters of length) are really very low. Considering the main material is waste reused (PET bottle, capacity of 2 – 3 litres; 10 meters of ½" plastic hose recycled; 30 pieces of synthetic fabric, with 1 m x 10 cm), other accessories cost about US$ 5.00, including PVC glue, plastic Tee and plastic elbow. The workforce to manufacture the standard unit is initially

estimated on US$ 5.00. Consequently, the total variable cost per 10 meter - unit is US$ 10.00, or US$ 1.00 per meter.

Figure 2: PETI-BR system and installed in a site for cultivating a cassava crop.

CONCLUSION
PETI-BR is an appropriate technology, low-cost/low-priced and focused on social and humanitarian programs. It should be understood as a non-profit enterprise and the devices can be manufactured by the community in which it will be used. It has no moving parts and the manufacturing process is very simple. The production materials can be easily obtained, even in small towns. It is not necessary power for operation. PETI-BR also contributes to the reuse of materials, contributing to sustainability. Finally, PETI-BR is a grassroot technology and can be made and used by anyone.

FUTURE WORK
The next step is validated the Project in the field experience that is being carried out with cassava crops, and compare the results with conventional irrigation techniques. It is expected to use efficiency indicators in terms of water save, productivity and ecological footprint.

KEYWORDS
Fabric waste, subsurface textile irrigation system, semiarid, sustainability, grassroot technology.

REFERENCES
[1] Informal Urban Communities Initiative. "Soda Bottle Wick Irrigation." Available on http://sqwater.be.washington.edu/wp/irrigation-system/. Web. 2016.

[2] Asabrasil. "Semiárido." 2015. Retrieved from http://www.asabrasil.org.br/Portal/Informacoes.asp?COD_MENU=105.

[3] De la Concha Vázquez, & Masó Marcet. "Irrigação Enterrada nas Uvas." 2015. Retrieved from http://poritex.com.br/irrigacao_uvas.htm.

Preparation and Characterization of Flame Retardant PLA Fibers with Phosphorus-containing Flame Retardant

Senlong Yu, Hengxue Xiang, Jialiang Zhou, Meifang Zhu
State Key Laboratory for Modification of Chemical Fibers and Polymer Materials,
College of Materials Science and Engineering, Donghua University, Shanghai, China
yusenlongzmf@163.com

INTRODUCTION

The bio-based biodegradable materials have been regarded as one of the optimal substitutes for petroleum-based polymers due to the energy shortages and environmental pollution. Poly (lactic acid) (PLA), as the typical example of renewable and degradable polyesters, has been widely applied in many fields because of its excellent biodegradation, superior mechanical properties, etc. [1-4]. Unfortunately, PLA is flammable due to its own intrinsic molecular chain structure and elements. Up to now, the most common way to improve the flame-retardant property of PLA is melt blending [5-13]. Most of the existing flame-retardant PLA products are plastics and seldom involve with the fibers. Since the spinnability of PLA will be sharply deteriorated with the introduction of flame retardants. In this work, we presented an appropriate method to prepare FR-PLA fibers with low flame retardant loading by melt spinning. The thermal stability, combustion performance, char residues structure, mechanical property of fibers were investigated.

APPROACH

The fibers were prepared by melt spinning: 1. Preparation of FR-PLA masterbatch: 70 wt.% PLA (Mn=1.6×10^5, PDI=1.2) and 30 wt.% OP (melt point=176.4 °C) were blended at 200 °C and then pelletized in a twin screw extruder pelletizer; 2. Preparation of FR-PLA fibers: the calculated neat PLA and FR-PLA masterbatch were dried at 100 °C for 8h before melt spinning. The spinneret temperature were 235 °C, 230 °C, 227 °C and 223 °C for neat PLA, 6OP/94PLA, 8OP/92PLA and 10OP/90PLA, respectively.

RESULTS AND DISCUSSION

Thermal stability of fibers was investigated by TGA test (Fig. 1). The temperature of maximum decomposition rate of FR-PLA is higher than that of neat PLA, which proves that the thermal stability of FR-PLA is significantly improved by OP. Furthermore, the weight percent of char residue at 700 °C of FR-PLA is much higher than neat PLA, which indicates that OP could promote the charring of PLA during combustion.
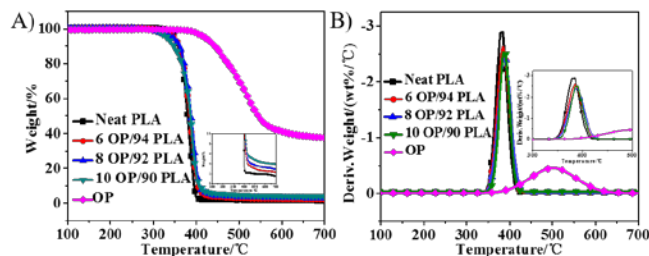

Fig. 1. TGA (A) and DTG (B) curves of fibers in nitrogen.

The flammability of fibers was evaluated by LOI and UL-94 tests (Fig. 2A). Compared to 20.5 % of neat PLA, the LOI value goes up to 27.3 %, 28.6 % and 29.7 % with the addition of 6 wt.%, 8 wt.% and 10 wt.% OP in PLA. Besides, the UL-94 grade can pass V-0 by the presence of 10 wt.% OP. The combustion process of samples in air is shown in the Fig. 2B. Compared with neat PLA, all the FR-PLA samples exhibit self-extinguishing phenomenon and the cotton can't be ignited by the drippings.
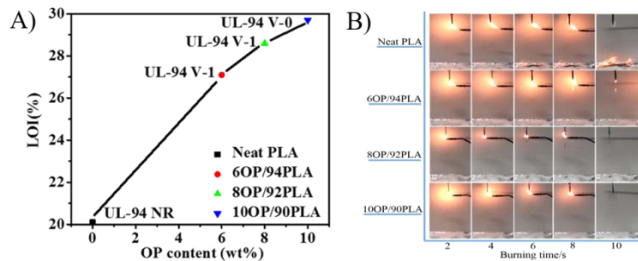

Fig. 2. Flame retardant property (A) and combustion behavior (B) of neat PLA and FR-PLA fibers.

The surface morphology of char residues was investigated by SEM (Fig. 3A). For neat PLA, the residue is a fragmental char layer with numerous flaws and pores. While the residues of FR-PLA are much more compact, which effectively improves the flame retardance of PLA.

Raman was used to investigate the graphitic degree of char residues (Fig. 3B). Generally speaking, the lower ratio of I_D/I_G signifies the better flame retardance, I_D and I_G are the integrated intensities of the D and G band [14-16]. As shown in Fig.3B, the I_D/I_G ratio follows the sequence of neat PLA (2.64) > 6OP/94PLA (2.62) > 8OP/92PLA (2.53) > 10OP/90PLA (2.50). It's clear that the results of LOI and UL-94 correspond with the SEM and Raman analysis.
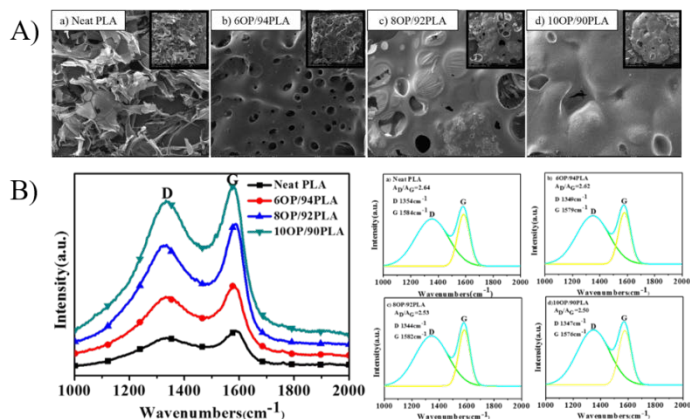
Fig. 3. The SEM micrographs (A) and Raman spectra (B) of the char residues collected after TGA experiment.

The result of mechanical property test was shown in the Fig. 4. The breaking strength of PLA fibers decreases from 3.3 cN/dtex to 2.3 cN/dtex, as the increasing of OP content from 0 to 10 wt.%. This might be because that the regularity and crystallinity of PLA are destroyed by OP, which will finally affect the breaking strength.
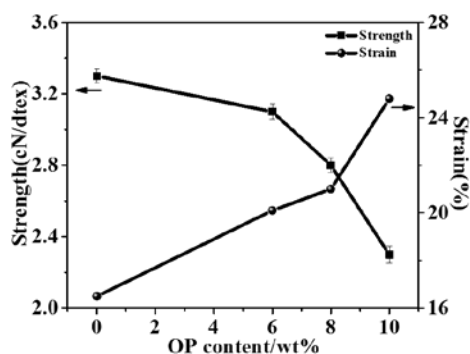

Fig. 4.The mechanical property of fibers.

CONCLUSION

The neat PLA and FR-PLA fibers with different OP content were prepared by melt spinning. The results of TGA showed that the addition of OP could significantly improve the thermal stability of PLA. The LOI and UL-94 tests revealed that OP could effective inhibit the burning of PLA. The SEM and Raman analyses suggested that the density of char residue and graphitization degree increased with the addition of OP, which were considered as the key points to improve the flame retardance and anti-dripping performance of the PLA. However, the breaking strength of PLA fibers decreased from 3.3 cN/dtex to 2.3 cN/dtex with the increasing of OP from 0 to 10 wt%. Hence, the future work is to improve the mechanics performance of FR-PLA and the organic/inorganic hybrid technology may be an ideal choice.

KEYWORDS

Poly (lactic acid), polysulfonyldiphenylene phenyl phosphonate, melt spinning, flame-retardant fiber.

REFERENCES

1. G. Donald. *J. Polym. Environ.*, 2001, 9: 63.
2. A. Bhatia, R. Gupta, S. Bhattacharya, H. Choi. *Korea-Aust. Rheol. J.*, 2007, 19: 125.
3. A.J.R. Lasprillaa, G.A.R. Martineza, B.H. Lunellia, A.L. Jardinia, R.M. Filhoa. *Biotechnol. Adv.*, 2012, 30: 321.
4. H.L. Luo, G.Y. Xiong, Q.Q. Li, C.Y. Ma, Y. Zhu, R.S. Guo, Y.Z. Wan. *Fiber. Polym.*, 2014, 15: 2591.
5. J. Gong, N. Tian, X. Wen, X. Chen, J. Liu, Z. Jiang, E. Mijowska, T. Tang. *Polym. Degrad. Stabil.*, 2014, 104: 18.
6. P. Jiang, X.Y. Gu, S. Zhang, J. Sun, R.W. Xu, S. Bourbigot, S. Duquesne, M. Casetta. *Polymer*, 2015, 79: 22.
7. H. Lin, S. Liu, L. Han, X. Wang, Y. Bian, L. Dong. *Polym. Degrad. Stabil.*, 2013, 98: 1389.
8. S. Li, J. R. Jie, H. Yuan, T. Yu, W. Yuan. *Polym. Int.*, 2010, 59: 242.
9. H. Lin, L. Han, X Wang, Y. Bian, Y. Li, L. Dong. *Polym. Adv. Technol.*, 2013, 24: 576.
10. M. Shabanian, N. Kang, D. Wang, U. Wagenknecht, G. Heinrich. *Polym. Degrad. Stabil.*, 2013, 98: 1036.
11. J. Zhan, L. Song, S. Nie, Y. Hu. *Polym. Degrad. Stabil.*, 2009, 94: 291.
12. X. Liu, D. Wang, X. Wang, L. Chen, Y. Wang. *Polym. Degrad. Stabil.*, 2013, 98: 1731.
13. R. Zhang, X. Xiao, Q. Tai, H. Huang, J. Yang, Y. Hu. *J. Appl. Polym. Sci.*, 2013, 127: 4967.
14. Y. Zhang, Y. Ni, M. He, X. Wang, L. Chen, Y. Wang. *Polymer*, 2015, 60: 50.
15. W. Yang, W, Sun, W. Chu, C. Jiang, J. Wen, Chin. *Chem. Lett.*, 2012, 23: 363.
16. Z. Chen, L. Zhao, Z. Wang. *Polymer*, 2013, 54: 5182.

Study of Mechanical Properties on PA-6 Electrospun Nanowebs Substitution Membrane and Diaphragm Tissue

Elham Mohsenzadeh[1], Nabyl Khenoussi[1], Laurence Schacher[1], Dominique Adolphe[1], Neda Shah Hosseini[1], Amir Houshang Hekmati[2], Christiane Wagner-Kocher[1,6], Joseph Hemmerlé[3], Anne Schneider[3,4], Nadia Bahlouli[5]

[1]Laboratoire de Physique et Mécanique Textiles, EA 4365 – UHA Mulhouse, France
[2]Department of Textile Engineering, Faculty of Engineering, South Tehran Branch, Islamic Azad University, Tehran, Iran
[3]Institut National de la Santé et de la Recherche Médicale, UMR S 1121– INSERM Strasbourg, France
[4]Service de Chirurgie Pédiatrique-Hôpitaux Universitaires de Strasbourg – Strasbourg, France
[5]Laboratoire des sciences de l'ingénieur, de l'informatique et de l'imagerie, UMR 7357 ICUBE – Strasbourg, France
[6]Laboratoire de Mécanique et Génie Civil – LMGC, Université de Montpellier – Montpellier, France

elham.mohsenzadeh@uha.fr

STATEMENT OF PURPOSE

Diaphragm is composed of a peripheral part (muscular fiber) and a central part (tendon). The tendon is the upper part of the diaphragm, in contact with the lungs and is closer to the front than to the back of the thorax, so that the posterior muscular fibers are longer. The central tendon is composed of several planes of fibers, whose arrangement gives strength and rigidity to the membrane (1-3). In this study a comparison between the tensile mechanical properties of tendon part of diaphragm and electrospun PA-6 nanofibers has been done.

INTRODUCTION

Diaphragm is the main breathing muscle in the body which is convex from the top and concave from the bottom. Its location depends on the respiration, body and viscera position. It is a dome shaped membrane divided into two sides made of both muscles and tendons which function as a barrier between the thoracic cavity and the abdominal cavity. Through the diaphragm there is a passage between these two cavities by three large holes such as aortic, esophageal and caval opening (3-4). A bottom view of diaphragm surface is shown in figure 1.
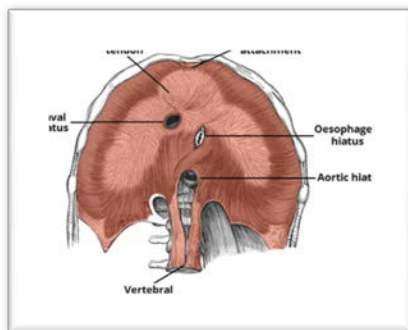

Figure 1. Bottom view of diaphragm (three openings) (3).

The diaphragm formation takes place between the fourth week and the third month of pregnancy. Congenital diaphragmatic hernia (CDH) is a rare defect that occurs while the baby is developing in the womb and it affects about 1 in every 2,500 babies. In the diaphragmatic hernia, the abdominal organs such as the stomach, small intestine, spleen, part of the liver and the kidney may take up part of the chest cavity. This process prevents the lungs from growing normally. Depending on the period in which the embryonic anomaly occurs, the consequences and therefore the type of diaphragmatic hernia will be different. There are several forms of diaphragmatic hernia according to the location and size of the defect. There is a common problem for all types of hernias: pulmonary hypoplasia which will alter the patient's respiratory system. The main goal of treatment is to move abdominal organs from the chest cavity back to the abdominal cavity. This hole can be closed by a simple suture, or may require in many cases prosthetic replacement. There are several types of membrane which can be used as prostheses (4). The goal of this research is to simulate the mechanical properties of electrospun PA-6 nanofibers to tendon part of diaphragm to use them as prosthesis for hernia treatment. Tensile features of electrospun PA-6 nanofibers with different times of the electrospinning as prosthetics membrane are compared with the tensile properties of tendon part of diaphragm.

EXPERIMENTAL

This research is based on the experiment that has been done previously in our Laboratory and Icube. Electrospinning of Polyamide-6 due to its good mechanical and physical properties with 3 different times of electrospinning (3,6 and 9 hours of electrospinning) by using single needle electrospinning machine was done. The average fiber diameter was calculated from 30 single nanofibers in each photo by ImageJ software from the images obtained by (Scanning Electron Microscopy) SEM. The process of electrospinning was done in the conditions which are shown in table 1.

Table 1. The electrospinning parameters for PA-6.

Concentration	20 wt.%
Applied voltage	30 kV
Distance	17 cm
Feed rate	0.1 ml/h
Temperature	28 °C
Needle diameter	0.4 mm

The fresh pork diaphragm (right and left side) was taken from Strasbourg Hospital and the mechanical test has been carried out on fresh samples. Mechanical test on pork's

diaphragm has been done in order to obtain a mechanical idea of feasible and the nearest case to human diaphragm. MTS machine was used for uniaxial tensile test on electrospun nanowebs and tendon samples. This machine consists of two grips for holding the sample and a loading cell. The uniaxial tensile test condition has been written in table 2.

Table 2. Tensile test condition.

Load-cell capacity	100 N
Elongation rate	10 mm/min
Sample dimension	10×25 (mm)^2
Temperature	$20 \pm 2°C$
RH	$65 \pm 2\%$

All of the electrospun nanoweb and tendon samples were cut with the same dimension of 10×25 (mm)^2. Tendon samples were cut from right and left side of the diaphragm, vertically and horizontally based on the tissue direction and they kept moist with sterile water to maintain certain moisture during the experiment until they were put to the tensile machine. To keep the samples stronger between the grips different types of frames were tested.

RESULTS AND DISCUSSION

The samples were categorized by their cutting direction (vertically or horizontally) based on tendon fiber direction and their location on diaphragm (right or left side) to make the result compression easier. The uniaxial tensile test was done for each sample and from obtained data the force-strain% curve of each test was traced. Then the maximum force and strain% was noted at rupture point and samples' behavior during the tensile test was observed. Double-faced sandpaper frame with water proof backing was selected as the best frame to avoid slipping the samples from the grips during the test. The same method was used to investigate mechanical properties of electrospun PA-6 nanofiber samples with 3, 6 and 9 hours of electrospinning time. Table 3 gives a summarized view of mechanical resistance of pork's tendon and PA-6 electrospun nanofibers which have been obtained from the above presented tests.

Table 3. Interval force and strain % of each sample.

	Side/ Time	Interval Force (N)	Interval Strain %
Vertically Tendon	Right	(7.6-16.3)	(32.7-49.9)
	Left	(10.1-22.2)	(15.4-52.5)
Horizontally tendon	Right	(13.1-17.7)	(27.3-42.6)
	Left	(8.7-16.6)	(46.1-52.2)
PA-6 Electrospun samples	3h	(11.5-23.1)	(4.1-10.8)
	6h	(15.5-18.2)	(7.5-8.2)
	9h	(16.1-18.2)	(5.7-9.1)

As the result shows mechanical study on pork's diaphragm revealed that its left and right side shows approximately same mechanical properties. The cut direction of tendon (vertical or horizontal) does not have a significant effect on mechanical properties. The comparison between mechanical results of tendon and electrospun nanofibers shows, 3h electrospun PA-6 nanofibers are close to tendon in the level of interval force.

FUTURE WORK

As future work we will concentrate to produce more elastic nanowebs which can simulate better mechanical properties of tendon part of diaphragm.

KEYWORDS

Electrospinning, Soft tissue, Tendon, Congenital diaphragmatic hernia (CDH), Uniaxial tensile test

REFERENCES

1) Saadé, J., Ladjal, H., Behzad, S., Beuve, M., Azencot, J. "Modélisation biomécanique du diaphragme humain: du CT-4D au modele du mouvement." *Reconnaissance des Formes et Intelligence Artificielle*, 2012: 978-2.
2) Rehan, V.K., Laiprasert, J., Wallach, M., Rubin, L.P., McCool, F.D. "Diaphragm dimensions of the healthy preterm infant." *Pediatrics*, 2001, 108(5): e91-e91.
3) Turgeon, J., Bernard-Bonnin, A-C., Gervais, P., Ovetchkine, P., Gauthier, M. *Dictionnaire de Thérapeutique Pédiatrique Weber*. 2nd Ed. DeBoeck, 2008. 1490.
4) Craighero, S., Promayon, E., Baconnier, P., Lebas, J. F., Coulomb, M. "Dynamic echo-planar MR imaging of the diaphragm for a 3D dynamic analysis." *European Radiology*, 2005, 15(4).

Highly Oriented Nanofibers Produced by Electrospinning

Neda Shah Hosseini[1], Nabyl Khenoussi[1], Laurence Schacher[1], Dominique Adolphe[1], Amir Houshang Hekmati[2], Yann Heitter[1], Jean Beyer[1]

[1]Laboratoire de Physique et Mécanique Textiles EA 4365 – UHA Mulhouse, France

[2]Department of textile engineering, Faculty of Engineering, South Tehran branch, Islamic Azad University, Tehran, Iran

neda.shahoseini@gmail.com

STATEMENT OF PURPOSE

This project consists of production of Polyamide-6 (PA-6) nanofiber with patterned structure by using novel collectors in electrospinning. These collectors (under patent process) will allow producing both oriented and non-oriented nanofibers in one scaffold for biomedical applications. These static collectors make it possible to have different nanofibers' structure and produce tunable oriented electrospun nanofibers scaffolds.

INTRODUCTION

Improving the organization of patterned scaffold helps to provide a better structure which mimics the native Extra Cellular Matrix (ECM) environment [1]. Electrospinning is one of the most utilized techniques to produce electrospun mats in nanoscale diameters with different morphologies and structures of nanofibers. In this process, a positively charged polymer solution jet is drawn through a needle by applying a high voltage electrostatic force, then nanofibers are collected over a grounded metallic collector. In electrospinning process collectors have a very important role to change the structure of nanofibers in the nanoweb. Usually, in the electrospinning process, the nanofibers are collected randomly on the flat collectors. [2] Different collector types with different designs such as static plate, rotating drum, parallel electrode, rotating disc, etc. which have been developed [3, 4]. Depending on collector type, nanofibers orientation can be changed from totally random to highly oriented arrangement [5, 6].

Generally, collectors are divided into two groups, static and rotating collectors. Rotating collectors are mostly based on rotating drum or rotating disk. To use rotating collector in electrospinning process, mandrel must be in the very high speed up to thousands of rpm. Hence, fiber breakage might be occurred. Moreover, the difficulty of detaching the mat and the presence of extra rotating engine can be problematic in the whole process. On the other hand, static collector because of the electrostatic field profile, the jet stretches itself across the gap towards the electrodes which may leads to produce aligned nanofibers. The advantages of these collectors over rotating collectors are easy detachment of mat from the collector and achievement of aligned and unidirectional oriented fibers.

Laboratory of Textile Physics and Mechanics (LPMT) of the University of Haute Alsace has been focused on nanofibers' orientation and structure for several years. In the previous work, it has been demonstrated the potential of 3D printing technology when it is combined with an electrospinning method to produce highly oriented 3D polymeric scaffolds in nanoscale diameter as a novel method. [7] In this work, a new method is investigated to produce highly oriented nanofibers using patterned collector as a new method which is under the patent process.

MATERIALS AND METHODS

Scaffold fabrication

The polymeric solution is composed of PA-6 and formic acid as a solvent. The 20 wt% concentration solution was stirred magnetically for at least 24 hours at 50 °C. Fabrication of advanced collectors using new method was done. Afterwards, PA-6 (20 wt%), with the mentioned parameters reported in table I, was electrospun over the patterned collectors by electrospinning machine designed and built in LPMT [8]. The patterned scaffolds on the collectors were achieved with an average fiber diameter of 200 nm. The morphological properties of nanofibers in the produced scaffolds were examined by SEM and ImageJ software on the basis of 30 measurements.

Table I. The electrospinning parameters for PA-6 20 wt% on the patterned collectors.

Concentration (wt %)	20
Applied voltage (kV)	30
Distance (cm)	20
Needle gauge (mm × mm)	0.45
Feed rate (ml/h)	0.1
Average diameter (nm)	200

The electrospinning was performed on the fabricated collector and the morphological characterization was investigated. To estimate the local orientation of nanofibers, ImageJ software has been used. It evaluates the local orientation and isotropic properties such as coherency of every pixel of the image. The coherency parameter C is defined as the ratio between 0 and 1, with 1 indicating highly oriented structures and 0 indicating isotropic areas.

RESULTS AND DISCUSSION

SEM micrographs presented in Fig. 2 shows the morphological properties of nanofibers and their structure in the produced scaffold. The images clearly present the oriented and non-oriented parts in the scaffold. The results show that structured collectors allow

producing nanowebs templates made of nanofibers with alternative pattern of oriented and non-oriented area.
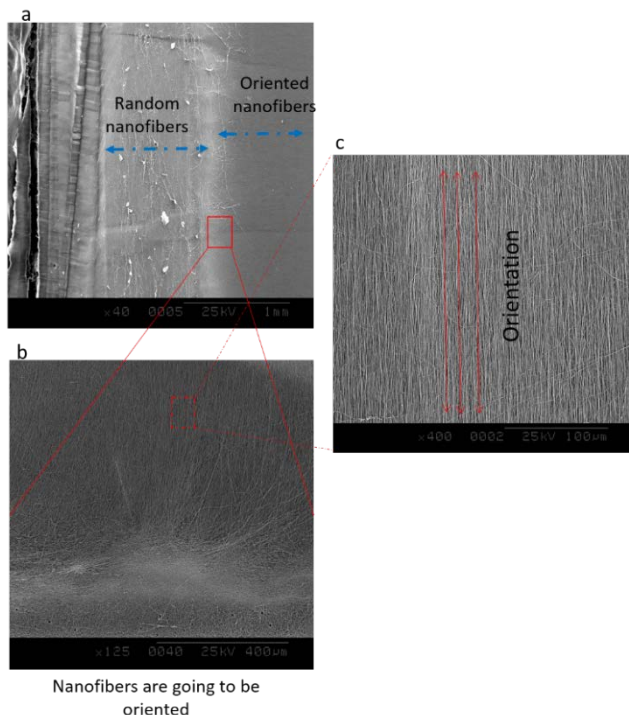

Figure 1. Oriented and non-oriented parts 40X (a), magnification 125X (b), and oriented nanofibers (c).

According to the orientation measurement results obtained thanks to by ImageJ software, the feasibility of a new generation of collector to obtain highly oriented nanofibers has been proven, presented in table II.
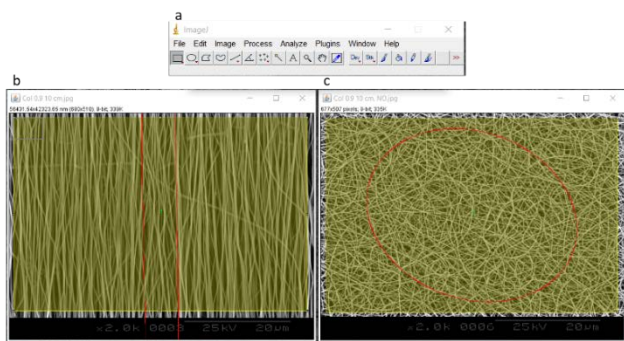

Figure 2. ImageJ analysis, significant differences between two parts in a sample.

Fig. 2 presents two different parts in the same sample which proves the significant difference in the case of orientation. The oriented nanofibers are mostly organized at the angle of 89.12° with coherency of 0.948 which is near 1. On the contrary, the coherency of random nanofibers on the other part, is approximately 0.1, as it is presented in table II.

Table II. orientation and coherency of produced random and oriented nanofibers.

Patterned collector	Orientation	Coherency
Oriented nanofibers	-89.12°	0.948
Random nanofibers	-19.79°	0.127

According to the recent studies, achieving these rate of orientation with the static collector is promising for the targeted application.

CONCLUSION

This work has investigated the potential of a new generation of collectors in the electrospinning process to produce highly oriented nanofibers in electrospun nanoweb. The obtained results without using any dynamic collectors in the terms of orientation is unique and promising.

KEYWORDS
Electrospinning, Nanofibers, Polyamide 6, Orientation, imageJ

REFERENCES
[1] Li, Wan-Ju, et al. "Electrospun nanofibrous structure: a novel scaffold for tissue engineering." *Journal of Biomedical Materials Research*, 2002, 60.4 (20: 613-21.
[2] Vaquette, Cedryck, Cooper-White, John Justin. "Increasing electrospun scaffold pore size with tailored collectors for improved cell penetration." *Acta Biomaterialia*, 2011, 7.6: 2544-57.
[3] Teo, W.E., Ramakrishna, S. "A review on electrospinning design and nanofibre assemblies." *Nanotechnology*, 2006, 17.14: R89.
[4] Shah Hosseini, N., Bölgen, N., Yetkin, D., Yılmaz, N.Ş, Khenoussi, N., Adolphe, D., Heitter, Yann, Hekmati, A.H., Schacher, L. "Novel Patterned 3D Electrospun Scaffolds and Their Effect on Cartilage Cell Attachment." *Biomedical Electrospun Materials & Applications (BEMA) Conference*, Mulhouse, France, December 2014
[5] Lavielle, Nicolas, et al. "Structuring and Molding of Electrospun Nanofibers: Effect of Electrical and Topographical Local Properties of Micro-Patterned Collectors." *Macromolecular Materials and Engineering*, 2012, 297.10: 958-68.
[6] Wu, Yiquan, et al. "Template-assisted assembly of electrospun fibers." *Polymer*, 2010, 51.14: 3244-48.
[7] Shah Hosseini, N., Khenoussi, N., Adolphe, D., Hekmati, A.H., Schacher, L., Bölgen, N. "Producing electrospun 3d scaffold by using 3d collectors for controlling cell response." *Proceedings from The Fiber Society Meeting and Technical Conference*, Philadelphia, Pennsylvania, USA, Fall 2014.
[8] Khenoussi, N., Schacher, L., Adolphe, D.C. "Nanofiber production: study and development of electrospinning device." *Experimental Techniques*, 2012, 36.2: 32-39.

An Approach to Improve the Reduction Process of Vat Dyeing by Sodium Borohydride

Duygu Şenol[1], Mehmet Kanık[2]

[1]Kahramanmaraş Sütçü İmam University, School of Advanced Vocational Studies, Department of Design, Kahramanmaraş, Turkey

[2]Uludağ University, Faculty of Engineering and Architecture, Department of Textile Engineering, Nilüfer, Bursa, Turkey

duygunsenol@ksu.edu.tr

OBJECTIVE

The aim of this study was to investigate improving the conventional Sodium dithionite reduction process which has caused ecological and industrial problems for vat dyeing. For this purpose, the application possibilities of whether Sodium Borohydride is feasible and effective in the reduction (vatting) stage of vat dyeing was researched.

KEYWORDS: Vat dyes, sodium dithionite, sodium borohydride, reduction.

INTRODUCTION

Industrially, vat dyes are the second biggest dye group with 17% after the reactive dye group at 50% in the cellulosic coloration process. The most popular and the oldest vat dye is indigo due to the widely used dyestuff for blue jeans (Bozic and Kokol 300, Preston 224, Kulandainathan et al. 47, Xin et al. 260, Bechthold et al. 135).

Vat dyes provide excellent fastness properties which can't be achieved by any other dye processes, particularly to washing, light, and chlorine bleaching. Vat dyes are used for all industries where the highest fastness is required like workwear, uniforms, and furnishings etc. Additionally, dyeing is a complicated process (Fig. 1) which includes reduction and oxidation mechanisms (Waring and Hallas 74).
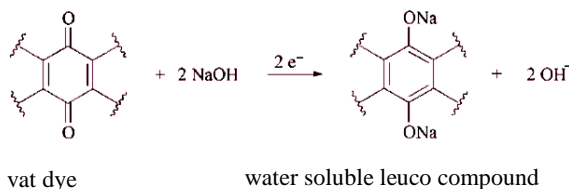

Figure 1. Reduction process of vat dye in an alkaline medium

Vat dyes are applied as a water soluble leuco form by a reduction process in a high alkaline medium (pH 11-14) to the fabric conventionally, which is applied substantively to cellulosic fiber. Following this, the dye is reoxidized with atmospheric oxygen to an insoluble pigment form in the fiber (Kulandainathan et al. 143).

Commercially, Sodium dithionite ($Na_2S_2O_4$) is the most powerful reducing agent for industrial vat dyeing processes due to the economic aspects of a short fixing time and good levelness properties for continuous dyeing. However, Sodium dithionite is decomposed oxidatively and thermally rapidly (Fig 2.), so this causes more stoichiometric requirements of dithionite for the process, poor reproducibility of dyeing, and toxic by-products (Bozic and Kokol 299, Meksi et al. 149).

$$2Na_2S_2O_4 + H_2O \longrightarrow Na_2S_2O_3 + 2NaHSO_3$$
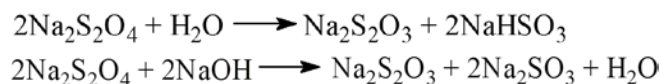$$2Na_2S_2O_4 + 2NaOH \longrightarrow Na_2S_2O_3 + 2Na_2SO_3 + H_2O$$

Figure 2. Decomposition reactions of Sodium dithionite in an alkali and aqueous medium (Preston 224).

Recently, a few investigations have been reported that the Sodium dithionite process can be replaced by metal catalyzed sodium borohydride ($NaBH_4$) and the borohydride process provides high color yields (K/S) depending on the amount of catalyst and temperature of the dye bath (Meksi et al. 187).

RESULTS AND DISCUSSION

In this investigation, comparative studies between conventional Sodium dithionite and Sodium Borohydride (SBH) reduction processes were carried out by measuring the redox potential of dyebath, color yield (K/S), and fastness properties of cotton fabrics dyed with vat red 14, vat blue 66, and vat orange 9. The results show that Sodium borohydride is not sufficient alone for the vatting (reduction) step of dyeing. For this reason, SBH was applied with different concentration rates of Sodium dithionite (Sodium dithionite/SBH 5:0; 5:0.5; 4.5:0.5; 4:1; 3.5:1.5; 3:2; 2:3; 2.5:2.5; 1,5:3,5; 1:4; 0.5:4.5; 0:5 g/l) combinedly and there weren't big differences between wash fastness degrees and K/S values of vat dyes except vat blue 66 as was expected.

On the other hand, wet and dry rubbing fastness which is tended to have poor values for vat dyes, increased 0.5-1 degrees with combined Sodium dithionite and SBH process (4.5:0.5 g/l).

When SBH and Sodium dithionite were combined, the redox potential changed to values more negative than −950 mV during dyeing process. Redox potential results indicate that in the presence of SBH, reduction yield was improved under controlled conditions.

In order to assess the effect of SBH on reproducibility, standard deviations of K/S values of reduction processes were analyzed. Analysis showed that although K/S values are decreased slightly by adding SBH, reproducibility is increased distinctly. It was established that differences of K/S values of Sodium dithionite treatments for 3 vat dyes have big standard deviation values ($\sim\pm2$) compared with the combination of SBH ($\sim\pm0.01$) and sodium dithionite processes.

CONCLUSION

Color yield and fastness properties of vat dyeings with the combined process of Sodium Dithionite/SBH were found that comparing the fastness of dyeings obtained with standard Sodium Dithionite processes was improved.

In addition to the improvement of color and rubbing fastness, the reproducibility disadvantage of Sodium dithionite is eliminated by combining process, which is caused by the economically and ecologically limitations of conventional process. SBH provided a stabilizing effect on the Sodium dithionite compound by means of preparation of Sodium dithionite solutions in situ without hazardous decomposition products at normal temperature and storage conditions (Fig 3.).

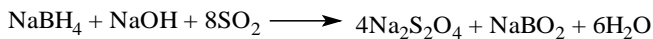$$NaBH_4 + NaOH + 8SO_2 \longrightarrow 4Na_2S_2O_4 + NaBO_2 + 6H_2O$$

Figure 3. Sodium Dithionite preparation with alkali Sodium Borohydride solution in situ (Ko and Lewis 1992).

According to the experimental results, a recipe for vat dyeing would be suggested as follows:

- 2 g/l Dispersing agent
- 3 g/l Levelling agent
- 1 g/l Vat dye dispersing agent
- X g/l Vat dye
- 4.5 g/l Sodium dithionite
- 0.5 g/l Sodium borohydride solution (12%)
  pH was adjusted to 12.8-13

REFERENCES

1. Bechthold, T., Burtscher, E., Kühnel, G., Bobleter, O. "Electrochemical Reduction Process in Indigo Dyeing." *JSDC*, 1997, 113: 135-44.
2. Bozic, Mojca, Kokol, Vanja. "Ecological Alternatives to the Reduction and Oxidation Processes in Dyeing with Vat and Sulphur Dyes." *Dyes and Pigments*, 2008, 76: 299-309.
3. Ko, Jeremy, Levis, Steven H. *High Yield Sodium Hydrosulfite Generation*. US Patent 5,094,833. 1992.
4. Kulandainathan, M., Anbu Patil, Kiran, Muthukumaran, A., Chavan, R.B. "Review of the Process Development Aspects of Electrochemical Dyeing: Its Impact and Commercial Applications." *Society of Dyers and Colourists, Color. Technol.*, 2007, 123: 143-51.
5. Meksi, N., Kechida, M., Mhenni, F. "Cotton Dyeing by Indigo with the Borohydride Process: Effect of Some Experimental Conditions in Indigo Reduction and Dyeing Quality." *Chemical Engineering Journal*, 2007, 131: 187-93.
6. Meksi, N., Ticha, M.B., Kechida, M., Mhenni, F. "Using of ecofriendly a-hydroxycarbonyls as reducing agents to replace sodium dithionite in indigo dyeing processes." *Journal of Cleaner Production*, 2012, 24: 149-58.
7. Preston, Clifford, Ed. *The Dyeing of Cellulosic Fibers*. Dyers' Company Publication Trust, 1986.
8. Xin, J.H., Chong, C.L., Tu, T. "Colour Variation in the Dyeing of Denim Yarn with Indigo." *JSDC*, 2000, 116.9: 260-5.
9. Waring, R., David and Hallas Goeffrey. *The Chemistry and Application of Dyes*. New York: Plenum, 1994.

Hybrid Textile for a Novel Heart Valve Prosthesis Design

Amna Amri, Antoine Vaesken, Frederic Heim

Laboratoire de Physique et Mécanique Textiles (LPMT), ENSISA, Université de Haute Alsace, Mulhouse, France

amna.amri@uha.fr

INTRODUCTION

Trans-catheter (non-invasive) aortic valve implantation has become an alternative technique to surgical valve replacement for an increasing number of patients [1]. However, the biological tissue currently used in clinical practice as valve leaflet material remains expensive to harvest and fragile. Heim et al. showed already in vitro that textile polyester could be an alternative solution to replace valve leaflets. In vivo, it appears that the interaction between fibrous material and living tissues depends highly on the size of the fibers used [2]. Thus, hybrid textile combining fibers of different diameters could provide mechanical resistance and promote favorable tissue-fabric interaction.

The aim of the current work was: (1) to develop an in house force spinning system that allows to produce fine PET non-woven fibers; (2) to design a heart valve combining a PET woven substrate with a non-woven PET layer (3) to assess some important characteristics of the obtained material.

APPROACH

Force spinning

Force spinning is a simple, efficient and a versatile method to produce fine PET fibers. The system developed in house is composed of a motor, an infrared heater, a rotary reservoir with orifice and a collector (Fig.1). The polymer is heated until its melting point. When the chamber rotates, the centrifugal force induces a jet of the heated polymer through the orifice. The polymer viscosity and the rotational speed influence the jet elongation and consequently the fiber diameter. Under the temperature gradient, the jet is solidified and the formed non-woven fibers are deposited on the collector.
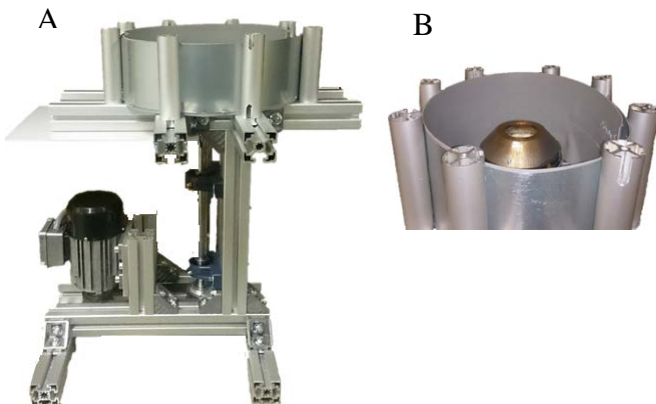

Figure 1. (A) Force Spinning system (B) Upper part of the Force Spinning system: the collector with the rotary reservoir.

Textile hybrid assembling and valve design

A layer of non-woven microfibers obtained with the force spinning system is deposited on the surface of a woven PET substrate (Fig.2). In order to create an adherence between those two layers, the material was first heated while a constant load was applied. Then local melted areas were created using an ultrasonic hand held welding gun.
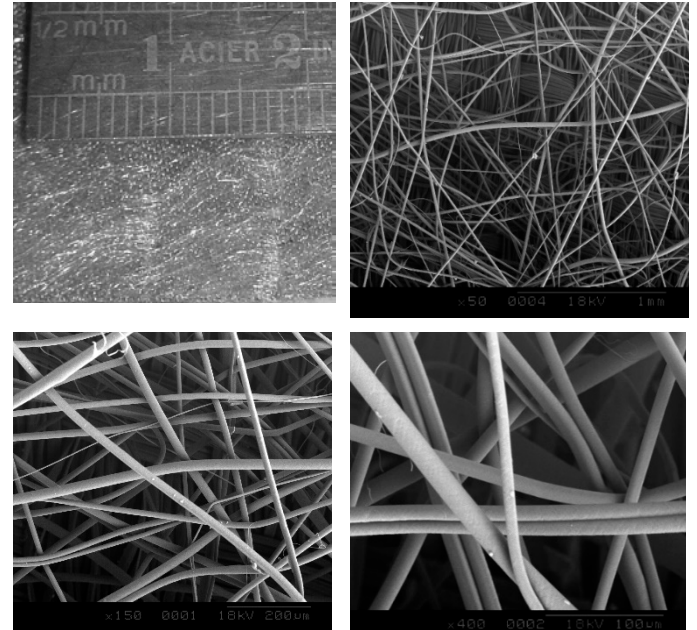

Figure 2. The Hybrid Textile.

Heart valve prototypes (Fig.3) were manufactured according to the procedure already described in a previous work [3].
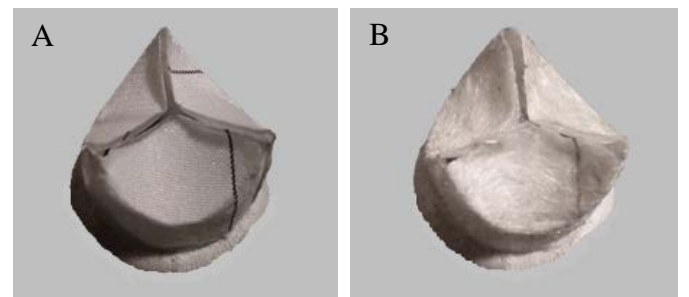

Figure 3. Heart valve prototypes (A) Monolayer Textile (B) Hybrid Textile.

Textile characterization

Characterization tests have been performed in order to assess the influence of the added layer on the following parameters which are critical for the heart valve performances: surface density, roughness, bending stiffness, permeability. Moreover, the valves dynamic regurgitation was assessed in a heart pulse duplicator.

RESULTS AND DISCUSSION

The characteristics presented in table I show that the added non-woven layer of microfibers, besides increasing the textile density, increases the bending stiffness of the valve leaflets and the roughness of their surface.

	Surface density (g/m²)	Bending stifness (mN.cm)	Roughness (µm)
Textile	132,8	0,0014	9,9
Hybrid Textile	147,8	0,0028	26,9

Table 1. Characteristics of the used materials.

Regarding the permeability, figure 4 compares a monolayer textile with a hybrid textile. One can observe that for the hybrid textile, the permeability is slightly reduced (by 7% on average). This leads to less regurgitation for the valve.
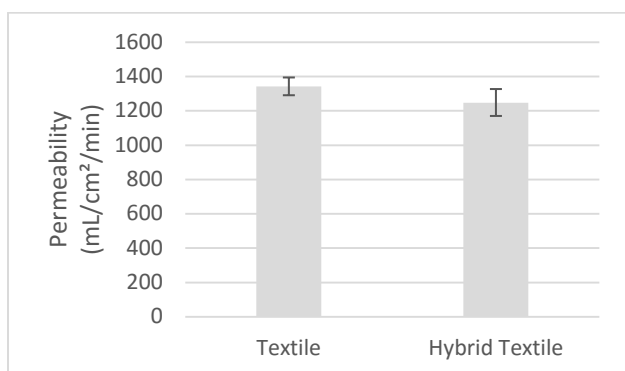

Figure 4. Permeability.

Despite a larger bending stiffness value, early dynamic tests performed in the valves show that the valve behavior doesn't seem to be modified with the non-woven layer. Actually, the permeability of the material being slightly reduced, it seems that the pressure applied on the valve leaflet generates a larger closing force which compensates the inertia due to the larger stiffness. The final behavior of the hybrid valve is therefore not really modified.

CONCLUSION

According to these early results it appears that it is possible to create a hybrid textile combining layers of fibers with various sizes. The material shows lower permeability and consequently lower regurgitation which is one of the most sought characteristics for a heart valve. The force spinning process enables obtaining oriented fibers and a controlled porosity which means a controlled specific surface, which may lead to a better controlled interaction between the textile valve and the host cells. In order to investigate other interesting features of this innovative hybrid textile, further tests should be performed.

KEYWORDS

Heart valve, Hybrid textile, Force Spinning

REFERENCES

[1] Kidane, A., et al. "Current Developments and Future Prospects for Heart Valve Replacement Therapy." *Journal of Biomedical Materials Research Part B: Applied Biomaterials*, 2009, 88B (1): 290-303.
[2] Heim, F., Durand, B., Chakfe, N. "Textile Heart Valve Prosthesis: Manufacturing Process and First In Vitro Performances." *Textile Res J.*, 2008, 78: 1124-133.
[3] Heim, F., Durand, B., Chakfe, N. "Textile Heart Valve: Novel Shaping Process and Material Performances." *Mater. Manuf. Processes*, 26 (10): 1303-309.

Advantages of a High-throughput Tensile Measurement System for Filaments Used in Fibre-reinforced Plastics

Yann Leray, Nigel Winsey, Steve Bucknell
Dia-Stron Limited, Andover, UK
yann.leray@diastron.com

INTRODUCTION

Carbon or ceramic filaments have been used for decades to mechanically enhance the strength and elasticity of polymer based matrix plastics. The mechanical characterization of these fibres or filaments, especially in uniaxial tensile deformation, is commonly evaluated to understand and to predict the behaviour of composites parts (1).

Tensile testing of such filaments is usually carried out on a Universal Testing Machine (UTM) where the filament is mounted onto a card frame using adhesive drops to anchor the sample in place at a specific gauge length (2). Great care must be given to specimen preparation to avoid premature tensile failure (3). For example, the filament should be mounted without shearing it. While setting up the card frame into the UTM, any misalignment will create bending stresses at the grippers resulting in premature break (4). Another practical issue arises from cutting both sides of the card frame prior to test start: in that case, the cutting action can easily snap the specimen before testing. These experimental problems often reduce significantly testing productivity and contribute to measurement errors.

Another aspect of filament tensile testing is the determination of the filament cross-sectional area to convert tensile force values into tensile stress values. Estimation of filament mean diameter is generally determined on Scanning Electron Microscope (SEM) micrograph (5). Alternative methods of cross-sectional area measurements include the use of optical gauges or filament vibroscopic techniques (6). These dimensional testing methods can present a number of disadvantages including long measurement time, specimen coating prior to dimensional measurements, or cross-sectional area calculations derived from material properties such as linear density.

To increase testing productivity and to tackle limitations of existing measurement methods, Dia-Stron Limited, a leading manufacturer of innovative and automated modular testing systems for single fibres and filaments, designed and developed a new automated metrology platform to perform dimensional and tensile testing of single carbon or ceramic filaments.

APPROACH

The presented measurement solution was developed to overcome the low productivity associated with the manual testing of mechanical properties of single fibres or filaments.

Sample preparation

As part of a new automated metrology platform, a filament mounting method was developed, based on a plastic tab system to align, mount and secure samples in place. Filament samples are located onto two plastic tabs presenting a self-aligning feature. The filament sample is then secured in place by dispensing a drop of epoxy based adhesive cured by UV light. A digital dispensing device helps with consistent and repeatable dosing. The filament specimens are stored on a sample cassette for easy and safe handling.

Dimensional measurement module

A dimensional measurement module, the LDS0200 – Laser Diffraction System, was designed for direct, non-contact diameter measurements. The measurement principle is based on laser diffraction. When a filament specimen is automatically placed in a collimated monochromatic laser beam, two symmetrical effects appear on each side of the filament section, similar to two new sources of coherent light, producing interferometric fringes perpendicular to the specimen. Deviation of the incident rays of light is due to the material tangential effect, creating a diffraction phenomenon. An optical system concentrates the fringe signal on a linear CCD sensor. The period of the diffraction fringes is a direct measure of the filament diameter, down to a few microns. The LDS0200 is calibrated, temperature compensated and insensitive to vibrations due to the high speed scanning rate.

Tensile measurement module

A tensile measurement module, the LEX820 – Linear EXtensometer, was developed as a high resolution extensometer designed especially for brittle filaments or fibres that fail at low strain values. At its heart, a DC micrometer drive offers smooth travel combined with high positional repeatability to acquire detailed stress/strain data. A 20N S-beam load cell is mounted on the LEX820 to capture force data and offers excellent linearity and low compliance.
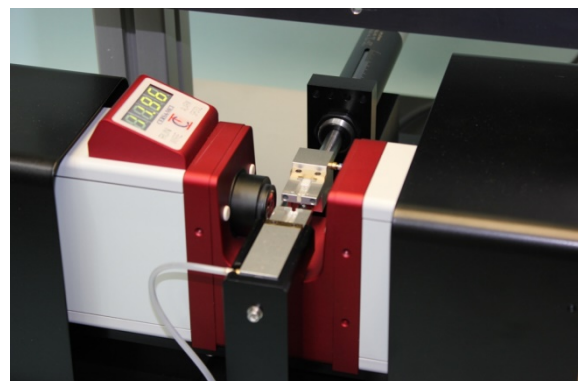

Figure 1: Integrated LDS0200 and LEX820 sub-system.

Automation platform

Both the LDS0200 and the LEX820 are integrated into a single metrology sub-system (Figure 1) to guarantee straightness and orthogonality of the filament specimen with the laser beam for higher diameter measurement precision. The LDS0200 automatically tilts around the sample to correct for any misalignment in the measurement system.

The integrated metrology sub-system is mounted onto an automation platform where a pick & place robot transports efficiently and safely fragile specimens from the storage cassette to the measurement modules. Specimens are loaded into a set of pockets (Figure 2) mounted on the LEX820 measurement module.
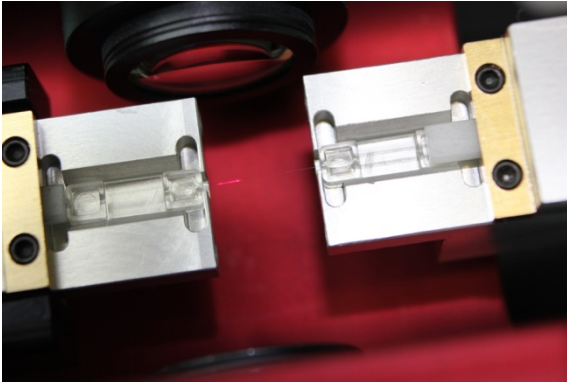

Figure 2: Specimen loaded into module pockets.

RESULTS AND DISCUSSION

After briefly describing experimental details, a set of dimensional and tensile data of commercial grade carbon and ceramic filaments will be presented. System compliance correction will be exposed as well as a Weibull analysis of the tensile strength data (7). Correlation between measured values and commercial datasheet values shows good agreement. Finally, specimen preparation and measurement timings will be shared to demonstrate testing productivity gain.

CONCLUSION

A new automated metrology platform for dimensional and tensile testing of filaments was presented. This high-throughput testing method offers significant advantages over manual methods based on a card frame approach. Generated data show good agreement with manufacturer datasheet values. In addition, the presented method is compatible with most common ASTM, ISO and JIS testing standards for filament samples.

KEYWORDS

Single Fibre, Single Filament, Carbon Filament, Ceramic Filament, Filament Diameter, Cross-Sectional Area, Laser Diffraction, Tensile Test, Tensile Strength, Failure Strain, Compliance Correction, Weibull Analysis, Automation.

REFERENCES

(1) M. Mohite, et al. "Axial Tensile Testing of Single Fibres." *Modern Mechanical Engineering*, 2012, 2: 15156.

(2) *Carbon Fibre: Determination of the Tensile Properties of Single-filament Specimens*. ISO 11566:1996 Standard.

(3) F. Franceschi. "Influence of sample preparation on carbon fiber single filaments mechanical characterization." *Innovation with Carbon Materials Conference*, Dresden, July 2015.

(4) A.R. Bunsell. *Handbook of Tensile Properties of Textile and Technical Fibres*. Elsevier, 2009. 40-41.

(5) A.R. Bunsell. *Handbook of Tensile Properties of Textile and Technical Fibres*. Elsevier, 2009. 25.

(6) J.R. Davis. *Tensile Testing,* 2nd Edition. ASM International, 2004. 185.

(7) S. Van der Zwaag. "The Concept of Filament Strength and Weibull Modulus." *Journal of Testing and Evaluation*, 1989, 17(5).

The Potential of Use of High-value Protein Obtained from Poultry Waste as Medical Textile

Aleksandra Miletić[1], Nabyl Khenoussi[2], Branka Pilić[1], Christelle Delaite[3], Dominique Adolphe[2], Laurence Schacher[2]

[1]University of Novi Sad, Faculty of Technology, Novi Sad, Serbia
[2]Laboratoire de Physique et Mécanique Textiles, UHA, ENSISA, Mulhouse, France
[3]Laboratory of Macromolecular Photochemistry and Engineering, UHA, ENSCMu, Mulhouse, France
alexm@uns.ac.rs

INTRODUCTION

Recent development of medicine created changes in materials that are used as medical devices. Following the global demand of new materials that are obtained from natural sources, medicine also started to implement this kind of materials (Jianga, Carbonea and Lo). Natural polymers are very valuable for medical applications, especially in tissue engineering, wound dressings and controlled delivery and release of drugs, first of all because of biochemical similarity with natural tissues and low possibility of irritations after implantation. Until now, collagen, whey and soy proteins, chitosan, wool keratin and many other natural polymers are used for different medical applications. Polymer that is also very interesting is poultry keratin, especially because it is obtained from waste from poultry production (Wang and Cao).

It is known that approximately 10% of poultry weight goes on feathers and with increased production of poultry worldwide, feathers become environmental problem, because it is reused as low nutrition animal feed and low caloric fuel in very low percent (Ullah, Vasanthan and Bessler). Another thing that is well known is that 90% of feather weight is consisted of keratin which has a great potential of use. While wool keratin is used for many years, poultry keratin still searches for it's place on the market because the methods of extraction are not well developed yet, which is a direct consequence of special structure. Opposite to wool keratin which is a big molecule, poultry keratin consists of about 100 aminoacids connected into polymer chain, with highlighted secondary and tertiary structure (Zoccola, Aluigi and Tonin). In literature there are very few methods for the extraction of poultry keratin, which are using harmful substances in order to destroy spatial structure and ease the extraction.

Keratin can be processed using electrospinning method, with or without blending with other polymers, and forming very fine nanofibers.

OBJECTIVE

As the chicken is predominated type of poultry produced, chicken feathers are used as a source of keratin. The main aim of this work is to make an overview of extraction processes that are used by other researchers and to propose a new way of extraction using different agents. Procedures of purifying and processing of obtained keratin will also be presented.

RESULTS

Chicken feathers are examined before the extraction, in order to determine protein amount (which equals to keratin amount) using Kjeldahl method, to determine thermal properties with TGA and DSC methods, to determine presence of crystalline structure within the feathers using XRD and to determine the presence of some functional groups using FT-IR. After the extraction, purification and drying was performed, all analysis are repeated in order to notice changes that eventually occurred. Keratin obtained this way can be used in many applications, in form of thin film, fibers, in blends etc.

CONCLUSION

The process of keratin extraction from chicken feathers is proposed, but still there is a need for optimization of process itself. As two different spatial structures of keratin are present in feathers, α- and β-keratin, with different properties caused by tertiary structure, and there is a there is a transformational change between those, process might be optimized this way. Also, changes on keratin molecule can be useful as well.

KEYWORDS

Poultry waste, characterization, extraction, keratin.

ACKNOWLEDGMENT

REFERENCES

1. Jianga, Tao, et al. "Electrospinning of polymer nanofibers for tissue regeneration." *Progress in Polymer Science*, 2015: 1-24.
2. Ullah, Aman, et al. "Bioplastics from Feather Quill." *Biomacromolecules*, 2011: 3826-32.
3. Wang, Yun-Xian, Xue-Jun Cao. "Extracting keratin from chicken feathers by using a hydrophobic ionic liquid." *Process Biochemistry*, 2012: 896-99.
4. Zoccola, Marina, Annalisa Aluigi, Claudio Tonin. "Characterisation of keratin biomass from butchery and wool industry wastes." *Journal of Molecular Structure*, 2009: 35-40.

Development of New Measurement Method of Transversal Friction Between Fibers

H.E. Gassara, A. Sinoimeri, C. Wagner Kocher, G. Barbier

Université de Haute Alsace, Laboratoire de Mécanique et Physique Textiles, Mulhouse, France

houssem-eddine.gassara@uha.fr

OBJECTIVE

The mechanical behavior of fibrous assemblies, particularly the transverse behavior of fiber yarns and multifilament strands depends, inter alia, on the fiber-to-fiber contact and sliding. All studies on interfiber friction presented in the literature focus on cases where the relative interfiber motion occurs either in longitudinal-to-longitudinal or longitudinal-to-transverse direction. The transversal-to-transversal interfiber friction plays an important role as far as the mechanical transverse behavior of fiber yarns and multifilament strands are concerned. Note that measuring of frictional properties of very fine fibers is not easy because of very low levels of normal and tangential interfiber forces developed during the fiber contact. The present study proposes an original method to evaluate the case named here 'transversal friction'.

INTRODUCTION

The frictional force can be calculated following the Leonardo da Vinci [1] and Guillaume Amontons approach when two bodies slide over each other with a certain speed v, the tangential frictional force F is proportional to the coefficient μ of friction and the normal force N as follows:

$$F = \mu \cdot N \qquad (1)$$

Since 1950, the shear-adhesion theory of Bowden and Tabor [2] proposed new methods in the study of friction and cohesion. According to this theory the frictional force F is generally connected to the normal force N using the following equation:

$$F = \alpha \cdot N^n \qquad (2)$$

where the n index takes into account the type of deformation (plastic, elastic…) of the micro asperities of the two bodies.

Fiber surface characteristics are generally longitudinally oriented, as it can be seen from Figure 1. It follows that fiber-to-fiber or fiber-to-other body frictional behavior will depend strongly on the direction of inter-surface movement relative to the fiber axis.

Despite the large number of studies and measuring devices concerning fiber-to-fiber and fiber-to-other body friction, as far as fiber-to-fiber friction is concerned, they can be classified in two main groups according to their measuring principles: l-l friction type (case (a) in Figure 2) and l-t friction type (case (b) in Figure 2). Unfortunately, nothing is proposed in the experimental literature on the t-t friction measurement type (case (c) in Figure 2). Let's note that this friction type cannot be deduced from measurements in other directions.

MATERIAL AND METHOD

A new experimental device, designed to measure frictional forces between two filaments in contact is show in Figure 3.
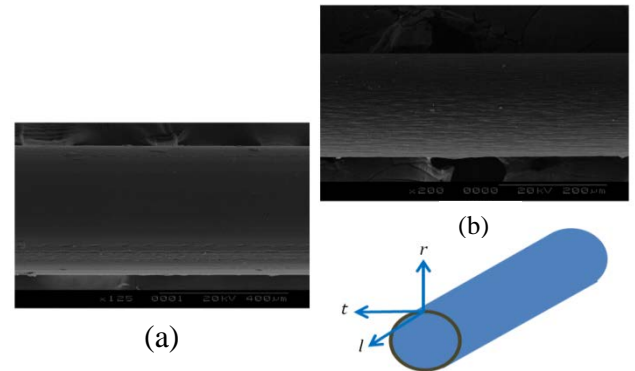

Figure 1. SEM pictures of PES (a) and PA 6-6 (b) fibers.
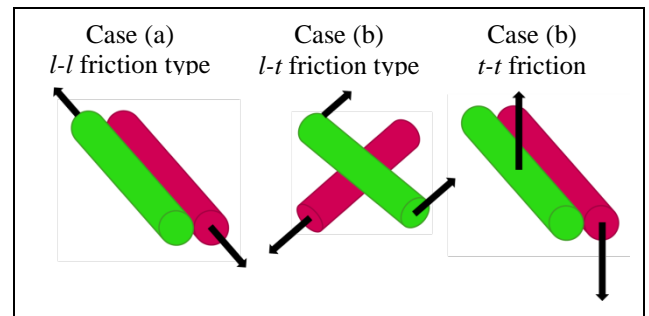

Figure 2. Frictional measurement in different configurations.
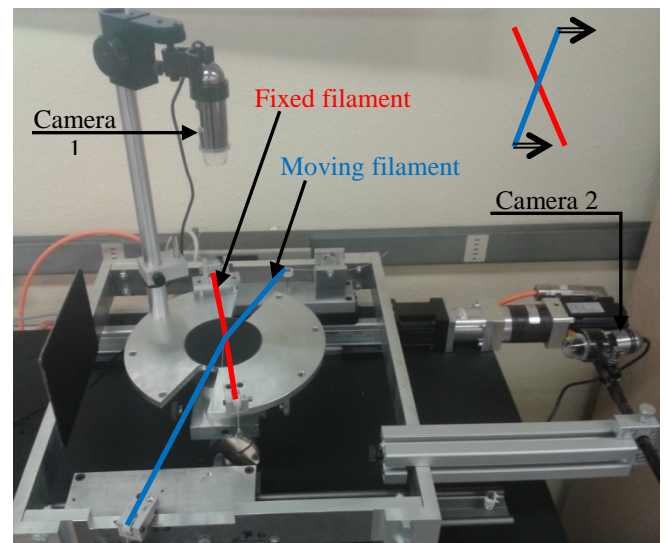

Figure 3. Experimental device.

Direct measuring of interfiber forces, normal and tangential, is very difficult due to their very low levels. On the other hand, the use of any contact sensor perturbs substantially the measure itself. For this reason, the authors have chosen to evaluate these forces by considering the equilibrium state (see Figure 4).
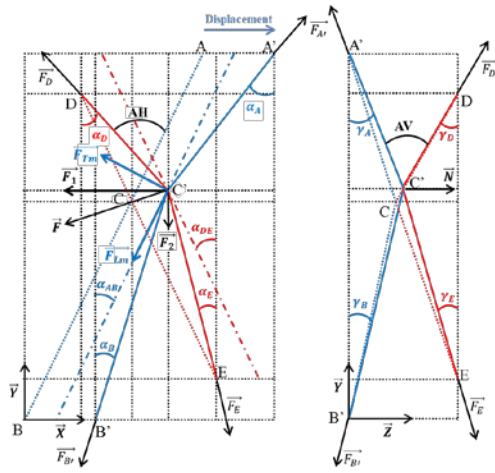
Figure 4. Top and side views of filaments in equilibrium.

Nine equations are provided by static equilibrium following x and y directions: moving filament alone, fixed filament alone and the two filaments considered together. Finally the equilibrium state may be written as follows:

$$\begin{pmatrix} A_{11} & \cdots & A_{15} \\ \vdots & \ddots & \vdots \\ A_{91} & \cdots & A_{95} \end{pmatrix} \begin{pmatrix} F_1 \\ F_2 \\ R \\ F_A \\ F_D \end{pmatrix} = \begin{pmatrix} B_1 \\ B_2 \\ \vdots \\ B_9 \end{pmatrix} \qquad (3)$$

Due to the experimental error, this system must be solved by the least squares method. The frictional coefficients, longitudinal and transversal, are calculated respectively by the rations F_L/N and F_T/N. A particular statistical analysis is performed in order to evaluate the confidence intervals of the calculated frictional coefficients.

RESULTS AND DISCUSSION

Figure 5 shows the effects of the angle between fibers and fiber tensioning on the calculated frictional coefficients.
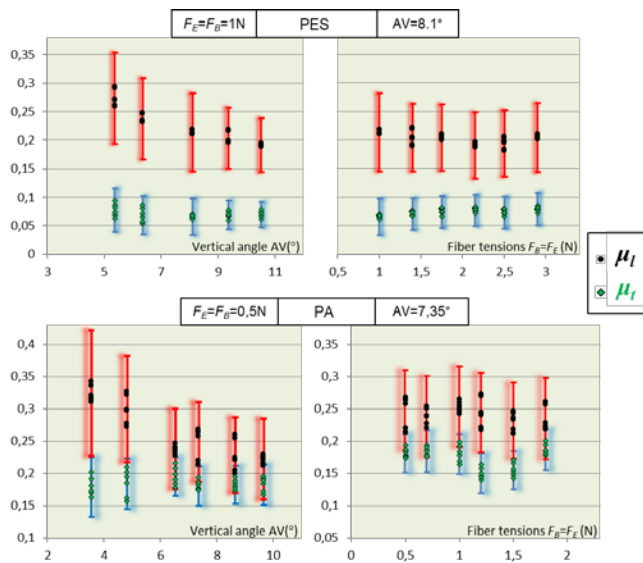

Figure 5. Effect of fiber tensions and vertical angle on the calculated transversal and longitudinal frictional coefficient.

It can be noted first that the frictional coefficients were not affected by fiber tension. As a matter of fact, it affects proportionally transversal, longitudinal and normal forces giving thus an invariable ratio F/N. Second, the longitudinal frictional coefficients decrease by increasing the vertical angle AV, whereas transversal frictional coefficients seem to be constant and independently of experimental factors. Finally, the transversal friction coefficients seem to be lower than the longitudinal one for both considered fibers. The longitudinal frictional coefficient measured by El Mogahzy and Gupta [3] device (not shown here) was of 0.4 for both Polyamide and Polyester fibers, which is superior to those obtained by the method proposed in the present work.

There are some inconsistencies in the presented results. There is no apparent reason to explain first why transversal frictional coefficient is independent of experimental condition whereas the longitudinal one isn't; and second, why the longitudinal frictional coefficient evaluated by another method is different and more important than the one evaluated by the present method. To conciliate these results, it will be interesting to consider how the fiber slippage occurs. Let's remember that in general, slippage takes place when the external force, tangent to the contact surface, becomes equal or greater than the frictional force $F_f = \mu N$. Let's also suppose two independent fiber-to-fiber frictional coefficients, longitudinal μ_L and transversal μ_T. During an experimental test described in the present study, external forces F_L and F_T change continuously. As long as these forces are both respectively lower than the limits $\mu_L N$ and $\mu_T N$, the slip does not occur. When even one of these two external forces exceeds its respective limit, the slippage takes place.

Following this reasoning, it results that in the present experimental device, the slippage occurs always in the transversal direction, giving thus 'real' and constant transversal frictional coefficient, whereas the longitudinal force has not yet attained its limit $F_L = \mu_L N$. The calculated longitudinal frictional coefficient results this way to be variable and underestimated.

CONCLUSION

A new device and an associated model have been developed in order to evaluate the transversal interfiber friction. The first results show a relative stability as far as the error effects are concerned. A relatively simple and original statistical approach is also developed to evaluate the confidence interval of these coefficients. This work is a first attempt of measuring the transverse interfiber friction. Other ideas and/or experimental devices would be very useful to validate the present method.

RÉFÉRENCES

[1] H.G. Howell, et al. *Friction in Textiles*. London: Butterworths Sc. Publications, 1959.
[2] F.P. Bowden, D. Tabor. *The Friction and Lubrication of Solids*. 1964.
[3] Y.E. El Mogahzy, B.S. Gupta. "Friction in Fibrous Materials, Part II: Experimental Study of the Effects of Structural and Morphological Factors." *Text. Res. J.*, 1993.

9 782955 656006

TEC-IT.COM